

AGARD

ADVISORY GROUP FOR AEROSPACE RESEARCH & DEVELOPMENT

7 RUE ANCELLE, 92200 NEUILLY-SUR-SEINE, FRANCE

AGARD LECTURE SERIES 205

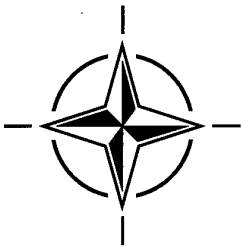
Smart Structures and Materials: Implications for Military Aircraft of New Generation

(Structures et matériaux intelligents — les retombés pour les
aéronefs militaires de la nouvelle génération)

DISTRIBUTION STATEMENT A

Approved for public release
Distribution Unlimited

The material in this publication was assembled to support a Lecture Series under the sponsorship of the Structures and Materials Panel and the Consultant and Exchange Programme of AGARD presented on 30-31 October 1996 in Philadelphia, USA, 18-19 November 1996 in Amsterdam, the Netherlands, 21-22 November 1996 in Paris, France.



NORTH ATLANTIC TREATY ORGANIZATION

Published October 1996

Distribution and Availability on Back Cover

AGARD

ADVISORY GROUP FOR AEROSPACE RESEARCH & DEVELOPMENT

7 RUE ANCELLE, 92200 NEUILLY-SUR-SEINE, FRANCE

AGARD LECTURE SERIES 205

Smart Structures and Materials: Implications for Military Aircraft of New Generation

(Structures et matériaux intelligents — les retombés pour les aéronefs
militaires de la nouvelle génération)

The material in this publication was assembled to support a Lecture Series under the sponsorship of the Structures and Materials Panel and the Consultant and Exchange Programme of AGARD presented on 30-31 October 1996 in Philadelphia, USA, 18-19 November 1996 in Amsterdam, the Netherlands, 21-22 November 1996 in Paris, France.

19961119 045



North Atlantic Treaty Organization
Organisation du Traité de l'Atlantique Nord

DTIC QUALITY INSPECTED 4

The Mission of AGARD

According to its Charter, the mission of AGARD is to bring together the leading personalities of the NATO nations in the fields of science and technology relating to aerospace for the following purposes:

- Recommending effective ways for the member nations to use their research and development capabilities for the common benefit of the NATO community;
- Providing scientific and technical advice and assistance to the Military Committee in the field of aerospace research and development (with particular regard to its military application);
- Continuously stimulating advances in the aerospace sciences relevant to strengthening the common defence posture;
- Improving the co-operation among member nations in aerospace research and development;
- Exchange of scientific and technical information;
- Providing assistance to member nations for the purpose of increasing their scientific and technical potential;
- Rendering scientific and technical assistance, as requested, to other NATO bodies and to member nations in connection with research and development problems in the aerospace field.

The highest authority within AGARD is the National Delegates Board consisting of officially appointed senior representatives from each member nation. The mission of AGARD is carried out through the Panels which are composed of experts appointed by the National Delegates, the Consultant and Exchange Programme and the Aerospace Applications Studies Programme. The results of AGARD work are reported to the member nations and the NATO Authorities through the AGARD series of publications of which this is one.

Participation in AGARD activities is by invitation only and is normally limited to citizens of the NATO nations.

The content of this publication has been reproduced
directly from material supplied by AGARD or the authors.

Published October 1996

Copyright © AGARD 1996
All Rights Reserved

ISBN 92-836-1042-3



*Printed by Canada Communication Group
45 Sacré-Cœur Blvd., Hull (Québec), Canada K1A 0S7*

Smart Structures and Materials: Implications for Military Aircraft of New Generation

(AGARD LS-205)

Executive Summary

Over the last five years, smart structures and materials have emerged throughout the world as new technologies. The main applications concern both the military domain (new aircraft, space, engines and ships) and civilian fields such as aeronautics, motors, energy, health and the building trade. They offer many advantages:

- reduction of cost due to a reduction of duplication;
- reduction of weight;
- reduction of energy consumption;
- improvement of system performance, maintenance and repair.

The best methods for design and processing of affordable materials are only beginning to be addressed by researchers. Concurrent engineering and intelligent processing of materials concepts will be essential to enable smart materials to make the transition from the laboratory into applications.

This lecture series will offer designers, industrial, and maintenance personnel (military and civilian) a better view of these techniques. It will review and identify the important basic elements of intelligent structures and will present the fundamental principles of the main sensing approaches related to the possible applications. Because the subject is so broad, the applications discussed will be limited to aircraft.

Structures et matériaux intelligents — les retombés pour les aéronefs militaires de la nouvelle génération

(AGARD LS-205)

Synthèse

Au cours des cinq dernières années, les structures et matériaux intelligents ont fait leur apparition, partout dans le monde, comme étant des technologies nouvelles. Les principales applications concernent aussi bien les militaires (aéronefs, espace, moteur, et navire) que les civils (aéronautique, moteur, énergie, robustesse, et construction). Elles offrent de nombreux avantages:

- réductions des coûts en raisons de la diminution des duplications;
- réduction en poids;
- réduction en énergie consommée;
- l'amélioration des performances des systèmes, de la maintenance et des réparations.

Les meilleures méthodes pour la conception et les procédés pour disposer de ces matériaux à des coûts abordables commencent à être entrevus par les chercheurs; une approche de l'ingénierie et un traitement avisé de leur conception de ces matériaux sera essentielle pour la transition des laboratoires vers des applications industrielles.

Cette série de conférences offrira au concepteurs, au personnel de l'industrie et de la maintenance (militaire et civil) une meilleure vision de ces techniques. Elle résumera et identifiera des éléments de base des structures intelligentes les plus importants et présentera les principes fondamentaux d'approches pragmatiques en fonction des applications possibles. Compte tenu de l'ampleur du sujet ces applications seront limitées aux aéronefs.

Contents

	Page
Executive Summary	iii
Synthèse	iv
List of Authors/Speakers	vi
General Introduction by Dr. Ing. Christian Boller	I
Characteristics and Processing of Smart Materials by Prof. Haydn N.G. Wadley	1
Shape Memory Alloys and their Application by Dr. Ing. Christian Boller, Mr. Werner Brand, Ms. L. Catherine Brinson and Prof. Miin-Shiou Huang	2
Intelligent Processing of Smart Materials by Prof. Haydn N.G. Wadley	3
Fundamentals on Damage Monitoring by Dr. Ing. Christian Boller	4
Use of Neural Networks/Genetic Algorithms for Fault Detection and Sensor Location by Prof. G.R. Tomlinson, Dr. K. Worden and Dr. W. Staszewski	5
Active and Passive Damping Techniques by Prof. G.R. Tomlinson and Mr. J. Rongong	6
A Novel Approach to Structural Design using Biological Models by Mr. R. Wardle and Prof. G.R. Tomlinson	7
Smart Structures, MEMS and Smart Electronics for Aircraft by Prof. Vijay K. Varadan and Prof. Vasundara V. Varadan	8
Structural Health Monitoring of Aircraft Components by Dr. Jayanth N. Kudva, Mr. Allen J. Lockyer and Mr. Craig B. Van Way	9
Adaptive Aircraft Wing by Dr. Jayanth N. Kudva, Mr. Allen J. Lockyer and Dr. Kari Appa	10
Electromagnetic Antenna and Smart Structures by Prof. A. Priou	11
Exploratory Team on Smart Structures and MEMS of NATO, Panel 3, AC 243 RSG by Prof. A. Priou	12

List of Authors/Speakers

Lecture Series Director:

Dr. Ing. Christian BOLLER
Daimler Benz Aerospace AG Military Aircraft, LMT 2
D-81663 Munich
GERMANY
actually with Daimler Benz AG
Research & Technology Exchange Group
HPL0507
D-70546 Stuttgart
GERMANY

Prof. Haydn G. WADLEY
University of Virginia
Materials Science and Engineering
Thornton Hall
Charlottesville
VA 22903-2442
USA

Dr. Jayanth N. KUDVA
Northrup Grumman Corp
Dept 9B71/63
1 Hornet Way
El Segundo, CA 90245
USA

Prof. Vijay VARADAN
Centre for Engineering of Electronic and
Acoustic Material and Devices
The Pennsylvania State University
149 Hammond Building
University Park, PA 16802-1400
USA

Prof. G.R. TOMLINSON
University of Sheffield
Dept. of Mechanical
and Process Engineering
Mappin Street
Sheffield S1 3JD
UK

Prof. A. PRIOU
Radar Technologies Division Head
DGA/DRET/STRDT/G22
26 Boulevard Victor
F-00460 ARMEES
France

CO-AUTHORS

Mr. R. WARDLE, Mr. J. RONGONG
Dr. W. STASZEWSKI and Dr. K. WORDEN
Department of Mechanical Engineering
University of Sheffield, Mappin Building
Mappin Street
Sheffield S1 3JD, UK

Ms L. Catherine BRINSON &
Prof. Miin-HUANG
Department of Mechanical Engineering
Northwestern University
Evanston/Illinois 60201
USA

Mr. Werner BRAND
Daimler-Benz Aerospace (DASA)
Military Aircraft LME2
Postfach 801160
D-81663 Munich
Germany

Prof. Vasundara V. VARADAN
Shiou Research Center for the Engineering of
Electronic and Acoustic Materials
Pennsylvania State University
University Park, PA 16802
USA

Mr. Allen J. LOCKYER, Mr. Craig B. VAN WAY
and Dr. Kari APPA
Northrop Grumman Corporation
Military Aircraft Systems Division
Dept. 9B71/63, One Hornet Way
El Segundo, CA-90245, USA

General Introduction

Christian Boller

Daimler-Benz Aerospace, Military Aircraft

D-81663 München, Germany

actually with: Daimler-Benz AG, Research & Technology Exchange Group

D-70546 Stuttgart, Germany

SUMMARY

Development in disciplines such as sensing technology, computation, control, micromechanics, materials including processing and many others has made significant progress during the past decades. This progress has been mainly possible through an in-depth analysis of the different aspects in these disciplines. To consequently take more advantage of this progress a synergy between these different disciplines has to be established, resulting in what has been termed to be smart materials and structures. Smart (alternatively: active, adaptive, multifunctional or intelligent) materials and structures is - briefly explained - the integration of sensing and actuation elements into a structure or even more ambitiously into a material, with sensor and actuator being linked by a controller. Materials actually favoured for integration include optical fibres and piezoelectric materials with respect to sensors, piezoelectric/electrostrictive materials, shape memory alloys and electro-rheological fluids with respect to actuators and microprocessors, neural networks, fuzzy logic and various types of signal processing with respect to control. Since performance of military aircraft and spacecraft has progressed in a sequence of steps in the past, smart materials and structures technology can thus be considered to be a next step in enhancement.

THE WAY TO SMART MATERIALS & SYSTEMS

It is now more than a decade ago since people have started to talk about smart materials and structures. Various definitions have been given (e.g. Ahmad 1988, Takagi 1989, Measures 1989) and various expressions such as intelligent, multifunctional or adaptive are used, which sometimes need to be clarified. There is however some common sense in the way that a smart material or system incorporates sensors and actuators with both being linked via a controller. Trying to summarize the various definitions and expressions can result in a view as shown in Fig. 1.

A key question leading to smart materials and systems is: *Why cannot materials and systems with structural functions take over additional functions?* Their basic/traditional use is mainly related to passive functionality. It is therefore termed to be a *passive material or structure*. Adding sensors to the material or structure leads to what can be called a *sensory material or structure*. The term *active material or structure* can be used if the material or structure also includes actuators. Sophistication is im-

proved if sensors and actuators are linked via a controller allowing the material or system to adapt itself to various prescribed conditions which can be called an *adaptive material or structure*. The highest level that can be actually thought of is achieved when the adaptive material or system also includes a processor allowing itself to adapt to various conditions by self-learning. It can be specified to be the real *intelligent material or structure* and is in many cases a vision which still requires to be achieved.

	Sensor	Actuator	Controller	Processor
Intelligent Material & Structure	●	●	●	●
Adaptive Material & Structure	●	●	●	
Active Material & Structure	●	●		
Sensory Material & Structure	●			
Passive Material & Structure				

Fig. 1

A look into specific books, journals and conference proceedings shows that the wide range from sensory to intelligent materials and systems is covered under the expression of smart, adaptive or intelligent materials and structures. Technologies considered are not limited very much although there are some materials and technologies being actually favoured. These include optical fibers and piezoelectric materials with respect to sensors, piezoelectric and electrostrictive materials, shape memory alloys (SMAs) or electro-rheological (ER) fluids with respect to actuators and microprocessors, neural networks, fuzzy logic and various types of signal analysis with respect to control.

Activities in the world of smart materials and structures have mainly originated from applications in aerospace and have been published in a variety of conference proceedings and papers in journals. A first workshop on 'Smart Materials, Structures, and Mathematical Issues' was presented at the U.S. Army Research Office in 1988 (Editor: C.A. Rogers, 1988). In 1992 AGARD's Structures and Materials Panel organized a meeting on 'Smart Struc-

tures for Aircraft and Spacecraft' (AGARD, 1992) which has possibly been one of the first conferences on smart structures being fully related to aerospace. In 1994 the American Institute for Aeronautics and Astronautics (AIAA) and the American Society of Mechanical Engineers then performed the 'Adaptive Structures Forum' (AIAA, 1994), which has been mainly related to aerospace. A second forum of that kind was performed in 1996.

Another conference being very much related to aerospace is the International (originally U.S./Japan) Conference on Adaptive Structures (ICAST, 1991 - 1995), which was established in 1991 and has been held since every year. Other conferences where smart structures applications for aerospace are partially presented include the annual 'Fiber Optic Smart Structures and Skins' (SPIE, 1988 ff.) organized by SPIE since 1988, the annual 'Adaptive Structures and Materials Conference' and the biannual 'European Conference on Smart Structures and Materials', both being held since 1992.

Considering special aspects of smart structures the biannual 'International Conference on Intelligent Materials' (ICIM, 1992, 1994, 1996), being also established in 1992, needs to be mentioned as one of the most important conferences with respect to smart materials. Another important conference is the 'Actuator'-Conference organized biannually by VDI in Bremen/Germany. Beside these a variety of other international and national workshops, sessions, seminars, etc. are organized by various organizations.

There are also two international journals on smart structures and materials which is the *International Journal on Intelligent Material Systems and Structures* (published quarterly by Technomic Publ. Co. since 1990 and edited by C.A. Rogers) and the journal on *Smart Materials and Structures* (published quarterly by the Institute of Physics Publ. since 1992 and edited by R.O. Claus, G. J. Knowles and V.K. Varadan). A significant number of aerospace related smart structures applications are also published in the relevant aerospace journals such as the *ALAA-Journal* and others.

Educational books have also been published during the past years. A first compilation of various activities on smart structures and materials were the notes of a two-day seminar on 'Intelligent Material Systems & Structures' presented by C.A. Rogers, E. Crawley and R.O. Claus around 1990 (Rogers et al., 1990). This has recently been followed by a new book written by B. Culshaw in 1996 (Culshaw, 1996). As a result of the various worldwide activities going on in smart structures and materials at the moment further books can be expected to be published in due course.

A lot of motivation has been spread through the ideas generated and successfully realized for aerospace applications (e.g. Crawley and Anderson, 1989, Wada and Garba 1992, Fanson 1993). In the meantime applications are also considered with respect to military and civil transportation, starting with those for military aircraft and recently followed by those for automobiles and railway systems. This development becomes especially obvious when considering a wider range of sensor, actuator and control types than those mentioned before. Other types of

sensors can be those based on the change of electrical properties such as resistivity or capacity, thermal imaging or pressure. Actuators mainly used today are electrical motors, hydraulic or pneumatic actuators. These different types of sensors and actuators linked via control are the basis of advanced engineering systems actually available in products which easily fall into the range of smart/intelligent structures.

The sensing and actuation materials considered and mentioned before cannot be specified to be new anymore. Nor can this be said with respect to phototropic or electrochromatic glasses. It is more the challenge to combine these materials with conventional structural materials such as can be well done with polymerbased composites (Varadan and Varadan, 1993) or by introducing these materials into a wider industrial application. Another significant area being still exclusively related to research is the implementation of sensing and actuation functions on a microstructural or even molecular basis into a material (Shinya 1994; Hirukawa 1994; Takeuchi 1994).

Whenever the application of smart materials in engineering structures is considered, the following question has to be answered:

How has a smart structure to be designed to become cost-effective?

Answering this question can be done by using analytic approaches easily determining the boundary conditions of smart materials, followed by a study using cost analysis procedures.

EXAMPLES OF AVAILABLE SYSTEMS AND MATERIALS

When comparing the definition given above for a sensory, active, adaptive and intelligent or briefly a smart material or structure with materials and systems used today in military aircraft, it becomes obvious that smart structures have already been implemented somehow. Aircraft nowadays all contain a large number of sensors such as for sensing temperature, speed, acceleration, brightness, humidity, volume flow or electromagnetic signals or actuators allowing to move components, to exert forces, to inject a fluid or a gas or to reduce light intensity. All actuation is done by either human or electronic control, the latter requiring the type of sensors mentioned before. The smart structures available today are based on the fact that structural components are fully made out of passive materials with sensors and actuators being added to the system. They can be classified in the range from sensory to adaptive structures, while intelligent structures are still the vision to be followed in future research and development.

Although there is a variety of sensors, actuators and control algorithms already available in military aircraft today, it is far beyond the scope of this lecture series to present all available systems and their possible relation to smart structures. In a few papers (Agnes and Silva, 1992; Schmidt and Boller, 1992) major potential areas for applying smart structures in military aircraft have been identified, which in both papers turned out to be the following three:

- aircraft health and usage monitoring, which is a sensory system mainly related to identification and possibly validation of damage in structures,
- active and adaptive structures which is related to shape control, vibration damping and light transmissivity of structural components, using materials with sensing and actuation capabilities such as piezoelectrics, SMAs, ER fluids or electrochromatic glasses,
- smart skins, being load carrying structural elements with integrated avionics (antennae), which can be either a sensory, active, adaptive or even intelligent structure depending upon its term of use.

Regarding the kind of materials considered to be smart, piezoelectrics, SMAs and electrochromatic glasses are the ones already being used today. So far their application is limited to their traditional use such as sensors and often simply controlled actuators within the structures described below.

Sensory Structures

In aerospace condition monitoring is widely used in jet engines. A network of sensors monitors temperature and gas flow within the engine and thus informs if critical engine parameters are within the operational range. Integrated health and usage monitoring system (IHUMS) have become quite popular with helicopters and have been recently made commercially available for helicopters (Bristow, 1992). These systems have been developed for gears and are based on monitoring acoustic signals being generated from the various rotating parts of the gear. Other systems include the use of video cameras for monitoring flaps and landing gear positions of widebody aircraft or the ones used for monitoring operational loads of military and civil aircraft based on either strain or flight parameters, where a broad selection of systems has been described (AGARD, 1991).

Active Structures

De-icing systems such as used on leading edges of aircraft wings and on aircraft engines are a type of active structures widely known. They consist of a pressure or ultrasonic sensor and pneumatic or electrical heating actuation system.

Electrochromatic windows allowing to change light transmissivity is another active structure considered for windows of aircraft cockpits (Daimler-Benz High Tech Report, 3/1994). The window has a sandwiched cross-section including two transparent electrodes, two electrochromatic layers and an electrolytical polymer layer. A small current of 1 to 2 volts imposed by the electrodes on the system allows to change the colour of the electrochromatic layers as a result of a chemical process initiated by the electrical current.

Adaptive Structure

A type of adaptive structure being widely known is the autopilot systems used for navigation and control of aircraft.

Noise cancellation in aircraft fuselages is a major issue with turboprops. Noise is monitored at the locations where it should be cancelled using conventional microphones. The signals are analysed and processed for actively generating an anti-noise which is either emitted using conventional loudspeakers or recently by adapting some small piezoelectric plates to the inside panel of the fuselage (Fuller et al., 1992).

A major initiative has come from space applications. Various activities performed have been related to space station freedom remote and space crane manipulator system, space based radar, the main truss, active vibration isolation of stores, equipment, sensors, or pods. A lot of knowledge has been generated through the USAF Advanced Control Technology Experiment (ACTEX) for demonstrating active vibration suppression in space vehicle applications using embedded piezoceramic actuators in a smart strut (Das et al., 1992). Truss structures with in-line sensor/actuator systems for active damping and possibly even vibration suppression, which can be individually controlled in a space truss work, has been a major result of this and other programs (Wada and Garba, 1992). Other types of piezoceramic actuators have been developed allowing to avoid sensor (e.g. interferometer) jitter resulting from systems such as cryocoolers or solar array panels in space vehicles. These different kinds of active elements have allowed to develop concepts for performing in-orbit modal analysis of large space structures or on active vibration damping of a space based radar. Disturbance isolation, active vibration suppression and active optical pathlength compensation of telescopes and optical interferometers have been successfully used with the Articulating Fold Mirror (AFM) which forms part of the optical scheme for correcting the spherical aberration of the Hubble Space Telescope and in other fields (Fanson 1993). Each AFM utilizes six electrostrictive multilayer ceramic actuators which also contain the required sensor unit while control is performed for the six actuators in a central unit. Adaptive structures for in-space assembly is another area of consideration.

FUTURE TRENDS

A trial to summarize state-of-the-art and future trends in technological development of smart materials and structures is shown in Fig. 2.

The following three main areas are seen to actually drive the technological development:

1. Engineering structures made of passive materials with sensors, actuators, and controllers being added (attached) to the system in the way described before.
2. Data processing and control which mainly involves high performance computing, neural net-works, fuzzy logic and genetic algorithms as well as micro-electronics related to it.
3. Materials and micromechanics which includes all kinds of materials and components such as fibre optics, piezoelectrics, SMAs and polymers, ER-fluids, nanostructures, composite materials, liga and silicon technology.

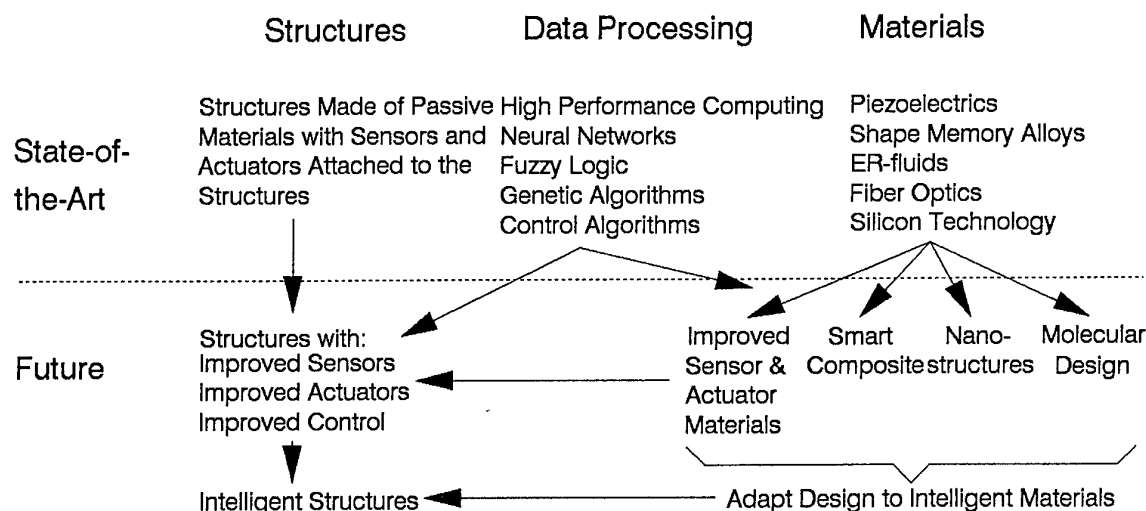


Fig. 2

With respect to the first area progress can be expected through improvement of the sensors, actuators, and control algorithms used.

Improvements achieved in the second area are applied for increase of the performance and/or the number of sensors and actuators used in the smart structure. Sensors and actuators can still be monofunctional and just attached to the structure considered.

The third area can again be split into three sections. The first section is related to improvement and possible development of materials with sensing and actuation functions. This includes topics such as improved ductility of piezoceramics, increase of piezoelectric induced strain as well as development of means for stroke amplification, higher Curie temperatures with piezoelectric polymers, better understanding of the constitutive behaviour of SMAs with respect to control of SMA actuation, extension of the range of possible transformation temperatures in SMAs, and much more.

The use of composite materials, which is related to the second section, has opened a wide field for integrating functional elements into these materials. This includes the integration of sensing or actuation elements such as fibre optics, piezoelectrics or SMAs. Studies recently performed involve determination of the effectiveness of these composite materials with respect to strength and performance. A lot of ideas have been generated in that area by integrating various types of sensors and actuators using technologies such as applied for printing electric circuit boards or other types of surface coating, thus leading to what is called a conformal smart skin (Varadan and Varadan, 1993) or generally a smart composite (Gardiner et al., 1993). Since such a type of composite will be able to take over sensing and actuation functions on a macroscopic and microscopic level, significant changes in design philosophies can be expected. However these new structural components have to meet the requirements set with respect to strength, environmental stability, cost, and reliability, the latter being achieved through redundancy in sensing and actuation elements allowing graceful degradation during operation. Activities similar to what is performed with smart composites is starting on a microscopic level in metallic and polymerbased materials

through implementation of particles with sensor and/or actuator functions in a way as having been initiated with the development of nanostructures. Finally it is worth mentioning that work is in progress trying to implement sensing and actuation functions on a molecular basis in polymers.

The third section can be related to work performed with respect to micromechanics including micromachines. Work performed here is mainly related to electronic, medical and surgical applications and has still not gained significance for being directly applied in transportation vehicles.

Analysing specific scientific papers leads to the conclusion, that smart materials and systems are mainly considered to be used in transportation vehicles for the following:

- monitoring the condition of a system/structure or the environment (situation awareness),
- exerting strokes and forces, and
- influencing dynamic behaviour.

Condition monitoring has become a major issue with composite materials where major concern exists with respect to barely visible impact damage (BVID) which occurs inside the structural material and can often not be seen from the outside. To minimize the effort required for inspecting the material or component with conventional Non Destructive Testing (NDT) technology, the NDT-technology is considered to become an integral part of the structure by implementing a network of appropriate sensors (Boller and Dilger, 1992). The types of sensors mainly considered are fibre optics (Measures, 1992; Tutton and Underwood, 1992) and piezoelectrics (Boller, 1994). Such structural health monitoring systems are actually mainly discussed for aircraft applications but could even gain interest when especially carbon fibre reinforced polymers will be more applied in railway systems and automobiles. Other issues include monitoring any condition which is required as an input for an adaptive or intelligent structure (e.g. monitoring the pressure profile for an adaptive wing).

Another important area related to sensory structures is smart skins. They are designed for control of aerospace structures such as acoustic noise and vibration, drag and

skin friction using advanced polymeric smart materials, MEMS (Microelectromechanical Systems) and built-in antennas (Varadan and Varadan, 1993). The objective is to develop something being denoted as "smart wall papers". Applications include smart helicopter rotorblades with microstrip patch antennas and detection and discrimination of hostile threats resulting from laser, radio-frequency and x-rays such as having been performed in the satellite attack warning and assessment flight experiment (SAWAFE) for actively filtered transparencies and conformal antennae (Obal et al., 1992). Wireless remote and continuous telemetry for application to rotorcraft and smart skin aerospace structures are further areas discussed (Varadan and Varadan, 1994).

Exerting strokes is done to statically change the position of a component. A lot of effort is actually placed on adaptation of the shape of aerodynamic profiles according to varying service conditions. When deformation speed is relatively low but strokes quite high, the use of SMAs is a solution to be considered (e.g. Misra et al., 1992). However this requires a precise control of temperature, which can become highly challenging when thinking of operational temperatures ranging between -50 and +120°C for aircraft applications. If deformation speed is a major requirement, piezoelectric actuators seem to be a considerable solution. A lot of studies have been performed with respect to active control of helicopter rotor blades using induced strain actuators where overviews have been given by Crawley and Anderson, 1989, Strehlow and Rapp, 1992, Barrett, 1995, or Giurgiutiu et al., 1995. It turns out that a hinged flap activated by a bimorph PZT actuator such as proposed by Spangler and Hall, 1989 is the most promising solution so far, especially since improvement has been gained with that system during the last years. Comparing this to conventional helicopter rotorblade design shows that the potential of active, adaptive and intelligent materials can only be taken full advantage of when design is adapted to the potential of these materials, which has been especially done here. Looking to applications in engines, control of valves using piezoelectric stack actuators seems to be an interesting field.

Reducing dynamic loads in any kind of engineering structures is a major field for considering intelligent materials and systems. Solutions have been proposed such as using piezoelectric stack actuators as part of an active acoustic noise control system between a jet engine and the fuselage (Sumali and Cudney, 1994).

Concepts, feasibility studies and windtunnel demonstrations for the control of aeroelastic response using smart structures in fixed and rotary wing aircraft applications have been performed. These include controlled transonic drag and tail buffeting reduction as well as active wing and panel flutter control and minimization/suppression using active means such as an active pylon or others. Decoupling of gyros from elastic aircraft vibration modes, helicopter rotor blade vibration suppression and control, and skin panel fatigue life extension are other areas widely discussed. Active landing-gears have been proposed for ride comfort (Catt et al., 1992).

With respect to missiles gunfire vibration reduction and active spoiler control are aspects to be mentioned.

To achieve large displacements required to reduce vibrations of relatively low frequency, much effort has to be placed into the activities of amplifying the low displacements generated by the piezoelectric actuators. Alternatives for these applications may exist by using other types of actuators such as based on ER-fluids (Naem et al., 1994).

Much effort is actually also going on in aeroelastic research using piezoelectric actuators for flutter and buffeting suppression and vibration damping (Heeg et al., 1994). Solutions here consider piezoelectric patches integrated into the aerodynamic profile, allowing to globally as well as locally influence the aeroelastic and aerodynamic behaviour. Finally the noise cancellation methods based on integrating piezoelectric patches into panels such as mentioned above is another activity in the field of reducing dynamic loads.

A variety of activities have started in the field of control where a good overview has been given in (AIAA 1996). These activities include flutter control, active control of helicopter rotorblades, sensor/actuator interaction, control of nonlinearities in actuators (e.g. piezoelectrics, shape memory materials) or decoupling of systems. In a large number of studies the use of neural networks for control has been examined.

General considerations also exist on actuator efficiency (Giurgiutiu et al. 1996, Sun and Rogers 1996), biometrics (de Rossi 1996) or evolutionary methods, where an overview is given for the latter in this lecture series (Tomlinson, 1996).

Based on the idea that smart structures and materials are considered to be the next step in enhancing the performance of aircraft and spacecraft, a variety of major initiatives have been generated such as the space activities at NASA-JPL (e.g. Controls and Structures Interaction (CSI) program, Precision Segmented Reflector (PSR) program, etc.), the US Air Force smart structures program, SDI or research and development programs going on in the area of adaptive wings (NASA/Lockheed, DASA/DLR/Daimler-Benz, Bae/Dowty) or in damage monitoring (e.g. the USAF Wright Laboratory Smart Metallic Structures Program and its relation to the USAF Aircraft Structural Integrity Program ASIP).

Based on the experience gathered so far with smart structures and materials, future needs have been expressed in various publications (e.g. Crawley, 1992, Agnes and Silva, 1992), which can be summarized as follows:

Sensors: There is still a great deal of work to be done with respect to design and optimization of sensors in the way that sensors can be tailored according to the specific needs they will be used for. One of these needs is monitoring of nonuniformly propagating acoustic signals in nonisotropic materials and the requirement for characterizing this for a range of layups structural components will be made of. Furthermore it would be desirable to distinguish between fibre and matrix cracking which would then allow to determine residual strength. Whenever this will be solved, sensing systems have to achieve a higher robustness, requiring some absolute or reference capability and not being completely relative.

Actuators: Based on commercially available actuation materials today (e.g. piezoelectric and electrostrictive) strain has to be increased by a factor of 3 to 10. Shape memory alloys show a good performance with respect to strain but their bandwidth in response time, constitutive behaviour, and others still need to be improved if ever a larger variety of applications is considered. Actuators on the basis of complex electrode patterns is an interesting possibility for increasing piezoelectric strain, but much more needs to be studied to understand the actuation, electrode, and host material interaction and thus the actuator's performance. Only if these actuation power improvements will be realized, benefits can be expected from systems such as considered for active flutter control.

Control: Aerospace systems mainly require non-linear adaptive controllers, which have to be based on real-time computing, miniaturized and of large bandwidth. Most of the control has been done on a mainly theoretical basis and for the control of discretized systems. Discretization is however not appropriate in a structural component, which therefore requires new ways of control. Distribution of control and definition of the various levels of control is another major issue to be considered.

Design: Since sensors and actuators are an integral part of a structural component, power conditioning and switching becomes important with respect to minimizing local heat loads, possibly leading to thermal degradation of the host material. Furthermore the integration of sensor and actuator elements into a structural material and component can significantly influence mass, stiffness and interfere with the load path, thus introducing new structural discontinuities of unknown significance. Another aspect is hermicity of embedded components which points special emphasis on reliably isolating the embedded components from environmentally deteriorating factors. Whenever smart materials and structures will have passed the laboratory stage, service liability, vulnerability to handling and damage, and repair will be of major significance. Before all, technology payoffs must be quantified and requirements established. Only when testing has been done on articles where key issues have been demonstrated understandably, more advanced flight worthy testing will be useful.

Manufacturing: Manufacturing of smart materials and structures is an issue which has not very much been considered before. It includes development of innovative techniques for packaging sensors, actuators and any other kind of electronics into structural materials and components, which have to become structurally robust in the way that they can survive stresses and strains they will be exposed during their in-service life. This is just one aspect of certainly a large number of others still to be explored.

CONCLUSIONS

Summarizing state-of-the-art and future trends in smart systems for aerospace applications leads to the conclusion that first applications start by adding sensors, actuators and controllers to a conventionally designed system based on passive materials. Progress in data processing technology provided today can be made use of at this stage, which mainly allows to increase the number of sensors or sensor information as well as to improve the performance of controllers applied. Parallel to this a large amount of

development has to be done in the area of intelligent materials. As long as their potential is not sufficiently described it is difficult to say if they can be used in reality. A look at three different R&D-programmes on adaptive aircraft wings in the USA, Germany and the UK respectively proves the conclusion made here to be realistic since they are all based on the following strategy: (1) Take a wing with its conventional sensors and actuators and improve control and data processing which allows to extend the use of existing flaps; (2) Implement sensors and actuators based on appropriate materials with known characteristics (e.g. piezoelectrics, SMAs, ER-fluids) and start to adapt the structural design according to these materials; (3) Use a smart composite system for design of the wing. It is the latter two steps which strongly require much more knowledge about active, adaptive and intelligent materials than we have today while the former step will mainly have to be focused on control.

This knowledge will be the basis for deciding if these active, adaptive and intelligent materials can be finally applied in accordance with the various requirements they will have to fulfil with respect to strength, environmental stability and compatibility, and especially cost. It is difficult for a material scientist to be aware of these requirements and it might be difficult for a designer in aircraft engineering to clearly understand the potential of new materials developed so far. To overcome this gap, to briefly determine the solution of best technological and economical potential and to always be on the track of minimum development time, procedures for validating the technological and economic potential have to be established.

It is advanced data processing, electronics, control, sensing and actuation which will help to let transportation systems of today to become somehow 'smart' tomorrow. It is however the introduction of smart materials which can significantly lead to a change in our engineering design philosophies towards intelligent structures. But none of all this can become reality if cost-effectiveness has not been proven.

REFERENCES

- AGARD, 1991; Fatigue Management; AGARD-CP-506
- AGARD, 1992; Smart Structures for Aircraft and Spacecraft; AGARD-CP-531
- Agnes G.S. and K. Silva, 1992; Aircraft Smart Structures Research in the USAF Wright Laboratory; AGARD-CP-531, Paper 27
- Ahmad I., 1988; "Smart" Structures and Materials; in: C.A. Rogers (Ed.); Smart Materials, Structures, and Mathematical Issues; Technomic, pp. 13 - 16
- Barrett R., 1995; All-moving Active Aerodynamic Surface Research; Smart Mater. Struct. 4, pp. 65-74
- AIAA/ASME, 1994; Adaptive Structures Forum; AIAA Proceedings
- AIAA/ASME/AHS, 1996; Adaptive Structures Forum; AIAA Proceedings
- Boller Chr. and R. Dilger, 1992; In-Flight Aircraft Structure Health Monitoring Based on Smart Structures Technology; AGARD-CP-531; Paper 17
- Boller Chr., 1994; Parameters and Techniques Based on Piezoelectric Sensing for Monitoring the Integrity of Composite Structures; Proc. of the 5th Internat. Conf. on Adaptive Structures; Technomic Publ. Comp.

- Bristow, 1992; Integrated Health and Usage Monitoring System (IHUMS); Aircraft Engineering, February 1992, pp. 12-13
- Catt T., D. Cowling and A. Shepherd, 1992; Active Landing Gear Control for Improved Ride Quality during Ground Roll; AGARD-CP-531, Paper 29
- Crawley E.F. and E.H. Anderson, 1989; Detailed Models of Piezoceramic Actuation of Beams; AIAA 89-1388-CP, pp. 2000-2010
- Crawley E.F., 1992; Intelligent Structures - A Technology Overview and Assessment; AGARD-CP-531, Paper 6
- Culshaw B., 1996; Smart Structures and Materials; Artech House Books
- Daimler-Benz High Tech Report, 3/1994; pp. 44-45
- Das A., G. Ombrek and M.W. Obal, 1992; Adaptive Structures for Spacecraft - A USAF Perspective; AGARD-CP-531, Paper 3
- De Rossi P.D., 1996; Biomimetic Materials and Structures; Proc. of ICIM/ECSSM '96, SPIE Vol. 2779
- Fanson J., 1993; Articulating Fold Mirror for the Wide Field and Planetary Camera; Proc. of the 4th Internat. Conf. on Adaptive Structures, Technomic, pp. 278-302
- Fuller C.R., S.D. Snyder, C.H. Hansen and R.J. Silcox, 1992; Active Control of Interior Noise in Model Aircraft Fuselages Using Piezoceramic Actuators; AIAA Journal, Vol. 30, No. 11, pp. 2613-2617
- Gardiner P., A. Kelly and A.R. Bunsell (Eds.), 1993; ECCM Smart Composites Workshop; Bordeaux/France; Woodhead Publ. Ltd.
- Giurgiutiu V., Z. Chaudhry and C.A. Rogers, 1995; Engineering Feasibility of Induced Strain Actuators for Rotor Blade Active Vibration Control; J. of Intell. Mat. Syst. and Struct., Vol. 6, pp. 583-597
- Giurgiutiu V., C.A. Rogers and R. Rusovici, 1996; Power and Energy Issues in the Induced Strain Actuation for Aerospace Adaptive Control; AIAA-96-1300-CP
- Heeg J., R.C. Scott and A.-M. R. McGowan, 1994; Aeroelastic Research: Using Smart Structures Concepts; in AD-Vol. 44, Aeroelasticity and Fluid Structure Interaction Problems, ASME, pp. 161-173
- Hirukawa H., S. Matsuoka, E. Takeuchi, K. Miyahara and Y. Muramatsu, 1994; Arrest Function of Fatigue Crack Growth by Phase-Transformed Oxide Particles; Proc. of the 3rd National Intelligent Materials Symposium, pp. 25-27 (in Japanese)
- ICAST, 1991 - 1995: Proc. of the Internat. Conf. on Adaptive Structures; Technomic Publ. Co.
- ICIM, 1992, 1994, 1996: Proc. of the Internat. Conf. on Intelligent Materials; SPIE
- Measures R., 1989; Smart Structures with Nerves of Glass; Progress in Aerospace Sci. vol. 26, pp. 289 - 351
- Measures R., 1992; Fibre Optic Sensing for Composite Smart Structures; AGARD CP-531, Paper 11
- Misra M.S., B. Carpenter and B. Maclean, 1992; Adaptive Structure Design Employing Shape Memory Actuators; AGARD CP-531, Paper 15
- Naem A.S.H., R. Stanway, J.L. Sproston and W.A. Bullough, 1994; A Strategy for Adaptive Damping in Vehicle Primary Suspension Systems; AD-Vol. 45/MD-Vol. 54, Adaptive Structures and Composite Materials: Analysis and Application, ASME; pp. 395-404
- Obal M., B. Saylor, H.S. Murray, M.R. Sweet, D. Holden and C. Moss, 1992; The Satellite Attack Warning and Assessment Flight Experiment (SAWAFE); AGARD-CP-531, Paper 7
- Rogers C.A. (Ed.), 1988; Smart Materials, Structures, and Mathematical Issues; Technomic Publ. Co.
- Rogers C.A., E.F. Crawley and R.O. Claus, 1990; Intelligent Material Systems & Structures (Two-Day Seminar); Technomic Publ. Co.
- Schmidt W. and Chr. Boller, 1992; Smart Structures - A Technology for Next Generation Aircraft; AGARD-CP-531; Paper 1
- Shinya N., M. Egashira and H. Fudouzi, 1994; Powder Particles Assembly Using Electron Beam for Creation of Multi-Functional Materials (manuscript prepared for publication)
- Spangler R.L. Jr. and S.R. Hall, 1989; Piezoelectric Actuators for Helicopter Rotor Control; Report #SSL 1-89, SERC 14-90, MIT Cambridge/USA
- SPIE, 1988 ff.: Proc. of: Fiber Optic Smart Structures and Skins II; The Internat. Soc. for Optical Engineering (SPIE)
- Strehlow H. and H. Rapp, 1992; Smart Materials for Helicopter Rotor Active Control; AGARD CP-531; Paper 5
- Sumali H. and H.H. Cudney, 1994; Electro-Mechanical Analysis of an Active Engine Mount Incorporating Piezoelectric Stack Actuators; AD-Vol. 45/MD-Vol. 54, Adaptive Structures and Composite Materials: Analysis and Application, ASME; pp. 211-218
- Sun F.P. and C.A. Rogers, 1996; Determination of the Electromechanical Conversion Coefficient of a Piezoelectric Stack Actuator under Impulsive Actuation; AIAA-96-1303-CP
- Takagi T. et al., 1989; The Concept of Intelligent Materials and the Guidelines on R&D Promotion; Science and Technology Agency, Tokyo/Japan
- Takeuchi E., S. Matsuoka, K. Miyahara, H. Hirukawa, Y. Ikeda, 1994; Arrest Function of Elevated Temperature Fatigue Crack by Metallic Dispersed Particle of Low Melting Point; Proc. of the 3rd National Intelligent Materials Symposium, pp. 31-33 (in Japanese)
- Tomlinson G.R., 1996; Adaptive Structures Based on Evolutionary Models; this volume
- Tutton P.A. and F.M. Underwood, 1992; Structural Health Monitoring Using Embedded Fibre Optic Sensors; AGARD CP-531, Paper 18
- Varadan V.K. and V.V. Varadan, 1993; Smart Materials, Smart Skins, and Composites for Aerospace Applications; in Proc. of the ECCM Smart Composites Workshop, Bordeaux/F, pp. 17-22
- Varadan V.K. and V.V. Varadan, 1994; Smart Materials, MEMS and Electronics Integration for Aerospace Applications; Proc. of the Internat. Aerospace Symposium (IAS), Nagoya/Japan, pp. 115-123
- Wada B.K. and J.A. Garba, 1992; Advances in Adaptive Structures at Jet Propulsion Laboratory; AGARD-CP-531, Paper 28

CHARACTERISTICS AND PROCESSING OF SMART MATERIALS

Haydn N.G. Wadley

Intelligent Processing of Materials Laboratory
School of Engineering and Applied Science
University of Virginia
Charlottesville, VA 22903

SUMMARY

Smart materials are revolutionary new engineering materials/intelligent structures that sense and respond to their environment. Emerging concepts for mission adaptable wings, helicopter blades and the active suppression of submarine noise are reviewed and used to identify the important basic elements of these intelligent structures. The fundamental principles of the main sensing approaches (based on piezoelectric, fiber optic, luminescent and other phenomena) are described together with the physical principles underlying approaches to actuation (piezoelectric/electrostrictive materials, magnetostriction, shape memory alloys and electrorheological fluids). The best methods for design and processing of affordable smart materials are only beginning to be addressed by researchers; concurrent engineering and intelligent processing of materials concepts will be essential to transition smart materials from the laboratory into applications.

1. Smart Materials and Structures

Smart (or intelligent) materials/structures are revolutionary new structural materials concepts that sense critical aspects of their environment and optimally respond/adapt to them[1]. The field has emerged in the past five years from increasingly intensive research and development activities in Japan, the USA and Europe. To better understand the idea of a smart materials/structures concept, consider three ongoing military application studies aimed at a) improving the performance of a bomber aircraft by the development of a mis-

sion adaptable wing (MAW), b) increasing the speed of attack helicopters by active blade vibration/twist control and c) active suppression of a submarine's acoustic signature.

1.1 Mission Adaptable Wing

Both the lift and the drag of an airfoil (e.g. a wing) are a sensitive function of the wing geometry (characterized by its camber) and the conditions under which it operates (the velocity of airflow over the wing and the ambient gas temperature/pressure). Normally, a fixed wing geometry is used that optimizes the lift/drag for the particular set of flight conditions deemed to be most mission critical, Fig. 1 [2]. For example, a minimum drag camber is used for subsonic, low level penetration of air defenses whereas a maximum lift configuration is used during aggressive maneuvers. Fig. 1 clearly shows that no single wing camber is optimal for all phases of a typical bomber aircraft's mission which involve both penetration and maneuvers.

One solution to this problem is a system of rotary actuators and linkages to hinge a flexible wing and thus change the camber, Fig. 2 [2]. This enables the camber to be adaptively controlled and the entire shaded region of lift-drag relations shown in Fig. 1 to be accessed with the mission adaptable wing. The resulting adaptive control surface can greatly improve maneuverability as shown in Fig. 3 [2]. The role of smart materials here is to replace the heavy slow mechanical system of actuation with smart adaptive panels that can be rapidly flexed over a wide range of angles [3,4]. This reduces weight allowing 30% higher payloads, 50% greater range and 30% increased maneu-

verability. The ability to continuously vary curvature over the airfoil without creating hinge lines also improves stealth performance.

1.2 Smart Helicopter Rotor Blades

There is a great deal of interest in expanding the flight envelope of future military helicopters. Today, this is very much determined by the dynamics of the rotor blades. In particular, the aeromechanical stability of the blades is a sensitive function of the inplane compliance of the blade - especially near the blade neck [5]. Soft inplane rotors give good aeromechanical stability, but the ideal compliance varies with flight conditions and a compromise is used in practice.

Variable camber flight envelope

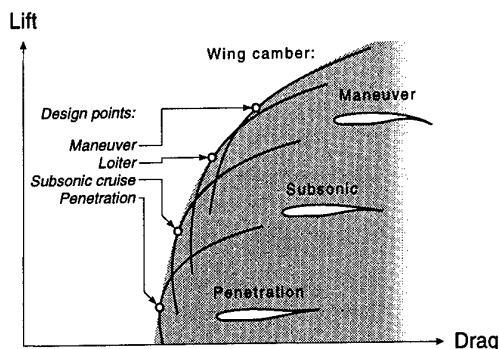


Fig. 1 Lift-drag relations for different wing cambers. By adaptively controlling the wing camber, the entire shaded region is accessible during a mission [2].

In addition, vibration and torsional deformations of the blades limit the airspeed of today's helicopters and contribute to significant fatigue damage requiring frequent overhauls and extensive maintenance [6]. By using smart materials whose effective compliance can be modulated, it will be possible to tune the blade neck stiffness for each flight condition encountered. Furthermore, the use of active patches and twist control "tendons" enables active compensation of vibrations and torsional

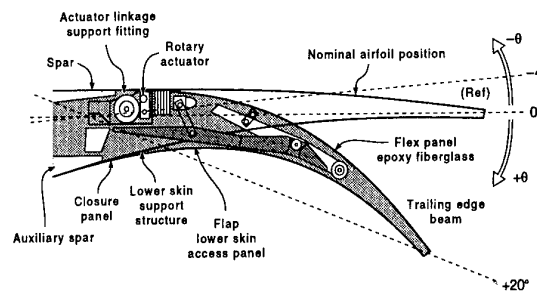


Fig. 2 A mission adaptable wing currently uses a system of mechanical rotary actuators and linkages to change the contour of the trailing edge mechanism of flexible skin wing [2].

Typical maneuver gains

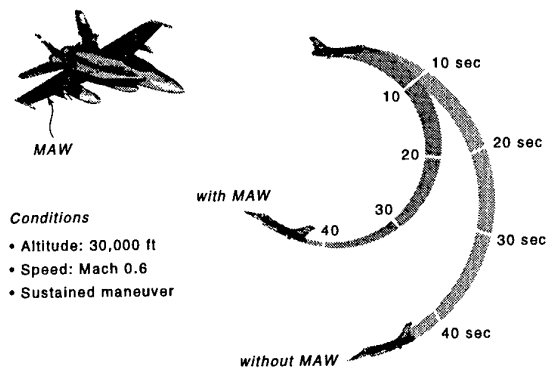


Fig. 3 The performance of maneuvers can be greatly enhanced with a mission adaptable wing [2].

deformations in future helicopter designs, Fig. 4 [3]. While these approaches will reduce noise and vibration, the weight savings from this approach are likely to be small, but could still significantly improve mission range. However, the largest pay-off will come from increased speed (from 160 to 200 knots) and greater maneuverability.

1.3 Active Coatings for Signature Suppression

Even today's most advanced submarines have acoustic signatures that emanate from the propulsion system, internal rotating machinery/

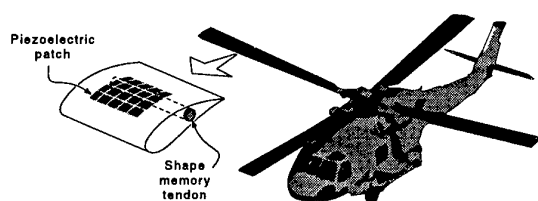
Helicopter blade vibration and twist control

Fig. 4 Adaptive control of blade neck compliance and blade vibration/twist enhances the performance of helicopters enabling 25% increases in maximum speed [3].

pumps and the flow of water over/around the hull. One of the most difficult problems to combat arises from the localized excitation of the acoustic modes of the hull. These couple effectively with the surrounding water and are readily detectable at long range. The role of smart materials here is as an active coating applied after the hull is assembled, Fig. 5 [3]. By embedding acoustic sensors in the coating, it is possible to measure the amplitude and frequency of an acoustic mode in the hull. If acoustic actuators are then built into the coating, it becomes possible to create 180° out-of-phase acoustic signals of an amplitude and frequency that match that of the acoustic mode. This results in destructive interference and a greatly reduced signal radiated into the surrounds.

This "active stealth" approach promises to greatly reduce acoustic signatures by 60dB or more [7]. While the acoustic displacements in this case are small (micrometers), a key feature of this smart materials application is the need for omnidirectional sound suppression across a relatively broad range of frequencies. For this to be accomplished, it is necessary to distribute the active coating widely over the surface of the submarine's hull and to use a coating that is carefully designed to span the range of vibrational frequencies encountered.

These three applications of smart materials/

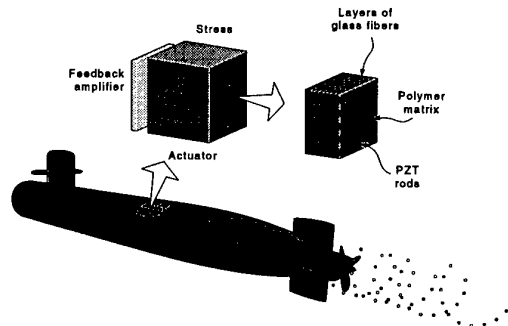
Active coatings for signature suppression

Fig. 5 Active coatings applied to the skin of a submarine sense sound waves emanating from the boat and emit out-of-phase signals which destructively interfere with the emissions. They result in large (60 dB or more) reductions across a wide band of frequencies and provide an active form of stealth [3].

structures embrace the key aspects of many other near-term smart material concepts under study [1,7,8]. Sensors measure the stresses, strains, displacements and temperatures within the components. Control systems recognize these and command signals to actuators that change shapes, elastic compliances and acoustic radiations in order to achieve a predetermined optimal response to the mission environment. It is important to recognize that these applications are our first tentative steps at the development of a potentially powerful new structural materials/structures technology that may eventually pervasively impact society.

2. Components/Processing of Smart Materials and Structures

Smart materials and structures are load carrying components that contain arrays of sensors and actuators embedded in such a way that overall mechanical properties are not adversely affected. The host material is usually a polymer or polymer matrix composite, though in principle, flexible structures built from metals

and ceramics are also possible. In fact, metal and ceramic structures containing embedded sensors that detect damage are already receiving much study for condition monitoring [9].

There would be no smart material without sensors. The last twenty years has witnessed intensive sensor development, and we are now able to draw upon a growing suite of sensor materials that includes piezoelectric and electrostrictive ceramics/polymers [10], embedded fiber optics [11,12] stress dependent luminescent and perhaps magnetic "tag" particles/fibers [13], ultrafast optical switching materials [7], microelectromechanical devices (MEMS) [14,15], solid state millimeter/microwave detectors [16] and sensitive magnetic sensors based on metal multilayers that exhibit giant magnetic resistance [17].

The incorporation of actuators in the material enables a structure to optimally respond to the environment in which it performs. These actuators must therefore "enable" changes of shape, modifications of elastic modulus, increases in damping or the excitation of destructively interfering acoustic signals. Today, we rely upon piezoceramics [18], shape memory alloys [19], electrorheologic fluids [20] and magnetostrictors [20] to accomplish this. These materials are being configured in novel ways to accomplish adaptive changes of smart structures.

These sensors and actuators are easily damaged during the sometimes aggressive conditions encountered during the synthesis of a composite component. It is essential that the temperatures, pressures and chemical environments used during the processing of smart materials are suitable for the synthesis of a composite with acceptable mechanical properties but do not damage its sensitive sensors/actuators. Processing is further complicated by the need to maintain components at optimal locations in the component. This can be a significant driver of cost. One approach to this extends filament winding/tape laying with directed energy heating to synthesize a composite structure layer by layer, Fig. 6 [22].

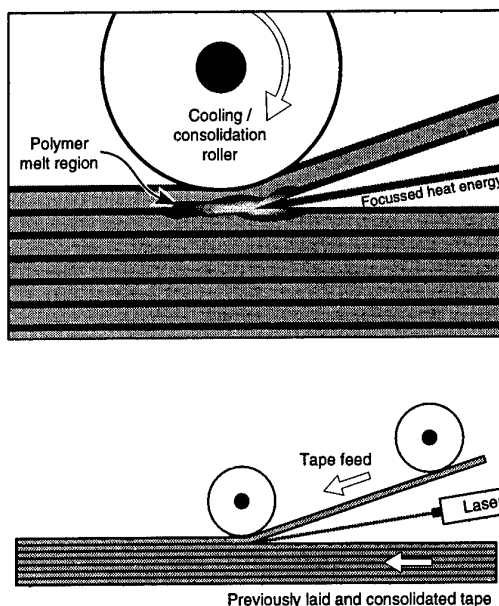


Fig. 6 McDonnell Douglas Aerospace has developed a versatile process for smart materials synthesis. Thermoplastic plies are laser heated and roll consolidated onto previous plies. Sensors/actuators are easily introduced and subjected to only a low temperature pressure transient [22].

A smart material/structure is not just a material containing sensors and actuators. The electrical signals to/from these devices must be routed through the component in a way that does not interfere with its performance, and the entire assembly must be placed under the authority of a closed loop feedback control system. Concurrent engineering design concepts [22], Fig. 7, and intelligent processing of materials [23] strategies for processing are enabling technologies for the affordable manufacturing of smart materials/structures.

3. Fundamentals of Embedded Sensing

A variety of approaches are available for sensing the environment within a smart material. They include the use of piezoelectric ceramics

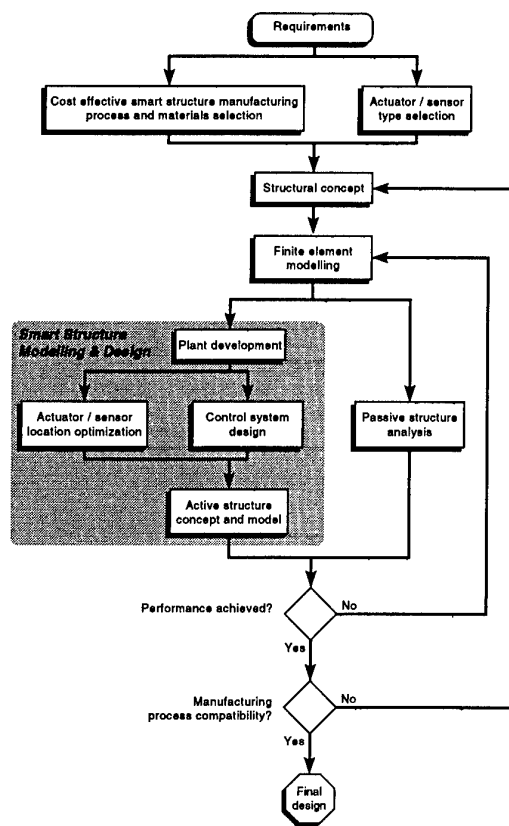


Fig. 7 Smart materials/structures are designed using a concurrent engineering methodology that simultaneously addresses component functionality (performance) and manufacturability [22].

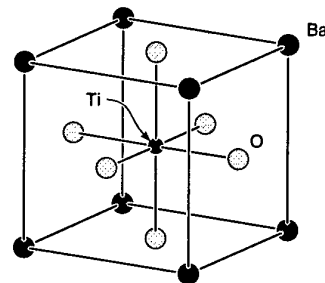
and polymers, electrostrictive materials, embedded fiber optics, luminescent fibers, MEMS sensors and various types of “tag” particles. The principles underlying the use of many of these are briefly reviewed below.

3.1 Piezoelectric Sensors

The application of a stress (or strain) to some materials results in the development of an electric charge on its surface; a phenomenon that is known as the direct piezoelectric effect. It is a property of most non-centrosymmetric structure materials. All crystalline materials belong to one of 32 symmetry point group classes. Twenty-one of these classes have unit cells that

are non-centrosymmetric (i.e. the arrangement of atoms in the unit cell is different after inversion about the unit cells center) and twenty of these exhibit piezoelectric behavior. Piezoelectricity is thus a fairly widespread phenomenon found in many insulating ceramics (e.g. quartz, lead zirconate titanate, barium titanate, lead titanate, etc.), some polymers such as polyvinylidene fluoride (PVF₂) and many semiconductors [24].

As an example, consider the high temperature perovskite crystal structure of barium titanate (BaTiO₃) as shown in Fig. 8 [25]. It is centrosymmetric and is not piezoelectric. However, below about 130°C (its Curie point), the titanium ion (which carries a 4+ charge) shifts in the X₃ direction, resulting in the non-centrosymmetric structure shown schematically in Fig. 9(a) [10]. This form of BaTiO₃ is piezoelectric, and the origin of the phenomenon is easily seen in Fig. 9(b)-(c). For example when a stress σ_3 (in Voigt notation) is applied, the crystal is elongated in the X₃ direction, the 4+ charge on the titanium ion moves further upwards from the center of the cell, a positive charge appears on the upper crystal surface and a negative one is seen on the bottom surface.



Perovskite structure (idealized)

Fig. 8 The high temperature ($T > 130^\circ\text{C}$) structure of BaTiO₃. It has a centrosymmetric structure and is not piezoelectric [25].

The strength of the piezoelectric effect can be quantified using a piezoelectric modulus (or piezoelectric strain coefficient), d , defined by

$$\Delta P = d\sigma$$

Where ΔP is polarization charge (coulomb) per unit area (m^2) and σ is the stress (Nm^{-2}). Thus the units of d are CN^{-1} . Since the polarization is a vector and stress is a second rank tensor, d is a third rank tensor. In voight notation, it can be written as a matrix with components d_{ij} where i is the direction of polarization and j is the stress direction (see Fig. 9).

If a piezoelectric crystal is attached to, or embedded within, a smart material, any mechanical stress (static or dynamic) introduced into the crystal causes a polarization to develop. This can be sensed by monitoring the resulting voltage that is developed across the crystal. It is related to the electric field, E , developed across the crystal, and so a figure of merit for a piezoelectric stress (or strain) sensor is the piezoelectric voltage coefficient tensor, g , (units of VmN^{-1}) given by

$$g = \frac{d}{\epsilon\epsilon_0} = \frac{E}{\sigma}$$

where ϵ_0 is the free space permittivity ($8.85 \times 10^{-12} \text{Fm}^{-1}$) and ϵ is the dimensionless dielectric constant (the dielectric susceptibility divided by the free space permittivity). Tensor component values for some commonly used

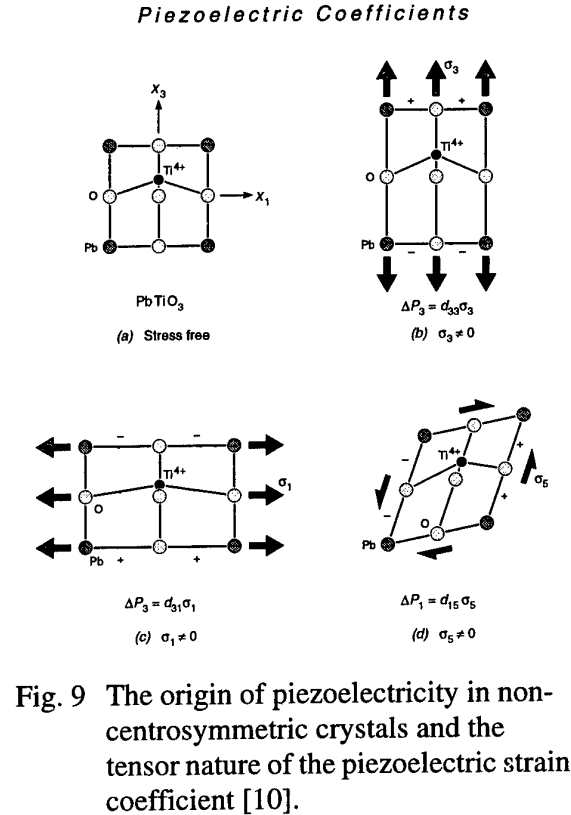


Fig. 9 The origin of piezoelectricity in non-centrosymmetric crystals and the tensor nature of the piezoelectric strain coefficient [10].

piezoelectric materials are given in Table 1 [26].

Many of the best piezoelectric materials are polycrystalline. They are synthesized by con-

Table 1: Piezoelectric and Relative Permittivity Constants for Selected Piezoelectric Materials [26].

Material System	Piezoelectric Strain Constants ($\times 10^{-12} \text{C/N}$)			Relative Permittivity(ϵ)	
	d_{33}	d_{31}	d_{15}	ϵ_{33}	ϵ_{11}
Barium Titanate	d_{33}	d_{31}	d_{15}	ϵ_{33}	ϵ_{11}
Barium Titanate*	37	-34.5	392	168	2920
Lead Zirconate Titanate* (PZT-2)	152	-60	440	450	990
Lead Zirconate Titanate (PZT-5H)	593	-274	741	3400	3130
Lithium Niobate	6	-1	68	30	84

*Uniaxially poled polycrystalline material.

solidating and then sintering ceramic powders [24]. Usually, this results in no overall piezoelectric effect because the polarization vectors of individual grains are random. However, by cooling these materials through their Curie points under a strong uniaxial electric field, the polarizations of each domain can be lined up, creating large values of the piezoelectric constant, Fig. 10, and enabling the sensitive detection of transient stresses associated with elastic wave propagation/vibration of structures. Because the poling effect only disappears upon reheating a polycrystalline piezoelectric ceramic above its Curie point, these materials can also be used for some elevated temperature applications (e.g. up to about 300°C for PZT-5H). Higher temperatures are achievable with single crystal materials. For example, lithium niobate (LiNbO_3) can be used up to 600°C in reducing environments and at much higher temperatures in the presence of small oxygen partial pressures (its Curie point is 1138°C).

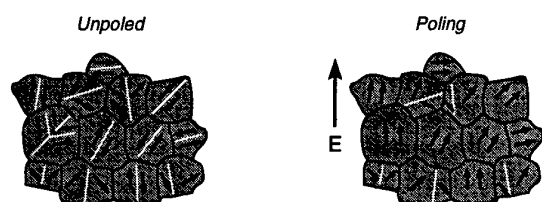


Fig. 10 Cooling a polycrystalline piezoceramic in a strong uniaxial field results in an overall piezoelectric effect.

The piezoelectric sensors are used to convert transient mechanical stresses to voltages that can be amplified and used to monitor the vibrations of a structure. It is important to realize that the signal from these devices may not faithfully replicate the amplitude of the transient stresses in the structure. This arises because the transducers themselves are finite dimensional structures and so exhibit elastic resonances of their own. The sensitivity of the transducers is a maximum near these resonances and are governed by the geometry of the sensor. Since the basic process of transduc-

tion involves the propagation of transient elastic stresses from the structure (or its environment) into the piezoelectric sensor element itself, a second design criterion is minimization of elastic wave reflections at the sensor's surface. These increase as the difference in the acoustic impedances (the product of density and acoustic velocity) of the sensor/surroundings increases. The acoustic impedance of a typical piezoceramic sensor, $Z_s = 30 \times 10^6 \text{ Kg m}^{-2} \text{ s}^{-1}$, while that of say water is $1.5 \times 10^6 \text{ Kg m}^{-2} \text{ s}^{-1}$. Polymer transducers such as polyvinylidene fluoride (PVF_2) have $Z_s = 3.22 \times 10^6 \text{ Kg m}^{-2} \text{ s}^{-1}$, and are much better matched to water, but they are less sensitive than PZT. One solution is to use composite transducers made up of arrays of ceramic sensors embedded in a low acoustic impedance polymer, Fig. 11 [26].

Composite Transducer

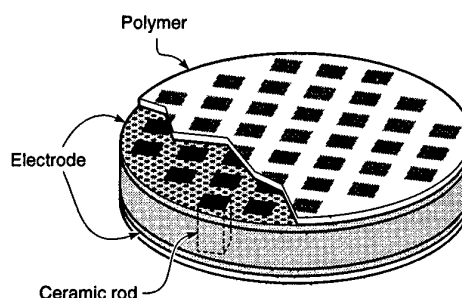


Fig. 11 Example of a composite transducer in which PZT rods/disk sensor elements are distributed in a polymer matrix [29].

3.2 Fiber-Optic Sensors

The emergence of optical fiber communications technologies in the 1970's has enabled the development of embedded optical sensors for process condition monitoring and for smart materials/structures applications [27]. Most concepts have addressed the measurement of strain. Strain affects the refractive index (i.e. the optical velocity) of the fiber [28] and

changes the fiber's dimensions. Several techniques have been developed to exploit both of these effects [29], and many applications are underway using commercially available sensors [30,31].

The simplest case to consider is the two fiber Michelson interferometric fiber optic sensor shown in Fig. 12 [29]. In this approach a coherent laser signal is optically propagated along two fibers of differing lengths. The ends of each optical fiber are silvered to ensure almost complete reflection of the signal back to a photodetector. The two signals travel different distances and so their individual signals are out of phase resulting in interference. If a strain is now applied to the body in which the fiber ends are embedded, the extra change in length and the strain induced refractive index change of the longer fiber results in a change in the degree of interference which is registered as a voltage change from the photodetector that is related to the strain.

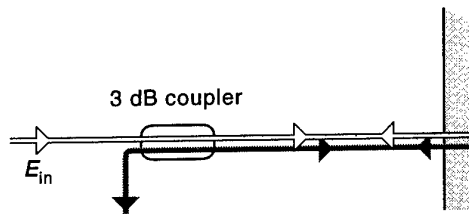


Fig. 12 A Michelson interferometric fiber optic sensor for measuring strain.

While this type of sensor has been successfully used in laboratory settings for measuring acoustic emission [31], it is not well suited to smart structural applications because it requires the embedding of a pair of sensors which can seriously weaken a structure, its common mode rejection is weak (both fibers may "see" the strain field and so cancel the differential response) and it is quite noise sensitive. The latter issue can be very serious in some applications because if one arm of the interferometer experiences a significant disturbance, the photodetector signal changes and the strain sensitivity changes. As a result, com-

mercially available sensors are based upon one of four different approaches: Fabry-Perot cavities, two mode fibers, polarimetric sensors and intracore Bragg gratings.

The Fabry-Perot approach is very simple yet sensitive and can be designed as a single-ended device or as part of a continuous fiber, Fig. 13. In either case, a coherent optical signal is reflected from two reflectors and the reflections are combined at a detector. Path length differences result in interference at the detector and an output signal that is a function of the spacing and refractive index between the reflectors. Multiple reflections in the cavity then result in a sensor with very high strain sensitivity.

Fabry-Perot fiber optic sensor configurations

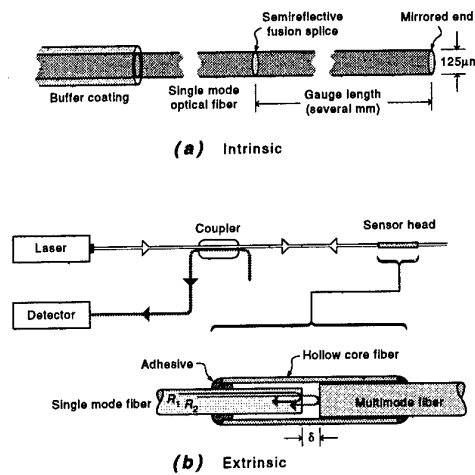


Fig. 13 Fabry-Perot fiber optic strain sensors use multiple reflections between pairs of reflectors to create an interference signal that depends linearly upon axial strain [32].

Suppose a Fabry-Perot sensor is embedded in a body to which a load is applied in the fiber direction. This results in a uniaxial stress, σ_z , in the fiber direction. If the fiber does not perturb the stress field of the body, and Hooke's law is obeyed, the uniaxial strain in the body, $\epsilon_z = \sigma_z / E$ where E is the body's Young's mod-

ulus (Pa). For a well bonded fiber, the matrix and fiber axial strains are the same for axial loading of the body, and so the phase change is given by

$$\Delta\phi = Sl\epsilon_z$$

where l is the gauge length and S is a phase-strain sensitivity index. For the "extrinsic" type of sensor in Fig. 13(b) (of the Michelson type),

$$S = kn \left[1 - \frac{n^2 P_e}{2} \right]$$

where k = the free space propagation constant, n is the refractive index of the fiber core and P_e is an effective strain optic coefficient. For isotropic materials, P_{11} and P_{12} are the only two independent strain optic coefficients [33] and it can be shown that

$$P_e = [P_{12} - \nu(P_{11(12)} + P_{12})]$$

where ν is the Poissons ratio of the fiber.

This simple theory predicts a linear relationship between phase change and axial fiber strain. It even gives a good estimate (within 5%) for ϵ_z when the loads are axial. However, for a general loading, the fiber does perturb the strain field of the host and a more complicated analysis is needed [12]. The detector voltage is also a nonlinear function of the phase difference so this sensor's output is a nonlinear function of strain.

The interferometric sensor can be improved by using an e-core two-mode fiber in the gauge section to maintain the optical polarizations (and so avoid polarization fading). These elliptical cored fibers [34] change the transverse spatial mode distribution of light within the sensor. The basic idea [29] is to propagate a lowest order transverse mode in the lead-in fiber and then transmit this into a short section of e-core optical fiber that allows two transverse optical modes to propagate at the wavelength of the single lead-in fiber mode. This can be accomplished with simple fusion splicing. Polarimetric sensors use the change of polarization of light travelling in a high birefri-

gence fiber to sense strain [32]. They require quadrature detection, special demodulation schemes, and are, as yet not very practical.

The intracore Bragg grating fiber optic sensor approach shown in Fig. 14 is much more attractive for smart structures and is widely used [32,35]. These sensors use a periodic grating that modulates the refractive index of the fiber core. The back reflected spectrum has a sharp peak whose wavelength, λ_B , is given by

$$\lambda_B = 2n\Gamma$$

where n is the core's effective refractive index and Γ is the modulation length. Strain in the axial direction changes Γ and n and so shifts the peak position. Measures [36] has shown that the peak shift for a particular linearly polarized mode is given by

$$\Delta\lambda = \lambda_B [1 - P_e] \epsilon_z$$

where λ_B and P_e are for the Bragg wavelength and effective strain optic tensor for the polarization mode of observation. The output of this sensor ($\Delta\lambda$) is thus a linear function of the strain, though again, the effects of a general state of stress will complicate analysis.

These fiber optic sensors respond to both strain and temperature. The latter is usually unknown in a smart materials application and is thus a potential source of error. One method for dealing with this is to use a second fiber to monitor temperature only (i.e. by decoupling) it from the strain field. This can be simply achieved by inserting the sensing end of a fiber in a hollow capillary prior to embedding in the host (see Measures et al [32] for further discussion).

3.3 Luminescent Fibers

Several techniques have been developed for measuring stress using the luminescence of Cr^{3+} ions in $\alpha\text{-Al}_2\text{O}_3$ [13,37]. The approach is based upon the quite strong stress dependence of the R1 and R2 emission frequencies from chromium-doped alumina. The level of Cr^{3+} doping can be quite small and most commercial grades of alumina contain more than

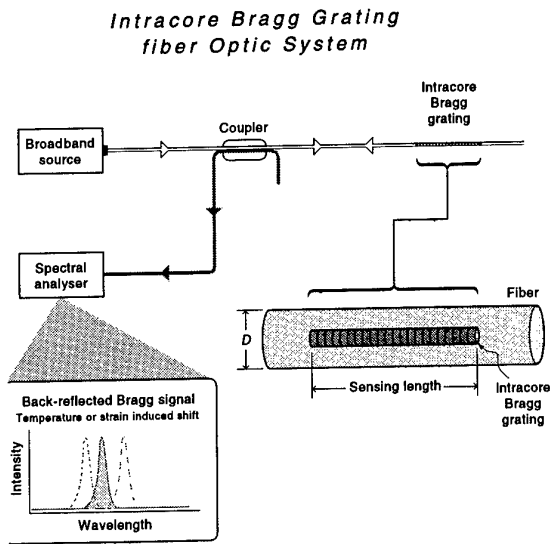


Fig. 14 The Intracore Bragg Grating fiber optic sensor uses a shift of Bragg frequency to sense strain.

enough chromium for this sensor application. The recent development of techniques for synthesizing single crystal alumina fiber with moderately good optical propagation characteristics now enables sensors to be embedded in composites (even metal and ceramic matrix composites processed at 1000°C and above) and their internal strains sensed.

Luminescence arises from the radiative decay

(emission of a photon) from an excited electronic state. The conditions for luminescent emission are rather stringent and only a relatively small percentage of molecules luminesce. In the case of Cr^{3+} embedded in the $\alpha\text{-Al}_2\text{O}_3$ lattice decay occurs from two crystal field split excited states resulting in two emission peaks with wavelengths of about 693 and 694 nm. The positions of both peaks are a function of stress. When the c-axis of the alumina crystal is aligned with the σ_3 principal stress, the line shifts $\Delta\nu$ are given by

$$\Delta\nu = \Pi_{11}(\sigma_{11} + \sigma_{22}) + \Pi_{33}\sigma_3$$

where for the R1 line, the piezospectroscopic coefficients, Π_{11} and Π_{33} have values of 3.0 and $1.8 \text{ cm}^{-1}/\text{GPa}$ respectively. Thus, the peak shifts are linearly related to stress, and are sufficiently large to be measurable using a spectrometer with a fine spacing grating. The approach is being used to interrogate residual stress fields in composites and has been used in the laboratory to measure stresses induced by applied loads. When alumina powder is dispersed as tag in a suitably transparent matrix, the technique could also be used to observe stress distributions in structures under load provided the matrix is optically transparent.

Table 2: A comparison of actuators for smart materials.

	PZT G-1195	PVDF	PMN	TERFENOL DZ	NITINOL
Actuation Mechanism	Piezoceramic	Piezo Film	Electrostrictor	Magnetostrictor	Shape Memory Alloy
Max Strain ($\times 10^{-6}$)	1000	700	1000	2000	20000
Young's Modulus	9	0.3	17	7	{4(m) 13(a)}
Bandwidth	high	high	high	moderate	low

(m) = martensite (a) = austenite

4. Actuators

The actuators in a smart material/structure provide the mechanism for the structure to adapt to its surroundings by suppressing vibrations or changing the structure's shape. In the future, one might imagine that more sophisticated needs will emerge (e.g. self healing of damage, active dielectric property control, local thermal control, etc.). However, even current needs are challenging since they require actuation authority over a broad bandwidth spectrum (from a few Hz for MAW's to hundreds of kHz for active vibration suppression) and over a wide range of displacement amplitudes (e.g. from tenths of micrometers for vibration control to millimeters/centimeters for a MAW application). A variety of approaches are available/emerging including piezoelectrics/electrostrictors, magnetostrictive devices, shape memory alloys and electrorheological fluids (see Table 2 for a comparison of their capabilities).

4.1 Piezoelectric/Electrostrictive Actuators

Piezoelectric materials not only develop a polarization when subjected to a strain, they deform when an electric field is applied. The sign of the displacement is determined by the polarity of the field. This converse piezoelectric effect can be used to transmit acoustic signals and to suppress structural vibrations. If a strong electric field is applied (or weaker fields if the temperature just above the Curie point), the ferroelectric domains lose their poled alignment and become aligned with the new field. This domain flipping gives rise to a strain that then depends only on the magnitude of the electric field (and not on its polarity as with piezoelectricity) and is known as electrostriction [25].

Typical (polycrystalline) piezoelectric ceramics like PZT are able to generate strains of 0.1-0.2% (at about 10kV/cm) before the applied voltage reaches the threshold for dielectric breakdown. However, these large fields can change the poling and lead to a form of piezoelectric fatigue so that the strain obtained

reduces with the number of electric field cycles. Electrostrictive materials such as lead magnesium niobate (PMN) are able to achieve similar strains but show no effect of cycling [10]. The magnitude of both the piezoelectric and electrostrictive contributions to deformation are a function of the ceramics' microstructure - the largest deformations are almost always obtained from single crystal materials, and are motivating research aimed at affordable methods for their synthesis.

The Sonofanel™ concept is a recent example of a piezoelectric smart material application [38]. These panels are used in underwater applications for active surface control. They are based upon a two dimensional array of axially poled PZT cylinders, Fig. 11. The array is fabricated using low cost injection molding, Fig. 15. This is followed by firing in air to both burn out the organic binder and to sinter the ceramic powders. The sintered preforms are then poled by cooling through the Curie point in an axial electric field. The region between the piezoelectric rods is subsequently filled with a castable polymer polyurethane that may contain up to 40% hollow polymer microspheres to increase elastic compliance and reduce density. Both surfaces are then ground flat to expose the piezoelectric rod ends. PZT piezoelectric accelerometers (sensors) are introduced and the assembly is bonded to glass-reinforced polymer (GRP) face sheets using a conducting epoxy. Shielding (to avoid cross talk) is also added prior to a final encapsulation in polyurethane, Fig. 16 [38].

Piezoelectric actuators can also be used to control vibrations in say helicopter rotors. These applications require the actuator to counteract the different modes of bending/torsion for a beam-like structure. This can be accomplished using pairs of piezoelectric sheets bonded to either side of a beam, Fig. 17.

4.2 Magnetostrictive Actuators

When most solids are placed in a magnetic field, they change their length[39]. For many materials the effect is very small, but for ferromagnetic materials below their Curie points,

Piezocomposite Transducer Preform Injection Molding

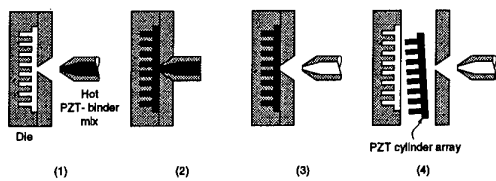


Fig. 15 A schematic diagram showing the injection molding process used for low cost manufacturing of ceramic cylinder array. (1) Hot powder-binder mixture in a nozzle. (2) Injection of mix into die. (3) Mix cools to form a solid (green) part. (4) Net-shape array is ejected [38].

Smart Panel™ with Integrated Accelerometer

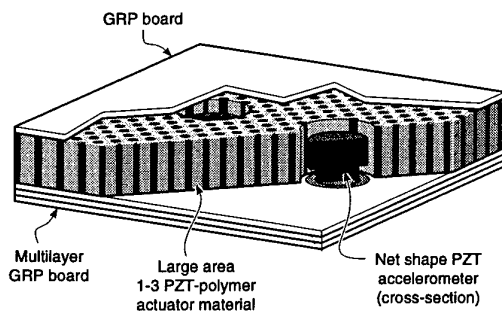


Fig. 16 Schematic cut-away view of a 0.1mx0.1m Sonofanel™ smart panel showing integrated velocity sensors (accelerometers) and the piezoelectric actuator array [38].

larger magnetostrictive strains of $\sim 10^{-3}\%$ are possible, and in a few of the rare earth systems, strains of more than 0.1% can be achieved[21]. The atomic origin of the phenomenon arises from spin-orbit coupling of the outer electrons. The effect is shown (in greatly exaggerated

Bending of Bars using Piezoceramic Materials

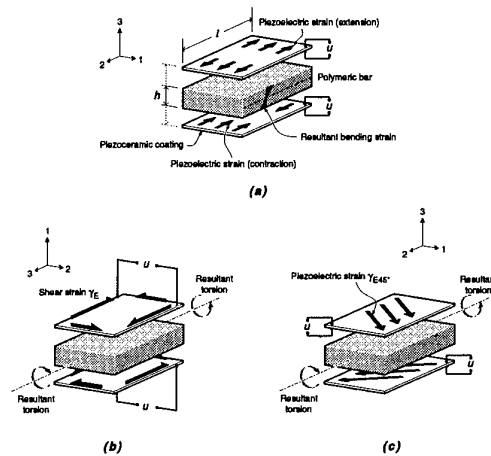


Fig. 17 Bending (a) and torsion (b and c) of a rectangular cross-section beam can be controlled with piezoelectric uniaxial/shear strain layers bonded to either side of the beam [5].

form) in Fig. 18 [39].

At a more macroscopic level, magnetostriction is associated with the field-induced movement of magnetic domain walls, Fig. 19. These domain walls are defined by the angle between the magnetization vectors of adjacent domains on either side of the wall. Two types exist: 180° walls and non- 180° walls (usually called 90° walls for simplicity). In Fig. 19, as in most polycrystalline ferromagnetics, both types exist. The movement of 180° walls reverses the direction of magnetization and does not cause a length change (see Fig. 18) and so magnetostriction arises from the motion of the 90° boundaries.

The largest ($\sim 1\%$) magnetostrictions are observed in hexagonal rare earth compounds containing Tb and Dy which have very anisotropic 4f electron distributions. However, their Curie temperatures are too low ($T_c < 240\text{K}$) for most smart materials/structures applications. In the last twenty years or so TbFe₂ (terfenol) and SmFe₂ (samfenol) Laves phase compounds have been synthesized with magneto-

Magnetostriction

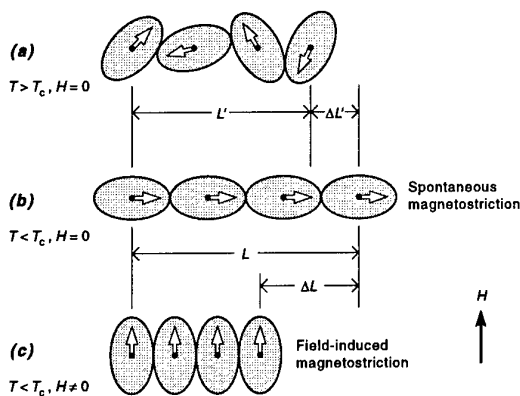


Fig. 18 A row of four atoms is shown together with their magnetic moments. Above the Curie temperature (T_c), the moments are randomly oriented and the material is paramagnetic. Below T_c the moments spontaneously align because of spin-spin coupling and a "spontaneous" magnetostriction occurs even when the magnetic field intensity, H , is zero. Applying a magnetic field perpendicular to this spontaneous alignment realigns the moments and results in a field-induced magnetostriction [39].

strictions as high as 0.36% at ambient temperature [21]. The magnetic field intensities required for these large magnetostrictions are relatively small and can be easily achieved by encircling a bar of say terfenol with a small solenoid. Thus, a prototypical magnetostrictive actuator consists of a rod of magnetostrictive material, a coaxial solenoid and a plunger housed in rigid body, Fig. 20 [40]. Since these devices have high inductances, they are best operated at frequencies below a few kHz. A Northrop Grumman, magnetostrictive-based actuator system is being evaluated for mission adaptable wing applications [41].

Iron Crystal Magnetostriction

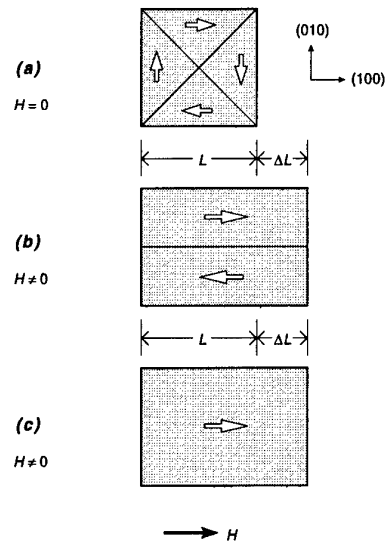


Fig. 19 Magnetostriction of a cubic ferromagnetic occurs by the movement of 90° domain walls.

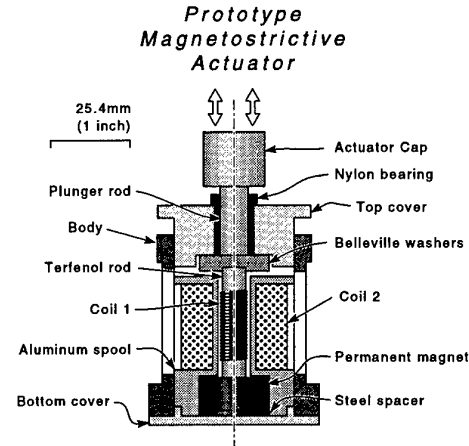


Fig. 20 A prototypical magnetostrictive actuator [40].

4.3 Shape Memory Alloys

When high forces or large displacements are required in a smart materials application (e.g. to change the camber of a mission adaptable wing), designers are increasingly making use

Table 3: Material Systems that exhibit the shape memory effect [42].

Alloy	Composition	M_s ($^{\circ}\text{C}$)	Transformation Temperature Hysteresis ($^{\circ}\text{C}$)	Ordered or Disordered	Volume Change
AgCd	44~49at.%Cd	-190~-50	~15	ordered	-0.16
AuCd	46.5~50at.%Cd	30~100	~15	ordered	-0.41
CuAlNi	14~14.5wt.%Al 3~4.5wt.%Ni	-140~100	~35	ordered	-0.30
CuAuZn	23~28at.%Au 45~47at.%Zn	-190~40	~6	ordered	-0.25
CuSn	~15at.%Sn	-120~30		ordered	
CuZn	38.5~41.5wt.%Zn	-180~-10	~10	ordered	-0.5
CuZnX (X=Si,Sn,Al,Ga)	few wt.% x	-180~100	~10	ordered	
InTl	18~12at.%Tl	60~100	~4	disordered	-0.2
NiAl	36~38at.%Al	-180~100	~10	ordered	-0.42
TiNi	49~51at.%Ni	-50~100	~30	ordered	-0.34
FePt	~25at.%Pt	~-130	~4	ordered	0.8~-0.5
FePd	~30at.%Pd	~-100		disordered	
MnCu	5~35at.%Cu	-250~180	~15	disordered	

of shape memory alloys (SMA's). The shape memory phenomenon is the ability of a material to remember its original shape either after suffering a mechanical deformation (the so-called one-way effect) or upon heating/cooling (the two-way effect) [42]. This remarkable phenomenon is exhibited by several materials that undergo thermoelastic martensitic transformations, Table 3. Today, materials based upon equiatomic NiTi alloys (Nitinol) are being extensively studied for a variety of applications [43].

Hornbogen has developed a scheme to simply show the various constitutive behaviors that can be encountered with a shape memory alloy. Fig. 21 shows the typical (normal) behavior found in many single phase materials: linear elasticity up to the yield strength (σ_{yp}) of the β -phase. The material also exhibits normal thermal expansion/contraction strains on heating/cooling. This behavior is found in all SMA's when they are used at a temperature

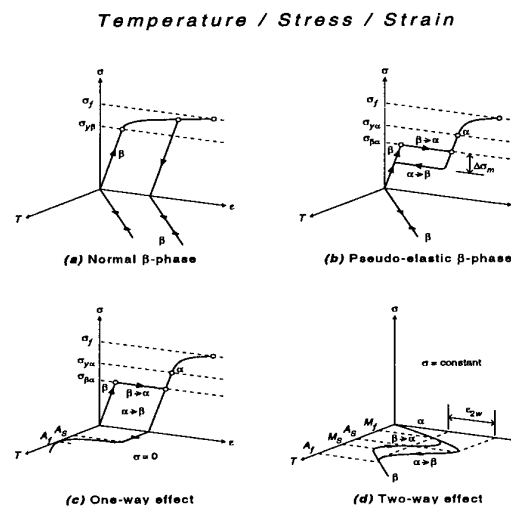


Fig. 21 The various types of constitutive response exhibited by a SMA that exhibits a $\beta \rightarrow \alpha$ martensitic transformation on cooling.

well above that where the martensitic transformation occurs. As the temperature is lowered (but still above the martensitic start, M_s , temperature) a stress can induce a transformation of the β -phase to the martensitic (α phase) at a stress $\sigma_{\beta\alpha}$. This gives a large strain increment which is recovered upon unloading as the α -phase retransforms back to β . The thermal strains are still "normal" in this test temperature region. If the test temperature is reduced further, Fig. 21(c), the reverse transformation does not occur on unloading and a permanent strain (ϵ_{1w}) remains. This can be removed (and the material returns to its original shape) upon heating and is the origin of the one-way shape memory effect. Thus, material in the form of say a spring (made by annealing a wire in die at $T \gg$ the austenite finish temperature, A_f) in the β -phase condition can be loaded (to a stress as high as $\sigma_{y\alpha}$) and it will inelastically deform an amount ϵ_{1w} . The original spring length is then returned upon heating (with an electric current perhaps). Since $\sigma_{y\alpha}$ can be quite high ($\sim 500\text{MPa}$), large stresses and big strains can be achieved via this effect. The two-way effect, Fig. 21(d), is very useful because it allows a large strain (up to 6%) to be repeatedly exerted by just heating or cooling the alloy through the $\beta \rightarrow \alpha$ and $\alpha \rightarrow \beta$ temperature region. This can be done (by a training procedure) so that the body returns to an original shape after each thermal cycle.

We have not addressed the issue of how a SMA is able to perform in such an unusual way. The reason lies in the mechanism by which the change of shape is achieved. We usually think that dislocations are responsible for inelastic deformations in malleable metals. Because of dislocation tangling, their deformations are usually not recoverable (beyond a very small amount associated with the Bauschinger effect). In SMA's, the deformation is achieved by a martensitic transformation. Fig. 22 shows how this can be achieved for the pseudoelastic and one-way effect cases of Fig. 21(b) and (c).

The two-way effect is a little more complicated and is based on the existence of many slightly different martensitic variants. The application

Lattice Correspondence

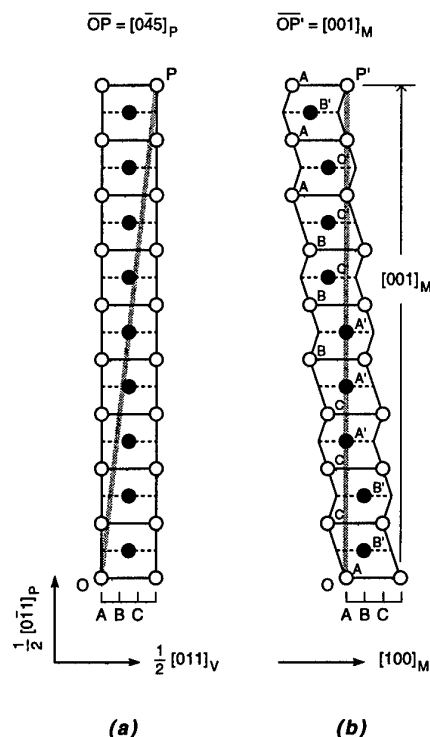


Fig. 22 A martensitically transformed structure results in an overall shape change. Reversing the transformation restores the original shape.

of a load to a pre-existing martensite can result in twinning/stacking fault formation and the creation of a different martensite variant, Fig. 23. By repeatedly deforming (training) the material, defects are introduced and retained in the structure. These predispose the selection of variants and result in a repeatable change of shape upon thermal cycling through the $\alpha \rightarrow \beta \rightarrow \alpha$ transformations.

SMA actuators can be designed using either the one- or two-way effect. Two-way (push-pull) behavior can be achieved with a one-way alloy behavior by using a "bias" force technique. For example, a two-way actuator using a spring to provide a bias is shown in Fig. 24. These materials are beginning to be introduced

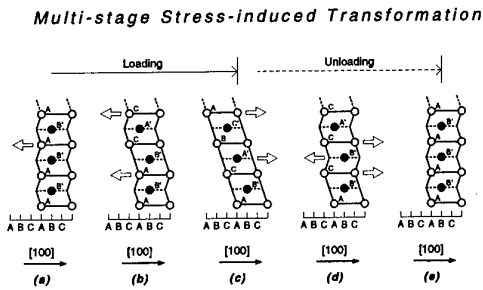


Fig. 23 In the two-way effect a training procedure is used to select the martensitic variants that give a desired shape change.

into MEMS devices creating a whole new range of future smart materials uses. Regardless of which type of SMA effect is used, these materials suffer fatigue degradation during prolonged use - especially when the loads are high. Furthermore, many processing operations can introduce undesirable microstructure changes and large residual stresses, and so the incorporation of these materials into a structure can be challenging.

Bias-type Two-way Shape Memory Component

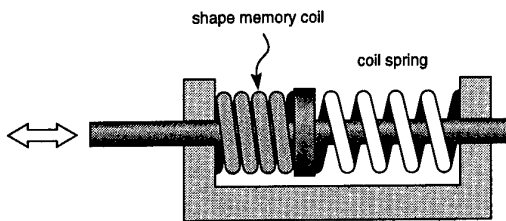


Fig. 24 A two-way actuator can be built using the one-way SMA effect and a simple spring.

4.4 Electrorheological Fluids

Electrorheological (ER) fluids are materials whose rheological properties (i.e. apparent viscosity) can be changed by the application of an electric field [20, 44, 45]. Fig. 25 shows an example of this for a typical ER fluid. We see

that the viscosity, η , (defined as the change in stress per change in shear strain rate, $\dot{\gamma}$) changes only slightly when an electric field is applied; what really changes is the shear stress τ_y needed to initiate flow. To a reasonable approximation a Bingham model describes the shear flow stress:

$$\tau_y = \tau(E) + \eta \dot{\gamma}$$

where $\tau(E)$ is an electric field (E) dependent flow stress obtained as $\dot{\gamma} \rightarrow 0$. ER fluids consist of a liquid dielectric (e.g. oil), polarizable particles (e.g. cornstarch) and an activator such as water. In a no field state, the particles are randomly distributed and the viscosity is governed by Newtonian flow around the particles. However, when a field is applied, the particles line up along field lines creating a more rigid structure that better resists shear.

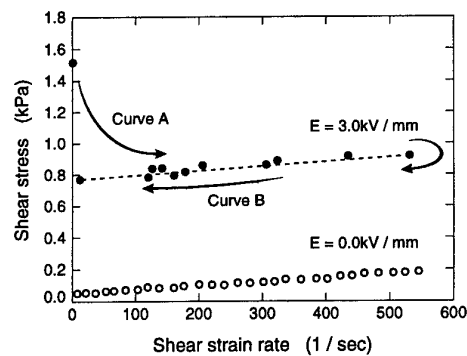


Fig. 25 Shear stress versus strain rate for an ER fluid with and without an electric field. The shear stress to initiate a shear strain is a strong function of the electric field.

General Atomics has recently developed a novel "smart material" by combining an electrorheological fluid with a very compliant elastomer to create an electro-active elastomeric structure (EAES) [46]. This avoids the need for fluid seals and results in a bulk material that can be applied as coating. By integrating acoustic sensors and electrodes into the material, it is possible to sense incoming acoustic signals in a marine environment and to then modify the elastic/damping characteristics of

the coating (using the ER effect) with millisecond time response.

Fig. 26 shows a schematic diagram of the General Atomics EAES smart material concept. It is composed of a soft silicone elastomer with an open cell structure. The cells are filled with an ER fluid consisting of polydimethyl siloxane silicone oil terminated with nonreactive CH_3 groups, polarizable particles (cornstarch) and water. Normally the EAES is soft (elastic modulus ~ 3500 Pa), but when an electric field is applied, the polarizable particles line up and the structure stiffens considerably. By varying the volume fractions of the constituents and the cell morphology of the elastomer, the properties of this material can be widely varied and tailored to suit specific applications, e.g. to control flow noise in hydroacoustic environments or acoustic isolation of hull mounted sonar systems.

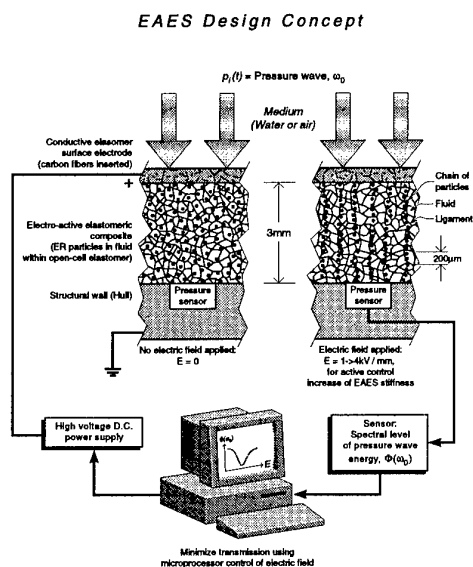


Fig. 26 A schematic diagram of the General Atomics EAES smart material concept [46].

5. Conclusions

This lecture has sought to introduce some of the emerging applications of smart materials and structures. The important concepts under-

lying these revolutionary new materials (sensing, recognizing and responding to the environment) have been reviewed. The need has been emphasized for sophisticated (concurrent) design and affordable synthesis/processing methodologies to enable these emerging materials concepts to become cost effective solutions to engineering problems.

Acknowledgments

I am grateful to Dr. Robert Crowe of the U.S. Defense Advanced Research Projects Agency for very helpful discussions about ongoing programs in smart materials and structures.

References

1. Steven Ashley, Mechanical Engineering, November, 1995, p. 76.
2. Ronald W. DeCamp, Richard Hardy and Douglas K. Gould, SAE International Pacific Air and Space Technology Conference, Melbourne, Australia, Nov. 13-17, 1987.
3. R. Crowe, Private Communication.
4. Advanced Materials and Processes, 9, 1995, p. 9.
5. H. Strehlow and H. Rapp, "Smart Structures for Aircraft and Spacecraft", AGARD Conference Proceedings 531, 1993, p. 5-1.
6. F.K. Straub and R.J. King, "SPIE Symposium on Smart Structures and Materials", San Diego, February 26-29, 1996.
7. A. Crowson, "Recent Advances in Adaptive and Sensory Materials and their Applications, Ed. C.A. Rogers and R.C. Rogers, Technomic Publishing Co. (Lancaster, PA), 1992, p. 811.
8. W. Schmidt and C. Boller, "Smart Structures for Aircraft and Spacecraft", AGARD Conference Proceedings 531, 1993, p. 1-1.
9. C. Boller and R. Dilger, "Smart Structures for Aircraft and Spacecraft", AGARD Conference Proceedings 531, 1993, p. 171.
10. L.E. Cross, "Smart Structures for Aircraft and Spacecraft", AGARD Conference Proceedings 531, 1993, p. 16-1.
11. T. Sato, H. Ishikawa and O. Ikeda,

- Applied Optics, 21(20), 1982, p. 3664.
12. J.S. Sirkis and H.W. Haslach, *Intell. Mater. Syst. and Struct.*, 2(1), 1991, p. 3.
13. H. Hough, J. Demas, T.O. Williams, H.N.G. Wadley, "Luminescence Sensing of Stress in Ti/Al₂O₃ Fiber Reinforced Composites", *Acta Metall. Mater.*, 43 (2), 1995, p. 821.
14. J. Bryzek, K. Petersen and W. McCulley, *IEEE Spectrum*, May, 1994, p. 20.
15. T. Honda, *Proc., IEEE Workshop on Micro-Electro-Mechanical Systems*, Oiso, Japan, Jan. 24-25, 1994.
16. A. Roberts and R.C. Compton, *Int. J. of Infrared and Millimeter Waves*, 11(2), 1990, p. 165.
17. E. Pennisi, *Science News*, 142, 1992, p. 140.
18. S.J. Cheng, D.C. Timm, Y. Lu, N. Shaikh and N.J. Ianno, *J. Int. Mater. Struct.* 6(3), 1995, p. 436.
19. D. Treppman, E. Hornbogen and D. Wurzel, *J. de Physique IV*, 5, 1995, p. C8-569.
20. K.D. Weiss, J.P. Coultier and J. Carlson, *Recent Advances in Adaptive and Sensor Materials and their Applications*, Ed. C.A. Rogers and R.C. Rogers, Technomic (Lancaster, PA), 1992, p. 605.
21. A.E. Clark, *ibid*, p. 387.
22. P.F. Lichtenwainer, *J. Mater. Eng. and Performance*, 2(5), 1993, p. 687.
23. H.N.G. Wadley, "Intelligent Processing of High Performance Materials", *Proc., 41st Sagamore Conference*, Eds. W.N. Roy, S. M. Walsh, Plymouth, MA, 1995, p. 57.
24. G.H. Hoertling, "Ceramic Materials for Electronics", Ed. R.C. Buchanan, Marcel Dekker (NY), 1986, p. 139.
25. B. Jaffe, W. Cook and H. Jaffe, "Piezoelectric Ceramics", Academic Press (NY), 1971, p. 49.
26. B.A. Auld, "Acoustic Fields and Waves in Solids", Vol 1, Krieger (Malabar, FL), 1990.
27. C.D. Butter and G.B. Hocker, *Applied Optics*, 17(18), 1978, p. 2867.
28. D. Brewster, *Phil. Trans. of Royal Society (London)*, 1816, p. 156.
29. R. Measures, "Smart Structures for Aircraft and Spacecraft", *AGARD Conference Proceedings*, 531, 1993. p. 11-1.
30. N. Fuerstenau, D.D. Janzen and W. Schmidt, *ibid*, p. 24-1.
31. F.A. Blaha and S.L. McBride, *ibid*, p.21-1.
32. K. Liu, S.M. Ferguson and R.M. Measures, "Fiber Optic Smart Structures and Skins II", *SPIE* 1170, 1989, p. 205.
33. D.A. Jackson and J.D.C. Jones, *Optical Acta*, 33, 1986, p. 1469.
34. K.A. Murphy, M. Miller, A.M. Vengsarkar, R.O. Claus and N.E. Lewis, *SPIE*, 1170, 1989, p. 566.
35. W.W. Morey, G. Meltz and W.H. Glenn, *Fiber Optic and Laser Sensors VII*, *SPIE* 1169, 1989, p. 98.
36. R.M. Measures, *Composites Eng.*, 2, 1992, p. 597.
37. Q. Ma and D.R. Clarke, *Acta Metal. Mater.*, 41(6), 1993, p. 1817.
38. R. Gentilman, D. Fiore, H. Pham-Nguyen, W. Serwatka, B. Pazul, C. Near, P. McGuire and L. Bowen, *SPIE Conf.*, "Smart Structures and Materials Symposium", San Diego, Feb. 28, 1996, p. 2721.
39. R.B. Cullity, "Introduction to Magnetic Materials", Addison-Wesley (London), 1972, p. 248.
40. M.W. Hiller, M.D. Bryant and J. Dmegaki, *J. Sound Vibration*, 134(3), 1989, p. 507.
41. "Smart Materials Alter Shape of Adaptive Aircraft Wings", *Advanced Materials and Processes*, 9, 1995, p. 9.
42. H. Furnakubo, "Shape Memory Alloys", Gordon and Breach Publishers (New York), 1987.
43. K.R.C. Gisser et al, *J. Chem. Education*, 71(4), 1994, p. 334.
44. T.C. Jordan, M.T. Shaw, *IEEE Trans on Electrical Insulation*, 24(5), 1989, p. 849.
45. H. Block, J.P. Kelley, *J. Phys D: Appl Phys.*, 21, 1988, p. 1661.
46. T. D. Gulden, C. R. Harder, P. W. Trester, W. Keith and S. Austin, *Active 95*, Newport Beach, Ca, 1996, p. 1311.

Shape Memory Alloys and their Application

Christian Boller and Werner Brand

Daimler-Benz Aerospace, Military Aircraft

D-81663 München, Germany

actually with: Daimler-Benz AG, Research & Technology Exchange Group

D-70546 Stuttgart, Germany

L. Catherine Brinson and Miin-Shiou Huang

Department of Mechanical Engineering, Northwestern University

Evanston/Illinois, USA

SUMMARY

Shape memory alloys (SMA) have gained increasing attraction within the development of aircraft structures. One of the major reasons is, that they allow a recovery of deformation as a result of a transformation process between martensite and austenite, where transformation occurs between characteristic temperature values when being initiated by temperature. So far deformation capabilities of SMAs is mainly taken advantage of by using their two extreme conditions, such as clamped or loose for a fixing element. Continuous control of deformation during this transformation process however allows to take much more advantage of SMAs capabilities but this requires a clear description of the SMAs constitutive behaviour which is actually an important area of research. The paper starts by analytically describing the SMAs constitutive behaviour using an approach being well understandable for engineering applications. After having explained the basic mechanisms of SMAs it will be shown how these can be analytically implemented into the calculation process for determining the behaviour of a simple engineering structure with an integrated SMA-actuator. Finally examples are described, where controlled deformation of a SMA in a smart structure is considered at present.

INTRODUCTION

Shape memory alloys (SMAs) have gained increasing attraction within the development of various engineering structures during the past decade. Although these alloys have been known for a long time, major impetus is coming from the introduction of an adaptive structure design philosophy.

SMAs have been used extensively for medical and surgical [Funakubo (Ed.), 1987] devices and toys. Applications are also known for switches and grips, mainly for automotive and robotic devices, as well as shrink fit type hydraulic tubing couplers. Within these applications only a two way functionality of the SMA is considered (e.g. on/off,

open/close, hold/release). However recently studies have been performed considering an adaptive airfoil for aeroelastic control [Lazarus et al., 1990], a thin-walled box type adaptive wing for static aeroelastic control [Song et al., 1991], an adjustable camber foil [Beauchamp et al., 1992], a winglet wedge section or an adaptive antenna [Misra et al., 1992]. With respect to composite materials, proposals have been given in [Rogers and Robertshaw, 1988] for SMA as a functional element in polymer-based composites.

The functionality requested from the SMA actuators within these latter studies is much more ambitious than that being made available so far. A much better understanding and analytical description of a SMA's constitutive behaviour is therefore required, which also requires much more experimental data compared to what has been made available so far. Furthermore the mechanical behaviour at the intersection between the SMA actuator and the structural material it is connected with has to be clearly understood. The initial step for making this feasible is to find a description of the constitutive behaviour of the functional elements (e.g. SMAs) used, which should be close to reality as far as possible and yet not too complex in handling. With respect to controlling the behaviour of SMA actuators this has to be done by a clear analytical description of the main features of the constitutive behaviour of these alloys. Initial work in this area has been based on Tanaka's approach which has been derived from principles of SMA's thermodynamical behaviour [Tanaka, 1986]. The constitutive relationship resulting from this approach has been formulated by Liang (1990) and is used within this paper in a version extended by Brinson (1993).

Although this approach cannot fully reflect the high complexity of SMAs it possesses the advantage of being relatively well understood in engineering science by macroscopically describing the SMA phenomenon. It therefore builds a good basis for designers to receive motivation in considering the implementation of SMAs into the design of their engineering structures. More complex descriptions of the SMAs constitutive behaviour

being based on the Ginzburg-Landau-model can be found in Falk (1990), Hoffmann and Niezgodka (1990), Müller and Huibin (1991), and Stalmans et al. (1994).

It is the objective of this paper to propose an extended analytical as well as numerical solution to especially account for the nonlinear behaviour of a SMA activated cantilever beam. Application of the solution will be shown numerically and partly be verified experimentally.

THE SMA CONSTITUTIVE LAW

A key element for the design of engineering structures is the analytical description of the constitutive (e.g. stress - strain) behaviour of materials used. With a large number of structural materials this can be easily expressed by using Hooke's law. With SMAs this however becomes much more difficult.

The governing mechanism responsible for the deformation in the SMAs is a transformation process between martensite and austenite. It can be initiated either by a change in temperature, where transformation occurs between characteristic temperature values (Fig.1a) and/or by a change in stress, where characteristic stress values define the incident of transformation (Fig.1b). In the former case (Fig.1a), when stress remains constant, transformation to austenite starts at temperature A_s (austenite start) and is completed when heating up to a temperature A_f (austenite finish) while during cooling transformation to martensite starts at temperature M_s (martensite start) and is completed at temperature M_f (martensite finish). In the latter case (Fig.1b) the characteristic transformation temperatures A_s , A_f , M_s and M_f change according to a linear function when stress is applied to the SMA. To account for the shape memory effect below M_s , two critical stresses σ_s^{cr} and σ_f^{cr} for conversion to martensite are additionally included.

SMAs lead to large pseudoelastic shape deformations when being loaded above a characteristic stress level. In contrast to conventional metals these pseudoelastic deformations can however be recovered when heat is applied above a characteristic temperature.

A selection of five different examples showing this behaviour at different temperatures is given in Fig.2.

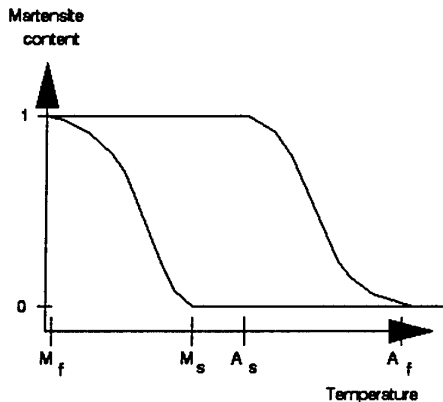


Fig. 1a.

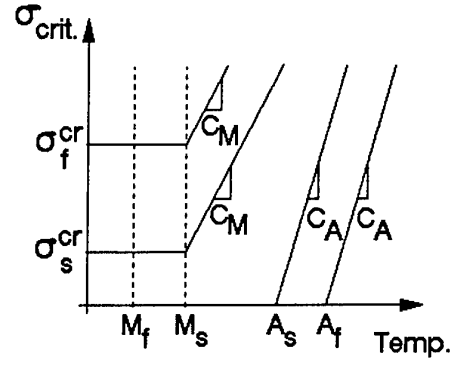


Fig. 1: Critical stresses for transformation of martensite twin conversion as function of temperature

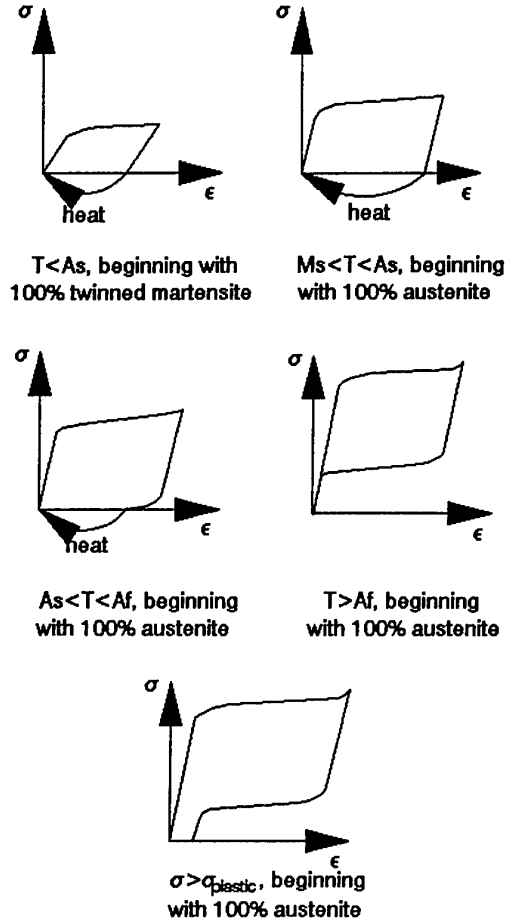


Fig. 2 Stress-Strain-Behaviour of SMAs

A solution accounting for the two types of transformation (stress and temperature induced) has been given in [Brinson, 1993] by splitting the martensite fraction ξ according to the following equation:

$$\xi = \xi_s + \xi_T$$

where ξ_T represents the fraction of the material that is purely temperature-induced martensite with multiple variants, and ξ_s denotes the fraction of the material that has been transformed by stress to a single martensite variant. The constitutive behaviour of SMA is described

by the following equation derived in more detail in [Brinson, 1993]:

$$\sigma - \sigma_0 = D(\xi)\epsilon - D(\xi_0)\epsilon_0 + \Omega(\xi)\xi_s - \Omega(\xi_0)\xi_{s0} + \Theta(T - T_0) \quad (1)$$

where σ , ϵ , ξ and T is the stress, strain, martensite fraction and temperature respectively, while D , Ω and Θ denotes modulus of the SMA material, transformation tensor, which are linear in ξ , and thermal coefficient. The initial state (or initial conditions) of the SMA is represented by the index 0.

Since D depends on the martensite fraction ξ a reasonable assumption has been made by Sato and Tanaka (1988) and Liang (1990) which can be described as

$$D(\epsilon, \xi, T) = D(\xi) = D_a + \xi \times (D_m - D_a) \quad (2)$$

with D_m the modulus value for the SMA as 100% martensite and D_a is the equivalent value as 100% austenite.

Based on Liang's suggestion [Liang, 1990] and extended by Brinson (1993), Ω also depends on ξ and can be written as follows:

$$\Omega(\xi) = -\epsilon_L \times D(\xi) \quad (3)$$

Theoretical studies examining phase equilibrium and transformation kinetics have also developed expressions for the martensite fraction as a function of free energy and temperature. Liang and Rogers (1990) have developed an empirically based cosine solution to represent the martensite fraction as a function of stress and temperature during transformation, which agrees well with their experimental findings. One of Liang's findings (in accordance with data from other authors) which have been extended by Brinson (1993) has been that the characteristic transformation temperatures A_s , A_f , M_s , and M_f change according to partly linear functions when stress is applied to the SMA where an approximation is shown in Fig. 1b.

Coupling Eq.(1) with transformation kinetics shown in Fig. 1b leads to the following set of equations being explained in more detail in [Brinson, 1993].

Conversion to Martensite

for $T > M_s$ and

$$\sigma_s^{\sigma} + C_M \times (T - M_s) < \sigma < \sigma_f^{\sigma} + C_M \times (T - M_s)$$

$$\xi_s = \frac{1 - \xi_{s0}}{2} \cos \left(\frac{\pi}{\sigma_f^{\sigma} - \sigma_s^{\sigma}} \left[\sigma - \sigma_f^{\sigma} - C_M (T - M_s) \right] \right) + \frac{1 + \xi_{s0}}{2} \quad (4a)$$

$$\xi_T = \xi_{T0} - \frac{\xi_{T0}}{1 - \xi_{s0}} (\xi_s - \xi_{s0}) \quad (4b)$$

for $T < M_s$ and $\sigma_s^{\sigma} < \sigma < \sigma_f^{\sigma}$

$$\xi_s = \frac{1 - \xi_{s0}}{2} \cos \left[\frac{\pi}{\sigma_f^{\sigma} - \sigma_s^{\sigma}} (\sigma - \sigma_f^{\sigma}) \right] + \frac{1 + \xi_{s0}}{2} \quad (4c)$$

$$\xi_T = \xi_{T0} - \frac{\xi_{T0}}{1 - \xi_{s0}} (\xi_s - \xi_{s0}) + \Delta_{T\xi} \quad (4d)$$

where, if $M_f < T < M_s$ and $T < T_0$

$$\Delta_{T\xi} = \frac{1 - \xi_{T0}}{2} \left(\cos \left[a_M (T - M_f) \right] + 1 \right) \quad (4e)$$

else $\Delta_{T\xi} = 0$

Conversion to Austenite:

for $T > A_s$ and

$$C_A \times (T - A_f) < \sigma < C_A \times (T - A_s)$$

$$\xi = \frac{\xi_0}{2} \times \left(\cos \left[a_A \times \left(T - A_s - \frac{\sigma}{C_A} \right) \right] + 1 \right) \quad (5a)$$

$$\xi_s = \xi_{s0} - \frac{\xi_{s0}}{\xi_0} (\xi_0 - \xi) \quad (5b)$$

$$\xi_T = \xi_{T0} - \frac{\xi_{T0}}{\xi_0} (\xi_0 - \xi) \quad (5c)$$

The appropriate use of ξ_s and ξ_T may be well understood when considering the following two examples:

- The SMA is under stress free conditions ($\xi_{s0} = \xi_{T0} = 0$) and is heated above A_f . When cooled down again the final conditions will be $\xi_T = 1$ and $\xi_s = 0$, because martensite was induced by temperature.
- The SMA starts from stress free conditions ($\xi_{s0} = \xi_{T0} = 0$) and is continuously loaded at a constant temperature above A_f until a fully martensitic stage is achieved. Final conditions are now $\xi_s = 1$ and $\xi_T = 0$, because martensite was induced by stress.

Thus, differentiation between ξ_s and ξ_T allows to describe the boundary conditions as follows:

- * $\xi_s = 0$ $\xi_T = 0$ $\rightarrow T > M_s$ (with $\sigma = 0$)
- * $\xi_s = 1$ $\xi_T = 0$ \rightarrow at any temperature, if the stress is above the critical finish value
- * $\xi_s = 0$ $\xi_T = 1$ \rightarrow twinned martensite ($T \leq M_f$)

All equations given so far are valid as long as applied strain does not exceed recovery strain of 8%. As strains up to 8% mainly cover the range of allowable strains in engineering applications, this description of the constitutive behaviour of the SMAs can be used to describe the deformation of adaptive engineering structures being actuated by these alloys.

Verification of the Approach

Prior to any verification and validation it has to be emphasized that reliable data on the constitutive behaviour of SMAs is still very limited. Liang (1990) and Dye (1990) have determined some data on NiTi-alloys which are mainly the basis throughout this paper. Some additional data of NiTi-alloys showing the full hysteresis at temperatures above A_f have been recently published by Schlegel (1995). A comparison of these data with the analytical approach is shown on Fig. 3.

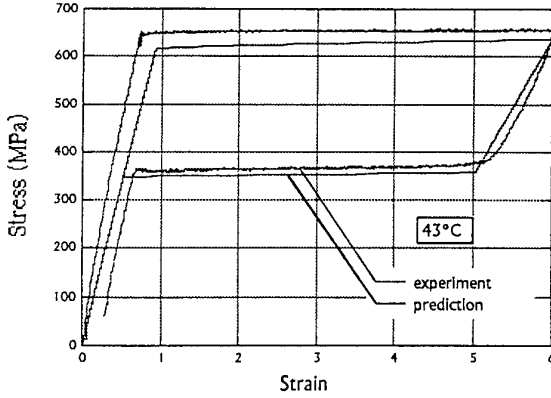


Fig. 3 Stress-Strain Comparison of Experiment and Numerical Approach

Although this analytic approach allows to describe the constitutive behaviour of a NiTi-alloy there is still a variety of other types of SMAs where a verification is still required. One example is copper based alloys (e.g. NiTiCu) that undergoes a double phase transition (Fig. 4) where an extension is required for the analytic approach presented here.

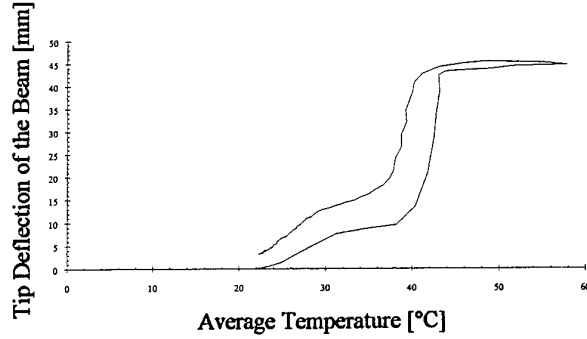


Fig. 4 Stress-Strain-Behaviour of NiTiCu (Experiment)

THE CANTILEVER BEAM MODEL

Linear Behaviour

A variety of applications have been proposed for using SMAs in engineering structures [e.g. Funakubo 1987, Lazarus et al. 1990, Song et al. 1991, Beauchamp et al. 1992, Misra et al. 1992, Rogers & Robertshaw 1988, Van Humbeeck et al. 1991]. The complexity of most of these structures makes understanding of the interaction between the SMA actuator(s) and the structure quite difficult. Beam models are therefore one of the ideal solutions to extract the essentials of this interaction. Although a variety of beam models being activated by a SMA actuator have been discussed, coupling between the beam interaction and the SMA constitutive law has only been partially considered. This however is an essential part yielding the stress, strain and martensite fraction of the activated SMA. Fig.5 shows the beam model considered here. It consists of a cantilever beam and a SMA wire at the bottom, which is only fixed to the beam at the beam's tip.

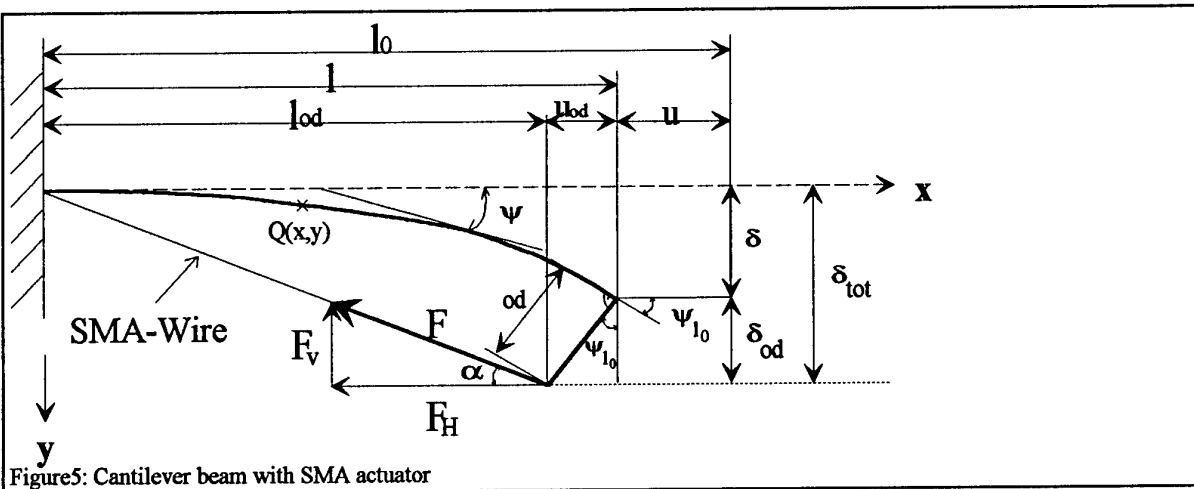


Figure5: Cantilever beam with SMA actuator

To determine the mechanical behaviour of the beam model, equations describing

- a) the constitutive behaviour of the SMA actuator and
- b) the deflection curve of the beam model

have to be established. It is assumed that the beam and SMA wire show no plastic deformation and (for the linear theory) that the beam tip deflection is small compared to the beam length ($w'(x)$ small). The constitutive behaviour of the SMA wire discussed in the preceeding chapter is given by Eq. (1). Determination of the beam deflection starts from formulating the equilibrium of horizontal, vertical and moment forces as follows:

$$F_H = -F \cos \alpha \quad (6)$$

$$F_V = -F \sin \alpha \quad (7)$$

$$M(x) = F_H (\delta - w(x) + o_d) - F_V (l_0 - x) \quad (8)$$

and

$$\delta_{o_d} = o_d \cos \Psi_{l_0} \approx o_d = \frac{t}{2} + r + \text{offset}$$

with t , r and offset being the thickness of the beam, radius of the SMA wire cross section and a constant offset distance of the beam's surface respectively.

Considering :

- (i) the linearized differential equation of the deflection curve

$$-EIw''(x) = M(x) \quad (9)$$

where E is Young's modulus of the beam and I the moment of inertia of the cross section respectively,

- (ii) the general solution of Eq. (9)

$$w(x) = C_1 \cos kx + C_2 \sin kx + C_3 x + C_4 \quad (10)$$

where

$$k = \sqrt{\frac{F}{EI}} \quad (11)$$

and

- (iii) the required boundary conditions finally leads to the following deflection curve

$$w(x) = o_d \left[\frac{\cos kl - 1}{\sin kl} (\sin kx - kx) - \cos kx + 1 \right] \quad (12)$$

which only depends on the applied force F and the horizontal displacement u . A more detailed description of the derivation is given in [Boller et al., 1993].

Determination of u starts from

$$u = \int_0^{l_0} (ds - dx) \quad (13)$$

with ds being an infinitesimal small element of the deflected beam. As long as $w'(x) \ll 1$ Eq. (13) can be approximated to be

$$u \approx \frac{1}{2} \int_0^{l_0} w'^2(x) dx \quad (14)$$

Eq. (12) can now be inserted into Eq. (14) thus leading to

$$u - \frac{1}{2} \int_0^{l_0} \left\{ o_d \times k \left[\frac{\cos kl - 1}{\sin kl} (\cos kl - 1) + \sin kx \right] \right\}^2 dx = 0 = g_1(F, u) \quad (15)$$

Including the characteristic equation for the angle of inclination at $x = l_0$:

$$w'(l) - \tan(\Psi_{l_0}) = 0 = g_2(F, u, \Psi_{l_0}) \quad (16)$$

as well as those for the stress and the strain in the SMA actuator

$$\sigma = \frac{F}{A_{SMA}} = g_3(F) \quad (17)$$

$$\varepsilon = \varepsilon_0 - \frac{l - l'}{l} = g_4(F, u, \Psi_{l_0}) \quad (18)$$

(with A_{SMA} being the cross section area of the SMA) a set of functions g_i ($i=1,4$) is obtained allowing to generally solve the problem. This number of functions is reduced by inserting $g_3(F)$ and $g_4(F, u, \Psi_{l_0})$ into Eq. (1), the SMA constitutive law, leading to a function $g_5(F, u, \Psi_{l_0})$. These remaining three equations g_1 , g_2 and g_5 now allow to determine the unknowns F , u and Ψ_{l_0} using Newton's iteration method. Performing this iteration requires the definition of an interval at least for one of the unknowns. Following the relationship shown in Fig. 1b a force F can only be implied by the transformation process when satisfying the following relationship

$$A_{SMA} C_A (T - A_f) < F < A_{SMA} C_A (T - A_s) \quad (19)$$

thus leading to the interval required for the iteration process.

Nonlinear Behaviour - Analytical Method

Taking full advantage of the SMA's actuation often leads to a situation where the assumption of linearized deformation is not valid anymore. This occurs especially for beams, when the ratio of stiffness versus length becomes small. Following Bernoulli-Euler's law

$$\frac{d\Psi}{ds} = \frac{M}{EI} \quad (20)$$

the bending moment at any point is proportional to the change in the curvature caused by the action of the load. Let α be the angle of inclination between the load and the horizontal. The bending moment at Q(x,y) is again (Fig. 5)

$$M(x) = F_H(\delta_{tot} - y) - F_V(l_{od} - x) \quad (21)$$

where

$$F_H = F \cos \alpha \quad (6) \quad \text{and} \quad F_V = F \sin \alpha \quad (7)$$

Inserting Eq.s (6), (7) and (21) into (20) and differentiating with respect to s yields

$$\frac{d^2 \Psi}{ds^2} = -\frac{F_H}{EI} \sin \Psi + \frac{F_V}{EI} \cos \Psi \quad (22)$$

with

$$\frac{dy}{ds} = \sin \Psi \quad \frac{dx}{ds} = \cos \Psi \quad (22a)$$

Introducing the following substitutions

$$v = \frac{s}{l_0} \quad \Theta = \Psi - \alpha \quad (23)$$

Eq. (22) can be transformed to the following second order inhomogeneous differential equation

$$\frac{d^2 \Theta}{dv^2} + c \sin \Theta = 0 \quad (24)$$

in which

$$c = \frac{l_0^2 F}{EI} = l_0^2 k^2 \quad (24a)$$

Multiplying Eq. (24) with $2d\Theta$ and integrating, yields

$$\frac{1}{2} \left(\frac{d\Theta}{dv} \right)^2 = c \cos \Theta + C_1 \quad (25)$$

With the boundary conditions

$$(\Psi)_{s=0} = 0 \quad \text{or} \quad (\Theta)_{v=0} = -\alpha \quad (26)$$

and

$$\left(\frac{d\Psi}{ds} \right)_{s=l_0} = \frac{F_H}{EI} \delta_{od} + \frac{F_V}{EI} u_{od}$$

or

$$\left(\frac{d\Theta}{dv} \right)_{v=1} = TC \quad (27)$$

with

$$TC = l_0 k^2 o_d \cos \Theta_b \quad \text{and} \quad \Theta_b = \Psi_b - \alpha \quad (27a)$$

C_1 can be determined, thus leading to

$$\left(\frac{d\Theta}{dv} \right)^2 = TC^2 - 2c \cos \Theta_b + 2c \cos \Theta \quad (28)$$

Hence

$$dv = \frac{ds}{l_0} = \frac{d\Theta}{\sqrt{TC^2 - 2c \cos \Theta_b + 2c \cos \Theta}} \quad (29)$$

Integrating ds from $\Psi=0$ to $\Psi=\Psi_b$ means a lower limit $\Theta = -\alpha$ and an upper limit $\Theta = \Psi_b - \alpha = \Theta_b$ in terms of Θ . Therefore,

$$l_0 = \int_0^{l_0} ds = l_0 \int_{-\alpha}^{\Theta_b} \frac{d\Theta}{\sqrt{TC^2 - 2c \cos \Theta_b + 2c \cos \Theta}} \quad (30)$$

Introducing a 'modulus' p ,

$$p^2 = \frac{TC^2}{4k^2 l_0^2} + \sin^2 \frac{\Theta_b}{2} \quad (31)$$

that governs the deflected shape, Eq. (30) results in

$$l_0 = \frac{1}{2k} \int \frac{d\Theta}{\sqrt{p^2 - \sin^2 \frac{\Theta}{2}}} \quad (32)$$

considering the integral without its limits initially.

Substitution of Θ by

$$p \sin \Phi = \sin \frac{\Theta}{2} \quad (33)$$

and differentiation leads to

$$d\Theta = \frac{2p \cos \Phi}{\sqrt{1 - p^2 \sin^2 \Phi}} d\Phi \quad (34)$$

which becomes

$$l_0 = \frac{1}{k} \int \frac{d\Phi}{\sqrt{1 - p^2 \sin^2 \Phi}} \quad (35)$$

when being introduced into Eq. (32).

Consequently the limits of the integration have to be transformed. Thus it can be written in context to Eq. (30) that

$$1 = \int_{-\alpha}^{\Theta_b} = \int_{-\alpha}^0 + \int_0^{\Theta_b} = -\int_0^{-\alpha} + \int_0^{\Theta_b} = \int_0^{\alpha} + \int_0^{\Theta_b} \quad (36)$$

The last step in Eq. (36) is possible, because the integrand of Eq. (30) is even.

According to Eq. (33) the limits of integration turn out to be:

$$\Theta_{l_0} \rightarrow \Phi_{l_0} = \arcsin \left(\sqrt{1 - \frac{p^2 TC^2}{4k^2 l_0^2}} \right) \quad (37)$$

$$\alpha \rightarrow \Phi_0 = \arcsin \left(\frac{\sin \left(\frac{\alpha}{2} \right)}{p} \right) \quad (38)$$

Hence l_0 is obtained in terms of Legendre's elliptic integrals of the first kind.

$$l_0 = \frac{1}{k} \left\{ F(p, \Phi_0) + F(p, \Phi_{l_0}) \right\} \quad (39)$$

As Eq. (39) still depends on two unknowns Ψ_{l_0} and α at least one additional equation is required. A first attempt in that way is obtained by calculating the horizontal deflection u .

Horizontal Deflection u

It is noted from Eq.s (29) and (34) that

$$ds = \frac{l_0 d\Theta}{\sqrt{TC^2 - 2c \cos \Theta_{l_0} + 2c \cos \Theta}} = \frac{1}{k} \frac{d\Phi}{\sqrt{1 - p^2 \sin^2 \Phi}} \quad (40)$$

As $dx/ds = \cos \Psi$ it is obtained that

$$dx = \frac{\cos(\Theta + \alpha) d\Phi}{k \sqrt{1 - p^2 \sin^2 \Phi}} \quad (41)$$

Expanding $\cos(\Theta + \alpha)$ and noting that

$$\cos \Theta = 1 - 2 \sin^2 \frac{\Theta}{2} = 1 - 2 p^2 \sin^2 \Phi \quad (42)$$

the following expression for dx is obtained,

$$dx = \frac{\cos \alpha}{k} \left\{ -\frac{d\Phi}{\sqrt{1 - p^2 \sin^2 \Phi}} + 2 \sqrt{1 - p^2 \sin^2 \Phi} d\Phi \right\} - \frac{\sin \alpha}{k} 2 p \sin \Phi d\Phi \quad (43)$$

Again, by changing the variable from Θ to Φ the limits of the integration become Φ_0 Φ_{l_0} . Hence

$$l = \frac{1}{k} \left\{ \cos \alpha \left[-F(p, \Phi_0) - F(p, \Phi_{l_0}) + 2E(p, \Phi_0) + 2E(p, \Phi_{l_0}) \right] + 2p \sin \alpha (\cos \Phi_0 + \cos \Phi_{l_0} - 2) \right\} \quad (44)$$

Even though Eq. (44) depends on Ψ_{l_0} and α via modulus p (see Eq.s (31) and (27a)), the length l remains as a further unknown. Thus an additional equation is required, which can be obtained by describing the tip displacement of the beam.

Tip displacement δ of the beam

A similar procedure as described for the horizontal deflection can be adopted for the derivation of the tip displacement of the beam.

$$dy = ds \sin \Psi = ds \sin(\Theta + \alpha) \quad (45)$$

By expanding $\sin(\Theta + \alpha)$ and expressing $\sin \Theta$ and $\cos \Theta$ in terms of Φ , the above expression leads to

$$dy = \frac{\cos \alpha}{k} 2 p \sin \Phi d\Phi + \frac{\sin \alpha}{k} \left\{ -\frac{d\Phi}{\sqrt{1 - p^2 \sin^2 \Phi}} + 2 \sqrt{1 - p^2 \sin^2 \Phi} d\Phi \right\} \quad (46)$$

Integrating between the same limits as for the horizontal deflection we obtain

$$\delta = \frac{1}{k} \left\{ \sin \alpha \left[-F(p, \Phi_0) - F(p, \Phi_{l_0}) + 2E(p, \Phi_0) + 2E(p, \Phi_{l_0}) \right] - 2p \cos \alpha (\cos \Phi_0 + \cos \Phi_{l_0} - 2) \right\} \quad (47)$$

Additionally to Ψ_{l_0} and α , the tip displacement δ remains again as an unknown. However a relationship between Ψ_{l_0} , α , l and δ can be derived from the geometric conditions of the beam shown in Fig. 5, thus being

$$\alpha = \arctan \left(\frac{\delta + \delta_{od}}{l - u_{od}} \right) \quad (48)$$

Final Iteration

If one inserts Eq.s (44) and (47) in Eq. (48), this results in a function f_2 which only depends on Ψ_{l_0} , α and F . Again a set of characteristic equations is obtained to determine the unknowns Ψ_{l_0} , α and the force F in the SMA wire, which will be determined by the function $g_3(F, u, \Psi_{l_0})$, the SMA constitutive law. The three characteristic functions are now

$$f_1(F, \Psi_{l_0}, \alpha) = \frac{1}{k} \left\{ F(p, \Phi_0) + F(p, \Phi_{l_0}) \right\} - l_0 \quad (49)$$

$$f_2(F, \Psi_{l_0}, \alpha) = \arctan \left(\frac{\delta + \delta_{od}}{l - u_{od}} \right) - \alpha \quad (50)$$

and g_3 mentioned with respect to the linear behaviour, where u in g_3 is expressed in terms of Ψ_{l_0} and α , thus leading to

$$\tilde{g}_3(F, \Psi_{l_0}, \alpha) \quad (51)$$

This set of functions can be solved by an expanded Newton's method. If one applies a temperature on the SMA wire, the stress, strain and martensite fraction of the SMA wire as well as the tip deflection, horizontal displacement and the angles of inclination Ψ_{l_0} and α of the beam are therefore obtained.

Nonlinear Behaviour - Numerical Method

The numerical solution method is very straightforward. First separate the problem into two functions:

1. Wire strain as function of the stress which is from SMA constitutive law (Eq.(1) and transformation kinetics equations):

$$\varepsilon_1 = f_1(\sigma) \quad (52)$$

2. Wire strain as a function of the load which is from the beam theory. A certain load applied to the beam results in a certain deformed shape of the beam and from that shape the amount the wire shortens can be calculated. This relates the load to the shortening of the wire. Now, the stress in the wire can easily be obtained by load/area and the strain by $(l-l_0)/l_0$. Consequently, one has another relation for the strain in the wire as a function of stress in the wire. (See step 3 for details of the deflected shape of the beam given the load.)

$$\varepsilon_2 = f_2(\sigma) \quad (53)$$

Subtracting ε_1 from ε_2 :

$$\varepsilon_1 - \varepsilon_2 = f_1(\sigma) - f_2(\sigma) = f(\sigma) \quad (54)$$

At a particular temperature, there is only stress for which $f(\sigma) = 0$. A binary search is used to find the stress by the following procedure:

$$\text{let } \sigma_{min} = 0 \quad \text{and} \quad \text{let } \sigma_{max} = \sigma_{critical}$$

Finding σ_{max} is a little tricky. Theoretically, it should be the critical buckling load which is not trivial to find for this configuration. However, in this procedure, any load guaranteed to be larger than the actual load will serve. Consequently, a case at 70°C is considered first (since 70°C is the maximum operating temperature and hence will occur the largest stresses). The critical load is determined initially for 70°C and then used to solve the problem at all temperatures (20-70°C).

The real stress must be bounded by σ_{min} and σ_{max} , that is

$$f(\sigma_{min}) \times f(\sigma_{max}) \leq 0$$

$$\clubsuit \text{ Then let } \sigma_i = (\sigma_{min} + \sigma_{max})/2$$

If $f(\sigma_{max}) \times f(\sigma_i) \leq 0$ then the real stress is between σ_{max} and σ_i . In this case let $\sigma_{min} = \sigma_i$. Otherwise, the real stress is between σ_{min} and σ_i . In this case let $\sigma_{max} = \sigma_i$. Go back to \clubsuit . With iteration, the range becomes increasingly smaller than the desired accuracy. The result is the desired approximate root.

3. There is no problem with the first function f_1 . However, there are complications for f_2 . With f_2 if the bending moment of the beam is known, then the problem is solved. But the bending moment depends on the shape of the beam (see Eq.(21)), which is naturally not known before the problem is solved. A gradual approach method was used to solve it. First it was assumed that the beam did not deform at all, and the load is applied at the tip of the offset device. Here, the moment distribution on the beam and consequently the shape of the beam can be calculated. (Of course the shape of the beam is not the exact shape of this load.)

\clubsuit Then the new shape was used to calculate the new moment distribution, and the new moment distribution to calculate the new shape. Since the moment is increasing, the beam deflection likewise increases.

Repeat (\clubsuit). At each iteration, the beam deflects further until the initial shape is the same as it should be under the given load. This is the solution to the given problem. See below for details of the solution at each iteration. Within step 3, the following must be solved at each iteration: When we assume a trial shape of the beam, the relevant equation for the nonlinear case is

$$\frac{w''(x)}{(1 + (w'(x))^2)^{3/2}} = M(w(x), x) \quad (55)$$

$$BC's: w(0) = 0, \quad w'(0) = 0$$

A 4th order Runge Kutta method was used to numerically solve the differential equation. This method uses the known function value and slope at one point to estimate the function value of the next point. However, it does not use the slope directly. Instead, this method calculates the slope of the midpoint and trial points and averages them. At each step, n , $w(x_n)$ is calculated from point x_{n-1} . Then the neutral axis length is summed up by

$$l = l + \Delta l$$

where

$$\Delta l = \sqrt{\Delta x^2 + (w(x_n) - w(x_{n-1}))^2} \quad (56)$$

So at the step where $l = l_0$, the desired solution is reached. For most cases

$$\text{step } n, l < l_0 \quad \text{step } n+1, l > l_0$$

Then interpolation can be used to compute the final solution.

Experimental Verification

In order to verify the analytical procedure for describing the linear and nonlinear behaviour of beams outlined before a set of experiments was done. Following the model shown in Fig. 5 an aluminium beam was clamped in vertical position (Fig. 6). As the verification of the beam's deformation has been the major target, the SMA actuator could be replaced by a conventional steel wire. Weights simulating the actuation force of the SMA actuator were fixed to the lower end of the wire. Possible friction due to the experimental setup was minimized as far as possible. To avoid ideal Euler buckling the actuation force was implied excentrically, thus allowing controlled bending of the beam. Within the series of experiments the following combinations of beam geometries were considered (all dimensions in millimeters):

Length	Width	Thickness
286	50	1
286	50	2
286	50	3
400	25	1
500	25	1

Figs 7 and 8 show a comparison between the numerical and experimental results for the beam's linear and nonlinear deformation behaviour respectively. Nonlinear deformation behaviour becomes only obvious for thicknesses of 1 millimeter. In neither of both cases (linear or nonlinear) a significant difference between experiment and theory is observed. Thus it can be concluded, that the analytical model proposed so far allows to describe realistically the deformation behaviour of the type of engineering structure considered.

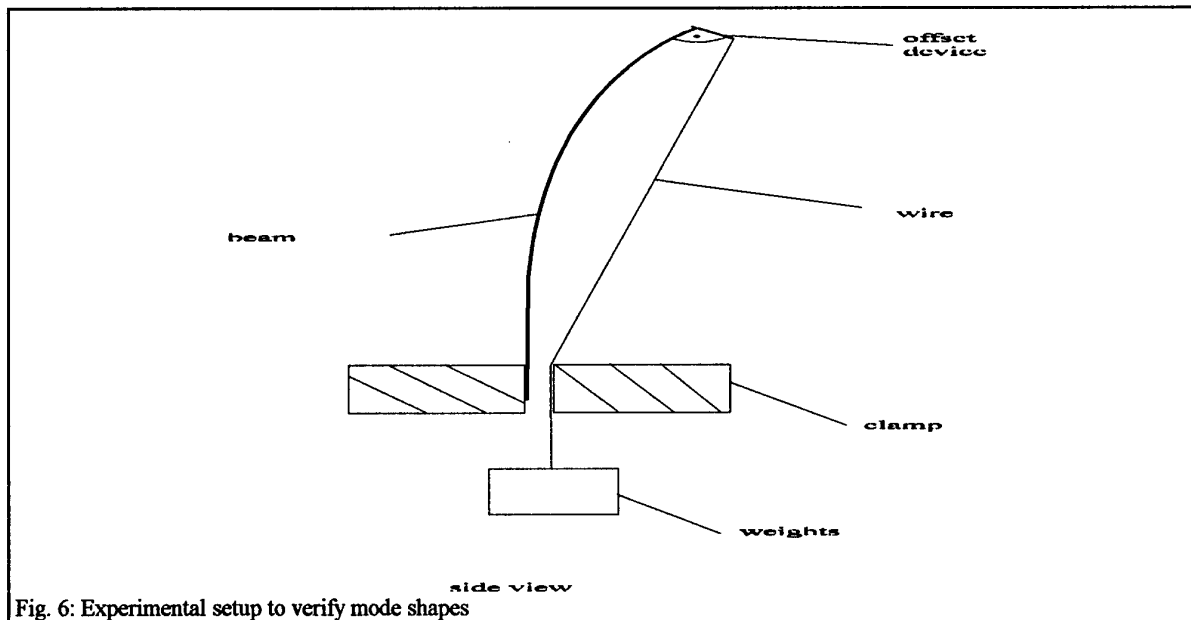


Fig. 6: Experimental setup to verify mode shapes

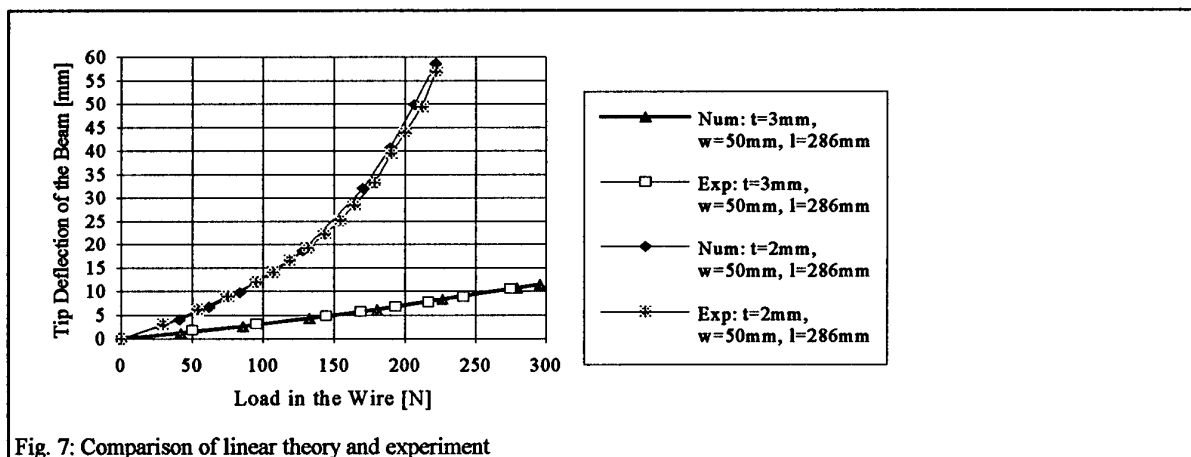


Fig. 7: Comparison of linear theory and experiment

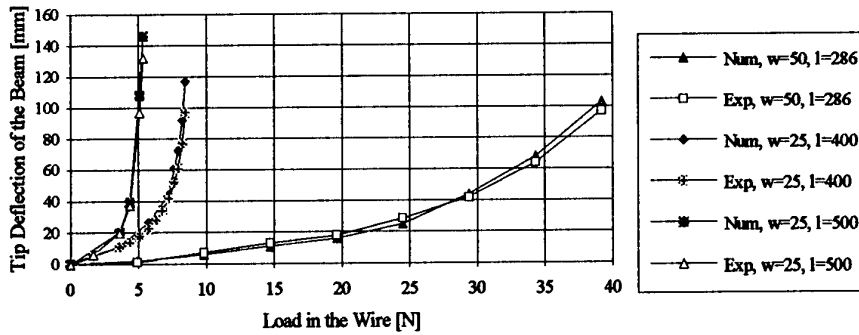


Fig. 8: Comparison of nonlinear theory and experiment

DETERMINING THE BEHAVIOUR OF STRUCTURE INTEGRATED SMA ACTUATORS

Based on the appropriate mechanical model it is now possible to determine what stresses, strains, martensite fraction and transformation temperatures will occur under

various loading conditions. The following examples are a selection of the variety of possible application. Material data for the SMA actuator were taken from literature [8,12]. The material used is NiTi₅₅. Table 1 summarizes the specific data required.

Moduli	Transformation Temperatures	Transformation Constants	maximum residual strain
$D_a = 67000 \text{ MPa}$	$M_f = 9^\circ\text{C}$	$C_M = 8 \text{ MPa}/^\circ\text{C}$	$\epsilon_L = 6,7\%$
$D_m = 26300 \text{ MPa}$	$M_s = 18,4^\circ\text{C}$	$C_A = 13,8 \text{ MPa}/^\circ\text{C}$	
$\Theta = 0,55 \text{ MPa}/^\circ\text{C}$	$A_s = 34,5^\circ\text{C}$	$\sigma_s^{cr} = 100 \text{ MPa}$	
	$A_f = 49^\circ\text{C}$	$\sigma_f^{cr} = 170 \text{ MPa}$	

Table 1: SMA material data

Stress σ and Tip Deflection δ

One of the interesting aspects is to determine what stresses in the SMA actuator and deflection of the beam's tip will occur when controlling the actuator's temperature. Figs 9 and 10 show the analytically determined results for two beams of different thickness with respect to these aspects. Dimensions of the beam are 286 mm in length, 50 mm in width and 2 and 3 mm in thickness respectively. The SMA actuator is assumed to have a circular cross section of 1 mm in diameter. The relationship between applied temperature and resulting stress in the SMA actuator is given in Fig. 9. Included are also the areas during which the transformation to austenite or martensite occurs. It can be seen that for both of the cases considered the SMA is not able to be fully converted into austenite without exceeding a limit stress in the SMA.

At the end of heating, a mixture of stress- and temperature-induced martensite and austenite exists in the SMA, as illustrated by the fact that the stress-temperature path never reaches the critical A_f line in Fig. 9. Note, however, that nevertheless a large stress is induced in the SMA wire. Care must be taken, therefore, in design of SMA actuator conditions: excessive heating in an attempt to „force“ full conversion to austenite in a stress restrained situation could lead to exceeding the critical stress for irreversible plastic deformation, thus destroying the shape memory effect in the case of the 3 mm thick beam, or leading to buckling for the 2 mm thick beam. Taking full advantage of the SMAs potential therefore allows to

reduce the diameter of the SMA for the beam with $t=2 \text{ mm}$ and requires an increase of the SMA's diameter with respect to the beam of 3 mm thickness.

When cooling down again a non-significant decrease in stress and deflection is observed up to the point where conversion to martensite is initiated. Beyond that point a remarkable decrease in stress and deflection starts where the stress function mainly follows the function of stress vs. temperature for transformation to martensite. When returning to the point of initial temperature of 20°C a residual stress is observed. These residuals result from the critical stresses σ_s^{cr} and σ_f^{cr} and can only disappear when the actuator is heated above A_f under a stress free condition. Whenever implementing SMA actuators into engineering structures it has to be kept in mind that residual deflection of the structure can occur. Note that upon further heating and cooling a closed loop cycle would be obtained, starting from the endpoint of the first cycle. Achievable deflections versus applied temperature are given in Fig. 10 for the two examples mentioned above. The results show the potential of achievable deformation for the engineering structure considered.

Based on this description and analytical model it can be interesting to determine, to what extent the deflection behaviour of the beam can be described for a sequence of temperature cycles and how specific material characteristics such as fatigue induced stress relaxation can be included into the analytical model. Deformation control

via temperature becomes highly difficult when structural deformation behaves nonlinear. Fig. 11 shows the calcu-

lated results for the beam with 1mm thickness. The controllable temperature range is only about 3°C.

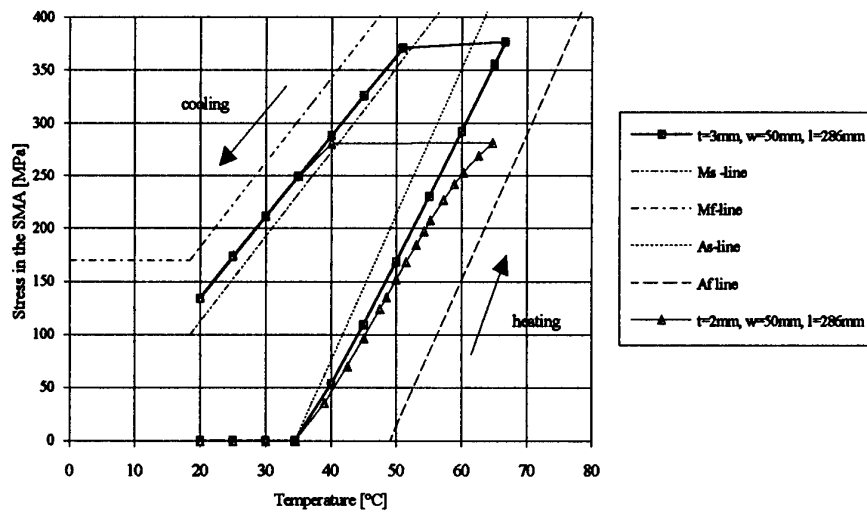


Fig. 9: Temperature dependent stress in the SMA actuator: $\xi_{S0} = 0.290$, $\xi_{T0} = 0.710$, $\epsilon_0 = 2.01\%$, $\sigma_0 = 0$

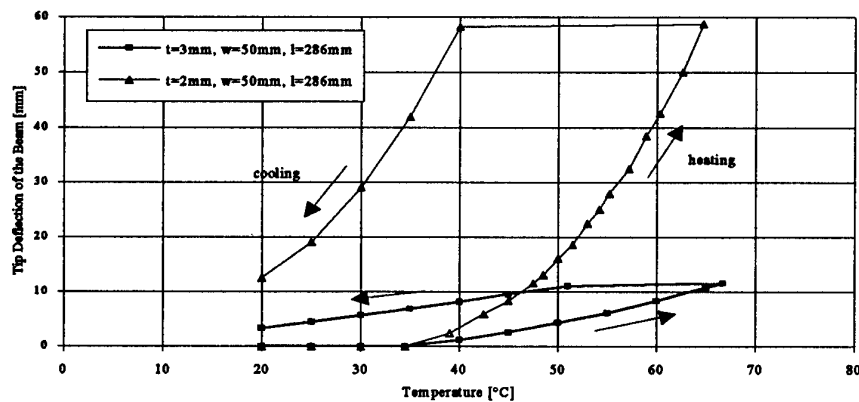


Fig. 10: Beam tip deflection vs. temperature applied in the SMA for the linear theory: $\xi_{S0} = 0.290$, $\xi_{T0} = 0.710$, $\epsilon_0 = 2.01\%$, $\sigma_0 = 0$

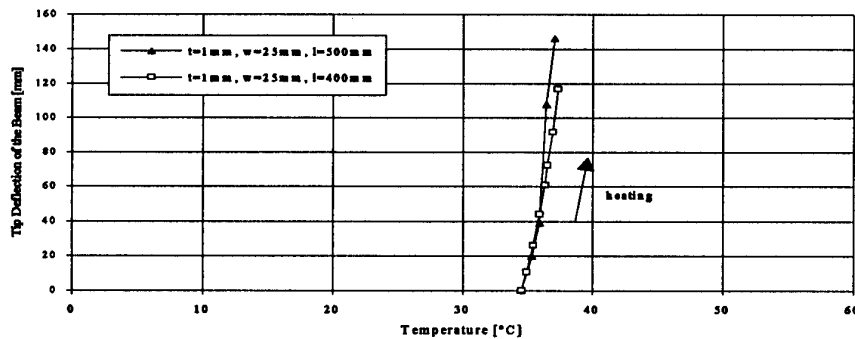


Fig. 11: Beam tip deflection vs. temperature applied in the SMA for the nonlinear theory: $\xi_{S0} = 0.590$, $\xi_{T0} = 0.410$, $\epsilon_0 = 3.97\%$, $\sigma_0 = 0$

From these few analytical results it can be concluded, that an increase in structural stiffness leads to a decrease in useable SMA transformation potential while a decrease in structural stiffness leads to decrease in controllability of structural deformation with respect to the temperature applied.

Martensite Fraction ξ

Another parameter possible to be determined by the procedure mentioned above is the martensite fraction ξ . Fig. 12 shows the relationship between stress and temperature induced martensite fraction and applied temperature. As the SMA actuator has to be prestrained before being integrated into the structure, neither of the martensite fractions is 1 or 0 at the beginning. When heating up the SMA wire and cooling it down again the martensite state of the beginning of the heating process cannot be reached again, being a result of the critical stress σ_s^{cr} and σ_f^{cr} . The ability of the SMA wire to

induce deformation in the beam is because of the stress-induced transformation of detwinned martensite and subsequent conversion to austenite and recovery of strain upon heating. While the exact rates of conversion of twinned and detwinned martensite and austenite relative to one another during the transformation are somewhat artificial (since no direct experimental data is available), the kinetic law used here is consistent with the end states and uses reasonable assumptions for smooth progress of the transformation. Thus it is illustrative to examine how the martensite fraction changes as the temperature changed in this restrained control environment. When the transformation kinetics of the SMAs are better understood, the new information can be easily incorporated into the constitutive model. As this is accomplished, more accurate design and analysis of actuators can be performed, taking into account the transformed and untransformed fractions of material and using this information of potential load and strain capability in control algorithms.

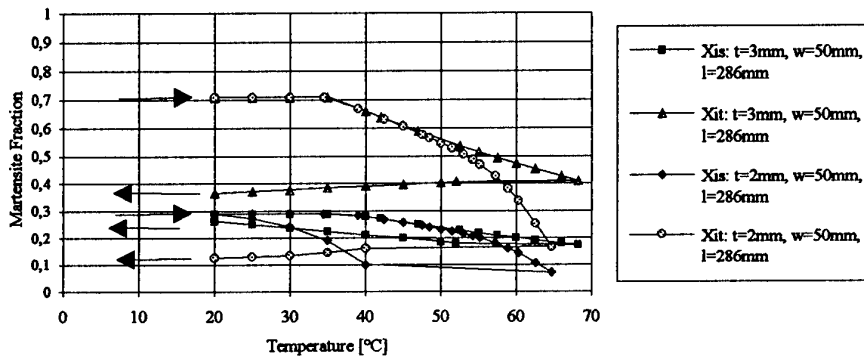


Fig. 12: Stress and temperature dependent martensite fraction in the SMA actuator, $\xi_{s0} = 0.290$, $\xi_{t0} = 0.710$, $\epsilon_0 = 2.01\%$, $\sigma_0 = 0$

POTENTIAL APPLICATION OF SMAs IN AIRCRAFT STRUCTURES

So far potential application of SMAs in aircraft has been limited to shrink fit type hydraulic tubing couplers. This is understandable, because this application neither requires precise temperature control nor does it require the need of taking full advantage of the SMAs transformation potential.

However, when considering aspects such as the change of aerodynamic shapes, control of deformation, the use of SMAs' potential becomes highly important. Although such applications have been widely proposed so far, they are unlikely to succeed as long as the basic understanding of the SMA actuators in engineering structures is not clarified. With the calculation process described above, a contribution to the clarification process is given. It will enable to determine the structural deformation behaviour as well as the amount of SMA actuators required. Furthermore the calculation process outlined so far can be extended to the determination to what amount actuation in a structure will be reduced as a result of repeated load and temperature cycles. This is especially important when considering aircraft structures under service conditions. To give an example, service temperatures in aircraft structural components can easily range between -50 and $+120^\circ\text{C}$,

which makes control of transformation process via temperature highly difficult. Furthermore this control of temperature becomes even more complicated when the actuator has to withstand variations in applied stress resulting from the actuators load carrying function and a service load sequence applied to the structure. Finally it has to be kept in mind, that a significant difference in Young's modulus between the SMA actuator and the structural material can lead to high stress concentrations at the intersection of these two components.

Keeping all these aspects in mind does not mean, that SMAs have only a limited application in aircraft. However, what it simply proves is, that a large amount of basic analytical and experimental work has to be performed before going into specific applications. This will help to design optimized SMA activated adaptive structures for aircraft (e.g. on the basis of a composite material or structure) making applications of the structures a reality.

CONCLUSIONS

The complexity of SMAs and SMA activated structures as well as the limit of structure integrated SMAs under temperature control has been presented in the examples described above. This complexity is especially true when considering the nonlinear deformation of engineering

structures. It can be seen on the one hand, that it is highly difficult to shape soft structures with the help of temperature controlled SMAs and on the other hand SMAs are restricted in their applicable potential to shape stiff structures. This has to be kept in mind when activating aircraft panels, flaps or wings by SMA actuators.

The examples given for the linear and nonlinear beam model show good coincidence of theoretical prediction and experimental data with respect of the tip deflection, horizontal displacement and angles of inclination of beam and load. Although this has not been proved experimentally yet, it can already be assumed, that analytically implementing an SMA actuator with the respective constitutive behaviour into an engineering structure leads to realistic results when using the theoretical model described here. Experimental verification is therefore underway to be performed as the next step.

When implementing a SMA in a structure the coupling at the intersection between the SMA and the remaining structure must be well understood. This is especially important when laminating SMAs into a composite material. As the SMA must act against the stiffness of the structure shear stresses occur at these intersections, which can cause displacements and even slips of single laminate layers and thus reducing the functionality of the whole laminate. Furthermore complete integration of the SMA actuator in a matrix material leads to states of multiaxial stresses and strains which require an appropriate constitutive law for the SMA. Such laws have not been established yet, but are necessary for describing the stress and strain of the SMA perpendicular and crossways to the load direction. As a result of this lack in such laws and for the time being the SMA actuator has to be fixed at his ends only. This allows to take advantage of most of the SMAs' transformation potential.

REFERENCES

- Beauchamp, C.H., R.H. Nadolink, S.C. Dickinson and L.M. Dean, 1992:* „Shape Memory Alloy Adjustable Camber (SMAAC) Control Surfaces“, 1st European Conf. on Smart Structures and Materials, pp. 189-192
- Boller, Chr. ; Brand, W. ; Brinson, L.C. ; Huang, M.S. 1993:* Some Basic Ideas on the Design of Adaptive Aircraft Structures Using SMA Alloys, Proc. of the 4th Int. Conf. on Adaptive Structures, Technomic Publ. Co.
- Brinson, L.C. 1993:* One Dimensional Constitutive Behavior of Shape Memory Alloys: Thermomechanical Derivation with Non-Constant Material Functions and Redefined Martensite Internal Variable“, J. of Intell. Mater. Syst. and Struct., pp. 229-242.
- Dye, T.E., 1990:* An Experimental Investigation of the Behaviour of NITINOL, M.S. thesis, Virginia Polytech. Inst. & State Univ.
- Falk F., 1990:* Phase Transitions and Nonconvex Energy Functions ; in K.-H. Hofmann and J. Sprekels (Ed.s): Free Boundary Problems - Theory and Application V - VI, London: Longman
- Funakubo, H., ed. 1987:* Shape Memory Alloys, translated from the Japanese by J.B. Kennedy, New York: Gordon and Breach Science Publishers.
- Hoffmann K.-H. and M. Niezgodka, 1990:* Mathematical Models of Dynamical Martensitic Transformation in Shape Memory Alloys; J. of Intell. Mater. Syst. and Struct., Vol. 1
- Lazarus, K.B.; Crawley, E.F. und Bohlman, J.D. 1990:* "Static Aeroelastic Control Using Strain Actuated Adaptive Structures", Proc. of 1st Joint U.S./Japan Conf. on Adaptive Structures, Technomic Publ. Co.
- Liang, C. 1990:* The Constitutive Modeling of Shape Memory Alloys; Ph.D. thesis, Virginia Polytech. Inst. & State Univ.
- Liang C. and C.A. Rogers, 1990:* One-Dimensional Thermomechanical Constitutive Relations for Shape memory Materials; J. of Intell. Mat. Syst. and Struct., Vol. 1, pp. 207 - 234
- Misra M.S., B. Carpenter and B. MacLean, 1992:* Adaptive Structure Design Employing Shape Memory Actuators“, Smart Structures for Aircraft and Spacecraft, AGARD- CP-531, Paper 15
- Müller I. and X. Huibin, 1991:* On the Pseudo-Elastic Hysteresis; Acta Metall. Mater. 39
- Rogers C.A. and H.H. Robertshaw, 1988:* Shape Memory Alloys Reinforced Composites, Engineering Science Preprints, 25, ESP25.88027, Society of Engineering Sciences
- Sato Y. and K. Tanaka, 1988:* Estimation of Energy Dissipation in Alloys due to Stress-Induced Martensitic Transformation; Res. Mechanica, 23, pp. 381 - 393
- Schlegel M., 1995:* NiTi-Formgedächtnislegierungen unter zyklischer Beanspruchung im pseudo-elastischen Zustand; Doctoral Thesis Ruhr Universität Bochum/Germany
- Song, O.; Librescu, L. und Rogers, C.A. 1991:* "Static Aeroelastic Behavior of Adaptive Aircraft Wing Structures Modelled as Composite Thin Wall Beams", Internat. Forum on Aeroelasticity and Structural Dynamics.
- Stalmans R., J. Van Humbeeck and L. Delaey, 1994:* A Generalized Thermodynamic Model to Predict Shape Memory Behaviour; AMD-Vol. 189/PVP-Vol. 292, ASME Winter Annual Meeting, Chicago/USA, pp. 39 - 44
- Tanaka, K. 1986:* A Thermomechanical Sketch of Shape Memory Effect: One Dimensional Behavior, Res Mech., 18: pp. 251-263
- Van Humbeeck, J., M. Chandrasekaran and L. Delaey, 1991:* Shape Memory Alloys: Materials in Action, Endeavour, New Series, Vol. 15, pp 148-154

INTELLIGENT PROCESSING OF SMART MATERIALS

Haydn N. G. Wadley

Intelligent Processing of Materials Laboratory
School of Engineering and Applied Science
University of Virginia
Charlottesville, VA 22903

SUMMARY

Intelligent Processing of Materials (IPM) is an emerging methodology for simulating and controlling the processing and manufacture of materials. It is finding widespread application during the manufacture of electronic, photonic and composite (i.e. high performance) materials, primary metals such as steel/aluminum and is an enabling technology for smart materials/structures synthesis/processing. IPM simulation tools seek to create, at the level of an engineering workstation, a "virtual" version of a process. They combine process models for a material's response to processing stimuli (e.g. pressure, temperature, environmental conditions, etc.) with characteristics of the process equipment to predict the material's performance defining attributes at the completion of the process. IPM controllers are an innovative extension of today's state-of-the-art in control technology. They exploit the recent availability of non-invasive sensors that sense critical product variables during the process. This new knowledge about the state of the process, together with the process models, can be used to plan and execute feedback control schemes leading to smart materials with "goal state" combinations of performance defining property attributes.

1. INTRODUCTION

The two aims of this lecture are to 1) describe an "idea" that has come to be called Intelligent Processing of Materials and 2) to review ongoing efforts to apply it to the processing of high performance composites as

an example of how it could be used for smart materials applications.

IPM has recently emerged as a new technology for designing and controlling the synthesis and processing of materials⁽¹⁾. It is beginning to pervasively impact the design and manufacture of many of today's advanced materials under development for military and civilian systems. For example, it is used during the growth of ceramic fibers for high performance composites⁽²⁾, for the production of novel alloy powders used in aircraft engines^(3, 4, 5), during the manufacture of metal and ceramic matrix composites^(6, 7), for the deposition of coatings for oxidation protection⁽⁸⁾, and in the production of high thermal conductivity substrates for the thermal management of multichip modules⁽⁹⁾. It is also being widely explored by the defense electronics community, for example, to improve the yield and performance of infrared imaging sensors⁽¹⁰⁾ and to speed the development of new device technologies based upon quantum well structures⁽¹¹⁾. The primary metals industry also continues to vigorously pursue its application through collaborative programs with the National Institute of Standards and Technology (NIST) and the Department of Energy^(12, 13). The processes to which it has been applied are likewise diverse and include continuous casting, extrusion, steel refining, Bridgman and Czochralski crystal growth, inert gas atomization, spray deposition, hot isostatic pressing, chemical vapor deposition (CVD), molecular beam epitaxy, etc.

2. IPM OVERVIEW

So what is IPM, and why is it attracting so much interest today? IPM can most easily be described with the aid of a sketch that schematically illustrates both the design and the control of one processing step during the manufacturing of a material, Figure 1. Let's begin at the lower right of the diagram with the box "Goal-State Property Envelope". Much of the motivation for IPM's development has come from the growing realization that successful materials are carefully engineered products that possess an optimum balance of properties (including cost) that make them best suited to a particular type of application. For example, Nextel 610TM alumina fibers recently developed by the 3M Company have extraordinarily high strengths (and stiffnesses) at low and intermediate temperature. This is because they have a fine (nanocrystalline) grain size and contain few defects. They are also chemically compatible with aluminum alloys, and are reasonably inexpensive. This particular combination of properties is almost ideal for directionally reinforcing aluminum alloys⁽¹⁴⁾. However, the fine (nanocrystalline) grain size that imparts low temperature strength to Nextel fibers results in significant creep at high temperatures (above say 1000°C) and other more creep resistant fibers would be necessary to ensure dimensional stability of other types of metal matrix composites (MMC) intended for higher operating temperatures. Furthermore, if the fiber's cost is too high, designers may choose to select a conventional high strength alloy steel, nickel, or titanium alloy instead of the aluminum matrix composite and trade off the penalty in performance against lower system cost. In fact, all materials in service today face intense competition of this type and markets only exist for those materials that can satisfy the increasingly stringent needs of designers whose products must now compete in a global marketplace.

Turning again to Figure 1, we see that a balance of properties leads to a "Goal-State Microstructure" because properties are, for the

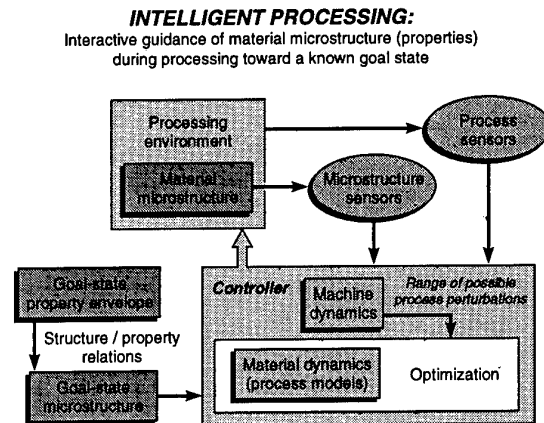


Fig. 1 The IPM loop for a hypothetical materials processing step.

most part, composition and structure sensitive. Thus, the high strength of Nextel 610TM fibers is derived from their fine grain size and small flaw size population, the cut-off wavelength of a $\text{Hg}_{1-x}\text{Cd}_x\text{Te}$ infrared detector depends critically on the value of x ⁽¹⁵⁾, the oxidation rate of Si_3N_4 coatings varies by orders of magnitude when the grain size is changed⁽⁸⁾, and the damage tolerance of metal/ceramic matrix composites is lost when the fiber-matrix interface is allowed to form reaction products⁽¹⁶⁾. An important issue here is that frequently the many properties of interest to a designer are each affected differently by composition/microstructure, and a delicate balance must be struck to obtain the needed property combinations. So we see that today's successful materials must have an "engineered" composition/microstructure which meets a design's specification. They should do this within the smallest possible tolerances so that conservative "design factors" can be eliminated or reduced, and the material's performance fully exploited.

Now let us look at how the processes for materials synthesis and processing have been designed and controlled in the past. The box marked "Processing Environment" in Figure 1 symbolically represents any materials manufacturing process, e.g. it might be a

microwave reactor used to deposit diamond wafers for thermal management applications⁽¹⁷⁾, a sintering furnace to control oxide fiber grain size or a liquid phase epitaxy reactor for depositing $\text{Hg}_{1-x}\text{Cd}_x\text{Te}$. Conventionally, processes like these would be controlled by sensing and attempting to hold constant, the variables of the process, i.e. in a CVD reactor, reactant gas flow rates, microwave power, and the temperature of the substrate upon which deposition occurs. The set-points for these would have been established by trial and error and would correspond to those that had given the highest yield (and lowest cost) material that satisfied the design needs of, let's say, a heat sink for a multichip module. When the windows in process space are wide, and the tolerances on microstructures large, this trial and error approach can expeditiously lead to an acceptable set of process conditions. In fact, most of the materials in use today have used this strategy quite successfully. But, when society tightens the microstructural tolerances, and competition drives the development of new materials and processes with reduced "processability windows", the conventional approach begins to break down. This might first be recognized by a very low yield for the process. But it is also characterized by long lead times to commercialization, questionable quality and very high cost. When placed in the context of today, where the market for materials is rapidly fragmenting into a multitude of small volume "niche" materials, we see that better approaches to processing are needed if we are to continue fielding new materials at the rate of the recent past.

Intelligent Processing of Materials is one approach that is widely used today to win a high stakes game amongst new materials that seek to become a part of tomorrow's engineering materials base^(1, 18, 19). As a feedback control methodology, it is predicated upon the development of "microstructure sensors", Figure 1. These are new sensor technologies originally developed by the nondestructive evaluation community, with a

capability to more directly sense the product being formed and allow inference of its quality defining attributes⁽²⁰⁾. A good example is eddy current (proximity) sensors which can be used during the hot isostatic pressing of alloy powders⁽²¹⁾ and metal matrix composites⁽²²⁾ to measure the remaining porosity during consolidation. Other sensors have been developed for measuring liquid-solid interfaces during solidification of metals/alloys⁽²³⁾ or semiconductors^(24, 25), texture in rolled steel/aluminum alloys^(26, 27), grain size during recrystallization⁽²⁸⁾, fiber diameter⁽²⁹⁾/ crystallographic orientation⁽³⁰⁾ during single crystal sapphire growth, etc. When the appropriate sensor technology exists (or can be developed at a reasonable cost), it becomes possible to attempt feedback control of the product's microstructure and to therefore directly attack the problem of performance variability.

However, this is not as simple as implementing feedback control of process variables. For one thing, there is no direct way to control microstructure - the only variables available for direct actuation have to do with the processing equipment, i.e. heat flux distributions, gas/liquid flow rates, pressures, and so on. One way to use the new sensor measurements for feedback control is to know beforehand what is referred to as "Material Dynamics" in Figure 1, and use this for model-based control. The material dynamics are just a mathematical description (usually greatly simplified) of the process that predict the relationships between the variables one can directly actuate and the microstructural quantities of interest. This process modeling has been an area of intense study during the past two decades and excellent models for many of the phenomena encountered in processing now exist. For example, the density of alloy powder preforms during hot isostatic processing (HIPing) or sintering can be predicted with models developed by Ashby and his coworkers⁽³¹⁾. The software for doing this on a personal computer is widely available⁽³²⁾ and software products are being introduced for handling more complex near net shape

problems⁽³³⁾. By numerically integrating these models, one can even simulate the evolution of the process with time and so predict the material dynamics. Knowledge of the machine's dynamics (i.e. its heating and pressurization rate limits in the HIP case) then allows the prediction of the outcome of any realizable process, and the possibility of implementing the two IPM modalities: designing optimal process schedules via process simulation and using model-based feedback control⁽³⁴⁾ to achieve goal-state microstructures.

In cases where the models are difficult to develop, or are too complex for treatment by the more formal methods alluded to above, other more heuristic approaches are being developed using neural nets⁽³⁵⁾, fuzzy-logic⁽³⁶⁾ and expert systems⁽³⁷⁻³⁹⁾. Indeed, it was an early reliance upon these artificial intelligence techniques that led to the coining of the term Intelligent Processing of Materials. It was not that the community engaged in its development were proposing that other methods were in some way unintelligent!

3. MMC PROCESSING

The designs of future high speed aircraft and propulsion systems have generated a need for stiff, strong, light, oxidation, and creep-resistant materials that can be used at high temperatures^(40, 41). These needs cannot be satisfied by the materials available today, and researchers are developing a variety of advanced composite materials composed of light metal/intermetallic matrices reinforced with silicon carbide or aluminum oxide fibers. The matrices of interest include conventional titanium (e.g. Ti-6Al-4V) or nickel alloys, as well as intermetallics based on Ti_3Al (α_2 -phase), TiAl (γ -phase), Ni_3Al , NiAl , etc.

Metal and intermetallic matrix composites are difficult to process. Contact between molten titanium alloys and the ceramic fibers for more than a second or two results in aggressive chemical reactions, fiber dissolution, and a loss of critical matrix/fiber

properties⁽⁴²⁻⁴⁵⁾, which results in a serious reduction of composite strength⁽⁴⁶⁾. Similar problems are encountered when embedding fiber optic sensors in metals. A variety of novel processing approaches are being developed to bypass this. They include foil-fiber-foil⁽⁴⁷⁾, vapor phase fiber coating⁽⁴⁸⁻⁵⁰⁾, powder cloth⁽⁵¹⁾, and molten spray deposition⁽¹⁹⁾. Each reduces or even eliminates liquid-fiber contact, but all require additional lay-up and consolidation processing to achieve a near net shape composite.

The use of molten droplet spray deposition methods has shown significant early promise for the deposition of conventional and intermetallic titanium alloys on prealigned ceramic fiber arrays⁽¹⁹⁾. The result is typically a 200 μm thick monotape containing parallel, evenly spaced 140 μm SCS-6 silicon carbide fibers in a porous matrix. The monotapes are layed-up to create a preform with the desired fiber architecture and then either hot isostatically or vacuum hot pressed to near net shape^(52, 53), Figure 2. The mechanical properties of the composites formed in this way are determined by the properties of the constituent materials, i.e. the matrix, fiber and interface and by residual stresses/damage induced during processing^(54, 55). In particular, the matrix may be depleted of desirable phases near the fibers^(56, 57), extensive chemical reaction of the fiber's coating can occur⁽⁵⁸⁾ and the consolidation process can cause bending or even fracture of the composite's fibers which has been predicted to result in a dramatic loss of strength⁽⁵⁹⁾.

The dependence of these phenomena upon processing has now been analyzed and the material dynamics captured in new process models and simulation tools. These have been used to explore the processability of different composite systems, to identify optimum process schedules and, in conjunction with microstructure sensors, used for model-based feedback control. Each is now reviewed in more detail as an example of one way in which the IPM approach can be usefully used, and to

help identify where further efforts might be focused, and to explore its value for smart materials synthesis.

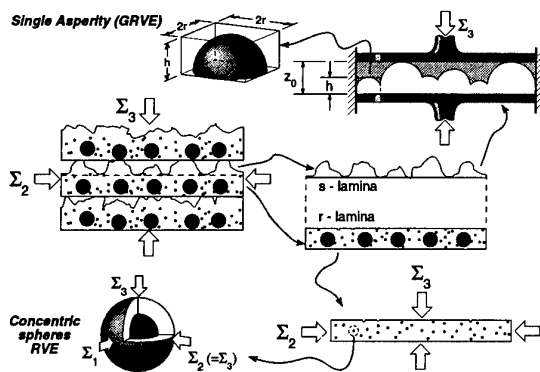


Fig. 2 The complex deformation behavior of a monotape lay-up (left) can be treated by considering the micromechanical response of representative volume elements to simplified states of stress⁽⁵³⁾.

4. CONSOLIDATION PROCESS SIMULATION

During the consolidation of a MMC monotape layup like that shown in Figure 2, densification occurs by the redistribution of matrix material. The fundamental mechanisms by which this is accomplished depends upon the temperature, applied load, and the matrix material. At low homologous temperatures and high pressures (relative to the material's yield stress), plasticity dominates; at high temperatures and low pressures, diffusional flow may be the most important mechanism while intermediate conditions activate power-law creep⁽⁵³⁾. The local forces that drive material transport by these mechanisms within the layup are also able to bend and sometimes fracture the fibers⁽⁵⁷⁾. This is mitigated by the use of high process temperatures which soften the material and facilitate consolidation with smaller local loads. However, prolonged high temperature exposure during processing results in chemical reactions between the fiber coatings and the

matrix with undesirable consequences for both. It also has an adverse effect upon the frictional sliding coefficient of the interface⁽⁵⁸⁾. All of these phenomena have complicated (nonlinear) dependencies upon the process's actuatable variables (temperature, pressure) and are time and material system dependent. They are also influenced by the way in which the previous monotape deposition step was conducted (since this controls the porosity inside the tape and the roughness of its surface). It is a formidable assignment to experimentally establish all this, and this would have to be redone each time the composite system were changed (e.g. as a fiber's strength was improved, or a matrix alloy's composition was refined) or if the conditions of the spray process were varied. Because of this, the consolidation cycles used so far have been suboptimal resulting in composites of sometimes questionable quality⁽⁵⁴⁾.

Recently developed process simulation software promises to overcome this⁽⁶⁰⁾. The simulations solve the fundamental micromechanical/chemical problems encountered in consolidation so that the material states can be calculated. The evolution of these states for any prescribed process cycle results in a temporal evolution of a composite's density, fiber fracture and fiber-matrix reaction.

4.1. Densification

Prior to consolidation, a plasma spray-deposited MMC monotape layup contains typically 35 to 45% internal porosity. Most of this porosity arises as a consequence of the surface roughness, the remainder being in the form of isolated voids within individual monotapes, Figure 2. Upon application of an applied stress, the layup densifies by the inelastic flow of material into the internal voids and by deformation of surface asperities at places where adjacent monotapes are pressed into contact. Recently, a model has been developed⁽⁵³⁾ to predict the density of a

MMC laminate as a function of the applied stress, temperature and time, given only the constituent materials properties and the geometrical parameters of the monotape (i.e. surface roughness distribution).

The complex internal deformation geometry problem is broken down by visualizing each composite monotape as consisting of two layers, or laminae, Figure 2. One, referred to as the "r"-lamina (reinforced lamina) contains the array of fibers, has all smooth sides and typically contains about 10% internal porosity in the form of isolated voids (the exact amount depends on how the spray process was performed), the other, referred to as the "s"-lamina (surface lamina), contains only the surface asperities. Densification of the s-lamina is treated in two stages: at lower relative densities ($D^s_0 \leq D^s \leq 0.85$, where D^s_0 is the initial relative density of the s-lamina), densification occurs by the blunting of asperities. This is referred to as "Stage I" by analogy to the situation encountered in powder consolidation⁽³¹⁾. At higher densities ($0.95 \leq D \leq 1$, where D is the matrix relative density), referred to as "Stage II", densification is more accurately described as the shrinkage of internal, closed voids. A smooth interpolation can be used to describe the transition between stages.

The model describing the Stage I densification of the s-lamina is based on an analysis of the contact stress required to cause blunting of a single hemispherical asperity of radius, r . The results of this unit cell analysis are given in Table 1 in the form of force-density relations for cases where the dominant deformation mechanisms are either plastic yielding, power-law creep, or diffusional flow. The overall response of the s-lamina is obtained by combining the predicted behavior for a single asperity with a statistical model describing the variation in size (r) and height (h) of the asperities on a typical monotape. Two probability distribution functions (ϕ_r and ϕ_h) are introduced, representing the probabilities of encountering asperities of a given radius and height, respectively. The

applied stress necessary to achieve a given densification rate (represented by the rate of change of s-lamina thickness, \dot{z}) is given as the sum of the forces acting on all asperities currently in contact multiplied by the total number of asperities per square meter, ρ :

$$\Sigma(z, \dot{z}) = \rho \int \int_{z=0}^{z_0\infty} \phi_h \phi_r F_c(h, r, D, \dot{D}) dr dh \quad (1)$$

Expressions for the probability density functions ϕ_r and ϕ_h , are given in ref. (53) along with numerical values for the statistical parameters used in the simulations presented below.

Table 1: Constitutive laws for Stage I deformation

<u>Mechanism</u>	<u>Constitutive Law</u>
Plastic Yielding	$F_c = 2\pi r \left(h - z_0 \frac{D_0}{D} \right) \beta \sigma_0$
Power Law Creep	$F_c = \left\{ z_0 \left(\frac{D_0}{D^2} \right) \dot{D} \right\} / \alpha \left[\left[rh - \frac{z_0 D_0}{D} \right]^{\frac{1}{2}-n} \right]$
Diffusional Flow	$F_c = \frac{r^2}{12\pi} g_u(D) a_c(D) \frac{kT (z_0 D_0 / D^2) \dot{D}}{\Omega (\delta D_b + 2\rho D_v)}$

The densification of the r-lamina (and of the s-lamina during Stage II) occurs by the shrinkage of internal voids; these are assumed to be spherical, non-interacting and of uniform size (implying that only homogenous stress distributions are considered). The components of the strain rate are given by the gradient of a potential function, Φ^m where m represents the assumed mechanism of deformation [i.e. plastic yielding (p), power-law creep (c) or diffusional flow(d)]:

$$\dot{E}_{ij} = \Delta \frac{\partial \Phi^m}{\partial \Sigma_i} \quad (2)$$

Here, Δ is a scalar multiplier which may depend on the loading path. Potential functions

used to describe the density-dependent material response for the cases of either plastic yielding, power-law creep or diffusional flow are summarized in Table 2.

Table 2: Potentials used for Stage II densification

<u>Mechanism</u>	<u>Potential</u>
Plastic Yielding	$\Phi^p = \left(\frac{\Sigma_e}{\sigma_0}\right) + \left(-2q(1-D)\cosh\left(\frac{3\Sigma_m}{2\sigma_0}\right)\right) - 1 = 0$
Power Law Creep	$\Phi^c = \frac{B}{n+1} \left\{ a(D)^2 \Sigma_e^2 + b(D)^2 \Sigma_m^2 \right\}^{\frac{n+1}{2}}$
Diffusional Flow	$\Phi^d = \frac{\Omega}{kTR^3} \left\{ \frac{5\pi}{6} \left(\delta D_b + \frac{2}{\pi} R D_v \right) \Sigma_c^2 + \left(\sigma D_b + \frac{3}{4} r_p D_v \right) \Sigma_m^2 \right\}$

The total principal strain rate components within each lamina are obtained as the sum of the contributions from each of the mechanisms:

$$\dot{E}_i = \dot{E}_{p_i} + \dot{E}_{c_i} + \dot{E}_{d_i} \quad (3)$$

For the case of constrained uniaxial compression, the densification rate is then obtained from $\dot{D} = -D\dot{E}_{kk}$.

The relative densities, for the s and r-laminae (D^s, D^r), at time, t , are computed as:

$$D^s(t) = D_0^s + \Delta D_p^s + \int_0^t \left(\sum_{j=1}^2 s_j (\dot{D}_c^s + \dot{D}_d^s) \right) d\tau \quad (4)$$

$$D^r(t) = D_0^r + \Delta D_p^r + \int_0^t (\dot{D}_c^r + \dot{D}_d^r) d\tau \quad (5)$$

where D_0^s and D_0^r are the initial densities of the s and the r-laminae respectively. As perfect plasticity is not a time-dependent mechanism, the increment of densification due to plasticity for each lamina is calculated (ΔD_p^s and ΔD_p^r) for every time step and added to the integral of the densification rate calculated for power law creep and diffusional flow.

Having calculated the relative density for the s and r-layers, rule of mixtures is used to calculate the composite's relative density (D):

$$D = D^s \cdot v^s + D^r \cdot v^r \quad (6)$$

where v^s and v^r are the volume fractions of the s and the r layers respectively.

A convenient way to show the densification response for a material is through the use of HIP maps popularized by Ashby^(31, 32) for powder consolidation. Figures 3 and 4 show examples for the Ti-24Al-11Nb (at %) and Ti-6Al-4V (at %) systems. These figures conveniently display the dependence of density upon pressure, temperature, and time, assuming the temperature and pressure are instantaneously applied and held constant.

4.2. Fiber Fracture

A fiber fracture model based upon micromechanical analyses of representative unit cells can be used to predict the overall response of a lay-up by calculating a sum of all the local (unit cell) responses⁽⁵⁷⁾. The general form of the unit cell chosen for analysis consists of a single fiber undergoing three-point bending due to forces imposed by (three) contacting asperities, Figure 5. An important parameter that determines the response of a given unit cell is the length of the fiber segment in bending which is governed by the statistically distributed asperity spacing. The deflection of the ceramic fiber, which is regarded as deforming elastically under all conditions, is calculated using simple beam theory and is a strong function of asperity spacing. From this deflection, the stress within

the fiber can be calculated and, for a fiber of known diameter, elastic modulus and strength distribution, the probability of its fracture can be determined.

While the unit cell response is relatively easy to describe (only a single ODE is required to be solved), prediction of the overall rate of fiber fracture is quite complicated because as densification occurs, and monotapes are pressed together, the number of asperities in contact along the length of any given fiber continually increases. As these new contacts are established, existing bend segments become sub-divided into smaller (stiffer) cells. Thus, the statistical distribution of bend segment lengths is density-dependent and in order to calculate the number of accumulated fractures at any time, the creation, deflection and elimination of bend cells must be tracked. Elzey and Wadley⁽⁵⁷⁾ have described an approximate approach for this and have developed a stochastic (Monte Carlo) model that has been implemented throughout an entire process cycle. Although complicated in principle, the model predictions have been obtained quickly in practice using a MathematicaTM program operating on a fast (486 processor) personal computer.

An important feature of the fiber fracture model is its dependence on densification; since the current density determines the number of bend cells, the distribution of cell lengths and the deformed heights of all unit cells, the density is used as an input to the fiber fracture model (instead of the applied pressure and temperature). This coupling of models is only one-way of satisfying this need; experimental densification data could also be used. The densification response is assumed not to depend on the number of fibers fractured.

There are many ways to present the outputs of a fracture model. One is to compute the number of breaks occurring per meter of fiber for a process conducted at a fixed densification rate (requiring continual change

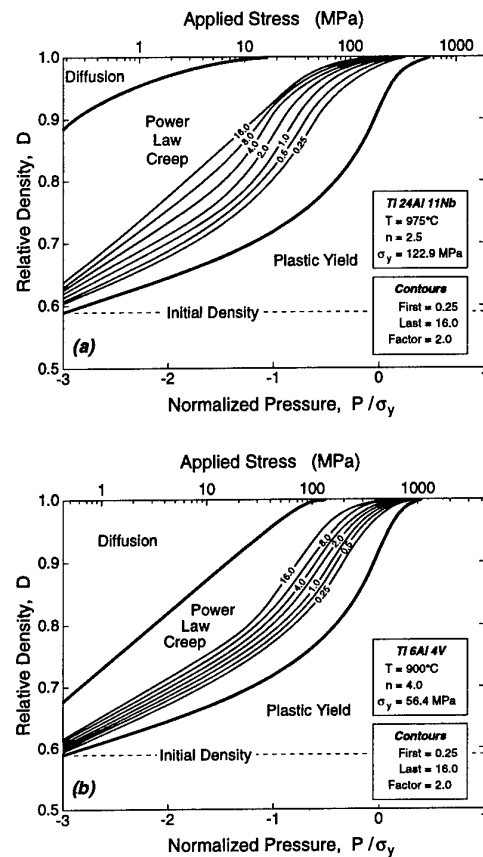


Fig. 3 Relative density versus pressures for various processing times (in hours). The bolder lines denote the locus of points where two mechanisms equally contribute to the density(53).

of applied pressure) and temperature. Figure 6 shows an example of this for the Ti-24Al-11Nb/SCS-6 system. Note how reducing the rate of densification (using a slow pressurization rate) and/or increasing the temperature reduces the damage.

4.3. Reaction Zone Growth

At elevated temperatures, titanium alloy matrices always react with reinforcing/sensing fibers and their protective coatings, eventually degrading the strength of the fiber and adversely affecting its properties. For example, it has been shown that in the Ti-24Al-11Nb/SCS-6 system, the sliding

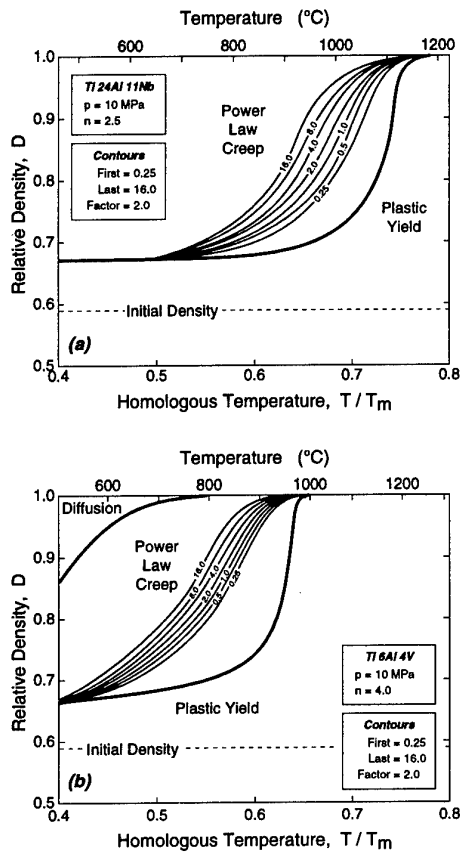


Fig. 4 Relative density versus homologous temperature for various processing times(53) (in hours).

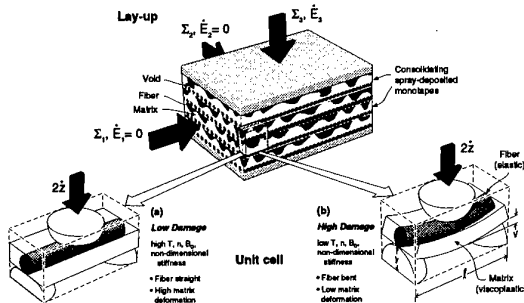


Fig. 5 A representative unit cell used to calculate the probability of fiber fracture during consolidation processing. Note how increasing the inelastic compliance of the matrix or the fiber's rigidity reduces the likelihood of fiber fracture(57).

resistance of the fiber/matrix interface becomes too great (so that damage tolerance is lost) once the thickness of the reaction zone exceeds a critical value of about $1.5\mu\text{m}$ (58). Based on studies of several titanium matrix composite systems, including Ti-24Al-11Nb/SCS-6 and Ti-6Al-4V/SCS-6, the thickness of the reaction zone has been shown to follow a simple parabolic law with respect to time:

$$\delta = kt^{\left(\frac{1}{2}\right)} \quad (7)$$

where k obeys an Arrhenius relationship of the form

$$k = k_0 \exp\left(-\frac{Q}{RT}\right) \quad (8)$$

in which k_0 is the pre-exponential reaction (diffusion) mobility, Q is the activation energy for the reaction and T is the absolute processing temperature.

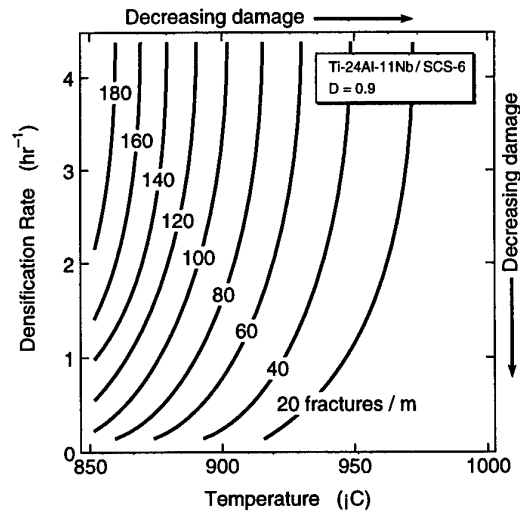


Fig. 6 A contour map showing lines of constant damage in a densification rate - homologous temperature space(57).

The reaction zone growth rate is obtained by differentiating equation 7 and substituting for k using equation 8:

$$\dot{\delta} = \frac{\left(k_0 \exp\left(-\frac{Q}{RT}\right)\right)}{2\delta} \quad (9)$$

4.4. Process Simulation

Models such as those described above, which relate processing conditions to changes in microstructure, may be combined to simulate the evolution of the microstructural “state” of a material during processing⁽⁶⁰⁾. The process simulation can be thought of as the virtual process; it uses the models for microstructural evolution (in this case relative density, fiber fracture and reaction zone growth), “admissible” input schedules (i.e. schedules that are constrained by the limitations of a hot isostatic press or vacuum hot press) and material parameters required by the process models, to predict the microstructure that results from any process cycle.

The process variables during HIPing or vacuum hot pressing, i.e. the inputs to the simulation, are the temperature and applied pressure. The inputs ($T(t)$ and $P(t)$) are time-dependent functions whose absolute values and slew rates are constrained to lie between upper and lower limits (determined by the particular machine used).

$$T_{min} \leq T \leq T_{max} \quad (10)$$

$$P_{min} \leq P \leq P_{max} \quad (11)$$

$$\dot{T}_{min} \leq \dot{T} \leq \dot{T}_{max} \quad (12)$$

$$\dot{P}_{min} \leq \dot{P} \leq \dot{P}_{max} \quad (13)$$

The simulation provides as output, the microstructural state variables as a function of time including the composite’s relative density (D), the cumulative number of fibers fractured (N_f) and the reaction zone thickness (δ). Put

another way, the simulation allows one to trace the path along which the microstructure evolves in a space whose axes correspond to the microstructural state variables.

4.5. Simulation Results

The simulation tool has been used to conduct numerical “experiments” as a way of identifying the relationships between the process conditions and the microstructural state of the composite⁽⁶⁰⁾. To illustrate the approach, results are presented for the consolidation of a conventional titanium alloy (Ti-6Al-4V) composite and one based on the α_2 intermetallic system (Ti-24Al-11Nb) both reinforced with SCS-6 fibers.

Figures 7-9 show the simulation results for a series of process cycles in which either the consolidation temperature or consolidation time have been systematically varied. Consider the α_2 matrix system of Figure 7 first. It shows that as the consolidation temperature is increased from 1100 to 1300K (while the slew rate for temperature is kept constant at $1^{\circ}(K/sec)$ for each simulation), the composite’s relative density at the end of the cycle also increases (ideally, it should be close to unity). Raising the temperature also results in a decrease in the number of fractured fibers but an increase in the thickness of the fiber-matrix reaction product. A small amount of damage may be tolerable for some applications, but reactions that result in more than about a $1\mu m$ thick reaction product result in unacceptable frictional sliding behavior⁽⁵⁸⁾. Figure 8 shows the effect of changing the “soak” pressure for a 1300K temperature, and again we see an increase in density as the pressure is increased, but too much interfacial reaction would occur before full density is achieved. Thus, none of the cycles shown in Figures 7 or 8 would result in a satisfactory composite.

This can be contrasted to the Ti-6Al-4V matrix system in Figures 9 & 10. Here we again see similar trends with the process

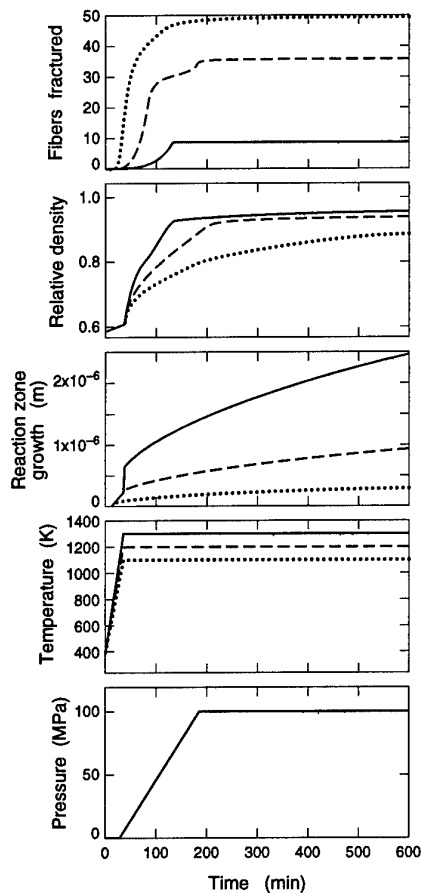


Fig. 7 Simulated consolidation of Ti-24Al-11Nb/SCS-6 system at 100MPa showing effect of changing the “soak” temperature(60).

variables, but in this system both minimal fiber fracture and acceptable levels of chemical reaction can be accomplished with a 1100K/100MPa cycle. Lowering the pressure further reduces the number of fiber breaks but also lowers the final density.

These simulation tools allow one to quickly explore “what if” questions and to use trial and error methods to rapidly converge on acceptable process cycles for the systems that can be processed successfully. They also allow the early determination of those that cannot! The tool also allows one to systematically explore the influence of the material system’s initial state on processing (i.e. on the final state of the previous process step). For example,

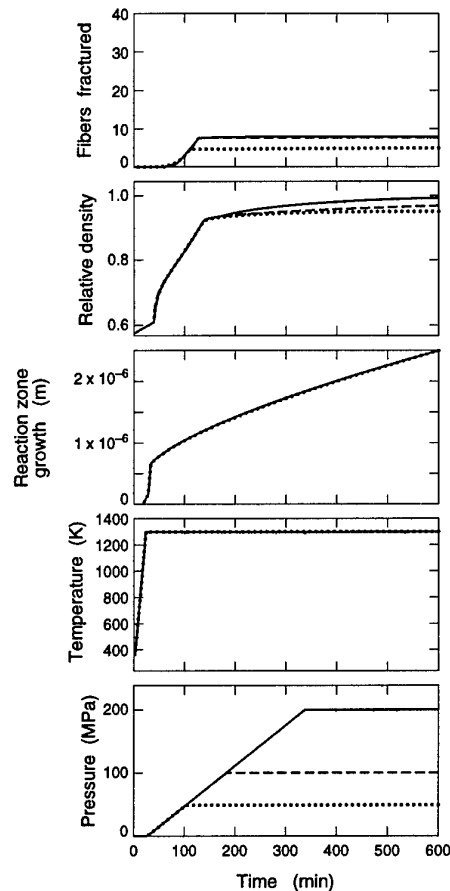


Fig. 8 Simulated consolidation of Ti-24Al-11Nb/SCS-6 system at 1300K showing effect of changing the “soak” pressure(60).

increasing the fiber’s reference strength or decreasing the roughness of the monotapes widens the window of processability and may enable the design of successful process cycles even for the $\alpha_2+\beta$ matrix composite system⁽⁵⁷⁾.

5. PROCESS PATH PLANNING

The use of simulation tools enables one to avoid costly and time consuming experimental trial and error during process design, but to this point it is still trial and error, and no guarantee can be made that human intuition will lead to the optimum process. One ought to be able to do better using formal optimization methods and find truly the best

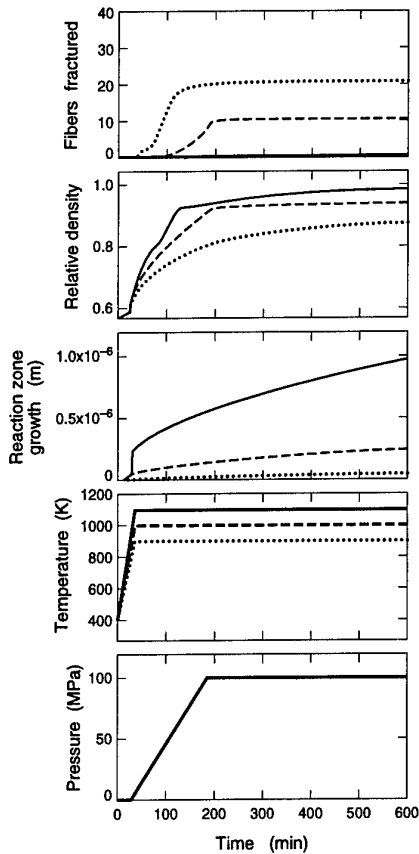


Fig. 9 Simulated consolidation of Ti-6Al-4V/SCS-6 system at 100MPa showing the effect of changing the “soak” temperature(60).

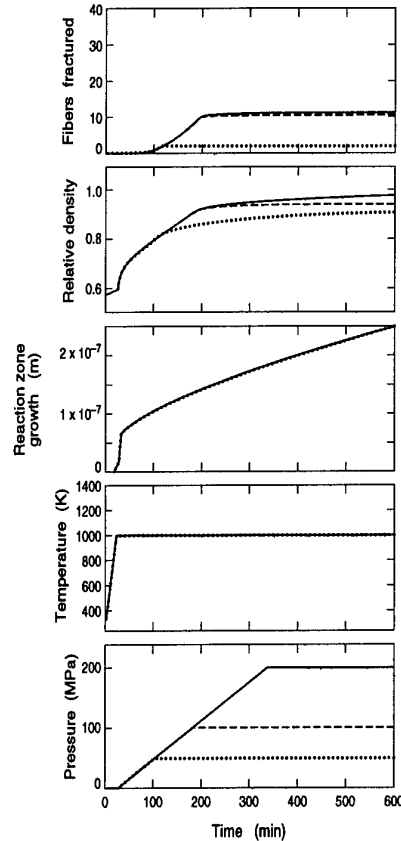


Fig. 10 Simulated consolidation of Ti-6Al-4V/SCS-6 system at 1000 K showing the effect of changing the “soak” pressure(60).

process cycle for a given set of initial conditions, material properties, machine dynamics and desired product goal state. Many different approaches have been developed by the process control community for path optimization. Vancheeswaran et al have explored one promising approach known as Generalized Predictive Control (GPC)⁽⁶¹⁾ which has the advantage of enabling one to fully exploit the predictive capabilities of process models.

GPC algorithms seek the inputs to a plant (the material and machine dynamics referred to in Figure 1) that drive the system's state variables (i.e. the microstructure) to a desired goal state⁽⁶⁵⁾. This approach was

chosen for study because the material's response to process stimuli vary greatly from between the beginning and end of a process cycle. Many other (considerably simpler) approaches could be used instead of GPC if the materials dynamics did not change during the process. The GPC method is a self-tuning technique encompassing a multi-step predictor to achieve a more robust control. It uses a receding horizon philosophy in which the controller predicts and accounts for the changes in the controlled variable (density, number of fiber fractures, reaction zone thickness,...) that will occur in the future using present process knowledge and candidate controller actions.

The optimization problem that needs to be solved is schematically shown in Figure 11. At any moment in the consolidation process, the material's state can be represented by a point in a relative density, reaction zone thickness, fiber deflection (i.e. probability of fiber fracture) state space. It will have reached this point along some path originating from the lower left in the figure. The consolidation process is irreversible, and so all future paths that are reachable by changing the machine conditions are enclosed in a generalized cone. The best (optimum) process path in state space will take the current material to the goal state.

To implement the GPC approach, one must know the dynamic responses of a) the machine used for consolidation and b) the material being consolidated, Figure 12. The predictive models discussed above serve the latter purpose well. The dynamic response of the HIP machine can sometimes exhibit complexity (e.g. coupling between temperature and pressure) but for exploring the process path optimization approach, this can be considerably simplified. To illustrate the approach, Vancheeswaran et al.^(61,67) have assumed that the machine dynamics, x_m , are ideal:

$$x_m = \eta = \begin{bmatrix} T \\ P \end{bmatrix} \quad (14)$$

$$\frac{d\eta}{dt} = u = \begin{bmatrix} \dot{T} \\ \dot{P} \end{bmatrix} \quad (15)$$

Therefore, the controller output is assumed to be the commanded values and rates, subject to satisfying the processing equipment's (limitations) constraints. The equipment constraints can be thought of as placing upper

and lower limits on the pressure and temperature and their slew rates:

$$\dot{T}_{mc} \leq \dot{T} \leq \dot{T}_{mh} \quad (16)$$

$$\dot{P}_{md} \leq \dot{P} \leq \dot{P}_{mp} \quad (17)$$

$$P_{min} \leq P \leq P_{max} \quad (18)$$

$$T_{min} \leq T \leq T_{max} \quad (19)$$

where \dot{T}_{mh} and \dot{T}_{mc} are the maximum heating and cooling rates, respectively, \dot{P}_{mp} and \dot{P}_{md} are the maximum pressurizing and depressurizing rates respectively.

The consolidation model can be written:

$$\dot{x}_h(t) = F(x_h(t), \eta(t)) \quad (20)$$

$$0 \leq G = (x_h(t), \eta(t)) \quad (21)$$

where

$$\dot{x}_h(t) = F(x_h(t), \eta(t)) \quad (22)$$

$$x_h(t) = \begin{bmatrix} D(t) \\ v_i(t) \\ r(t) \end{bmatrix} \quad (23)$$

represents the materials dynamic response and

$$\eta(t) = \begin{bmatrix} T(t) \\ P(t) \end{bmatrix} \quad (24)$$

Here $x_h(t)$ is a state vector whose components are the relative density of the material's s-lamina $D^s(t)$, the deflection of a fiber in the i-th unit cell $v_i(t)$, and the fiber's reaction zone thickness $r(t)$. $\eta(t)$ is defined as the environment vector, whose components are the applied temperature and pressure. The vector field $F(x, \eta)$ is complicated and is given

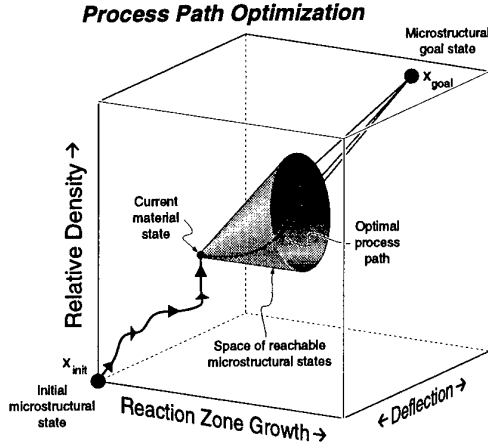


Fig. 11 The process path optimization problem encountered in consolidation processing of metal and intermetallic matrix composites(61).

by the time dependent mechanisms of the states described earlier. It can be written:

$$F(x_h, \eta) = \begin{bmatrix} \sum_{i=1}^2 S(x)(PLC_s(x_h, \eta) + Dif_s(x_h, \eta)) \\ (g(D, \eta) - h(v_i, T))_i \\ r(r, T) \end{bmatrix} \quad (25)$$

The time dependent densification mechanisms due to power law creep are denoted $PLC_j(x_h, \eta)$ and for diffusional flow by $Dif_j(x_h, \eta)$. The densification of the composite is modeled as two distinct layers, the s and the r layers, which are considered as independent states in the non-linear simulation. Since the density of the s -layer is modeled with two different geometries (Stage I and II), the smoothing functions described in Ref. (53) are also incorporated. The inequality constraint $G(x, \eta)$ is used as a way to introduce the plastic yielding (instantaneous) contribution to densification. Plasticity is modeled as a time independent mechanism (that is the densification response to an applied stress occurs instantaneously) and so the resulting

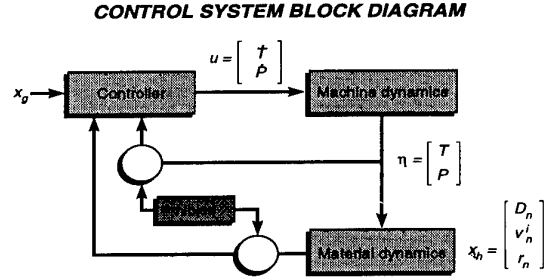


Fig. 12 The architecture of the composite consolidation control problem. The vectors u and h represent the plant controls. D_n , V_n and r_n are the materials (time evolving) density, the fiber deflection suffered by the i -th unit cell and the thickness of fiber-matrix interface(60).

vector field has finite discontinuities, which considerably compounds the problem.

5.1 Optimization Methodology

Implementation of the optimization scheme has been achieved by calculating the states (using locally linearized models) at discrete (2 minute) intervals during the process, out to a "look-ahead" horizon of 40 minutes (20 sampling intervals, N_l). An optimal process variable schedule, $\eta(t)$, can then be designed by perturbing the actuator input slew rates (which are constrained by the machine) such that they simultaneously lie in their admissible space and minimize an objective function which is a weighted function of the squared (Euclidean) distance between the projected future material states (based on the linearized model) and a user defined goal state. The function, E , to be minimized is:

$$E = \frac{1}{N_l^2} \sum_{k=1}^{N_l} k^2 [x(k) - x_g]^2 \quad (26)$$

The objective function is quadratic and uses an aggressive strategy by weighting the future more heavily than the present (because of k^2 in Eq. 26). The specifications

(constraints) and the objective function are easily proven to be convex and therefore the (locally) optimal temperature and pressure slew rates can be found by convex programming. The constraints in the convex optimization problem can be set up as a set of Kuhn-Tucker Equations and solved using the MATLAB optimization toolbox⁽⁶²⁾.

A sequential quadratic programming (SQP) method is then used to solve the problem and is guaranteed superlinear convergence by using a quasi-Newton updating procedure for accumulating second order information. Once the optimal values of the temperature and pressure slew rates are found, they are used as inputs to the simulation (non-linear models) which is then integrated forward by one sampling interval (2 minutes). A linearization is then conducted about this new operating point and the process is repeated.

Figures 13 & 14 show examples of optimal temperature and pressure cycles calculated using the GPC method together with the predicted temporal evolution of the state vector components. The goal state for this system was a relative density of one, a reaction product thickness of $0.6\mu\text{m}$ and zero deflection for each of the unit cells. The HIP machine was assumed to have a maximum operational temperature and pressure 1100K and 100MPa, a temperature slew rate of 1K/s and pressurization rate of 0.022MPa/s. This "good" result was obtained by also applying a time delay constraint on the pressure slew rate. When this is not included, the GPC designed cycle closely approaches the goal state density and reaction layer thickness but incurs significant fiber fracture very early in the process. This happens because the controller fails to increase the machine's temperature fast enough to soften the matrix and avoid large fiber deflections. Effects like this can also be overcome by increasing the weighting attached to fiber damage contributions to the current state - goal state vector (Eq. 26) during the convex optimization step.

6. SENSOR TECHNOLOGY

The direct measurement of a component's density throughout a consolidation process cycle allows one to rapidly evaluate the validity of consolidation models⁽⁶³⁾. It also enables one to implement feedback control about a planned path in state space provided the models for fiber fracture and reaction zone growth are reliable. The reliability of the fracture model depends on the reliability of densification kinetics and the assumed strength properties for the fiber. Since the former could be a directly sensed quantity, the feedback control approach requires only reliable fiber strength data and kinetic parameters for fiber-matrix reactivity. Both can be obtained to more than adequate precision with a few simple experiments.

During consolidation processing no mass change occurs and so the relative density can be obtained by making measurements of the volume or shape of the component during consolidation. This can be done using multifrequency eddy current techniques^(21, 22, 63). Probe-type sensors like those shown in Figure 15 have been used for measuring the separation distance between a fixed probe-tip and the (changing) position of the sample surface near the probe tip⁽²²⁾. Pairs of probes maintained a fixed (or known) distance apart then allow determination of a component's thickness. In a sense, they become eddy current calipers. Other probe array configurations can give the dimensional changes of even complex shaped parts if this is necessary.

The response of these eddy current probes depends upon the probe's design/operating frequency, the electrical/magnetic properties of the component, and the component's shape in the vicinity of the probe. Relationships between these parameters and the impedance of the probe/test circuit have been investigated to perfect the sensor's design and develop algorithms to analyze multifrequency impedance data so that the component's

dimensions may be deduced to the needed level of precision for model verification or feedback control. For axisymmetric configurations, the analytical approach of Dodd and Deeds⁽⁶⁴⁾, together with a network analysis of the test circuit, may be used to derive the fundamental relationships required. For samples of more complex shape, an electromagnetic finite element method can be used⁽⁶⁵⁾

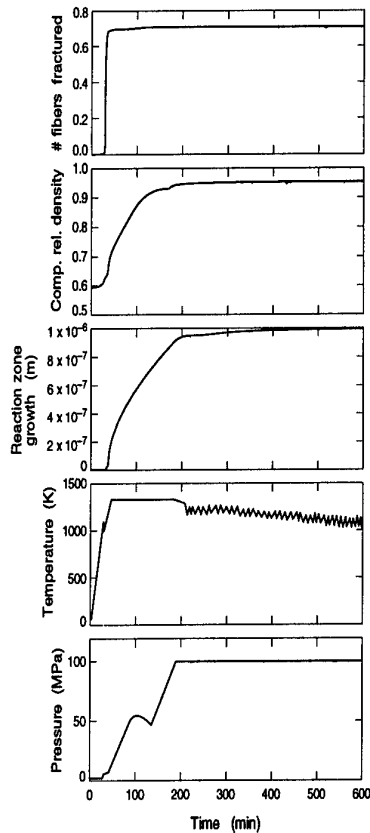


Fig. 13 Example of a calculated optimal temperature/pressure path and resulting microstructural evolution for the Ti-24Al-11Nb/SCS-6 system(61).

Normally, a two-coil design for each probe (as schematically indicated in Figure 13) is used so that the measured response is, to first order, independent of temperature (this avoids the need for active cooling of the sensor which is impractical in the HIP environment). The primary coil of the sensor, Figure 14, is

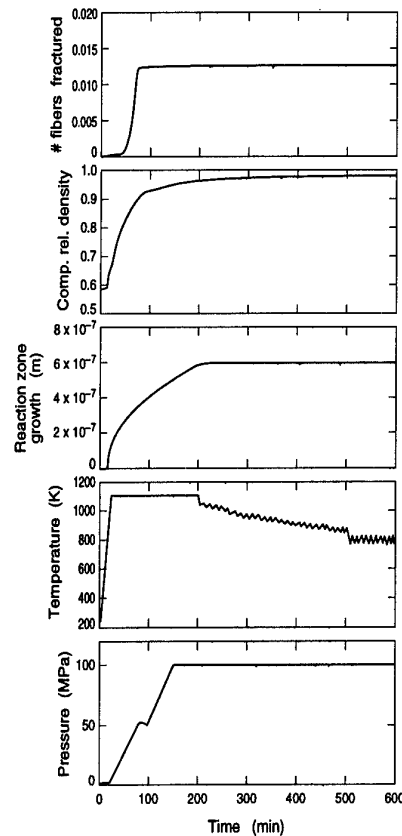


Fig. 14 Example of a calculated optimal temperature/pressure path and resulting microstructural evolution for the Ti-6Al-4V/SCS-6 system(61).

connected to a variable frequency oscillator with optional power amplification. The current (I_p), that flows in the solenoid generates an electromagnetic field, a fraction of which links the sample of interest and the secondary coil. By measuring the voltage drop (V_p), across a precision resistor (R) to ground, the value of the primary current (I_p) can be continuously monitored. The fluctuating electromagnetic field associated with the primary current induces eddy currents in the nearby conducting sample. The eddy currents, whose magnitude depends upon the rate of change of flux (which increases with frequency), act to oppose the change in field (Lenz's law) and thereby perturb the field of the primary coil. The perturbed field can be conveniently measured with a second coil aligned coaxially with the

primary. The voltage induced in the secondary coil (V_s), though small can be amplified, and if measured with a high impedance instrument, is independent of the secondary windings resistance, and thus the sensor's temperature.

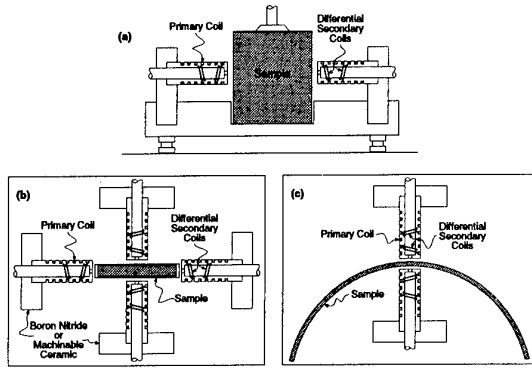


Fig. 15 Schematic illustrations of the use of eddy current probe sensors to measure shape (volume) changes during consolidation.

The ratio $V_s:V_p$ defines a sensor gain (G), and the difference in phase between primary and secondary, $\phi = \phi_s - \phi_p$, defines the measured phase. Then at any measurement frequency, the complex impedance components can be found from:

$$\text{Real}Z = (G/G_o)\text{Sin}(\phi - \phi_o) \quad (27)$$

$$\text{Imag}Z = (G/G_o)\text{Cos}(\phi - \phi_o) \quad (28)$$

where the subscript zero refers to the values of an empty coil located far from any conductor.

The impedance normalized by the empty coil value is plotted on the right in Figure 16 for two different distances h above a uniform conductor with the electrical conductivity of copper. At low frequencies, the rate of change of flux is small, and the eddy current density is low, but is distributed deeply within the sample because the skin depth δ is large (recall that $\delta = (2/\omega\sigma\mu)^{1/2}$ where ω is the radial frequency, σ the conductivity and μ the sample's permeability). At low frequencies there is quite a large change of phase because

the flux deeply penetrates the conductor, but almost no eddy current losses occur because the eddy current density is small, so the impedance is almost purely inductive (imaginary). As the frequency is increased, eddy current densities increase resulting in greater losses that are reflected by the increase in the real part of Z . The imaginary component decreases because the flux does not penetrate as deep into the sample. At very high frequencies, the skin effect limits the depth of flux penetration severely, and the total eddy current losses also decrease because the volume supporting the eddy currents becomes very small, and overpowers the increase in current density associated with the now very high rate of flux change.

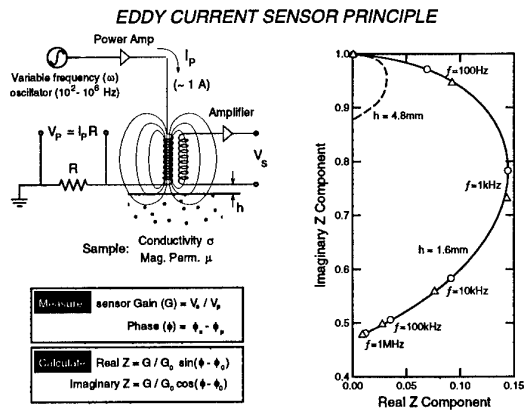


Fig. 16 The eddy current probe sensors measurement principle.

In the limit, the eddy current losses go to zero and the impedance curve intersects the imaginary axis at a value determined by the ratio of the flux linking the sample and the secondary coil to the total flux. Thus, as the sample densifies, and its surface moves away from the sensor (see for example the curve for $h=4.8\text{mm}$), fewer flux lines link the sample and the high frequency intercept moves towards the origin at ($Z=0+1j$).

Using an axisymmetric finite element model the sensor configuration shown in Figure 15 has been analyzed in detail⁽²²⁾. The analysis consists of solving for the unknown

magnetic vector potential \underline{A} over a range of frequencies for different lift-offs and sample conductivities and then computing the coil impedances. Model parameters such as coil diameter, coil length, the number of turns, the number of secondary coils and their placement, sample thickness, material parameters and loading conditions can then be easily studied, and optimized sensors designed for various applications. This has all been significantly simplified by the advent of user friendly electromagnetic finite element codes⁽⁶⁵⁾.

The governing equations for these types of problems follow from Ampere's Law:

$$\nabla^2 \underline{A} = -\mu \underline{J} \quad (29)$$

where μ is the magnetic permeability, \underline{A} the magnetic vector potential, and \underline{J} is the total current density. It is composed of two contributions:

$$\underline{J} = \underline{J}_{eddy} + \underline{J}_{coil} \quad (30)$$

The induced eddy current density within the sample can be written as,

$$\underline{J}_{eddy} = \sigma \underline{E} = -\frac{\sigma \partial \underline{A}}{\partial t} \quad (31)$$

where \underline{E} is the electric field and σ is the electrical conductivity. Substituting for \underline{J} in Amperes Law gives the governing differential equation:

$$\nabla^2 - \mu \sigma \frac{\partial}{\partial t} \underline{A} = -\mu \underline{J}_{coil} \quad (32)$$

With sinusoidal excitation,

$$\underline{J}_{coil} = J_{coil} e^{-j\omega t} \quad (33)$$

and,

$$\underline{A} = A e^{-j\omega t} \quad (34)$$

Thus, the governing equation reduces to the fundamental eddy current relation,

$$\nabla^2 \underline{A} + j\omega \mu \sigma \underline{A} = \mu \underline{J}_{coil} \quad (35)$$

The boundary conditions are that \underline{A} and its normal derivative are continuous across each boundary.

The impedance measured experimentally depends upon the average value of the vector potential at the location of the secondary coil:

$$Z = \frac{4\pi^2 N_s r_s f}{I_p} [Im(\underline{A}_{ave}) - jRe(\underline{A}_{ave})] \quad (36)$$

where f is the excitation frequency (Hz), N_s is the number of secondary coil turns, r_s is the secondary coil radius and I_p the primary coil current.

One usually measures an impedance normalized by the impedance of the probe when it is located far from a sample. This empty coil impedance, Z_o , is given by:

$$Z = \frac{4\pi^2 n_s r_s f}{I_p} [Im(\underline{A}_o) - jRe(\underline{A}_o)] = R_o + j\omega L_o \quad (37)$$

where \underline{A}_o is the vector potential in the absence of the sample, R_o is the equivalent resistive impedance component and ωL_o the empty coil's inductive reactance component. In general $\omega L_o \gg R_o$ and so the normalized impedance,

$$Z_n = \frac{R + j\omega L}{R_o + j\omega L_o} \equiv \frac{R}{\omega L_o} + \frac{j\omega L}{\omega L_o} \quad (38)$$

$$= [-Im(\underline{A}_{ave}) + jRe(\underline{A}_{ave})] / Re(\underline{A}_o)$$

For a differential sensor (i.e. one with two spatially separated opposingly wound pick-up coils), the impedance is calculated by algebraically summing the impedance of the individual secondaries.

The normalized high frequency impedance for a probe coil with a single secondary is shown versus lift-off in Figure 17 (curve 4). One sees that for larger separation distances, the effect of a small further change in separation distance becomes progressively

more difficult to observe. In practice, one is interested in the final stages of shrinkage of a sample when the surface has moved ~10% of the sample thickness away from the probe. If the probe diameter is substantially less than the sample thickness results in a loss of sensitivity to the elimination of a sample's final porosity.

One way to overcome this limitation is to increase the sensitivity at larger separation distances by increasing the sensor's diameter. But this increases the sensitivity to concurrent changes in lateral sample dimensions (length and width). An alternative approach involves the use of a differential secondary configuration. Figure 17 shows the calculated normalized impedance for several differential sensor designs (shown on the right) with secondary coil separations of 3.2, 6.4, and 9.6mm. The normalization practice now inverts the impedance plane diagram but one notes that there is now a much stronger effect of impedance upon lift-off.

The size of the impedance curve, can be controlled by varying the secondary coil separation. The effect of this separation upon the normalized imaginary Z-component versus lift-off relationship is shown in Figure 17. We see that the sensitivity to lift-off (i.e., the slope of the curve) is determined by the number and separation of the secondary coils. In particular, we note that there is considerable enhancement in far field sensitivity (i.e., lift-offs greater than 4mm) for these differential sensor geometries.

Based upon these results, sensors have been designed using boron nitride preforms and high temperature (e.g., platinum or molybdenum) windings and used to measure changes in the thickness of composite samples to better than 20 μ m precision during HIP cycles to temperatures in excess of 1000°C. They have been used both to evaluate the predictions of densification models and for on-line process control. The accuracy appears to be limited by thermal effects upon the dimensions of the sensors and changes to the electrical conductivity of its components and

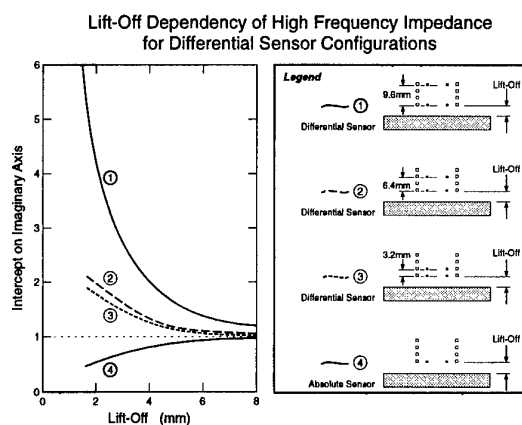


Fig. 17 Calculated sensor responses for different eddy current sensor probe designs(22).

the sample as the temperature varies. Further work is needed to understand the subtle consequences of these.

7. FEEDBACK CONTROL

The feedback control of microstructural states during composite consolidation is a formidable problem. The optimal controller will vary throughout the process, the dynamics are highly nonlinear, irreversible, and only some of the states are sensed. However, because the dynamics of composite consolidation are fairly slow (the process requires several hours to complete), a relatively small closed-loop bandwidth is required for successful control. Hence, the Nyquist sampling rate for the sensors is low and there is ample time (1-2 minutes) for computations in a control loop. In view of this, and given the difficulty of the feedback control problem, it has been logical to consider controller architectures that might normally be too computationally intensive for processes requiring faster sensor sampling rates.

One that may be suitable for this type of application is shown in Figure 18. It was originally designed to allow the control of density (D) and grain size (G) during the consolidation of powders using models

developed by Ashby and others⁽⁶⁶⁾. In view of the similarities between this and composite consolidation, it appears a good place to begin an attack of the composite problem. The architecture functions by constantly forming a local linearization of the material dynamics which is then used in a controller design procedure (in this sense it is similar to GPC path planning). The controller then attempts to establish a temperature and pressure schedule that steers the current material state, x_h to the desired goal state x_g .

The architecture shown in Figure 18, uses what is known as an observer based controller. In this approach the observer (estimator) uses the linearized process models to estimate future material states (by applying Kalman filtering) given the present estimated states $(\hat{D}, \hat{G}, \hat{T}, \hat{P})$, the sensed states (D, G, T, P) , the current actuator inputs (\dot{T}, \dot{P}) , and a gain matrix L . The observer based controller is then designed using linear quadratic regulator (LQR) theory. Here, the states (either estimated or sensed) are optimally fed back to the linearized system as inputs after they are acted upon by some gain matrix K to drive the system to the future material states. These problems have been rigorously studied and have well known solutions (to find K and L) involving algebraic Ricatti equations. To ensure stable observation and control of the system, coprime factorizations of the plant and the nominal controller are computed using the matrices K and L with formulas found in refs. (68, 69). At this point, a stable nominal controller has been found (for some point in the process) which adjusts the actuator inputs (U) to reduce the effects of sensor and actuator noise, Figure 19. The observer based controller is then continuously redesigned using new local linearizations of the system, as the process progresses through the consolidation cycle.

To drive the regulated variables (D, G) to their goal (x_g), a finite response Q filter is added to the system, Figure 19. W represents the set of exogenous inputs (the goal state (x_g), the sensor noises and actuator disturbances), Z

comprises the regulated variables (i.e. the controls, (\dot{T}, \dot{P}) , the machine states (T, P) and the material states (D, G) , U comprises the actuator inputs (\dot{T}, \dot{P}) , and Y the sensed outputs $(D, G, T, P$ and x_g). The nominal controller is then modified or augmented to produce a signal e (with the same number of dimensions as the sensed outputs Y), and an auxiliary input signal v (of the same size as the actuator inputs U). The important point to this controller architecture is that the map from e to v , H_{ev} is forced to zero, so that when a finite impulse response filter Q is inserted, the overall transfer matrix $G_{overall}$ assumes the form:

$$G_{overall} = H_{zw} + H_{zv}QH_{ew} \quad (39)$$

which will then have the affine structure in Q needed for convex optimization. This convex optimization results in the elements of the Q matrix Q_{ij} , such that the sensor and actuator noises are minimized, the closed loop system is stable, and the regulated variables are driven to their goal state.

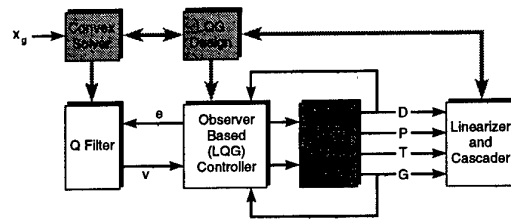


Fig. 18 Feedback control architecture designed to control density (D) and grain size (G) during the HIPing of powders⁽⁶⁶⁾.

The convex program is set up to minimize some objective function (in this case a weighted sum of the Euclidean distance between the goal state and the projected future states) to select the "best" controller (locally). Moderately sized convex programs can be solved easily in the available time. Once Q is found, controller specifications are complete, and the control is calculated and implemented

until the next sensor sampling of the process, whereupon the process is repeated. Figure 18 shows an example of a simulation conducted with this controller (assuming perfect sensing of D and G). The goal states are shown in dashed lines, and it is clear that for this case at least, the controller is able to practise the principles of IPM control.

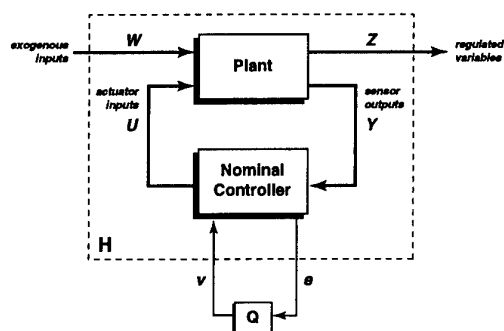


Fig. 19 System after closing loop with nominal controller.

This approach to feedback control has now begun to be applied to HIP consolidation processing of composites with encouraging initial results⁽⁶⁷⁾. The HIP consolidation of metal alloy powders/composites to a goal state microstructure occurs by similar mechanisms to other deformation processes such as vacuum hot pressing, isothermal forging, hot rolling, extrusion, superplastic forming/diffusion bonding, etc. These feedback control concepts may be a logical starting point for designing controllers for these processes also.

8. CONCLUSIONS

Intelligent Processing of Materials is a new way of designing and controlling advanced materials synthesis and processing. It is making a pervasive impact across a broad spectrum of materials and processes. Predictive process modeling, combined with convex optimization techniques, are beginning to allow materials engineers to rapidly design processes that result in the attainment of a goal state microstructure - a key step in the

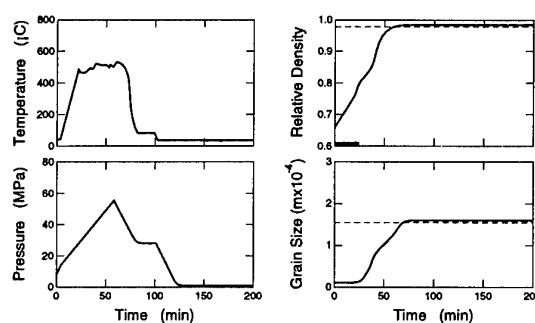


Fig. 20 Simulated performance of an IPM control system for alloy powder densification. The goal state microstructures are indicated by dashed horizontal lines⁽⁶⁶⁾.

development of a processing technology that will finally enable the high yield manufacture of highly engineered materials like smart materials/structures. When microstructure attribute sensors are available, a new (for materials synthesis/processing) type of IPM feedback control methodology becomes feasible. The first tentative steps in this direction have been made and at least one approach appears to hold promise. However, its application is paced by the emergence of new microstructure sensors. As the materials community finds ways to field non-invasive techniques based on eddy currents, laser ultrasonics, dielectric spectroscopy, microwave reflectivity, ellipsometry, etc. to satisfy these sensor needs, the extension of IPM as a feedback control method is likely to grow rapidly to reduce process costs and realize the potentially significant improvements in the yield/quality of high performance smart materials.

Acknowledgments

This lecture is based upon a presentation given at the U.S. Army 41st Sagamore Conference.

References

1. H.N.G. Wadley and W.E. Eckhart, JOM, 41, (10), 1989.

2. D.G. Backman, D. Wei, L.C. Filler, R. Irwin and J. Collins, in "Advanced Sensing, Modelling and Control of Materials Processing," Ed. by E.F. Matthys and B.G. Kushner, TMS (Warrendale), p. 3, 1992.
3. S.D. Ridder, S.A. Osella, P.I. Espina and F.S. Biancaniello, in "Thermal Structures and Materials for High-Speed Flight," Ed. by E.A. Thornton, AIAA (Washington, D.C.), p. 499, 1992.
4. B.G. Kushner and R.J. Schaefer, in "Intelligent Processing of Materials," Ed. by H.N.G. Wadley and W.E. Eckhart, TMS (Warrendale), p. 55, 1990.
5. R.J. Schaefer, in "Thermal Structures and Materials for High-Speed Flight," Ed. by E.A. Thornton, AIAA (Washington, D.C.) p. 523, 1992.
6. D.G. Backman, E.S. Russell, D.Y. Wei and Y. Pang, in "Intelligent Processing of Materials," Ed. by H.N.G. Wadley and W.E. Eckhart, TMS (Warrendale), p. 17, 1990.
7. H.N.G. Wadley, D.M. Elzey, L.M. Hsiung, Y. Lu and D.G. Meyer, in "Monograph on Flight-Vehicle Materials, Structures and Dynamics Technologies - Assessment and Future Directions," Ed. by A.K. Noor and S.L. Venneri, In Press, 1994.
8. J.R. Strife, W.Y. Lee, R.D. Veltri, C.F. Sack, R.J. Kee, G.H. Evans, R.S. Larson, D.S. Dandy, M.E. Coltrin, P. Ho and R.J. Buss, in "Thermal Structures and Materials for High-Speed Flight," Ed. by E.A. Thornton, AIAA (Washington, D.C.) p. 485, 1992.
9. M.E. Coltrin, unpublished work.
10. D.E. Witter, in "Intelligent Processing of Materials", Ed. by H.N.G. Wadley and W.E. Eckhart, TMS (Warrendale), p. 91, 1990.
11. Y. Lu, M.V. Moore, D.T. Queheillalt, and H.N.G. Wadley, in "Proceedings of Review of Quantitative Nondestructive Evaluation, Vol 13," Ed. by D.O. Thompson and D.E. Chimenti, (NY), 1994.
12. Y.W. Kim, in "Advanced Sensing, Modeling and Control of Materials Processing," Ed. by E.F. Mattheys and B.G. Kushner, TMS (Warrendale), p. 45, 1992.
13. D. Apelian et al, "On-Line Control of Metal Processing," NMAB-444, National Academy Press, 1989.
14. 3M Company Data Sheet.
15. R.M. Wood, "Optical Materials," Institute of Materials (London), p. 80, 1993.
16. P.E. Cantonwine, Master of Science Thesis, University of Virginia, 1993.
17. R.J. Koba, in "Diamond Films and Coatings," Ed. R.F. Davis, Noyes (Park Ridge, NJ), p. 147, 1992.
18. P.A. Parrish and W.G. Barker, JOM, 42 (7), p. 14, 1990.
19. D.G. Backman, JOM, 42 (7) p. 17, 1990.
20. R. Mehrabian and H.N.G. Wadley, JOM, 37 (2), p. 51, 1985.
21. A.H. Kahn, M.L. Mester and H.N.G. Wadley, in "Proc. 2nd International Conference on Hot Isostatic Pressing," Ed. by R.J. Schaefer and M. Linzer, ASM (Metals Park), p. 341, 1989.
22. K.P. Dharmasena and H.N.G. Wadley, in "Review of Progress in Quantitative NDE," Vol 10B, Ed. by D.O. Thompson and D.E. Chimenti, Plenum Press, (NY), p. 1757, 1991

23. F.A. Mauer, S.J. Norton, Y. Grinberg, D. Pitchure and H.N.G. Wadley, *Met. Trans B*, 22B, p. 467, 1991.
24. K.P. Dharmasena and H.N.G. Wadley, *J. Crystal Growth*, p. 553, 1993.
25. K.P. Dharmasena and H.N.G. Wadley, *J. Crystal Growth*, 1996, In Press.
26. R.B. Thompson and A.V. Clark, in "Intelligent Processing of Materials," Ed. by H.N.G. Wadley and W.E. Eckhart, TMS (Warrendale), p. 227, 1990.
27. R.B. Thompson, S.S. Lee and J.F. Smith, *Ultrasonics*, 25, p. 133, 1987.
28. C.B. Scruby, Private Communication, 1994.
29. D.G. Backman, D. Wei, L.C. Filler, R. Irwin, and J. Collins, in "Advanced Sensing, Modelling, and Control of Materials Processing," Ed. by E.F. Matthys and B.G. Kushner, TMS (Warrendale), 1992.
30. H.N.G. Wadley, Y. Lu and J.A. Goldman, *J.NDE*, In Press, 1994.
31. W.B. Li, M.F. Ashby and K.E. Easterling, *Acta Metallurgica*, 35, p. 2831, 1987.
32. M.F. Ashby, HIP 6.0 Software for HIP Diagrams, Dept. Eng., Univ. of Cambridge, UK, 1990
33. L. Christodoulou, BDM Product Sheet, 1993.
34. D.G. Meyer and H.N.G. Wadley, *Met Trans B*, 24B, p. 289, 1993.
35. S.A. Osella, in "Intelligent Processing of Materials," Ed. by H.N.G. Wadley and W.E. Eckhart, TMS (Warrendale), p. 339, 1990.
36. A.L. Moran and D.R. White, *JOM*, 42 (7), p. 21, 1990.
37. V.V. Badami, P. Nielsen and J.B. Comly, in "Intelligent Processing of Materials," Ed. by H.N.G. Wadley and W.E. Eckhardt, TMS (Warrendale), p. 369, 1990.
38. S.B. Dolins and J.D. Reese, in "Intelligent Processing of Materials," Ed. by H.N.G. Wadley and W.E. Eckhardt, TMS (Warrendale), p. 385, 1990.
39. M. Makhlof, R. Makhlof, R.K. Heinzmann, J. J. Baush, R.D. Sisson, in "Advanced Sensing, Modelling and Control of Materials Processing," Ed. by E.F. Matthys and B.G. Kushner, TMS (Warrendale), p. 223, 1992.
40. D.L. Anton and D.H. Shah, in "MRS Symposium Proceedings", 133, Ed. C.T. Liu, A.I. Taub, N.S. Stoloff, and C.C. Koch, MRS (Pittsburgh), p. 361, 1989.
41. J.R. Stephens, in "Metal and Ceramic Matrix Composites: Processing, Modelling and Mechanical Behavior," Ed. by R.B. Bhagat, A.H. Clauer, P. Kumar, and A.M. Ritter, TMS (Warrendale), p. 3, 1990.
42. N.A. James, D.J. Lovett, and C.M. Warwick, in "Composites: Design, Manufacture and Application, ICCM VIII," Ed. by S.W. Tsai and G.S. Springer, SAMPE, 2 (19), p. 11, 1992.
43. M.S. Misra and S.G. Fishman, *ibid*, p. 18A1.
44. T. Onzawa, A. Suzumura, and J.H. Kim, *ibid*, p. J1.
45. W.J. Whatley and F.E. Wawner, *J. Mater. Science Letters*, 4, p. 173, 1985.
46. S. Ochiai and Y. Murakami, *J. Mater. Science*, 14, p. 831, 1979.
47. D.R. Schuyler, M.M. Sohi, and R. Mahapatra, in "Interfaces in Metal-Ceramic Composites," Ed. by R.Y. Lin,

- R.J. Arsenault, G.P. Martins, and S.G. Fishman, TMS (Warrendale), p. 475, 1989.
48. D.A. Hartwick and R.C. Cordi, in "Intermetallic Matrix Composites," Ed. by D.L. Anton, P.L. Martin, D.B. Miracle, and R. McMeeking, MRS (Pittsburgh), 194, p. 65, 1990.
49. P.G. Partridge and C.M. Ward-Close, Int. Mat. Rev., 38, p. 1, 1993.
50. H.E. Deve, D.M. Elzey, J.M. Warren, and H.N.G. Wadley, in "Proceedings of 8th CIMTEC World Ceramic Congress and Forum on New Materials," Ed. by P. Vincenzi, 1994 (In Press).
51. P.K. Brindley, in "High Temperature Ordered Intermetallic Alloys II," Ed. by N.S. Stoloff, C.C. Koch, C.T. Liu, and O. Izumi, MRS (Pittsburgh), 81, p. 419, 1987.
52. D.M. Elzey, J.M. Kunze, J.M. Duva, and H.N.G. Wadley, in "Mechanical Properties of Porous and Cellular Materials," 207, Ed. L. Gibson, D.J. Green, and K. Sieradzki, MRS (Pittsburgh), p. 109, 1991.
53. D.M. Elzey and H.N.G. Wadley, Acta Metall. et Mater., 41 (8), p. 2297, 1993.
54. S.L. Draper, P.K. Brindley, and M.F. Nathal, in "Developments in Ceramic and Metal Matrix Composites," Ed. K. Upadhy, TMS (Warrendale), p. 189, 1991.
55. W.A. Curtin, Composites, 24, p. 98, 1993.
56. H. Hough, J. Demas, T.O. Williams, and H.N.G. Wadley, Acta Metall. et Mater., In Press, 1994.
57. D.M. Elzey and H.N.G. Wadley, Acta Metall. et Mater., In Press, 1994.
58. P.E. Cantonwine and H.N.G. Wadley, Composites Eng., 4 (1), p. 67, 1994.
59. J.M. Duva, W.A. Curtin, H.N.G. Wadley, Acta Metall. et Mater., In Press, 1994.
60. R. Vancheeswaran, D.M. Elzey, and H.N.G. Wadley, R. Vancheeswaran, D. M. Elzey and H. N. G. Wadley. Acta Metall. Mater., Vol. 44, No. 6, pp. 2175-2199, 1996.
61. R. Vancheeswaran, D.G. Meyer, and H.N.G. Wadley, Acta Metall. Mater., Submitted.
62. D.W. Clarke, C. Mohtadi, and P.S. Tuffs, Automatica, 23, p. 137, 1987.
63. H.N.G. Wadley et al, Acta Metall. et Mater., 39 (5), p. 979, 1991.
64. C.V. Dodd and W.E. Deeds, "Analytical Solutions to Eddy Current Probe-Coil Problems," J. Applied Physics, 19 (6), pp. 2829-2838, 1968.
65. Ed. B.E. MacNeal, MacNeal-Schwendler Corporation, MSC/EMAS Modelling Guide, 1991.
66. D.G. Meyer and H.N.G. Wadley, Met Trans B, 24, p. 289, 1993.
67. D.G. Meyer, R. Vancheeswaran, and H.N.G. Wadley, in "Model-Based Design of Materials and Processes," Ed. by E.S. Russell and D.M. Elzey, TMS (Warrendale), p. 163, 1992.
68. P.E. Gill, W. Murray, and M.H. Wright, *Practical Optimization*, Academy Press, London, 1981.
69. C.N. Nett, C.A. Jacobsen, and M.J. Balas: IEEE Trans. Automat. Contr., AC-29, pp. 831-32, 1984

Fundamentals on Damage Monitoring

Christian Boller

Daimler-Benz Aerospace, Military Aircraft

D-81663 München, Germany

actually with: Daimler-Benz AG, Research & Technology Exchange Group

D-70546 Stuttgart, Germany

SUMMARY

Within the paper, the following is discussed: existing load monitoring systems in aircraft and their use for fatigue damage evaluation; validation of different NDT-techniques with regard to their use for and integration into composite materials; validation of the use of structural health (damage) monitoring systems; parameters and techniques based on piezoelectric sensing for monitoring impact loads. It is concluded that structural health monitoring can have a beneficial effect in combination with composite materials.

INTRODUCTION

Aircraft are known to be highly complex systems. They are composed of a variety of electronic, hydraulic and propulsion systems and a light weight/high stiffness structure, that has to withstand severe loading conditions. In addition the whole system is highly safety critical and suffers degradation even when not being in service. Such complex systems require extended maintenance.

Because of safety criticality, most of the maintenance effort is related to monitoring. Only a smaller amount of maintenance should be related to repair. Manpower has become a major cost driving force in highly industrialized countries while increased competition in commercial aircraft business has led to low transport fares and highly sophisticated technology in military aircraft or space vehicle business requires extended care in functionality and reliability. Procedures for automated structural health or generally condition monitoring with high reliability are therefore considerable solutions for meeting the objectives of maintenance cost minimization, reliability, and functionality enhancement.

Beside these objectives, a variety of other requirements and reasons exist which includes:

- preservation of flight safety and improvement of operational capability
- maximization of aircrafts' availability through on-condition monitoring
- reduction of weight because of taking better advantage of the materials potential
- improvement of inspectability of composite materials' structures

- better understanding of the materials damage behaviour through simplification in detection, localization and possibly validation of damage such as cracks, delaminations and corrosion resulting from fatigue, impacts or mishandling
- saving fuel and thus reducing pollution.

Monitoring of aircraft structures is nowadays still fully performed on-ground using Non-Destructive Testing (NDT) procedures according to prescribed instructions and after fixed service time intervals. As these fixed intervals have been mainly based on severe flight conditions first attempts have been made to flexibilize these by on-condition monitoring using an aircraft loads monitoring system. Smart materials and structures technology including microelectronics and advanced data processing such as data bases, neural networks, fuzzy logic and artificial intelligence are emerging areas of science which might allow to integrate a NDT-system into an aircraft structure similar to the neural system in a human body. Fully automated aircraft structure condition monitoring would be enabled even to be used in-flight.

Materials mainly used today in aircraft structures are metals, metal matrix composites (MMC), and polymer-based composites. Ceramics is a further group of materials which is partly considered for jet engines and in structures with respect to hypersonic aircraft. The way how damage is generated highly depends on the material's ductility and homogeneity. Damage in ductile materials such as metals and MMCs is mainly characterized by cracks which generate on a microscopic level and slowly progress during a component's life. Monitoring however these cracks is quite troublesome and is mainly restricted to inspecting highly loaded areas such as notches or joints (rivets, bolts, welds, etc.). Determination of the incident where inspection becomes interesting is either defined by a prescribed inspection sequence or by monitoring the actual load sequence the component has gone through. Damage occurring from unexpected severe loads such as impacts can be well seen as a plastic deformation on the component's surface. Polymerbased composite materials often do not possess that amount of plasticity which leads to the fact that impacts can induce barely visible impact damages (BVID). These damages can only be monitored by using handheld non-destructive testing (NDT) equipment during an on-ground inspection. Smart structures technology can facilitate that inspection effort through the implementation of a sensor network into or onto these materials, allowing

continuous on-board monitoring. Finally damage in ceramic materials is mainly characterized by the distribution of the damage inducing microscopic failures (e.g. voids) which might not change over the component's service life and thus only needs to be determined once at the beginning of the component's life.

This paper will focus on existing load monitoring systems in aircraft to be used for fatigue life evaluation, validation of different NDT-techniques with regard to their use for being integrated into composite materials, validation of the use of structural health monitoring systems and parameters and techniques based on piezoelectric sensing for monitoring impact loads. In a subsequent paper the implementation of these ideas and techniques into real aircraft components will be discussed (Kudva, 1996).

STATE-OF-THE-ART OF IN-FLIGHT AIRCRAFT STRUCTURAL HEALTH MONITORING

When considering an aircraft from a health and usage monitoring aspect, four different areas within the aircraft are of major importance:

- the aircraft structure,
- hydraulic systems,
- propulsion systems, and
- electronics/avionics.

For propulsion systems health and usage monitoring are highly advanced. Whole in-flight Engine Condition Monitoring (ECM) systems have been developed and built which are already in use within various operators' fleets [Spragg et al. 1989, Haberding 1985]. This takes in engine data such as revolutions per minute, vibrations, temperatures, pressures and rate of fuel usage. By immediate data analysis, engine condition can be monitored long before in-flight malfunctions occur, and defects can be traced to a specific module within the engine. ECM has received FAA and JAA approval.

Since the widespread introduction of digital technology, the control and avionics systems of aircraft incorporate varying levels of Built In Test Equipment (BITE) to monitor system behaviour and to provide corrective action in the event of failures.

In-situ monitoring of aircraft structures or hydraulic systems is still limited to on-ground monitoring using NDT procedures such as eddy current, ultrasonics, pressurization or simply the naked eye [Achenbach and Thompson 1991].

In-flight monitoring, having gained large interest during the past decades, is performed nowadays by either monitoring strain or flight parameter sequences which are then used to derive a load sequence for the aircraft part considered. A description of this kind of monitoring is given in the following.

Strain Gauge Based Monitoring System

Initial work with in-flight monitoring was performed by bonding strain gauges to well selected areas in the aircraft and measuring strain sequences. On-ground, but even with sufficient computation capacity on-board, the strain sequences are then converted to stresses and/or loads

allowing a numerical evaluation of fatigue damage using mainly simple damage accumulation rules (e.g. Palmgren-Miner's rule).

This kind of monitoring system has been continuously developed through the past years mainly using improved bonding techniques, advanced electronics and data processing as well as improved sensors. Various examples are described in [AGARD 1991] where Fig. 1 shows one example for a military aircraft [Amabile and Giacobbe, 1991]. All strains measured with strain gauges are converted to digital signals and stored in-service in a Data Acquisition Unit (DAU). Within a following step the strain histories are then converted to stress histories and a detailed damage/fatigue life evaluation is performed for the last flight and the overall flight history of the aircraft. This damage/fatigue life evaluation might be performed either in-flight or on-ground.

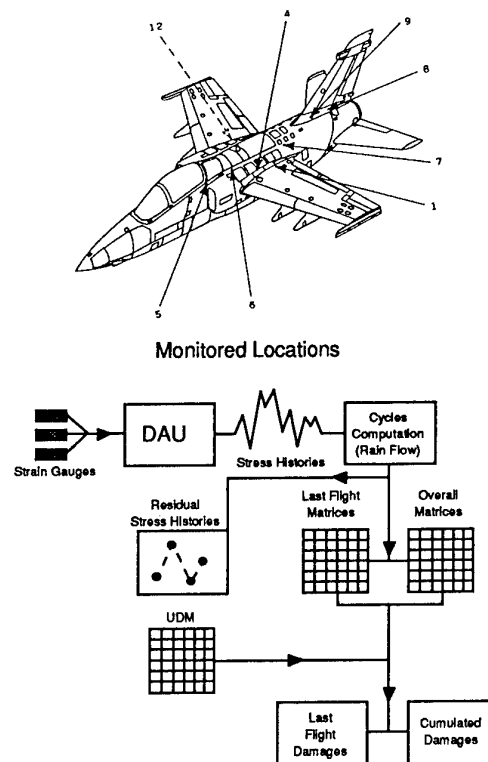


Fig. 1: Strain Gauge Based A/C Health Monitoring

Flight Parameter Based Monitoring Systems

Aircraft operators try to minimize the risk of complexity within an aircraft by avoiding additional sensors. Therefore strain gauges for simply monitoring loads might not be welcome. Instead sensors already available in the aircraft are used for monitoring the aircraft's load sequence. Early work started by using the g-meter for converting measured gravity accelerations to flight loads. This work was then extended including further flight parameters such as speed, altitude, air data, pressure, fuel quantity, flaps position, etc. for a more precise evaluation of loads. Fig. 2 shows an example of the Operational Loads Monitoring System (OLMS) developed for the Airbus A320 [Ladda and Meyer, 1991] and Fig. 3 the main procedure of the On-board Life Monitoring System (OLMOS) used for the Panavia Tornado military aircraft

within the German Tornado fleet [Bauer 1987, Krauß 1988].

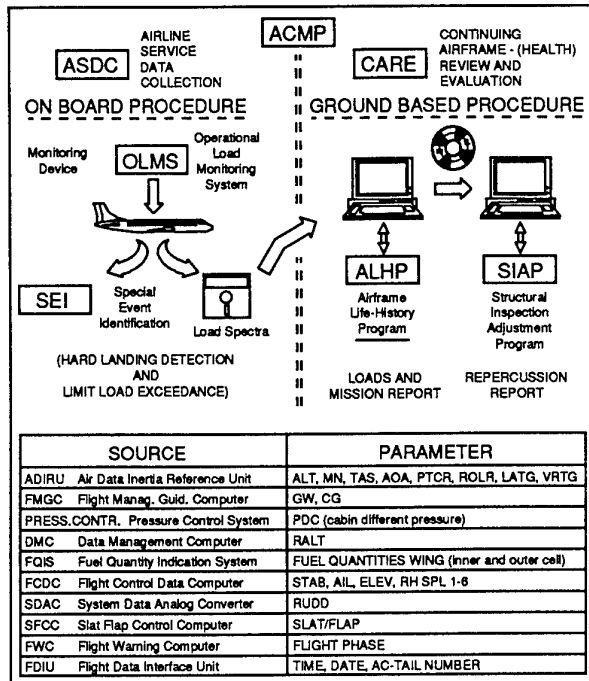


Fig. 2: OLMS, Flight Parameter Based A/C Health Monitoring [Ladda & Meyer 1991]

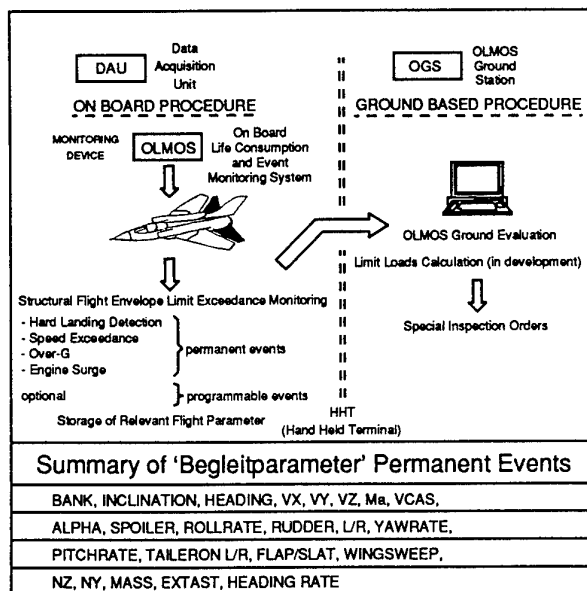


Fig. 3: OLMOS, Flight Parameter Based A/C Health Monitoring

Both systems are designed for on-board preprocessing of data, differing between special events (hard landings and limit load exceedances) and the general load spectrum. Even though the accuracy of the load sequence monitored is not fully satisfying at present a lot of improvement has already been gained in the past and further improvement can be expected from ongoing work. The optimum result obtainable with a flight parameter based system is therefore a load sequence identical to a load sequence measured with strain gauges.

Disadvantages with Actual Monitoring Systems

A loads monitoring system as described before is not able to monitor - or in other words - detect damage by additional use of numerical evaluation procedures. The difference between predicted and detected damage can be quite remarkable. A factor of two is very common in fatigue life predictions [Boller et al. 1983]. Furthermore structures exhibit large scatter in their damage behaviour. Fig. 4 is a typical example for a fatigue life curve [Simpson (Ed.) 1987]. The scatter in experimentally obtained fatigue lives easily varies by a factor of ± 2 around the mean value. The solid and dotted lines in Fig. 4 are the result of numerical fatigue life evaluation using different baseline data for the same material. It is obvious that the predicted fatigue life is significantly influenced by the appropriate selection of baseline data. Other factors are known to be the damage accumulation rule or the state of stress (uni-/multiaxial mean stress) applied. It can therefore be concluded that real monitoring of damage would be of great advantage to get more precise and reliable information.

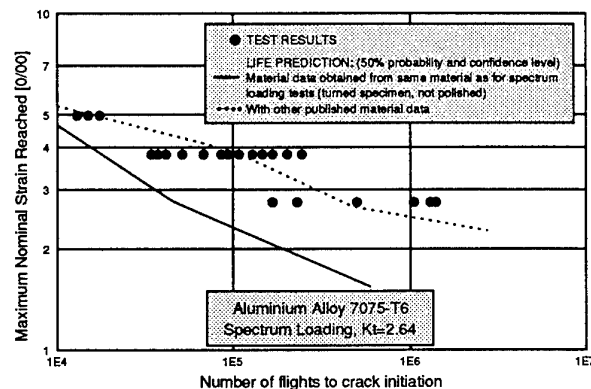


Fig. 4: Predicted versus Actual Fatigue Life [Simpson (Ed.), 1987]

The gap between predicted and real damage becomes even larger when considering composite materials. Damage evaluation for these materials is still at an early stage. Monitoring flight loads is hardly of great use to detect damage in composites such as fibre or matrix fracture, delamination or BVID. Composite structures nowadays are designed such that they can withstand all service loading conditions without experiencing damage. They could however be designed much more light weight if damage such as mentioned above could be monitored. This would lead

to make better use of composite materials potential without influencing the degree of security required.

Another aspect which cannot be covered by loads monitoring are environmental effects such as corrosion in metallic and humidity and temperature effects in composite structures - aspects which are becoming important with the increasing age of aircraft.

As a conclusion, considering safe-life as well as damage tolerant design and taking full advantage of materials' potential is only possible through continuous monitoring of material's condition applying NDT procedures. These NDT procedures must be applied on-board and even in-flight of an aircraft. An NDT system being an integral part of the aircraft can then lead to reduced manpower for inspection and ground times.

VALIDATION OF DIFFERENT MONITORING TECHNIQUES

A variety of NDT procedures is used within on-ground maintenance of aircraft structures nowadays. Apart from visual inspection, use of ultrasonics and eddy current are the procedures generally applied. Procedures such as computer tomography, holography, shearography, thermography, Barkhausen noise or magneto optical eddy current have recently gained more attraction because of improved availability of these techniques. Major applicability and

experience gained with these techniques has been with metals. A limited number of them is however also applicable to composite materials.

Requirements for On-Condition Monitoring

Future aircraft health and usage monitoring systems to be designed as built-in systems must be able to monitor damage on-condition. Major damage to be detected includes:

- fatigue and corrosion in metallic structures, and
- delaminations, especially BVID, in composite structures

resulting either from material degradation (aging) or mishandling including misrepair.

Damage has to be detected, localized and monitored in accordance with damage tolerance design principles.

On-condition monitoring is closely related to in-flight monitoring. The major criterion for selecting the appropriate NDT procedures is therefore in-flight applicability. Fig. 5 shows an overview of NDT Procedures with respect to applicability for in-flight monitoring, degree of development, degree of monitoring and type of damage monitored.

Monitoring Technology	Monitoring Qualities	In-flight Applicability	Degree of Development	Loads	Damage Identification	Damage Propagation	Fatigue Crack	Impact (BVID)	Delamination	Corrosion
Visual/Borescope		No -	+				+			+
Strain		Yes +	+	+			(+)			
Flight Parameters		Yes +	+	+			(+)			
Magnetic Particle		No -	+		+	+	+			
Eddy Current		No -	+		+	+	+	(+)	(+)	
Penetrant		No -	+		+	+	+		(+)	
Paintings		No -	-		+			+		
Chem. Sensing		Yes +	-		+					+
Radiography		No -	+		+	+	+	+	+	+
Modal Analysis		Yes +	+	+	+	+	+	+	+	?
Acoustic Emission		Yes +	+	+	+	+	+	+	+	(+)
Holography		?	-		?	?	?	?	?	?
Ultrasonics		Yes +	+		+	+	+	+	+	?
Shearography		?	-		?	?	?	?	?	?
Thermography		No -	-		+	+	+	+	+	
Barkhausen Noise		?	-	?	?		?			?
Magneto Opt. Eddy Curr.		No -	-		?	?	?			?
Comp. Aid. Tomography		No -	-		+	+	+	?	?	?

Fig. 5: Technology Selection for Health Monitoring Systems

The following NDT techniques turn out to show in-flight capability:

- strain
- flight parameters
- chemical sensing
- modal analysis

- acoustic emission, and
- acousto ultrasonics.

When considering well established NDT procedures which is generally identical to a high degree of development chemical sensing might still be excluded from the techniques mentioned before.

In-situ monitoring of damage is a further major criterion for an advanced aircraft health monitoring system which reduces the candidate NDT procedures to modal analysis, acoustic emission and acousto-ultrasonics. These latter procedures are also able to monitor various kinds of damage such as fatigue cracks, BVID, delamination or even corrosion. Depending on the kind and size of damage to be monitored these are the NDT procedures proposed to be considered in future health monitoring systems.

Acoustic emission (AE) has been successfully used for monitoring discontinuities, fatigue failures, materials behaviour, welds including welding process or stress corrosion cracking in pressure vessels, aerospace and engineering structures. Acoustic emission is the elastic energy being suddenly released when materials undergo deformation. It may be released from propagation of cracks and/or delaminations, friction, leakage or microscopic deformation or transformation. The elastic energy - or better acoustic signal - emitted from the damage is registered as acoustic signal of a frequency of in the range between 10 kHz and 1 MHz using a piezoelectric sensor well attached to the structure. Fig. 6a shows schematically a typical example of an AE signal. The signal is then analyzed and classified according to specific features such as amplitude, rise time, decay time, duration, counts, etc.

(Fig. 6b). Including time as a parameter allows damage source localization when at least three AE sensors are used. A good compilation of AE fundamentals and applications is given in [Miller & McIntire (Ed.s) 1987].

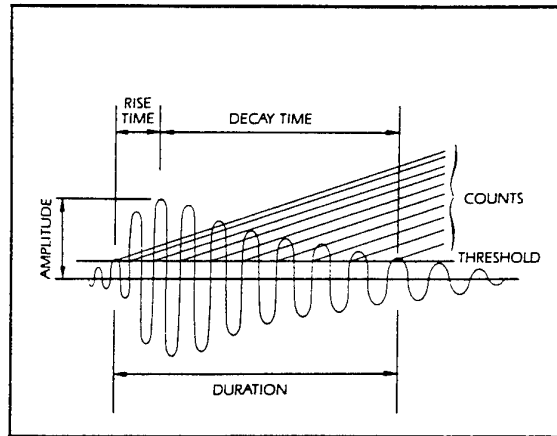


Fig. 6a: Definition of Simple Waveform Parameters [Miller & McIntire (Ed.s) 1987]

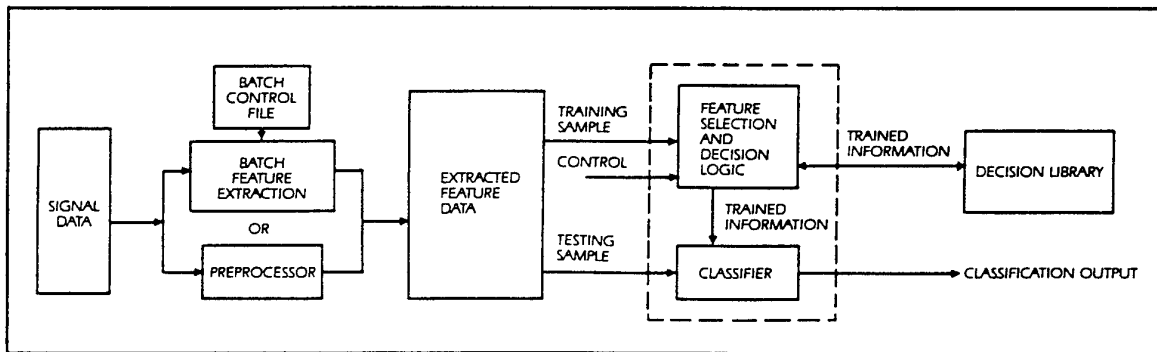


Fig. 6b: A Classification System for Treatment of Acoustic Emission Signals [Miller & McIntire (Ed.s) 1987]

Various studies have been performed during the past decades using AE for monitoring damage in aircraft structures [Bailey 1976, Scala 1986, Carlyle 1989, Fotos 1989]. Some of these studies report of having even applied AE for in-flight monitoring [Scala 1986, McBride 1989]. This has however been limited to either monitoring an aircraft structure in a rig test [Scala 1986] performed on-ground under simulated in-flight conditions or implementing an inertial loading apparatus with a precracked test specimen in a flying aircraft [McBride et al. 1989].

Other studies have been performed by pressurizing the cabin of commercial aircraft fuselages for the detection of fatigue cracks, corrosion, cracked lap joints and cracks around rivets and in forgings and wing splices [Fotos 1989]. The F-111 fighter/bomber aircraft has been tested in a chamber where the aircraft was periodically chilled to -40°C and stressed between $+7.3\text{ g}$ and -3.0 g and an AE system was used to locate sources of structural failure [Crlyle 1989]. Techniques were developed to eliminate

loading noise and a strategy was established to identify locations where sensors should be placed to obtain optimized signals. These developments have become feasible since handling, processing and interpretation of data has been improved through better computer technology and new attempts [McBride et al. 1991].

Acousto-ultrasonics is a technique which has been proved to be even more sensible than acoustic emission [Vary & Lark 1979, Hillger & Block 1986]. Fig. 7 illustrates the principle of this technique. It requires two probes, one of which is used to introduce ultrasonic stress waves into the structure and the other to pick up these stress waves at another position. As soon as the damaged area lies between the two probes the shape of the received acoustic signal changes because of change in material damping characteristics due to the damage (crack, delamination) occurred. Acousto-ultrasonics has not been an NDT procedure established within aircraft structures up to now but it

shows significant potential for future health monitoring systems.

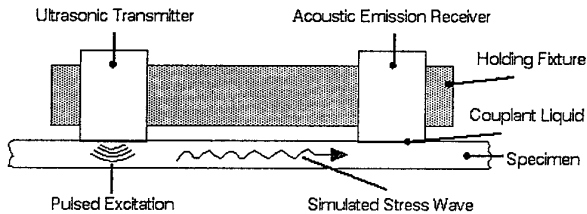


Fig. 7: Schematic Diagram of the Acousto-Ultrasonic Technique

Modal analysis is a further NDT procedure which is widely applied for monitoring space structures. It is based on monitoring vibration modes. These vibration modes change when damage occurs. Pandey et al. (1991) have shown the applicability of modal analysis for a cracked beam based on numerical (FEM) analysis. Tracy and Pardoen (1989) used modal analysis for monitoring damage in a delaminated beam where the analytical procedure is explained in more detail in a subsequent chapter. Hickman et al (1991) have shown on a demonstrator aircraft, that modal analysis could well be used for monitoring damage such as lost rivets or bolts. Similar applications are known with the Integrated Health and Usage Monitoring Systems (IHUMS) of helicopters (Bristow 1992). Other aircraft applications include monitoring of cracks in metallic aircraft fuselages (Robinson et al. 1996).

Sensor Selection

The three candidate NDT procedures, modal analysis, acoustic emission and acousto ultrasonics are all based on monitoring stress waves. The frequency of these stress waves range from a few Hz in modal analysis to 1 Mhz in acoustic emission. Registration of these waves is performed either using an accelerometer (especially with modal analysis), sensors based on either piezoelectric materials (ceramics or polymers) or optical fibers.

Traditionally acoustic emission and acousto ultrasonics testing has been performed using sensors made of *piezoelectric ceramics*. These sensors are highly sensitive and either work on a broad band or limited band/resonant basis. The working principle and different kinds of available sensors is well described in [Miller & McIntire (Ed.s) 1987].

Due to the fact that piezoelectric ceramics do not withstand higher strains, piezoelectric rubbers and paints have been developed (Hanner et al., 1989; Egusa et al., 1993). Manufacturing of these materials is based on the principle that a piezoceramic material is milled into a very fine particulate-sized powder, mixed to a rubber or epoxy resin and then polarized to again obtain the piezoelectric effect. Using that kind of material allows to easily shape the type of sensors and possibly actuators required according to very specific needs. Thus piezoelectric sensors can become an integral part of a component. Sensor networks can either be bonded or painted onto or even integrated into a component. Continuous retrieval of the signals emitted by

these sensors allows on-line determination of the component's loading and possibly even damage condition.

Work has also been published on the use of sensors made from *polyvinylidene fluoride PVDF* for either ultrasonics or acoustic emission application [Stiffler & Henneke 1983, Brown & Brown 1990]. PVDF has a molecular conformation of fluorine atoms opposite to hydrogen atoms along a carbon backbone. Because of the strong electronegativity of fluorine, PVDF molecules possess a large dipole moment leading to piezoelectric properties after processing. PVDF processing includes electrical poling, unidirectional mechanical stretching and thermal treatment. The product obtained is a piezofilm with maximum in-plane displacement sensitivity in the stretched direction as well as some out-of-plane displacement sensitivities. The film can be tailored in its geometrical shape according to specific needs. Its sensitivity is satisfactory when monitoring composite materials. Advantages have to be seen in lower cost, lower mass, higher flexibility, wide-band frequency response and the high internal damping.

A lot of development work has been spent in the past years using *fibre optics* for health monitoring of engineering and especially aeronautical structures [Glossop et al. 1990]. Major work has been reported in [SPIE 1988ff]. Optical fibres are mainly based on silicon but may even be made of sapphire when used in an ultra-high temperature environment (< 2400 °C). To obtain satisfactory reliability of signals measured, optical fibres usually have to be integrated into the material. As this is especially feasible with composite materials, fibre optic sensors have been used in various examples for monitoring the curing process and/or damage induced by impact or overloads. A detailed description of fibre optics technology including its applicability of fibre optic smart structures is given in Udd (Ed.) 1991, Measures 1992, Culshaw 1996.

Fibre optic sensors have several advantages compared to the electrically based sensors mentioned before such as light-weight, all passive configurations, low power utilization, immunity to electromagnetic interference, high sensitivity and bandwidth, compatibility with optical data transmission and processing, long lifetimes and low cost (as long as using silicon fibres). Disadvantages exist with reparability as long as optical fibres have to be integrated into the material and placed according to major occurring stresses and strains to obtain reliable data. Furthermore a lot of effort has to be made to simplify optical signal transmission between or out of structural parts leading mainly to development of smaller, lower cost and less sensible optical signal clutches.

Summarizing the advantages and disadvantages of the three types of sensors leads to the overview given in table 1.

The large effort performed in development of fibre optics technology as well as in improving performance of piezoelectric materials will certainly help to diminish the number of disadvantages mentioned above. It is therefore timely to consider the application and integration of these sensors into smart materials and structures especially under the aspect of structural health monitoring.

Type of Sensor	Advantage	Disadvantage
Piezoceramic	Large Experience;	Expensive; High Mass; No Flexibility
Piezopolymer	Low Cost; Low Mass; Flexibility; Wide-Band Frequency; High Internal Damping	Limited Experience; Low Temperature Stability
Optical Fibre	Electromagn. Immunity; Compatible to Optical Data Transmission; High Temp. Stability	Repairability; Signal Transfer Clutches; Need for Materials/Structures Integration

Table 1

VALIDATING STRUCTURAL HEALTH MONITORING

The variety of numerical tools available today allows to determine and validate the potential of technologies before starting an experiment. Even though the numbers calculated may not completely reflect reality, they might still be useful when compared to each other as long as they all contain a constant error. A large number of excellent studies have been performed for active and adaptive structures (e.g. Crawley and Anderson, 1989; Barrett, 1995) while comparatively less has been done for structure health monitoring.

A key aspect to be considered with Structural Health Monitoring Systems (SHMS) is the problem of how damage accumulates in the material selected which has

now been especially discussed for metals for nearly 70 years (Palmgren, 1929; Miner, 1945). Damage accumulation - as far as related to metals - is often assumed to follow linear relationships when being considered in numerical fatigue life evaluations. However in reality damage may often accumulate according to nonlinear relationships. An equation also allowing to account for these non-linearities can be written as

$$D = 1 - \left(\frac{N_r}{N_f} \right)^a \quad (1)$$

where D is damage, (N_r/N_f) the normalized fatigue life, N_r the residual fatigue life and N_f the total fatigue life respectively. As shown in Fig. 8 the case of linear damage accumulation is described when the exponent a equals 1 while in all other cases damage accumulates nonlinearly.

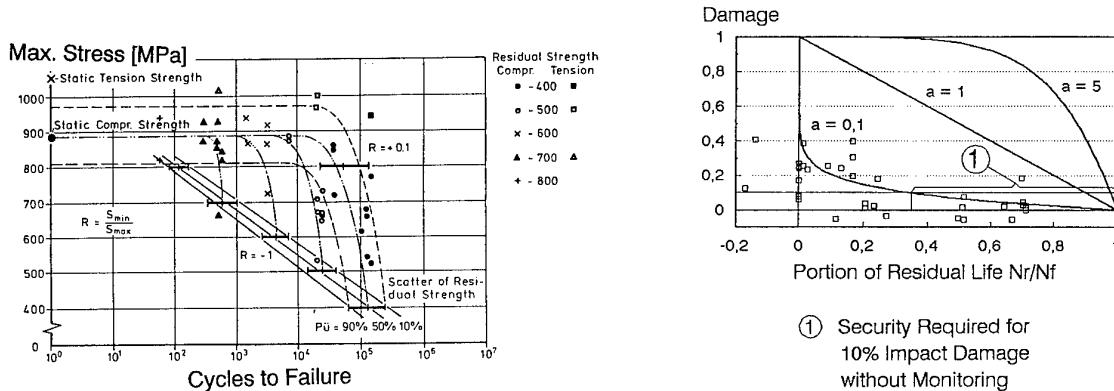


Fig. 8: Damage Accumulation Behaviour and Fatigue Life Curve for Composite Considered

Damage accumulation in composite materials is quite different when compared to metals. Since the approach mentioned above is however more of a phenomenological nature and stress versus fatigue life is also used to describe the fatigue behaviour of composites, Eq. (1) will even be applied here for characterizing the damage behaviour of composite materials.

Fig. 8 contains some data for a graphite composite laminate $[0_2/+45/0_2/-45/0/90]_s$ which Prinz, 1983 tested on flat unnotched specimens under reversed fatigue loading ($R = -1$). 64 specimens were tested until complete buckling under compression loading and used to determine the fatigue life curve which can be well described in a semi-log scale using the following equation

$$\log \left(\frac{N_i}{N_{ref}} \right) = k \times \left(1 - \frac{\sigma_i}{\sigma_{ref}} \right) \quad (2)$$

with N being the number of cycles, k the slope, and σ the applied stress while i and ref denote the actual and an arbitrary reference value respectively. Additionally 33 specimens were tested the same way but removed unfailed after N_i cycles and finally tested under a static compression test. The ratio of their compression strength $\sigma_{i,comp}$ compared to the mean compression strength $\sigma_{0,comp}$ of a virgin specimen has been taken as the basis to determine their degree of damage according to the following equation:

$$D_i = 1 - \frac{\sigma_{i,comp}}{\sigma_{0,comp}} \quad (3)$$

Since neither the virgin compressive strength nor the total fatigue life could be determined for these 33 specimens, the mean values of the fatigue life curve described with Eq. (2) have been taken to convert the damage determined under Eq. (3) to a damage being related to the number of cycles as described with Eq. (1) with N_r being

$$N_r = N_f - N_i \quad (4)$$

This explains the large scatter of the experimental data in Fig. 3 and why some of the data fall below a value of 0 for the damage and ratio of residual life respectively.

Composite components nowadays are often designed such that they do not require to be inspected during their whole life. This requires to always consider the most severe case which depends on how damage accumulates or in terms of Eq. (1) if a is < 1 or > 1 .

With $a > 1$ in eq. (1) the most critical situation is independent of the fact that the material/component contains a SHMS or not. In both cases the most critical situation exists when the impact occurs at the very end of the components life. Thus no gain in allowable stress can be achieved by using a SHMS for a material accumulating damage with $a > 1$.

For $a < 1$ the most severe service condition for a material/component without a SHMS is when the material/component is hit by an impact inducing a damage of D_{im} at the very beginning of its service life. The residual life of the material/component can be calculated using Eq. (1) which leads to

$$\frac{N_{r,i}}{N_f} = (1 - D_{im})^{1/a} \quad (5)$$

Since the material/component has to survive at least the first mission (time between maintenance) of N_m cycles during which the impact can occur, the normalized residual life becomes

$$\frac{N_r}{N_f} = \frac{N_{r,i}}{N_f} + \frac{N_m}{N_f} \quad (6)$$

Including Eq. (6) into Eq. (2) and having cycles and stresses based on the reference values N_{ref} and σ_{ref} respectively, leads to the relationship

$$\frac{\sigma_i}{\sigma_{ref}} = 1 + \frac{1}{k} \left[\log \left\{ (1 - D_{im})^{1/a} - \frac{N_m}{N_f} \right\} - \log \left(\frac{N_i}{N_{ref}} \right) \right] \quad (7)$$

which describes a fatigue life curve for fatigue lives including impact damage D_{im} .

Considering a material/component with a SHMS, which allows the material's/component's inspection at arbitrary intervals, the most critical condition is when the impact damage D_{im} is included just at the beginning of the last

mission. Following Eq. (1) the residual damage after the impact is

$$D_{r,m} = 1 - \left(\frac{N_m}{N_f} \right)^a \quad (8)$$

and the equivalent before the impact is

$$D_{r,i} = D_{r,m} - D_{im} = 1 - \left(\frac{N_m}{N_f} \right)^a - D_{im} \quad (9)$$

The residual life thus becomes

$$\frac{N_r}{N_f} = 1 - \left[\left(\frac{N_m}{N_f} \right)^a + D_{im} \right]^{1/a} \quad (10)$$

Including Eq. (10) into Eq. (2) leads to

$$\frac{\sigma_{i,SHM}}{\sigma_{ref}} = 1 + \frac{1}{k} \left[\log \left\{ 1 - \left[\left(\frac{N_m}{N_f} \right)^a + D_{im} \right]^{1/a} \right\} - \log \left(\frac{N_i}{N_{ref}} \right) \right] \quad (11)$$

with $\sigma_{i,SHM}$ being the allowable stress when using a SHMS.

To now determine the advantage that can be achieved by use of a SHMS, the ratio of the allowable stresses determined from Eqs (7) and (11) can be calculated, which leads to the following for $N_i/N_{ref} = 1$:

$$\frac{\sigma_{i,SHM}}{\sigma_i} = \frac{k + \log \left\{ 1 - \left[\left(\frac{N_m}{N_f} \right)^a + D_{im} \right]^{1/a} \right\}}{k + \log \left\{ (1 - D_{im})^{1/a} - \frac{N_m}{N_f} \right\}} \quad (12)$$

Based on the experimental data mentioned before the following standard values have been used for qualification of the shortcomings of using a SHMS:

$$k = 4,617; \quad \sigma_{ref} = 600 \text{ MPa}; \quad a = 0,1; \\ D_{im} = 0,3; \quad \frac{N_m}{N_f} = 10^{-3}$$

The fatigue life curve used and some variations in its slope k is shown in Fig. 9 while the resulting gain in allowable stress determined from eq. (12) and resulting from these different slopes can be seen in Fig. 10. It becomes obvious that the gain in allowable stress decreases with increase in k . A significant gain in using a SHMS is seen with very steep fatigue life curves (e.g. $k = 2$).

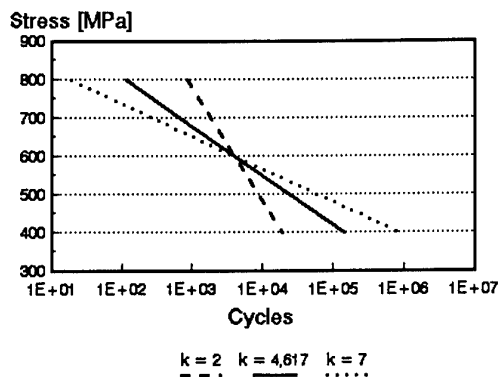


Fig. 9 Fatigue Life Curves Considered

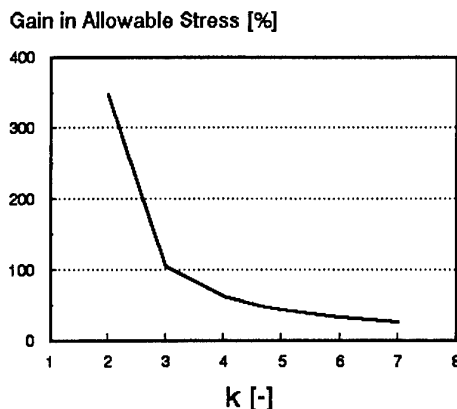


Fig. 10 Influence of Fatigue Life Curve Slope

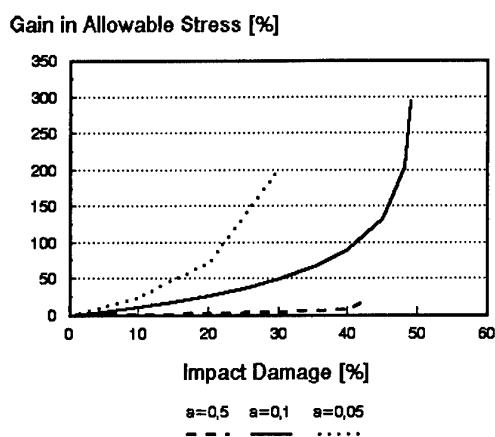


Fig. 11 Influence of Damage Size and Way of Damage Accumulation

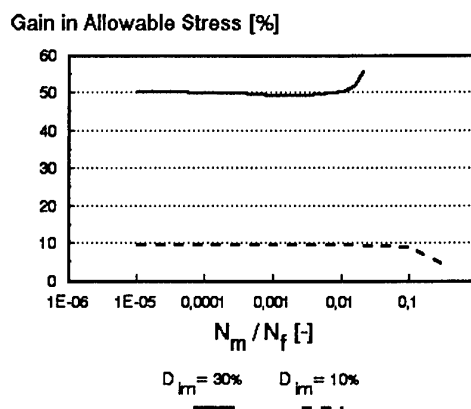


Fig. 12 Influence of Mission Length

The relationship between the gain in allowable stress and the induced impact damage D_{im} is shown for different values of the exponent a on Fig. 11. Generally the gain in allowable stress increases with an increase in allowed induced impact damage and reaches an infinite value when the induced damage reaches its maximum allowable value. The reason for infinity here comes from the fact that a component without a SHMS and the equivalent impact damage is not able to withstand any stress for that condition anymore. It also becomes apparent that the exponent a - and thus the way how damage accumulates - has a strong influence on the gain in allowable stress.

Finally Fig. 12 shows the influence of the length N_m of a mission which is considered to be here the time between the possibilities of maintenance, where no significant influence can be seen for the two standard examples shown.

Beside this possibility of increasing allowable stress and thus reducing structural weight a major advantage of using a SHMS is the reduction in inspection effort, which is mainly related to the manpower required. Quantifying this generally is quite difficult since every type of component mainly follows its specific inspection guidelines. However it can be said for a component designed to require no inspection, that implementing a SHMS has to be carefully considered. Reasons include that:

- the possible increase in allowable stress through use of a SHMS will increase the effort required for repair,
- the SHMS might require maintenance or
- the SHMS's mass might absorb the structural mass gained through the increase in allowable stress if the SHMS's mass cannot be used multifunctionally to also carrying loads.

The aspects to be considered can therefore be summarized as follows:

Aspect	Gain	Loss
Saving in Structural Material	x	
Increase in Payload	x	
Reduced Manpower Effort for Inspection	x	
Higher Availability Due to Less Inspection Time	x	
Cost of SHMS		x
Maintenance of SHMS		x
Increased Structural Mass through SHMS		(x)
Increased Structural Repair		x
Less Availability Due to Increased Repair		x

Based on these aspects and possibly others a quantitative balance has to be performed, allowing finally to determine if the SHMS is a cost-effective solution or not.

VALIDATION OF DIFFERENT MONITORING TECHNIQUES

From the large number of candidate NDT-techniques mentioned before, modal analysis, acoustic emission and acousto ultrasonics have been considered to be the most suitable for in-service structure health monitoring.

To prove the applicability and suitability of modal analysis a significant number of tests has been performed on bars and plates where cracks originated from the specimen's surface perpendicular to the applied normal stress (e.g. Pandey et al., 1991; Campanile, 1993). This type of crack is however not very common with composite materials. Instead delaminations have to be considered, which can be detected with much less sensibility when using modal analysis. Experimental results published in various papers (e.g. Lee et al., 1987; Balis Crema et al., 1985; Tracy and Pardoen, 1989) show, that the delamination's size must be at least 10% of the component's surface being monitored by a sensor for being reliably detected by that technique. This experimental fact can be well analytically explained by using some basic mechanic's equations compiled in (Tracy and Pardoen, 1989), for describing a delaminated beam that is divided into four sections (Fig. 13).

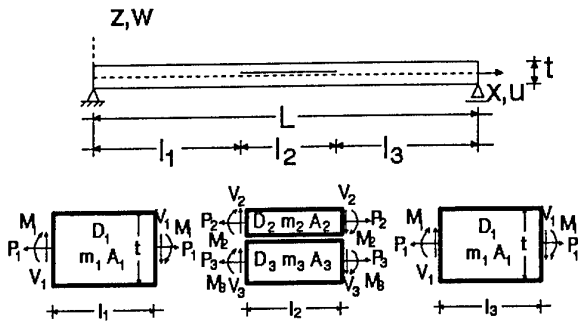


Fig. 13 Mechanical Model for Delaminated Beam

The governing differential equations are:

$$D_i \frac{d^4 w_i}{dx^4} - m_i \omega^2 w_i = 0 \quad (13)$$

$$\frac{dP_i}{dx} = A_i \times \frac{d^2 u_i}{dx^2} = 0 \quad (14)$$

with the following abbreviations used: A_i extensional stiffness, D_i bending stiffness and m_i mass. The solutions to eq.s (13) and (14) have the form:

$$w_i = C_{i1} \cosh(kx) + C_{i2} \sinh(kx) + C_{i3} \cos(kx) + C_{i4} \sin(kx) \quad (15)$$

$$\text{with } k^4 = m_i \frac{\omega^2}{D_i} \text{ and } U_i = B_{i0} + Bx \quad (16)$$

Considering boundary and continuity conditions and eliminating non-physical vibration modes leads to 14 equations with 14 unknowns which can be solved. Fig. 14 shows the resulting change in natural frequency versus the size of a delamination centered in the middle of the beam. Since modes higher than mode IV do not lead to significant higher sensitivity, results shown in Fig. 14 prove that only delaminations longer than 10% of the beam's length can be reliably recognized. Whenever designing a network of sensors for detecting delaminations by modal analysis, the distance of sensors should therefore not exceed 10 times the minimum delamination size to be monitored (e.g. 5-6 mm in diameter)

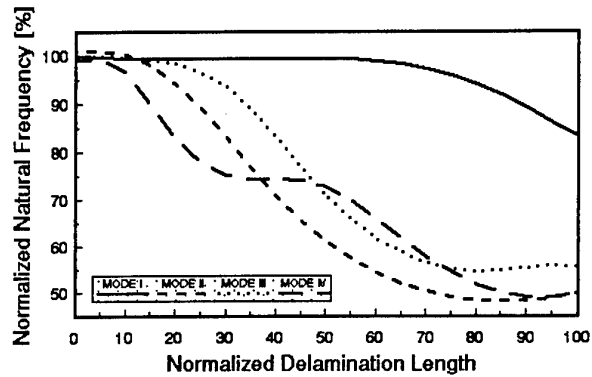


Fig. 14 Influence of Delamination Size on Natural Frequency

Acoustic emission is another candidate NDT-technique where limitations exist when using it for damage monitoring in large polymerbased composite components such as used for aircraft structures. A major reason for these limitations is the composite material's significant damping behaviour. To simply give an example, damping in a carbonfibre reinforced composite is approximately 6 dB/cm in fibre direction and 10 dB/cm transverse to fibre direction at a frequency of 1 Mhz (the upper limit usually monitored with acoustic emission). When considering an energy of 65 dB, which is usual to occur at the initiation of a delamination, a sensor is required approximately every 10 cm for reliably monitoring the damage. Bearing in mind that acoustic emission signals usually have a complex shape and are therefore difficult to read, effort required for data processing can become highly complex when considering aircraft components (e.g. panels, fins, etc.). Thus application of acoustic emission in that field still becomes highly troublesome.

Due to the fact that the measurable deformation, dynamic or acoustic signals emitted from delaminations in composite structures are relatively weak, they can be easily disturbed by other signals generated in an in-service environment and can thus lead to misinterpretations. A lot

of effort is therefore required to avoid that problem by using a large number of sensors and spending very much effort into data processing.

A way allowing to reduce the severity of that problem exists by emitting a well defined signal through the structure, which can be an acoustic signal as described before for the acousto-ultrasonics method, but can also be of another physical nature. Recently piezoelectric elements have been integrated into composite structures and have been used as sensors and actuators with success (Keilers & Chang 1995, Lalande & Rogers 1996, Shen et al. 1996, Esteban et al. 1996). Lalande and Rogers (1996) have shown results where a defined signal has been emitted from a piezoelectric sensor for the case of an undamaged and a damaged component. A difference in the frequency response can be clearly recognized. However using classical modal analysis by simply monitoring the frequency spectrum in the far field does not lead to any significant difference in the frequency response mentioned.

Another method being also related to the actuator/sensor principle has been based on Lamb wave theory (e.g. Victorov 1967, Kaczmarek, Simon & Delabarre 1996). In this case a longitudinal and transverse plate wave is emitted into a structure. The ability of these waves to propagate over long distances is highly advantageous. However much care is required to find the right angle for inducing the Lamb waves, especially when the structure to be monitored is of a geometric shape significantly different to that of a plate.

PARAMETERS AND TECHNIQUES BASED ON PIEZOELECTRIC SENSING OF IMPACT LOAD

Impact Phenomena

The governing equations for describing the behaviour of two structures under impact such as shown in Fig. 15 with an impactor and a beam are:

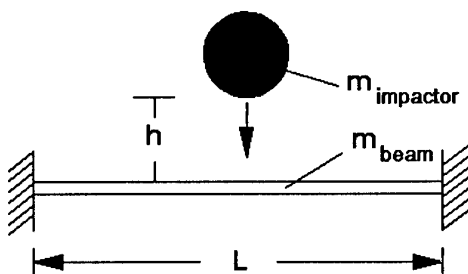


Fig. 15: Two Bodies under Impact

1. The equilibrium of impulse:

$$m_1 \times u_1 + m_2 \times u_2 = m_1 \times v_1 + m_2 \times v_2 \quad (17)$$

2. The equilibrium of energy:

$$\frac{m_1}{2} \times u_1^2 + \frac{m_2}{2} \times u_2^2 = \frac{m_1}{2} \times v_1^2 + \frac{m_2}{2} \times v_2^2 \quad (18)$$

3. The equations for the deformation/location of the beam:

$$w(t) = \sum_i A_i \times \sin(\omega_i t) \quad (19)$$

for the impactor:

$$w(t) = g \times \frac{t^2}{2} + v_0 \times t + w_0 \quad (20)$$

where the appropriate equations for speed and acceleration of the beam can be obtained by differentiation. Throughout these equations the following abbreviations have been used:

A	maximum amplitude
g	gravity
i	index
m	mass
t	time
u, v	speed
w	location
ω	frequency

and index 1 and 2 denoting the impactor and structure (beam) respectively and 0 the initial conditions (integration constants).

Within the following the impact is considered to behave ideal and fully elastic. When analyzing an impact two different conditions have to be considered:

1. the impactor's mass is less than or equal to the vibrating mass of the structure (beam)
2. the impactor's mass is larger than the vibrating mass of the structure.

Within the first condition, the impactor falls on the structure and is immediately rejected. Fig. 16 gives an example for the experimentally determined deformation versus time behaviour of a structure (e.g. a plate). It shows a single peak due to the impact at the initiation followed by the free vibrations of the plate.

When considering the second condition, three different stages within the time-deformation signal become important (Fig. 17).

The first stage, which can be explained analytically, is related to a multiple impact between impactor and the plate. The reason for this is, that after each impact the impactor reduces its speed but does not change its direction of motion. This lasts to continuous reimpacting until the impactor's speed is zero or it has changed its direction of motion, which leads to the initiation of the second stage. Fig. 18 shows schematically the deformation versus time relationship for both, the impactor and the structure.

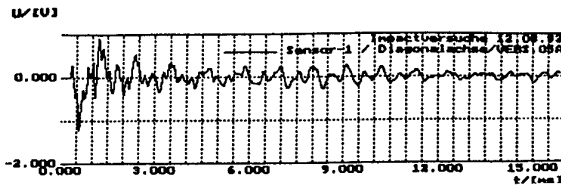


Fig. 16: Impact Signal for the Impactor's Mass = Vibrating Structural Mass (Experiment)

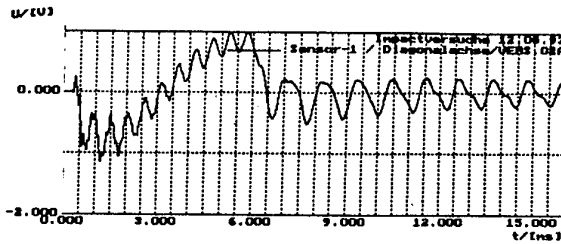


Fig. 17: Impact Signal for the Impactor's Mass >> Vibrating Structural Mass (Experiment)

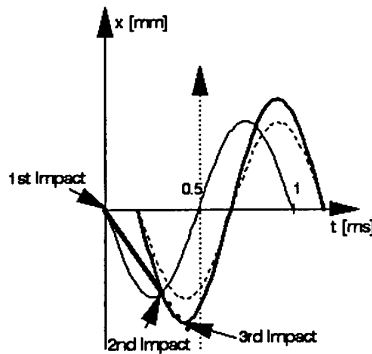


Fig. 18: Deformation vs. Time Behaviour During Impact (Theory)

During the second stage, when the impactor has changed its direction of motion, the speed of the impactor is lower than the structure's (e.g. beam's) speed. Thus the impactor is lifted by the structure. The impactor acts as a spring bearing and due to the roughness between the impactor and the structure a vibration mode is initiated for the structure which is equivalent to the vibration mode of the beam with a spring bearing at the location of the impact (Fig. 19).

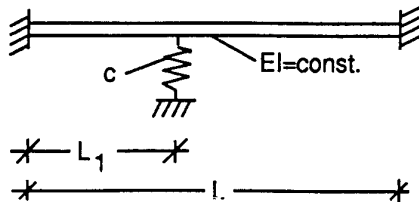


Fig. 19: Mechanical System During Impact

When the impactor's speed again becomes larger than the speed of the structure the third stage is initiated which finally contains the vibration modes of the freely vibrating structure.

Impact-Energy Monitoring Parameter

A good means for monitoring deformations and vibrations resulting from impacts is the use of piezoelectric sensors. Within the experiments described below some rectangular carbonfibre reinforced polymer plates were tested under impact loading using polymer-based piezoelectric sensors simply bonded onto the plate's surface. Sensor data obtained during the impact were automatically stored when passing a defined threshold level.

Signals monitored during the impact, where two examples are given in Figs 16 and 17, can be divided into the stage of interaction between impactor and structure and the stage of a freely vibrating structure. It can be seen, that the period of interaction between impactor and structure increases with increasing mass of the impactor (structure's mass is kept constant). In excess of the two experimental results shown above, various tests have been performed with different masses of the impactor dropped from different heights. Results from these tests, with the impact being located in the centre of the plate, are given in Fig. 20 as a relationship of duration of the time t^* of the interaction between impactor and structure versus the impactor's mass m .

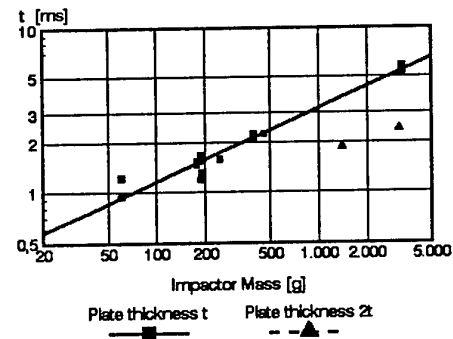


Fig. 20: Contact Time t^* vs. Impactor's Mass

Although these data scatter to some extent they generally show a good linear relationship in a double-logarithmic scale leading to the equation

$$t^* = B \times m^r \quad (21)$$

Determination of t^* has been done in a first step by visual analysis of the sensor signal, which might be one of the reasons for scatter in experimental results. An automated signal processing procedure for determining t^* is a next step to be done. Eq. (21) can however also be determined numerically using the set of equations mentioned above. It is the basis for determining the mass of an impactor detected by a piezoelectric sensor on a component's surface.

Another important value for determining impact energy is the impactor's speed. It can be seen from experiments that within a range of frequencies, which has been 100 Hz to

10 kHz for the sensors used here, the sensor output is a well described function of the impactor's speed and the structural stiffness. Within the impact tests described here this function has been linear and can be described by

$$U^* = c \times v \quad (22)$$

with U^* being the maximum voltage emitted from the piezoelectric sensor during the impact, v the impactor's speed just before the impact and c the slope of that linear relationship. Fig. 21 gives some results for impact tests with two plates of different thickness. The impactor's mass was varied significantly but did not have any remarkable influence on the relationship observed.

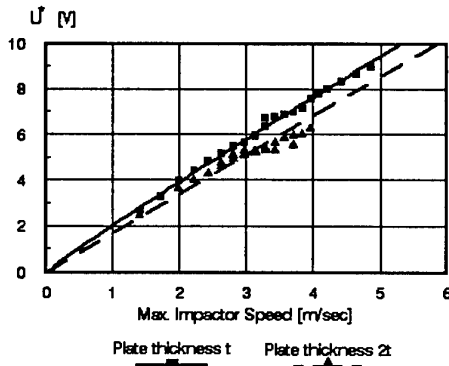


Fig. 21: Max. Sensor Voltage Signal vs. Max. Impactor's Speed

Matching Eq.s (21) and (22) together allows to define a parameter

$$P^* = \frac{m}{2} \times v^2 = \frac{1}{2} \times \left(\frac{t^*}{B} \right)^{1/2} \times \left(\frac{U^*}{c} \right)^2 \quad (23)$$

which is identical to the impact energy.

Plotting the known impact energy E_{kin} for the tests performed versus P^* determined with the piezoelectric sensors shows good correlation (Fig. 22).

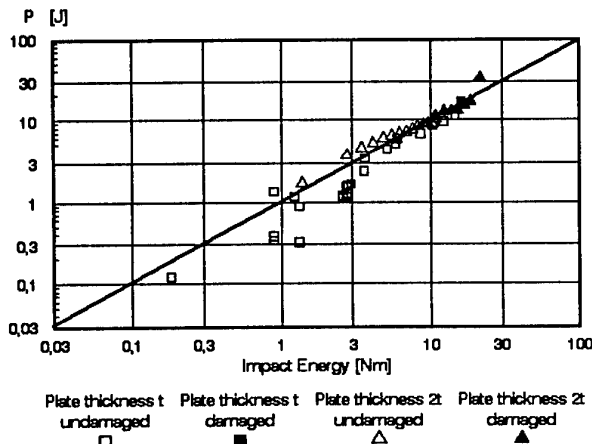


Fig. 22: P^* vs. Measured Impact Energy

Fig. 16 also contains data from tests where damage (delaminations) due to impact occurred. Damage was detected by use of ultrasonic testing. For plates with a thickness up to 5 mm damage could also be detected directly from the sensor signal, which was not possible for the thicker plates anymore. However also for this latter case the impact load can be determined from Eq. (23). Whenever P^* exceeds a threshold value, damage has to be expected in the component considered with high likelihood. Determination of that threshold value can be done by materials testing or reference to design guidelines. Results shown in Fig. 22 prove that P^* is a material constant being independent of the plate's thickness and thus the geometric shape.

Discussion

The parameter described so far allows to experimentally determine impact loads acting on components similar to the way fatigue loads are monitored nowadays. Application has been verified for rectangular plates clamped on all four sides and impacts loaded at the center of the plates' plane. Compared to conventional methods, such as the free vibration modes of a component (modal analysis) or the acoustic emission resulting from the damage (e.g. initiation of a delamination), sensor signals obtained with the P^* -method are much more intense, especially when considering small sizes of damage. Furthermore the effort for signal processing and analysis is very much reduced when compared to acoustic emission.

In this paper just the initiation of a method for monitoring impacts has been given which requires extension whenever applied to an engineering component. The next step is to identify how far impact loads induced at various locations on the plate can be monitored. Automation of signal analysis is another fundamental step for reliably determining the time t^* of interaction between the impactor and the structure as well as the maximum voltage U^* emitted from the piezoelectric sensor.

When applying the P^* -method to an engineering component a network of sensors may be required. Processing of data obtained from these various sensors could be done by using electronic devices such as analog signal storing elements, multiplexers and microprocessors. Additionally neural networks is another emerging technique to be considered for determining t^* and U^* as well as other values that might become important when extending the method to more general applications. An important guideline for designing the sensor network is to consider the distribution of impact criticality over the component's surface. Placing sensors simply to impact critical locations can help to reduce the effort for monitoring significantly.

So far the P^* -method has only been applied with sensors being attached to the specimen's surface. The advantage of doing so is that repair of the monitoring system is possible when a sensor or its contacts become damaged. However sensors have to withstand more severe environmental conditions when compared to the alternative of being integrated into the structure. This alternative needs to be considered because monitoring of impact loads might become quite difficult in very thick composite structures such as thicknesses above approximately 3 cm. Integration of these sensors into the composite material may

furthermore require consideration on how to minimize the effect of stress concentrations.

Last but not least it has to be mentioned, that reliably monitoring a component with the P^* -method is only possible when the monitoring system is working continuously. As soon as the system has been once switched off, inspection of a component is required by conventional non-destructive techniques.

As a conclusion the method presented here may be a step ahead of the traditional procedures used so far. However its application to real structures will still require achievement of a significant amount of further steps in development.

CONCLUSION

Structural health monitoring is one of the candidate applications suitable for introducing smart structures technology. In their actual stage structural health monitoring systems consist of sensors and sensor data processing and are limited to monitoring loads and evaluating damage. Technology exists for in-situ monitoring of damage even though its applicability is still limited to on-ground inspection.

When looking at the possibilities where contributions are made with respect to in-situ damage monitoring, the following fields can be identified:

1. Improvement in data processing and pattern recognition such as the use of data bases, neural networks and fuzzy logic. Especially the use of neural networks has gained significant importance (e.g. AIAA/ASME, 1994). The following lecture is therefore also related to fault detection by use of neural networks (Tomlinson, 1996).
2. Electronics and microsystems is another area that can highly contribute to improvement of signal processing. Increased miniaturization, power and reliability of these systems related with reduced cost have made them viable to even become an integral part of the structure and to perform a significant amount of data preprocessing (e.g. storage, amplification, filtering, etc.).
3. Emission of a well defined signal into a structure by use of a small localized actuator (e.g. a piezoelectric patch) and monitoring the change in impedance seems to be a monitoring procedure being quite promising when compared to the traditional procedures such as modal analysis or acoustic emission.
4. There is also an increased effort going on in implementing particles into composite materials leading to smart materials with intrinsic functions such as emitting specific noise or influencing magnetic or electric properties as a consequence of damage. Ideas following that idea have been reported by Schulte 1991, Neelakanta and Subramaniam, 1992, Lalande and Rogers 1996.
5. Technologies for adaptation and integration of sensors and actuators onto and into composite components have to be studied and developed with respect to improvement of the actuator/sensor and host material interface.

It is unquestioned that aircraft structural health monitoring is of significant importance with respect of direct operating and life cycle cost. Existing loads monitoring systems are a first step to monitor if aircraft have flown according to their design load spectra or not. The output of such systems can lead to either shorter or longer inspection intervals. These systems can be the basis for establishing a smart structural aircraft monitoring systems by taking advantage of the data and signal processes developed so far and improving them with the techniques mentioned above.

Actual security factors in aircraft design take into account the scatter in materials properties as well as the lack in knowledge of damage behaviour, the latter being especially related to composite materials. One of the important objectives with smart health monitoring systems is to improve detection of damage leading to taking better advantage the structural material's potential.

Integrating all the sensing, actuation and possibly even data processing techniques into the structural material by taking advantage of enhanced materials and micromechanics technology will finally lead to what is discussed in the lectures given by V.K. Varadan and V.V. Varadan within this lecture series.

REFERENCES

- Achenbach J.D. and D.O. Thompson, 1991: Towards Quantitative Non-Destructive Evaluation of Aging Aircraft; in: S.N. Atluri, S.G. Sampath and P. Tong (Ed.s): Structural Integrity of Aging Airplanes; pp. 1 - 13
 AIAA/ASME, 1994; Proc. of: Adaptive Structures Forum
 AGARD, 1991: Fatigue Management; AGARD-CP-506
 Amabile P. and T. Giacobbe, 1991: Proposal for the New Fatigue Management System for the AMX; AGARD-CP-506, Paper 9
 Bailey C.D., 1976: Acoustic Emission for In-Flight Monitoring on Aircraft Structures; Materials Evaluation, Vol. 34, No. 8, pp. 165 - 171
 Balis Crema B, A. Castellani and I. Peroni, 1985; Modal Test on Composite Material Structures Application in Damage Detection; Proc. of 3rd Internat. Modal Analysis Conf., Orlando/FA, pp. 708 - 713
 Barrett R., 1995; All-moving Active Aerodynamic Surface Research; Smart Mater. Struct. 4, pp. 65-74
 Bauer W., 1987: Event Monitoring Functions Introduced by the Onboard Life Monitoring System (OLMOS) into a German Aircraft; DFVLR-Mitt. 88-04, pp. 131 - 154
 Bolter Chr, P. Heuler, T. Seeger, O. Buxbaum, H. Oppermann, H.-G. Köbler and D. Schütz, 1983: Vergleich der Lebensdauervorhersage nach dem Kerbgrundkonzept und dem Nennspannungskonzept; FG Werkstoffmechanik, TH Darmstadt; Report No. FD-5/1983
 Bristow, 1992; Integrated Health and Usage Monitoring System (IHUMS); Aircraft Engineering, Febr. 1992, pp. 12-13
 Brown L.F. and R.H. Brown, 1990: Permanently Mounted Piezo Film Sensors for Structural Quantitative NDE; in: 1990 Review of Progress in Quantitative NDE
 Campanile L.F., 1993; A Modal Method for Structural Health Monitoring; Proc. of 4th Internat. Conf. on Adaptive Struct., Technomic Publ. Co.
 Carlyle J.M., 1989: Acoustic Emission Testing the F-111; NDT-International, Vol. 22, No. 2, pp. 67 - 73

- Crawley E.F. and E.H. Anderson, 1989; Detailed Models of Piezoceramic Actuation of Beams; AIAA 89-1388-CP, pp. 2000-2010
- Culshaw B., 1996; Smart Structures and materials; Artech House Books
- Egusa S., N. Iwasawa, 1993; Poling Characteristics of PZT/Epoxy Piezoelectric Paints; *Ferroelectrics*, Vol. 145, pp. 45 - 60
- Esteban J., F. Lalande and C.A. Rogers, 1996; Theoretical Modeling of Wave Propagation and Energy Dissipation in Joints; AIAA-96-1278-CP
- Fotos C.P., 1989; Acoustic Emission Technique Tests Aircraft Integrity; *Aviation Week & Space Technology*, August 28, 1989, p. 76
- Glossop N.D., S. Dubois, W. Tsaw, M. LeBlanc, J. Lymer, R.M. Measures, and R.C. Tennyson, 1990; Optical Fiber Damage Detection for an Aircraft Composite Leading Edge; *Composites*, Vol. 21, pp. 71 - 80
- Haberding R., 1985; Schwingungsüberwachung an Turboflugtriebwerken am Beispiel des Airbus A310; *VDI-Berichte* 568, pp. 167 - 181
- Hanner K.A., A. Safari, R.E. Newnham and J. Runt, 1989; Thin Film 0-3 Polymer/Piezo-electric Ceramic Composites; *Piezoelectric Paints; Ferroelectrics*, Vol. 100, pp. 255 - 260
- Hickman G.A., J.J. Gerardi and Y. Feng, 1991; Application of Smart Structures to Aircraft Health Monitoring; *J. of Intell. Mat. Syst. and Struct.*, Vol. 2, pp. 411 - 430
- Hillger W. and J. Block, 1986; Ultraschall- und Schallemissionsprüftechnik zur zerstörungsfreien Schadensanalyse an CFK-Proben; *Zeitschr. f. Flugwiss. u. Welt-raumforschung* 10, Heft 4, pp. 273 - 280
- Kaczmarek H., C. Simon and C. Delabarre, 1996; Evaluation of Lamb Wave Performances for the Health Monitoring of Composites Using Bonded Piezoelectric Transducers; *Proc. of ICIM'96 and ECSSM 96*, SPIE Vol. 2779, pp. 130 - 135
- Keilers Jr. C.H. and F.-K. Chang, 1995; Identifying Delamination in Composite Beams Using Built-In Piezoelectrics: Part I - Experiments and Analysis; Part II - An Identification Method; *J. of Intell. Mat. Syst. and Struct.*, Vol. 6, pp. 649 - 672
- Krauß A., 1988; Betriebslastenermittlung für Flugzeugentwurf und -entwicklung; 14. Vortragsveranst. DVM-AK Betriebsfestigkeit
- Kudva J.N., 1996; Structural Health Monitoring on Aircraft Components; this volume
- Ladda V. and H.-J. Meyer, 1991; The Operational Loads Monitoring System OLMS; AGARD-CP-506, Paper 15
- Lalande F. and C.A. Rogers, 1996; Qualitative Nondestructive Evaluation Research at CIMSS; *Proc. of ICIM '96 and ECSSM 96*; SPIE Vol. 2779, pp. 106 - 111
- Lee B.T., C.T. Sun and D. Liu, 1987; An Assessment of Damping Measurement in the Evaluation of Integrity of Composite Beams; *J. of Reinforced Plastics and Composites*, Vol. 6, pp. 114 - 125
- McBride S., M. Viner and M. D. Pollard, MacPhail, P.S. Bouwman and D.T. Peters, 1989; Acoustic Emission Detection of Crack Presence and Crack Advance During Flight; AGARD-CP-462, Paper 16
- McBride S., M. Viner and M. Pollard, 1991; Acoustic Emission Monitoring of a Ground Durability and Damage Tolerance Test; in: D.O. Thompson and D.E. Chimenti: *Review of Progress in Quantitative Nondestructive Evaluation*; Vol. 10B, Plenum Press, pp. 1913 - 1919
- Measures R., 1992; Fibre Optic Sensing for Composite Smart Structures; AGARD CP-531, Paper 11
- Miller R.K. and P. McIntire (Ed.s), 1987; Non-destructive Testing Handbook; 2nd Ed., Vol. 5, Acoustic Emission Testing; American Soc. for Non-destructive Testing
- Miner M.A., 1945; Cumulative Damage in Fatigue; *Trans. ASME, J. Appl. Mech.* 12, pp. 159-164
- Neelakanta P.S. and Subramaniam K., 1992; Controlling the Properties of Electromagnetic Composites; *Advanced Materials and Processes*, 3/92, pp. 20 - 25
- Palmgren A., 1929; Die Lebensdauer von Kugellagern; *VDI-Z* 69; pp. 337-341
- Pandey A.K., M. Biswas and M.M. Samman, 1991; Damage Detection from Changes in Curvature Mode Shapes; *J. of Sound and Vibration*, pp. 321 - 332
- Prinz R., 1983; Growth of Delaminations under Fatigue Loading; AGARD-CP-335; Paper 5
- Robinson N.A., L.D. Peterson and G.H. James, 1996; Health Monitoring of Aircraft Structures Using Experimental Flexibility Matrices; AIAA-96-1304-CP
- Scala C.M., 1986; A Semi-Adaptive Approach to In-Flight Monitoring Using Acoustic Emission; in: *Proc. of Review of Progress in Quantitative NDE*, San Diego, pp. 361 - 369
- Schulte K., 1996; Some Aspects on Health Monitoring in Composite Materials; *Proc. of ICIM '96 and ECSSM 96*; SPIE Vol. 2779
- Shen B., M. Tracy, Y.-S. Roh, and F.-K. Chang, 1996; Built-in Piezoelectrics for Processing and Health Monitoring of Composite Structures; AIAA-96-1310-CP
- Simpson D.L. (Ed.), 1987; Minutes of 20th ICAF, p. 5/23
- SPIE, 1988 ff.: Fiber Optic Smart Structures and Skins; SPIE Vol. 986 (1988), SPIE Vol. 1170 (1989), SPIE Vol. 1370 (1990), SPIE Vol. 1588 (1991), SPIE Vol. 1798 (1992)
- Spragg D., U. Ganguli, R. Thamburaj, R. Hillel and R.W. Cue, 1989; The Role of Inflight Engine Condition Monitoring on Life Cycle Management of CF-18/F404 Engine Components; AGARD R-770; Paper 4
- Stiffler R. and E.G. Henneke II, 1983; The Application of Polyvinylidene Fluoride as an Acoustic Emission Transducer for Fibrous Composite Materials; *Materials Evaluation*, pp. 956 - 960
- Tomlinson G.R., 1996; Use of Neural Networks/Genetic Algorithms for Fault Detection and Sensor Location; this volume
- Tracy J.J. and G.C. Pardoen, 1989; Effect of Delamination on the natural Frequencies of Composite Laminates; *J. of Composite Material*, Vol. 23, pp. 1200 - 1215
- Varadan V.K. and V.V. Varadan, 1996; Smart Structures, MEMS and Smart Electronics for Aircraft; this volume
- Vary A. and R.F. Lark, 1979; Correlations of Fiber Composite Tensile Strength with the Ultrasonic Stress Wave Factor; *J. of Testing and Evaluation*; pp. 185 - 191
- Victorov I.A., 1967; Rayleigh and Lamb Wave; Plenum, New York

USE OF NEURAL NETWORKS/GENETIC ALGORITHMS FOR FAULT DETECTION AND SENSOR LOCATION

G.R. Tomlinson, K. Worden and W. Staszewski

Department of Mechanical Engineering
The University of Sheffield
Mappin Street
Sheffield
S1 3JD
UK

1. SUMMARY

An approach to fault detection and sensor location using neural networks and genetic algorithms is described. A plate representing an aircraft panel is used as the structure and static strains, derived from a Finite Element model of the plate, are used as the supervised training set for the neural network. Having established a suitable diagnostic network, the process of optimal sensor location is carried out using a genetic algorithm for the diagnostic system. The final part of the paper briefly describes a new approach to fault detection using Novelty Measures which removes the need to use a supervised learning approach, common to most classical neural network procedures.

2. INTRODUCTION

Military aircraft of a new generation will be able to benefit from the significant advances that have been made in the pattern recognition methods that can employ a whole range of sensor signals such as Lamb waves, acoustic emissions and fibre optic outputs in fault detection procedures. Additionally, the location of the sensors can be optimised using recent developments based upon genetic coding algorithms which can assist the designers in locating the minimum number of sensors needed to locate/detect a fault to within a certain level of probability of success. The basic problem of fault detection essentially relates to pattern recognition using measurements taken from sensors which are distributed on a structure/component. The distribution/location of the sensors is embodied in the problem in that given the existence of an effective fault detection procedure, it is important to have a methodology as to where the sensors should be placed to ensure the optimum efficiency of the detection method. Clearly if one relates to the use of, for example, fibre optics and Bragg gratings for fault detection, then the optimal placement of the fibres and the gratings could result in a 'minimum intrusive' solution. There exist a large number of optimisation techniques but the more recent ones employing non-deterministic methods include neural networks, genetic algorithms, evolution strategies, simulated annealing and tabu search (references 1-5). This paper begins by presenting an approach to fault detection and sensor location using static strains as the supervised training data, derived from a numerical model of a plate meant to represent an aircraft skin panel. The strains are employed with neural networks and genetic algorithms to achieve the optimal placement of the sensors.

In the second part of the paper a new approach to fault detection is briefly described which has the advantage of not requiring a supervised learning procedure. This method, using Novelty Measures, has been reported by Worden (reference 5) and offers considerable potential for new generation aircraft. Although it utilises a neural network methodology, no dependability is placed on having an a-priori model of the system and as such it can be made insensitive to the boundary conditions or the non-stationary properties of an aircraft during flight.

3. ESTABLISHING THE DIAGNOSTIC NETWORK

The first stage in the fault detection procedure was to establish a neural network which was capable of detecting, with a high degree of confidence, pre-defined faults in the plate structure. Although there are no fixed rules for creating optimum neural networks, the input/output topology of the network was fixed by the geometry of the plate model and the number of 'measurement' locations. An aluminium plate, representative of an aircraft skin panel, of dimensions 300 mm x 300 mm x 3 mm thick with boundary conditions comprising two clamped edges and two simply supported edges as shown in Figure 1 was modelled using the FE ABAQUS code. Nine hundred, 8 noded quadrilateral shell elements on a regular 30 x 30 mesh were used. Damage was simulated by reducing the Young's modulus of various elements at 36 possible fault locations. Three different fault levels were simulated representing stiffness reductions of 10,000 (fault level 1), 10 (level 2) and 3 (level 3). The fault 'area' comprised nine elements as shown in Figure 2 and it was initially assumed that the static strains, due to both in-plane and bending loading conditions, were obtainable at 25 sensor locations, shown in Figure 3. Both normal and shear strains were computed and used as the training data set.

Thus, the input data was established as 25 real numbers (the normal or shear strains at the 25 sensor locations). The data was corrupted with zero-mean Gaussian noise to simulate experimental data. The output of the network had to report the existence or otherwise of a fault at the 36 fault locations, thus the input/output nodes of the network were 25 and 36 respectively. To determine the internal structure, ie number of hidden layers/nodes, a simple strategy was allowed; the network was trained to produce a value of 1.0 at output (fault location) 1 and 0.0 at the other outputs if the data set was associated with a fault at that location. Outputs

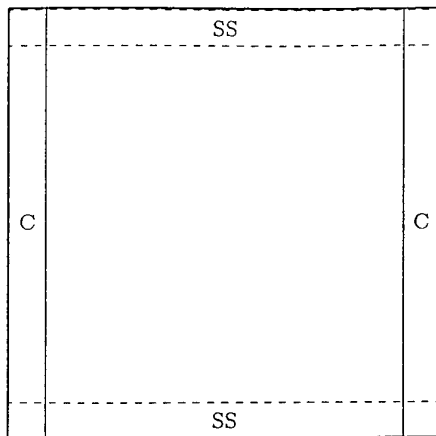


Figure 1: Boundary Conditions for the analysed plate
 SS = Simply supported
 C = Clamped

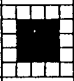
31	32	33	34	35	36
25	26	27	28	29	30
19	20	21	22	23	24
13	14	15	16	17	18
7		9	10	11	12
1	2	3	4	5	6

Figure 2: Numbering for fault locations and a typical fault area.

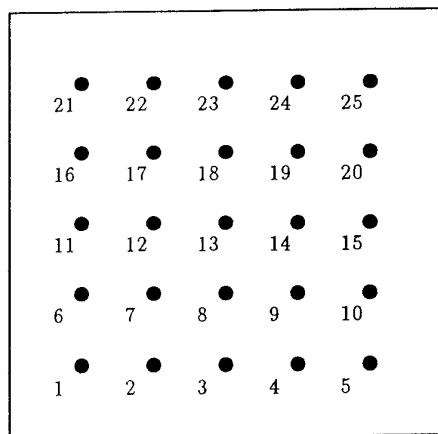


Figure 3: Sensor locations

2, 3 etc were similarly associated with faults at locations 2, 3 etc.

Using this strategy, the number of hidden layers was varied between zero and two and the number of nodes in the hidden layers was chosen by a trial and error procedure. The algorithm used was back-propagation with a hyperbolic tangent activation function (reference 7).

Three networks were trained, a linear network (25:36), a single hidden layer network (25:20:36) and a two hidden layer network (25:20:20:36). The best results were obtained with the single hidden layer network (25:20:36). Three different sets of normal (E11, E22) and shear strain (E12) were used. An example of the strain contours of the plate for a level 1 fault is shown in Figure 4. For each fault level, 200 copies of the strains were distorted by adding 1% and 5% Gaussian white noise which gave an initial training set of 7200 patterns. Figure 5 shows the output of the network for the E11 normal strain and fault level 1. The results represent output nodes 20 and 24 of the network for 7200 testing sets of input data to the network. The desired response should be unity between 3000 and 4000 points and zero elsewhere. The solid line is the ideal and the dotted line is the network response which shows good correspondence. The probability of mis-classification is a very important characteristic of the network and Table 1 shows the outcome of using the different types of strains. It is clear that the network performs better with the E12 shear strain than with the normal strains. This is simply due to the fact that the shear strain contours offer a better mapping than the normal strains, as can be observed from Figure 4. As the fault intensity reduces, the network performance reduces and if the noise levels increase at the same time the use of the normal strains E11, E22 would introduce probabilities of mis-classification which are unacceptable.

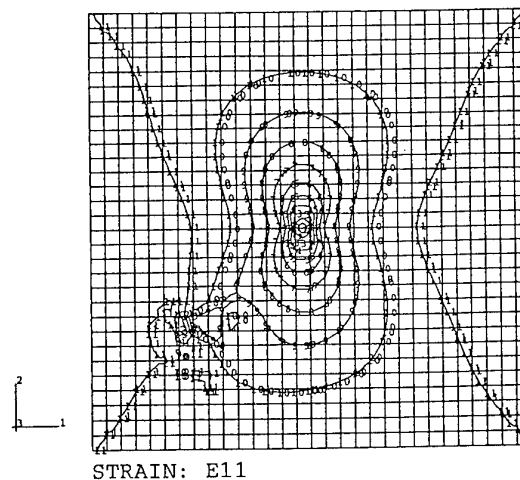


Figure 4 (a): Strain Contours for the Direct Strain E11

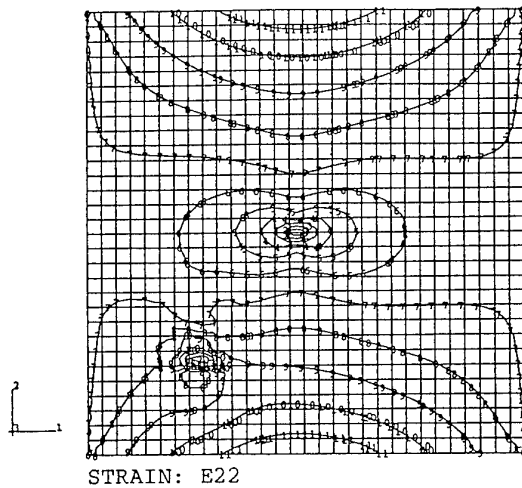


Figure 4 (b): Strain Contours for the Direct Strain E22

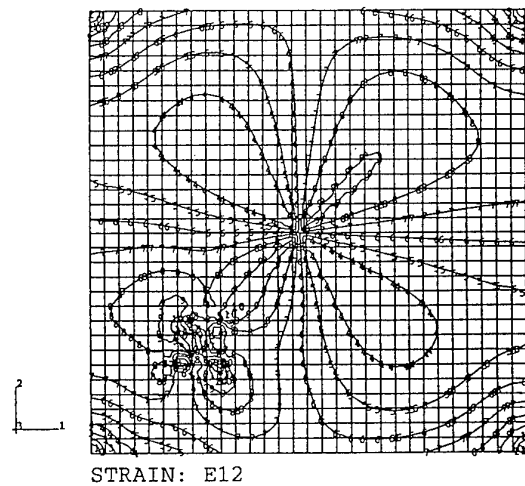


Figure 4 (c): Strain Contours for the Shear Strain E12

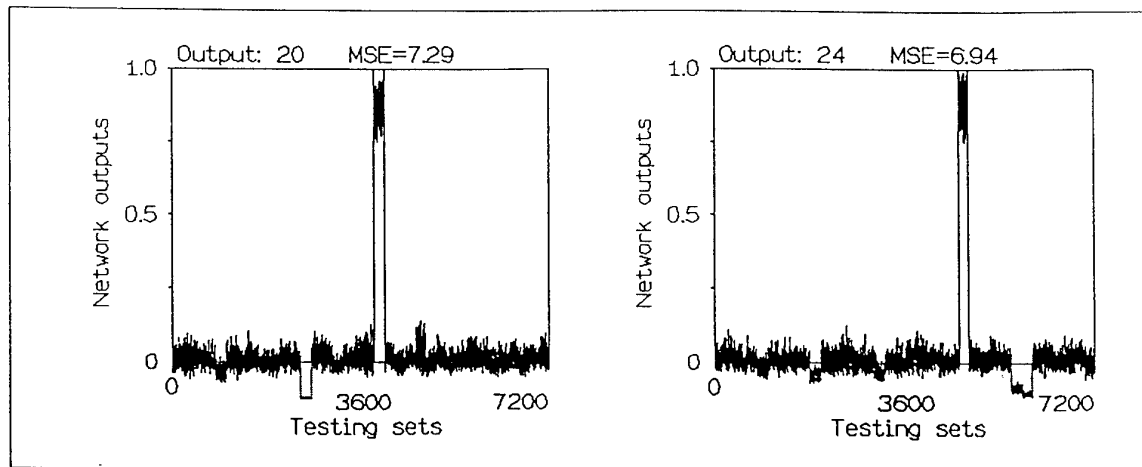


Figure 5: Neural network testing outputs. Network structure: 25:20:36. Strain data: E11. Fault advancement: 1. RMS noise level: 1%. Desired output (____). Measured output (----).

Fault advancement	Strain component	Noise level	
		1%	5%
1	E11	0	0.026
	E22	0	0.054
	E12	0	0.00014
2	E11	0	0.10
	E22	0	0.26
	E12	0	0.0094
3	E11	0.00014	0.5
	E22	0.0014	0.71
	E12	0	0.18

Table 1: Probability of misclassification. One hidden layer in the network structure used.

4. OPTIMAL SENSOR PLACEMENT USING A GENETIC ALGORITHM APPROACH

Genetic Algorithms (GAs) are search procedures which utilise the mechanisms of natural selection and genetics

(Ref 3). These procedures use random selection algorithms to do a highly exploitative search through a parameter space. The parameter space consists of genes which are coded as finite-length strings over some type of alphabet. The first step before the GA is to generate, at random, an initial population of possible solutions. The number of genes in a population depends on several parameters including the size of each individual gene and the size of the solution space. Having generated an initial population of genes, genes representing best solutions are chosen. To do this, a fitness function, which operates on encoded genes, is used to provide best solutions in the population.

The simple GA used involved the following operations:

reproduction - an artificial version of natural selection; a process in which individual fittest genes are copied to the next generation according to the given probability value.

crossover - a method of combination between pairs of genes in which the randomly chosen substrings from each gene are switched.

mutation - an operation involving random switching of gene binary digits.

new blood - new entirely random genes which form perturbations into the populations; these genes prevent a population from stagnating.

elite - a process in which the best solutions in a population are copied automatically into the next population to prevent the loss of the fittest genetic material.

Using the shear strain (E12) as the sensor signal, an integer coding was introduced as the genetic chromosome to represent the sensor location. For example (1 5 12 15 23) represents a solution in which sensors are located at positions 1, 5, 12, 15 and 23. The results for the different numbers of sensors is shown in Table 2 and Figure 6 where the probabilities of misclassification for a given number of sensors represents the minimum probability for the best sensor configuration.

These results have not been validated experimentally and thus it cannot be proved that the optimum solutions for the sensor placement have been found. However, methods based on symmetry and random placements (Refs 6, 7) have been shown to be inferior to the solutions generated by the GA.

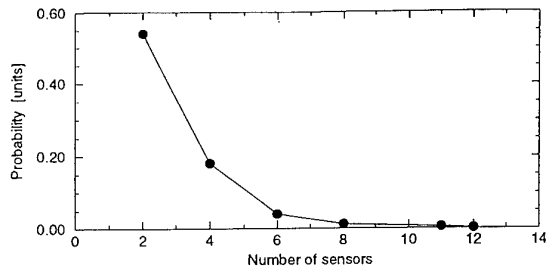


Figure 6: Summary of GA results - graphical representation of the probability of misclassification.

Number of Sensors	Sensor Pattern	Prob. value
12	1 2 3 5 9 10 11 16 20 21 23 25	0.0011
11	4 6 9 10 11 13 20 21 22 24 25	0.0051
8	1 5 8 11 15 16 23 25	0.012
6	4 6 15 16 23 25	0.040
4	5 7 16 24	0.18
2	2 23	0.54

Table 2: Probability of misclassification - summary of GA results.

5. A NEW APPROACH TO FAULT DETECTION BASED ON NOVELTY MEASURES

The previous sections dealt with the use of neural networks which require supervised learning procedures in order that they can be trained. This means that either numerical models such as FE have to be used to provide the training data or numerous experiments need to be carried out. However, a new approach to fault

detection that resolves these problems has recently been proposed (Ref 8). This is based on *novelty detection* in which the object is to monitor a sequence of patterns and if one (or more) arise which differ significantly from the statistics of the set, this is 'flagged up'. Neural networks are still used as the monitoring process, but in this case Auto-Associative Networks (AANs) are used. These are simply feed forward Multi-Layer Perception (MLP) networks which have a filter process whereby the data is passed through hidden layers which have fewer nodes than the input/output layers. Figure 7 shows an example of an AAN.

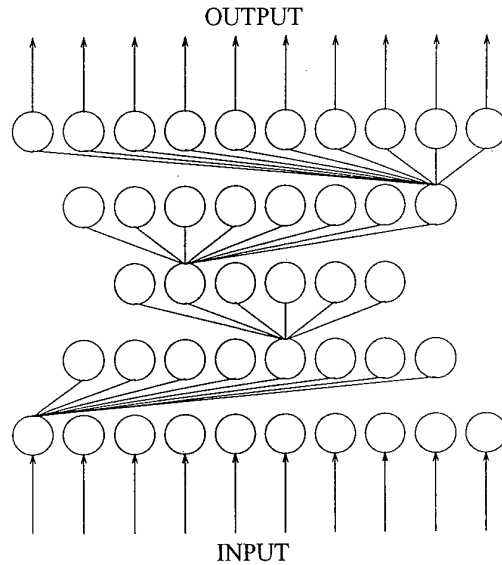


Figure 7: An example of an AAN (10:8:6:8:10)

The novelty index used in the following example is a very simple index, namely:

$$I(Z) = \|\underline{Z} - \hat{\underline{Z}}\|$$

where $I(Z)$ is the novelty index

\underline{Z} is a pattern vector

$\hat{\underline{Z}}$ is the network prediction of the pattern

Thus $I(Z) = 0$ represents a 'normal' condition. Damage is detected when $I(Z) \neq 0$.

5.1 A Numerical Example

This example is taken from Ref 12. Figure 8(a) shows the discrete system with a fault represented as a change in the stiffness of element k_{12} . Note that no *a priori* model is assumed and that only 'on-line' data is used.

The on-line training feature is the ratio of displacements (this could be strains, acoustic emissions etc) between the coordinate points 1 and 2. This ratio is called the Transmissibility function. The on-line training set was obtained by taking 1000 copies of the transmissibility patterns corresponding to the normal condition but corrupted with noise. Fifty regularly spaced points between 0 and 50 Hz were used from these functions as the training vector. A fault was introduced by reducing the stiffness of k_{12} by 1% and 10%. Figure 8(b) shows the Transmissibility functions

for these conditions and it can be seen that the 1% stiffness change produces zero discernible change.

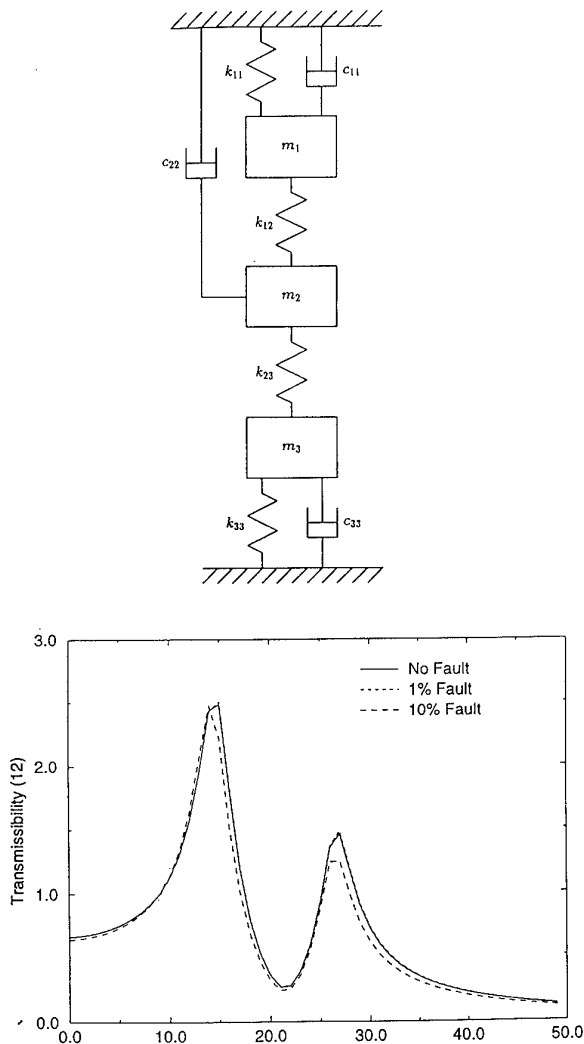


Figure 8: (a) Discrete system used for the simulation
(b) Transmissibility Functions for the various changes to element k_{12}

A network structure of 50:40:30:40:50 was used as the diagnostic and trained 'on-line' on the 50 sampled points from the noise polluted Transmissibility functions for the normal condition. Figure 9(a) shows the AAN output in terms of the novelty index over the normal training data. It can be seen that the mean level of the novelty index is around 0.2. When a fault is introduced and the novelty index is evaluated, the results are significant. Figures 9(b) and 9(c) show how the novelty index immediately detects the change when the fault occurs.

6. CONCLUSION

This brief paper has described state-of-the-art methods for fault detection/sensor optimisation. It has shown how a combination of advanced pattern recognition methods can be effectively employed for fault detection. Of particular significance is the 'on-line' novelty detection procedure which in principle may be employed with almost any sensor system and offers an important way forward for future work.

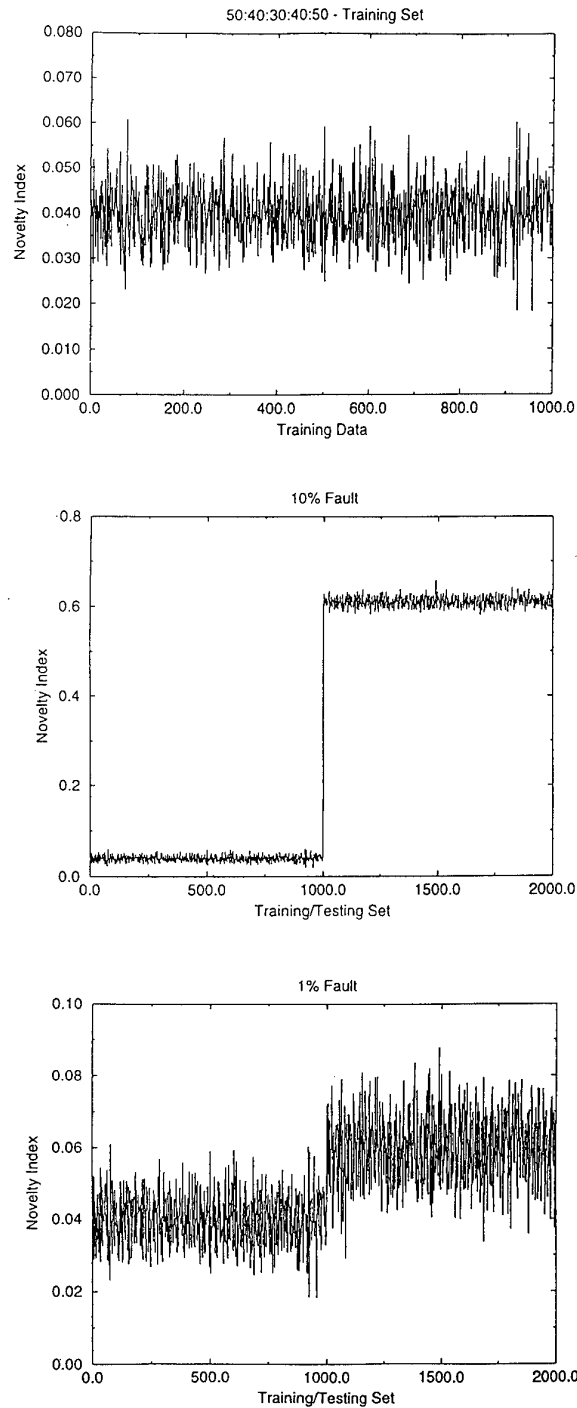


Figure 9: (a) AAN output on the unfaulted data
(b) AAN output with a 10% reduction in k_{12}
(c) AAN output with a 1% reduction in k_{12}

7. ACKNOWLEDGMENTS

The author is grateful to his co-researchers Dr Keith Worden and Dr Wieslaw Staszewski who have applied and developed the techniques and procedures used in this paper.

8. REFERENCES

1. Hopfield, J. J. and Tank, D. W., 'Neural Computation of Decisions in Optimization Problems', *Biological Cybernetics*, 52, 1985, pp 141-152.
2. Holland, J. H., 'Adaptation in Natural and Artificial Systems', University of Michigan Press, Ann Arbor, 1975.
3. Goldberg, D. E., 'Genetic Algorithms in Search, Optimization, and Machine Learning' Addison-Wesley Publishing Co Inc, Reading, Massachusetts, 1989.
4. Dekkers, A. and Aarts, E. H. L., 'Global Optimization and Simulating Annealing', *Math. Programming*, 50, 1991, pp 367-393.
5. Glover, F., 'Tabu Search, Part 1', *ORSA J. Computing*, 1, 1989, pp 190-206.
6. Staszewski, W. J., Worden, K. and Tomlinson, G. R., 'Optimal sensor placement for neural network fault diagnosis', *Proc. ACEDC '96*, University of Plymouth, UK, 1996.
7. Worden, K. and Burrows, A. P., 'Optimal sensor placement for fault detection'. Submitted to *Mechanical Systems and Signal Processing*, 1996.
8. Worden, K., 'Structural fault detection using a Novelty Measure'. Submitted to the *Journal of Sound and Vibration*, May 1996.

ACTIVE AND PASSIVE DAMPING TECHNIQUES

G.R. Tomlinson and J. Rongong
 Department of Mechanical Engineering
 The University of Sheffield
 Mappin Street
 Sheffield
 S1 3JD
 UK

1. SUMMARY

The use of passive and active damping techniques for minimising structural vibration is discussed. It is shown that passive damping, employing constrained viscoelastic layers requires careful consideration in terms of frequency and temperature in order to optimise the performance and that at high frequencies, the combination of longitudinal, flexural and radial modes can significantly modify the performance. When active methods are employed, dramatic improvements in the effective damping can be obtained and if this is combined with constrained viscoelastic materials, even greater improvements are found. This paper concludes with an overview of the concepts currently being applied and how Smart technologies should lead to effective solutions.

2. INTRODUCTION

Active and passive damping methods embrace a wide technology field encompassing materials, geometry, sensors, actuators and control techniques. Passive damping technology has addressed the problem of minimising structural vibration and noise by selective use of applying optimised damping materials to areas where the modal strain energy is high (reference 1) or, more recently, to 'potted joints' where the strain energy is dissipated in the joint material (reference 2). These methods are 'open-loop' and are effective only when structural resonances occur but have been shown to be capable of extending flight operations using damping wraps (constrained layer dampers) to slow down or stop crack growth in jet-engine vanes. The critical issues in using these passive methods relates to temperature when viscoelastic damping solutions are used (these being by far the most common) but the use of ceramic/enamel spray coatings is beginning to show promise (reference 3). Another limitation in the use of passive viscoelastic materials is that at low frequencies the loss modulus approaches zero and hence the ability to reduce low frequency resonances (eg. in space craft) is restricted.

If, however, a Smart concept is utilised in which sensors/actuators based on PVDF/PZT materials are used with the constraining layer system then both low and high frequency resonance effects can be controlled. These ideas are still being developed and several variants such as active damping and active constrained layer damping methods are being researched (reference 4).

This paper examines the use of passive damping methods for suppressing structural vibration, highlighting the care that needs to be given to the use of

such methods in order to obtain a good solution and then extends this to hybrid active/passive methods where the combination of viscoelastic materials with sensing and actuation is shown to offer advantages over pure passive methods.

3. PASSIVE DAMPING

This usually employs a high loss viscoelastic material in either a free or constrained layer construction. Constrained Layer Damping (CLD) is well established and has proved highly successful in suppressing unwanted vibration due to forced and flutter mechanisms in non-rotating fan vanes. The CLD method is by far the most popular as it is more effective in inducing cyclic strain energy into the constrained viscoelastic (damping) layer and as such this paper will concentrate on such methods.

To successfully apply CLD to a structure several important aspects have to be considered:

- the frequency and temperature dependence of the damping material;
- the mode shapes of the structure/component;
- the geometry of the composite CLD assembly.

These aspects have to be optimised for a particular application and the usual procedure is to employ the material property Master Curves with finite element calculations in order to predict the frequency response characteristics for a range of construction geometries (reference 5). The process can be speeded up considerably, by using, modal strain energy methods based on undamped eigenvalue/eigenvector finite element calculations to determine the regions of maximum strain energy (reference 6). From this the effective modal damping can be estimated using a modal strain energy ratio,

$$\eta_{\text{mode}}^{(i)} = \frac{\eta_s V_s + \eta_v V_v}{V_{\text{TOTAL}}} = \frac{\eta_v V_v}{V_{\text{TOTAL}}} = \eta_v \text{MSE} \quad (1)$$

where MSE is the modal strain energy ratio, η_s is the loss factor of the initial undamped structure in the mode i , η_v is the loss factor of the damping material and V_{sv} represents the strain energy in the structure (viscoelastic) material. For relatively simple structures such as beams, plates and rings, analytical methods can be used based on Rayleigh-Ritz or Virtual Work principles (references 6,7) but for large, complex

structures the finite element approach offers the best solution.

An example of the importance of carrying out modal strain energy analyses is shown in Figures 1 and 2. These figures show the results of a finite element analysis of a simple straight and curved beam with a constrained layer. It can be seen from Figure 1 that although the effect of curvature of the beam does not affect the modal strain energy ratio, there is a frequency range where two maxima (at 3.7 kHz and 6.2 kHz) and one minimum occurs (at 5 kHz). The maxima are where both shear and radial effects occur, as can be seen from the mode shape plot of the straight beam in Figure 2(a). In Figure 2(b), the mode shape at 5 kHz shows a longitudinal mode, producing little shear (and hence little strain energy) in the constrained layer. Thus it is essential to recognise that the type of relative motion between the damping treatment and the initial structure can result in a significant increase or decrease in the modal strain energies and hence in the effective modal damping.

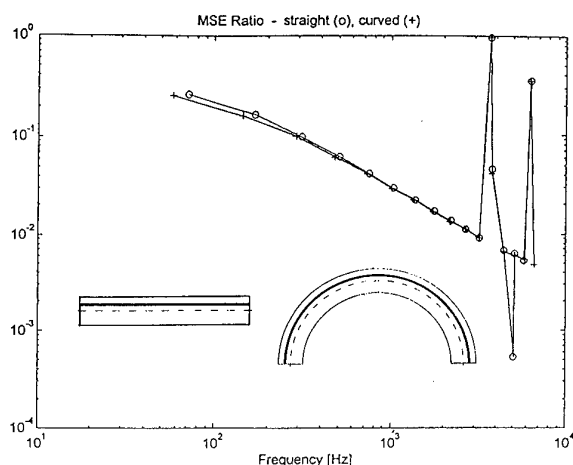


Figure 1: Modal Strain Energy for straight and curved CLD beams

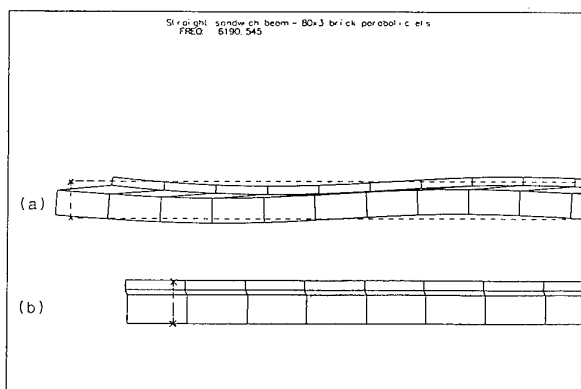


Figure 2: Mode shapes of the straight beam
(a) 6.2 kHz and (b) 5 kHz

A novel approach to passive damping is the use of 'potted joints'. This concept is shown in Figure 3 and the results of finite element predictions compared with experimental results is shown in Figure 4. Significant reduction in the vibration transmissibility levels are achieved between the vibration path entering the end

blocks and the carbon fibre vane after the material and the 'potted joint' geometry was optimised (reference 7).

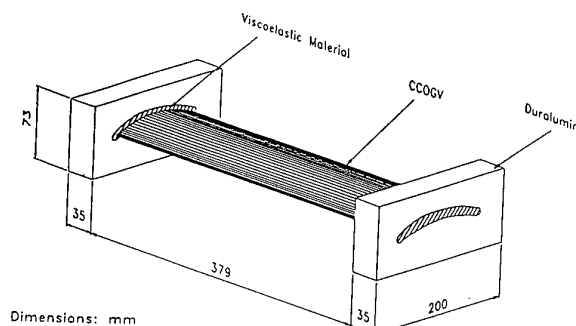


Figure 3: Potted joint assembly

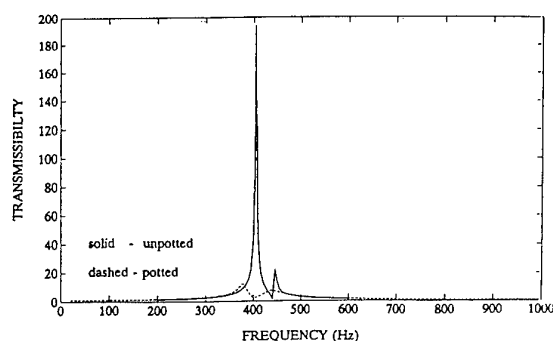


Figure 4: Comparison of potted and unpotted vibration transmissibility characteristics at 100°

4. ACTIVE DAMPING

The classical definition of active damping in Smart Structures terminology is to attach directly to a structure a sensor/actuator, which could typically be collocated PZT patches or a PVDF sensor and a PZT actuator patch and to feed back the sensor signal, appropriately modified in gain and phase, to the actuator to control or 'damp' the unwanted resonant characteristics. If the conditions of observability and controllability are satisfied, good results can be obtained (reference 8). However, if one is going to utilise an active damping solution it is possible to combine the best of passive and active damping procedures. This section of the paper concentrates on the recent developments in this technology which offers the potential for application to new generation military aircraft.

4.1 Active Damping Concepts

Several approaches to active damping are under investigation. Figure 5 shows the concepts which range from active CLD to active/passive CLD. The mathematical models which are used to develop the equations of motion of these composite constructions usually employ energy methods in which the strain and kinetic energies are formulated for the structure, the actuators and the viscoelastic materials. These are then combined with Lagranges equations to formulate the equations of motion (Ref 6). Alternatively, finite element models have been used to form the mass and complex stiffness matrices (Ref 8). The control laws used with the active damping methods range from simple velocity feedback methods to LQR optimal control theory (Ref 7). Whichever approach is used,

the objective of ACLD is to enhance the damping, via appropriate strain control, by shear deformation of the viscoelastic layer.

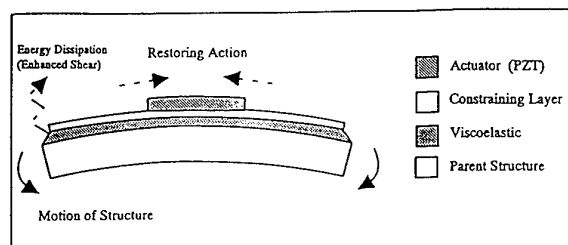


Figure 5 (a): Active Constrained Layer Damping

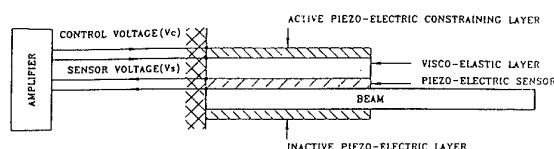


Figure 5 (b): Alternative version of ACLD

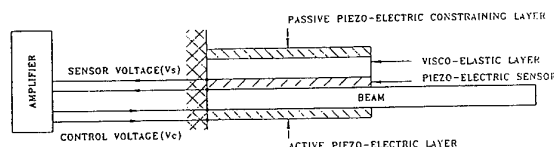


Figure 5 (c): Active/Passive CLD

Figure 6 shows the basic mechanisms involved in which the shear angle γ has to be maximised under the control action of the piezoelectric actuator (denoted p in the figure). This is very different to the classical active damping (AD) approach in which the actuators are bonded directly to the structure and it is the controlling 'moments' which provide the vibration suppression.

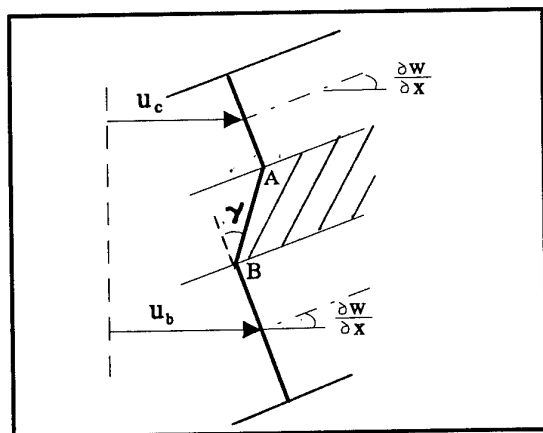


Figure 6: Shear angle of the viscoelastic layer

In order to compare AD with ACLD a simple experiment will be described. The experimental configuration is shown in Figure 7 in which a beam structure employed symmetrically placed constraining layers and PZT actuators. This allows the actuators to be used 'out-of-phase' creating flexural induced damping or 'in-phase' creating longitudinal induced damping. An identical beam was also manufactured with the PZT actuators placed directly on the beam

surface to provide an active damping (AD) comparison. The sensor was an accelerometer located at the tip of the beam which was employed with velocity feedback control to the actuators. Ref 6 provides full details of the governing equations of motion for the system. In the first set of tests the PZT actuators were excited using a 0-10 kHz band limited random signal (100 v ptp); in-phase to excite the longitudinal modes and out-of-phase to excite the flexural modes, the response at the tip of the beam being measured by the accelerometer. The idea was to maximise the shear strain in the viscoelastic layer to minimise the vibration at the tip of the beam. Figures 8 and 9 show the results for the longitudinal and flexural behaviour for the AD and the ACLD configurations. It is clear that better damping performance is obtained via the ACLD configuration.

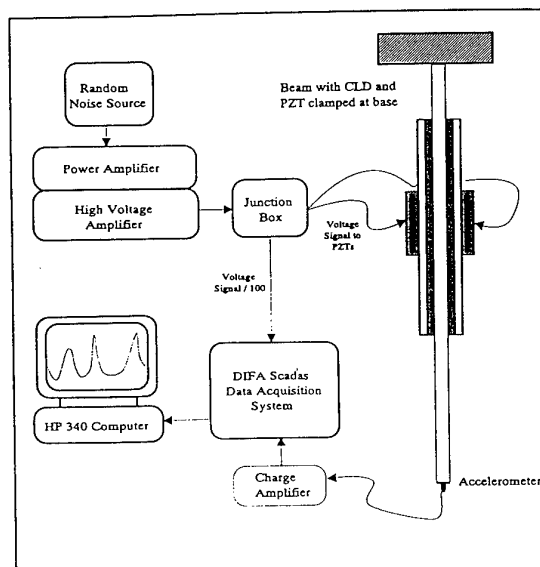


Figure 7: Experimental arrangement used for symmetric (longitudinal) and asymmetric (flexural) ACLD studies

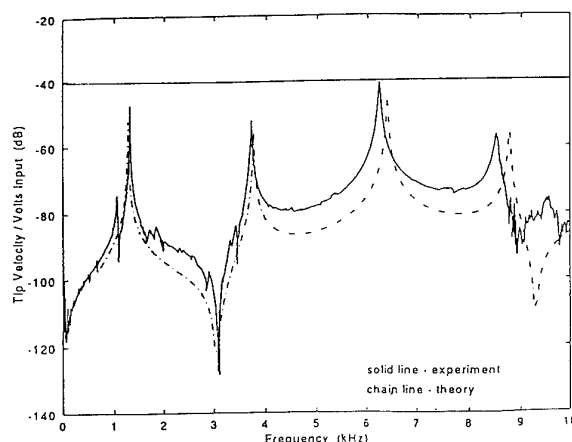


Figure 8 (a): PZT patches directly bonded to the beam - longitudinal vibration characteristics

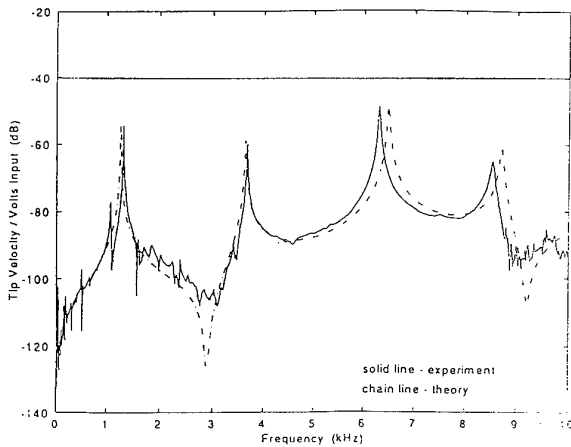


Figure 8 (b): As in Figure 8 (a) but with the PZT patches bonded to the constraining layer

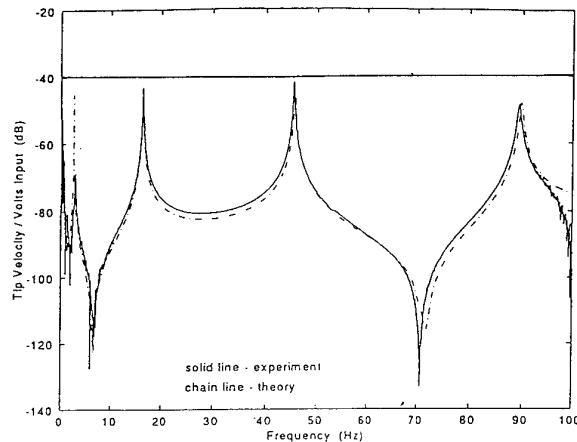


Figure 9 (a): PZT patches bonded directly to the beam - flexural vibration characteristics

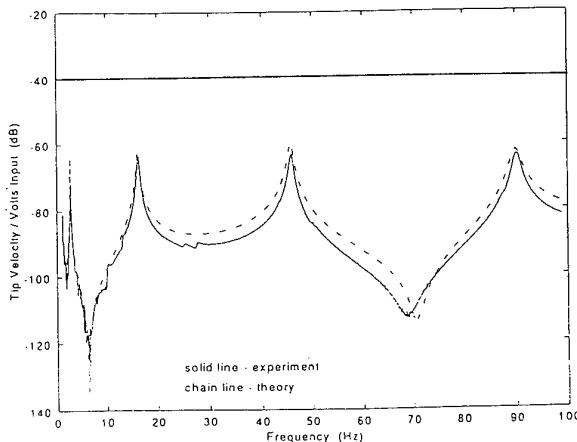


Figure 9 (b): PZT patches bonded directly to the constraining layer

In order to validate the apparent gain in damping performance, a conventional control test was carried out using the actuators driven by the feedback voltage from the accelerometer. Again, the ACLD and the AD (ie. the actuators driving the constrained layer system and the actuators being bonded directly to the beam respectively) beams were used. However, in this second set of tests, the cantilever beam assembly was

mounted on a vibration exciter and driven at its base in flexure in order that the beam tip to base input vibration transmissibility could be measured. The location of the actuators/sensors was not optimised and in particular it was deliberately chosen to locate these in a *non-collocated* manner in an attempt to demonstrate the effectiveness of ACLD. Figure 10 shows the variation in the base-to-tip transmissibility as the feedback gain to the actuators was increased. It can be seen that for the beam with no constraining layer, large values of transmissibility were observed at the various resonant frequencies and the third mode became unstable (due to non-collocation of sensor/actuator) at a relatively low feedback gain of about 50. The ACLD system, however, reduced the resonance peaks over the entire frequency range used and also reduced the vibration levels of the fourth mode of vibration which was almost unaffected by the conventional AD approach, owing to the spatial positioning of the actuators not being optimised for that mode.

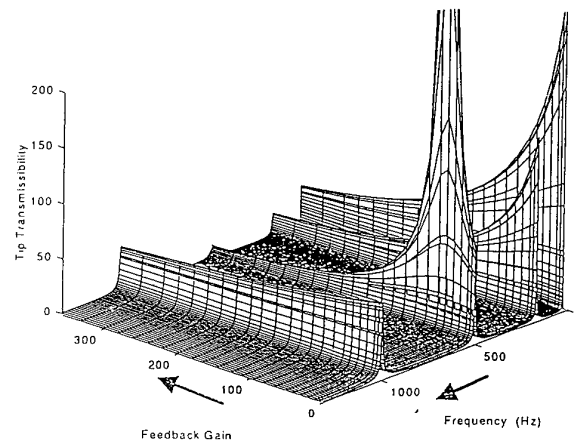


Figure 10 (a): Tip/Base transmissibility characteristics as a function of the feedback gain - PZT patches bonded directly to the beam

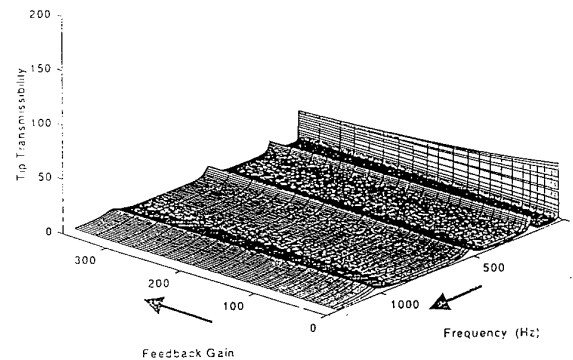


Figure 10 (b): As Figure 10 (a) but with the PZT patches bonded directly to the constraining layer

An additional advantage of the ACLD is shown in Figure 11. It is seen that for the AD configuration much higher voltages are needed to achieve the same feedback gain levels. For example, if the maximum voltage to the PZT actuators was limited to 200V (peak), the maximum feedback gains would be 50 for the AD configuration and 270 for the ACLD configuration before non-linearity occurs in the PZT material, hence giving greater controllability.

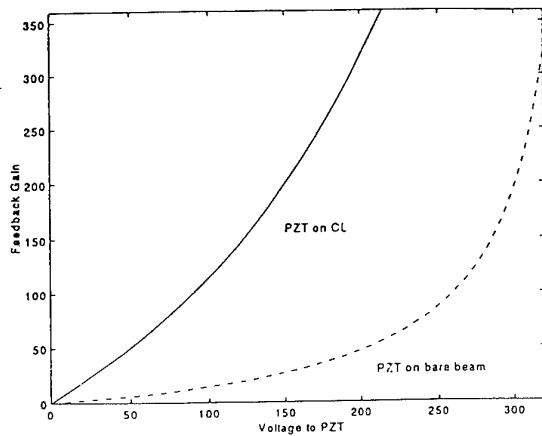


Figure 11: Feedback gain versus PZT excitation voltage for the PZT patch on the constraining layer (CL) and on the beam directly

5. CONCLUSIONS

Active damping is a strong candidate for smart structures. If this is combined with passive damping to create an active constrained layer damping configuration, significant benefits can be derived over a wide frequency range. Although this paper has not gone into great detail regarding active damping, the main concepts have been highlighted and it is clear that the use of PVDF/PZT materials for sensors and actuators can provide an effective combination for active damping in smart structures.

6. ACKNOWLEDGEMENTS

The author would like to acknowledge Mr J. Rongong who provided the material for this paper.

6. REFERENCES

1. Johnson, C. D. and Kienholz, D. A., 'Finite element prediction of damping in structures with constrained viscoelastic layers', *AIAA Journal*, 20, (9), 1981, pp 1284-1290.
2. Oyadiji, S. O. and Tomlinson, G. R., 'Controlling the vibration levels of vibrating vanes using viscoelastic materials', *ASME Design Eng Conf*, Vol 84-3, Pt C, 1995, pp 709-718.
3. Futamata, M., Fuji, A., Nakahira, H. and Harada Y., 'Effects of thermal spray coating on sound and vibration damping. II. Damping characteristics of continuous sound', *J. High Temp. Soc. Japan*, 15, (5), 1989, pp 234-241.
4. Tomlinson, G. R., 'An overview of active/passive damping techniques employing viscoelastic materials', *Proc 4th ICIM Conference*, Lyon, 1996, pp 656-669.
5. Graphical presentation of the complex modulus of damping materials, BS7544: 1991, ISO10112: 1991.
6. Rongong, J. A. et al 'Modelling of a hybrid constrained layer/piezoelectric approach to active damping', submitted to the *ASME Journal of Vibration and Acoustics*, 1995.
7. Liao, V. H. and Wang, K. W., 'On the active-passive hybrid vibration control actions of structures with active constrained layer treatments', *ASME Design Eng Conf*, DE-Vol 84-3, Pt C, 1995, pp 125-141.
8. Baz, A. and Ro, J., 'The concept and performance of active CLD treatments', *Journal of Sound and Vibration*, 28, 1994, pp 18-21.

A Novel Approach to Structural Design using Biological Models

R. Wardle*

G. R. Tomlinson†

Dynamics Research Group
Department of Mechanical Engineering
University of Sheffield, Mappin Building
Mappin Street, Sheffield S1 3JD, UK

1 SUMMARY

Methods of adapting the placement and properties of material within structures subject to static and dynamic loading are presented. It is shown that for a statically loaded cantilever a spatially local adaptation process can produce a structure which has a topology and material properties much improved from the original. For a dynamically excited structure an evolutionary method is used to add free-layer damping to the surface of the structure, reducing the amplitude of vibration while minimising the mass of additional damping material.

2 INTRODUCTION

Biological analogies are used in many aspects of engineering design. In structural engineering, many comparisons can be drawn between biological load carriers such as trees and animal limbs and man-made structures such as cantilevers, and it is natural to ask whether the evolutionary processes which act to remodel bone and wood can be used to remodel engineering structures, making them more suited to their function. The remodelling, or *functional adaptation*, is generally aimed at eliminating material which contributes little to the desired structural goal, while adding new material where an enhancement could be achieved or where alteration is necessary due to damage or changed loading conditions. We can express this adaptation in the form of a cellular model, the cells of which are subject to 'birth and death' rules. These rules are essentially local functions of some relevant property of the structure under consideration; for example, a 'cell' might live or die depending on the level of stress it experiences. As well as the addition or removal of structural material an existing cell's properties may change; for example a cell's Young's modulus may increase to stiffen a part of a structure.

The subject of this paper is an investigation into how evolutionary methods, in contrast to traditional optimisation schedules, may be used to produce more efficient (in terms of load bearing capacity per mass of structure) load-bearing structures. An evolutionary approach is used to alter the Young's modulus of a cantilever structure in response to an imposed load. Elements of the structure are also subjected to a 'birth-death' schedule which eliminates 'unwanted' elements while producing new elements in parts of the structure which are over-stressed (see (ref. 6) for a similar approach).

The investigation is extended to include a demonstration

of how an evolutionary approach can be used to alter the dynamics of a structure subjected to a time-varying load through the progressive addition of structural damping. A common technique in the suppression of excessive vibration in structural components is the addition of damping materials to the surface of the structure. This technique of passive vibration suppression utilises the energy dissipation properties of viscoelastic materials to reduce structural resonance amplitudes. By adding a layer of viscoelastic material to the surface of the base material, strain energy can be transferred into the viscoelastic where the energy of vibration can be dissipated. If the damping material is added gradually using an evolutionary approach, placement of the material can be optimised.

3 EVOLUTION OF A STATICALLY LOADED STRUCTURE

3.1 Finite Element Model

The statically loaded structure was evolved from a cantilever plate, 30 cm long, 20 cm deep and 2.5 mm thick (figure 1), which was assumed initially to have the mechanical properties of aluminium (Young's modulus of $70 \times 10^9 \text{ N/m}^2$, Poisson's ratio of 0.3 and mass density of 2700 kg/m^3). The plate was built-in at one end and loaded at a point 10 cm from the free end with a load of 10 N. The plate was divided into 0.5 cm square elements which formed both the finite element mesh and the cells for the evolutionary procedure.

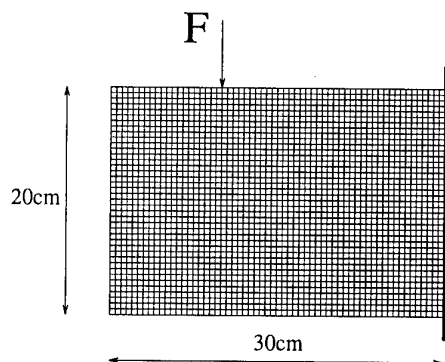


Figure 1: Finite Element Model

3.2 Evolutionary Procedure

The aim of the evolutionary procedure was to change the Young's modulus of each element depending on the stress

*e-mail: r.wardle@sheffield.ac.uk

†e-mail: g.tomlinson@sheffield.ac.uk

level in that element. The von Mises stress was used as the element stress. Following Inou, Shimotai and Uesugi (ref. 2), and Worden and Tomlinson (ref. 5), a non-linear stress-modulus adaptation curve was used to control the evolution (figure 2), as it is known that this high degree of non-linearity is required to produce an organised structure. The procedure was a local adaptation process, meaning that the state (modulus) of an element depended only on its current modulus and level of stress. This condition is necessary if the procedure is to mimic the adaptation process of a natural material such as bone (ref. 1). The following procedure was applied to the structure: (1) Set up the initial plate structure as a finite element model. (2) Calculate the von Mises stresses in the structure. (3) Change the Young's modulus of surviving cells in the structure, based on the element stresses. (4) Remove cells which do not contribute to the load-bearing function of the structure; add cells in areas which are over-stressed. (5) Go to step 2. The procedure was continued until a stable structure emerged, or until a pre-determined number of iterations was exceeded.

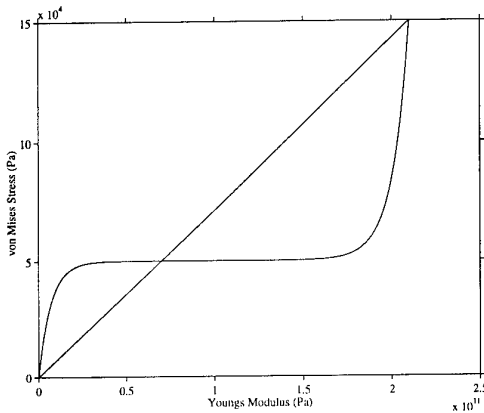


Figure 2: Stress/Modulus Adaptation Curve

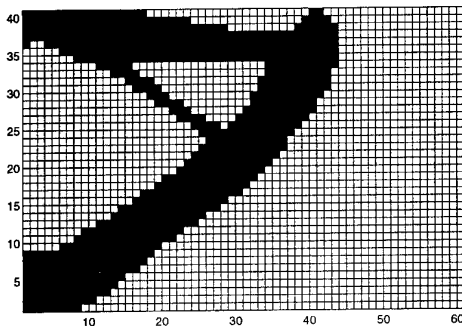


Figure 3: Structure after 200 Evolutions

3.3 Results And Discussion

Initially, a method of cell elimination followed in (ref. 5) was used, where an inefficient cell was given a very low modulus. It was found that this method produced some anomalous structures and led to particular difficulty in dynamic analyses; consequently, the evolutionary procedure

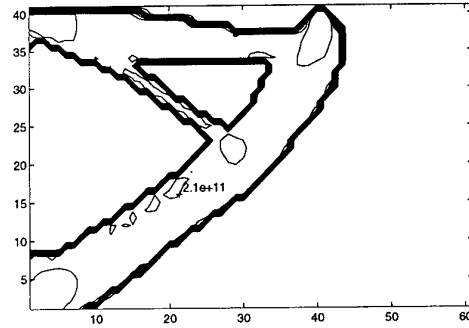


Figure 4: Final Distribution of Young's Modulus

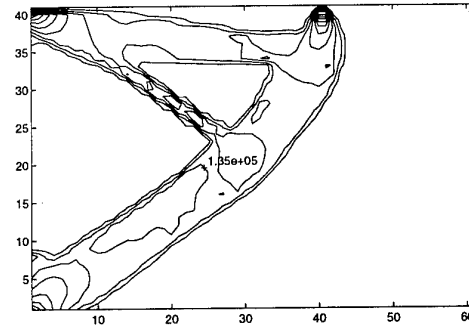


Figure 5: Final Distribution of von Mises Stress

removed elements from the FE model altogether rather than simply assigning them a low modulus. The resulting structure resembles those proposed by Michell (ref. 3) (figure 3). It is noted that to produce a Michell-like structure a highly non-linear stress-modulus curve must be used in the evolution process. In fact, this is equivalent to producing a material with a non-linear stress-strain relationship, and in the 'best' structures (i.e. the highly organised, near-Michell type structures), the non-linear stress-strain relationship approaches a linear one where the Young's modulus, and stress, are constant throughout the structure — see figures 4 and 5. The contour values on these figures are given in pascals. Hence the resulting structure is taken to be of the shape shown in figure 3 with a modulus value of 210 GPa.

4 EVOLUTION OF A DYNAMICALLY LOADED STRUCTURE

4.1 Structural Damping Using Viscoelastic Materials

It is possible (and commonplace) to reduce vibration levels in structures by adding passive damping in the form of layers of viscoelastic material attached to the surface of the structure. It is an attractive method because the materials are easy to apply (as only the exterior of the structure needs to be accessible) and it is relatively effective. In order to operate efficiently the damping material must be placed on the surface in positions of high strain energy so that the energy dissipation per unit mass of viscoelastic is high. One way of estimating the effectiveness of the added damping method is to model the structure with the viscoelastic coating layer using the finite element method (FEM). The damping is estimated using the *modal strain energy* method (MSE) (ref. 4). Assuming the damped

modes of vibration are similar to the undamped modes, and that initially frequency and temperature dependence on the elastic moduli of the viscoelastic is ignored (no damping behaviour), a modal analysis will give the strain energy distribution in the base structure and in the viscoelastic. The *loss factor* for the r th mode is given by

$$\eta^r = \sum_{j=1} \eta_j \frac{SE_j^r}{SE^r} \quad (1)$$

where SE^r is the total strain energy for the r th mode, η_j is the loss factor of the j th material, and SE_j^r is the strain energy in the j th material for the r th mode. Hence, since for a combination of viscoelastic and metallic structure, we can assume $\eta_m \ll \eta_v$, where the m subscript refers to the metal and the v to the viscoelastic, and hence

$$\eta^r \approx \eta_v \frac{SE_v}{SE^r} \quad (2)$$

The strain energy distribution in each mode shows where the viscoelastic material must be placed to produce the maximum amount of damping for the lowest amount of added material (which adds mass and expense); the coating layer should be present primarily in these areas of high surface strain energy. The placement of the damping layer depends upon the judgement of the designer, and suffers from the added difficulty of the conflicting requirements of damping in multiple modes.

This paper proposes an alternative method of viscoelastic damping layer placement which utilises the evolutionary approach. An initial eigenvector analysis is performed which gives the strain energy distribution per mode, for a given number of modes. Viscoelastic material is then added to the surface at positions of relatively high surface strain energy, where the strain energy is considered for all desired modes. In this preliminary investigation, the analysis was limited to consideration of the first mode.

4.2 Finite Element Model

The structure optimised for static loading in the previous section was selected for the dynamic analysis (figure 3). The final structure (figure 6) was composed of a 'metallic' material with Young's modulus of 2.11×10^{11} N/m², Poisson's ratio of 0.3 and mass density of 2700 kg/m³, a product of the optimisation procedure. The FE model of this structure was highly discretised, using 0.5 mm 'blocks'. This was an artifact of the previous optimisation procedure, and also made the addition of viscoelastic elements easier. The base structure was assumed to have a structural (Rayleigh stiffness proportional damping) of around 0.5 % near the first frequency.

The viscoelastic material itself was an idealised abstraction to simplify the analysis. The material was modelled using the complex modulus method, where the Young's modulus of an element is given by $E^* = E' + jE''$, E' being the storage modulus and E'' the loss modulus. For the purposes of this study E^* was assumed to be independent of frequency. The properties of the viscoelastic were taken as 'typical' values (ref. 4), with the loss factor $\eta = 1.0$, and $E' = 33 \times 10^6$.

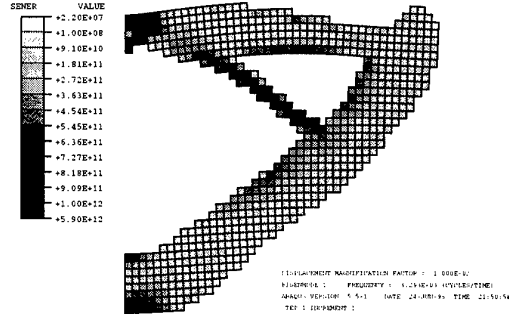


Figure 6: 1st Mode

4.3 Evolutionary Procedure

In a modal strain energy analysis, placement of viscoelastic material for damping can be done by eye. The aim of this study is to develop a more systematic method of damping material placement which places material only where it is needed. In the case of multiple-mode damping, it is expected that the evolutionary method will place damping in locations which may not be immediately obvious.

In this initial study, some simplifications were made to enable the work to concentrate on the effectiveness of the growth process. First, instead of concentrating on modes demonstrating the largest amplitudes at resonance, only the first mode was considered for damping treatment. Generally, the first mode will be among those modes which suffer from large amplitude vibrations; and the coarseness of the finite element mesh made some of the higher mode shapes to be of suspect accuracy. The viscoelastic layer was of a single, constant thickness, represented by a single 'block' element in the finite element model. The 'blocks' were placed only where they would contact elements of the structure along an element edge (elements were not allowed to join at corners). The iterative procedure for adding viscoelastic elements was

1. An eigenvector analysis for the first mode only was performed on the structure using the ABAQUS finite element package.
2. The strain energy in each element was recovered from the FE results file, and a 'strain energy threshold' was defined as

$$\widehat{SE} = \lambda \times \text{maximum}(SE) \quad (3)$$

with

$$SE = \{SE(x_i) | x_i \text{ is a surface element}\}$$

where $SE(x_i)$ is the strain energy in element x_i . $\lambda < 1$ is a variable parameter which specifies the proportion of edge elements to remove at each step, and was set to 0.9.

3. All surface elements which have a strain energy greater than \widehat{SE} 'grow' an adjacent viscoelastic element, if possible. Growth of viscoelastic is limited to positions directly 'north', 'east', 'south' and 'west' of the element under consideration. Elements

which grow their maximum number of elements are no longer considered to be surface elements and are removed from the set SE.

4. The cycle is repeated from step 1.

4.4 Results And Discussion

Free-layer damping was added as described until the entire structure was 'coated' with a single-thickness layer of material; it took 107 iterations of the cell-addition procedure for the structure to become completely covered. The state of the damping layer is shown after 7 iterations (figure 7), 20 iterations (figure 8), 50 iterations (figure 9) and 80 iterations (figure 10). Grey represents the base structure, while black shows the location of the viscoelastic.

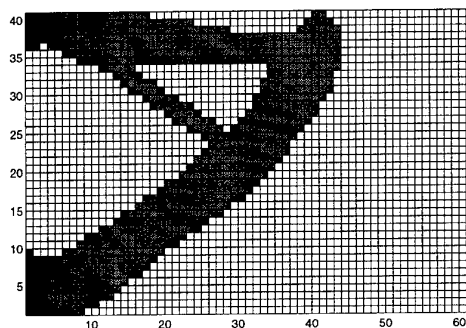


Figure 7: 7 Iterations

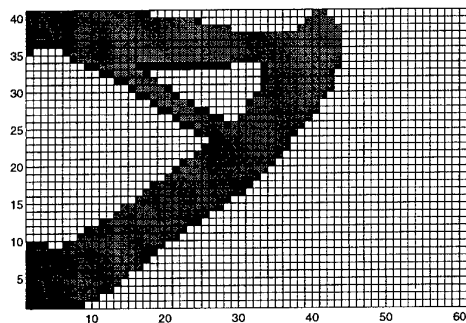


Figure 8: 20 Iterations

At each point in the evolution, the loss factor was esti-

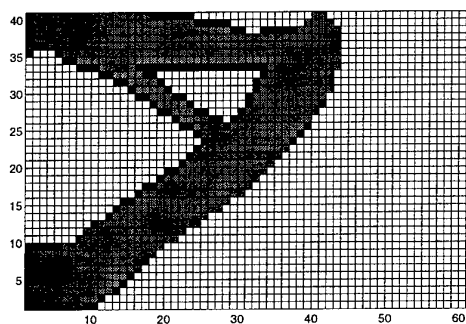


Figure 9: 50 Iterations

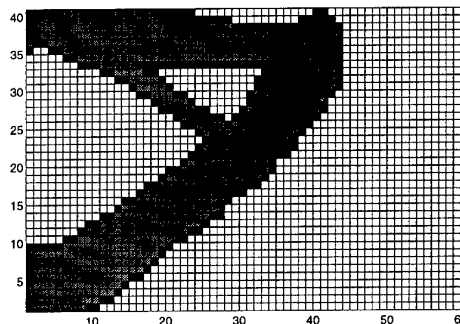


Figure 10: 80 Iterations

mated using the modal strain energy method. The evolution of the loss factor is shown in figure 11 as a function of the proportion of mass of viscoelastic to mass of the base structure; when the structure is totally covered the mass of the viscoelastic is almost 10% that of the base structure. The initial study is represented by the 'Material 1' curve; the other curves are explained below. The normalised amplitude of vibration, $\frac{X}{F/k}$, reduces quickly over the first few iterations, and then reduces much more slowly up to total coverage. This is important as it is shown that a 'by eye' estimate of the amount of damping may be an over-estimation of the actual damping required — the asterisks in figure 11 are damping values against relative mass for 'by eye' estimations (see below). By examining an evolutionary curve as shown, the minimum sufficient amount of damping may be added to reduce vibration levels below a specified amount, while keeping the added mass of damping material to a minimum. Figure 13 shows a structure which has had damping added 'by eye' i.e. using good judgement based on the surface strain energy distribution from the initial undamped eigenvector analysis. Figure 14 shows the same case but with a double-thickness layer. Referring to figure 11, the asterisk at relative mass of around 0.055 is the performance of the structure with the 'normal thickness' damping layer. The other asterisk represents the performance of the 'double thickness' damping layer. While the absolute level of

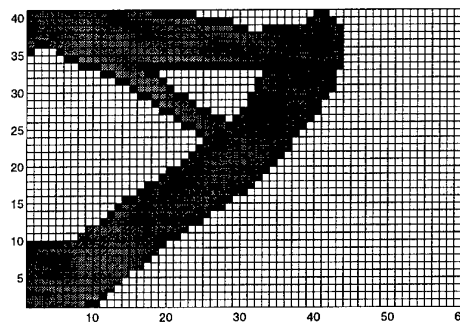


Figure 13: Placement of Damping 'by eye' — Normal Layer

added damping may not appear to be impressive, this may be attributed to three things. First, the model is discretised in a way which does not lend itself well to transferral of energy to the viscoelastic via the extensional principle.

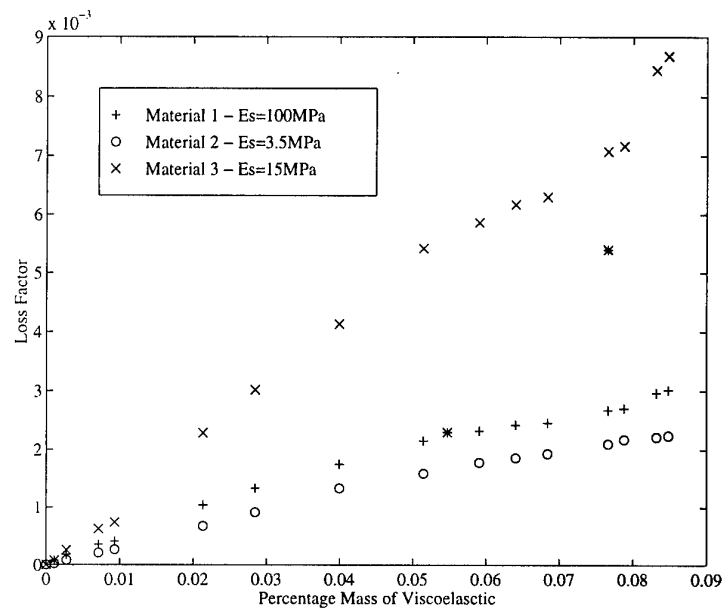


Figure 11: Loss Factor as a Function of Relative Mass of Viscoelastic

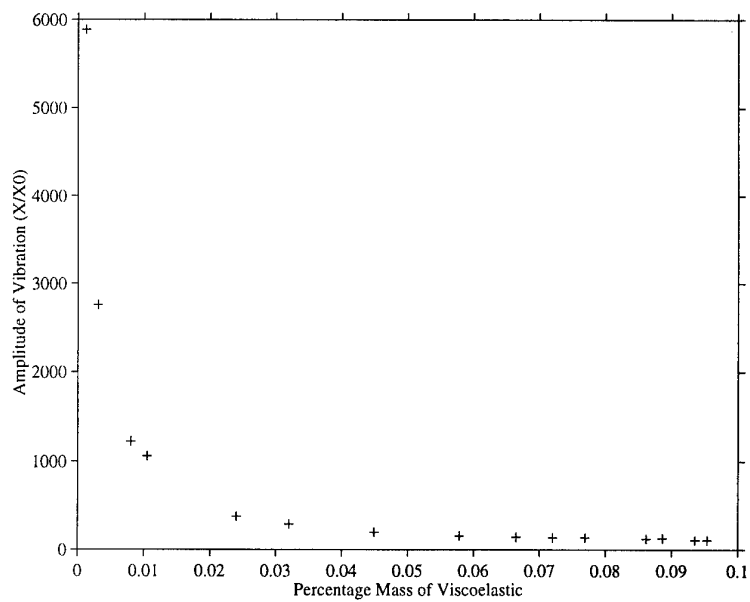


Figure 12: $\frac{X}{F/k}$ as a Function of Relative Mass of Viscoelastic

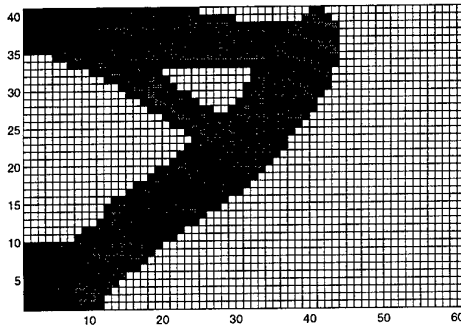


Figure 14: Placement of Damping 'by eye' — Thick Layer

This could be easily remedied by the construction of a better finite element model. Secondly, the damping used is of the free-layer type, which is recognised as having an inherently limited potential for energy dissipation (ref. 4). It is known that $\eta \propto t_n$ for free-layer damping and it can be demonstrated that the thickening of the damping layer at any point in the evolutionary process leads to much greater damping. The absolute damping could therefore be increased through the use of thicker layers or alternatively (and preferably) a *constrained layer* of viscoelastic material. The current study was conducted using free-layer methods for simplicity, but further work would be carried out using constrained-layer methods. Lastly, the properties of the viscoelastic were idealised to a certain extent, and it was found that lowering the modulus of the material produced more strain and hence larger losses. The effect of changing the damping material properties can be seen in figure 11, where 'Material 2' has loss factor $\eta = 1.0$, and $E' = 1 \times 10^6$, while 'Material 3' has loss factor $\eta = 0.7$, and $E' = 5 \times 10^6$. Material 3 is based on the properties of the viscoelastic ISD112 at 20°C, 3kHz. It is evident that the mechanical properties of the damping material have a strong effect on the structural loss factor. No attempt has been made to take this into account in this study.

5 CONCLUSIONS

The proposed method allows viscoelastic damping material to be placed on the surface of a structure in a slowly evolving manner. The advantages of such a technique are that it is possible to place 'just enough' damping on a structure, and the required location of the damping is known. In contrast, 'by eye' estimation places an indeterminate amount of damping into the system which in many cases may be too much and hence wasteful of damping material. This is particularly important where large structures such as aircraft are concerned. In this study, the 'normal thickness' damping performance can be seen to coincide with the evolution of the damping material; for a given application this level of damping may be too much and hence material is being wasted. The 'double thickness' layer shows the significant effect of adding more viscoelastic.

The proposed method is currently limited in a number of respects. Firstly, the finite element model itself is not robust; the way in which it has been discretised leads to a lack of smooth surfaces which introduces stress concen-

trations, which in themselves cause element addition. A smooth-surface model may not evolve in the same manner. This is initially the most pressing deficiency, but it is one which is easily remedied. Secondly, a model of a real system would be required to take into account real properties of the viscoelastic, including the frequency dependence of the Young's modulus. It is seen that the loss factor varies significantly for a fairly small change in the properties of the damping material. Whether or not this is significant depends upon the application to which the evolutionary damping placement method is applied, and it is not the aim of this study to perform material property optimisation.

The method is currently limited to the addition of damping for one specific mode — no attempt has been made to modify the behaviour at modes above the first. It is expected that as the evolutionary method attempts to alter the viscoelastic layer, conflicts in placement will arise, ultimately producing the 'best compromise' of damping over a range of modes. The procedure must then be expanded to allow the removal of elements for this to occur. Once a damping element has been added, it stays on the model — no provision is made for the removal of damping elements which may become unnecessary during the evolution. As it stands, the process is guaranteed to produce a final, stable state (when all the surface is covered). The addition of a rule to remove elements may produce unwanted states in the evolution such as limit cycles. It may be difficult to determine these in advance.

6 ACKNOWLEDGEMENTS

Thanks to Jem Rongong for invaluable assistance with ABAQUS, especially in the modelling of viscoelastic materials.

7 REFERENCES

1. S. C. Cowin and D. H. Hegedus, "Bone Remodeling I: Theory of Adaptive Elasticity", *Journal of Elasticity*, 6, 3, July 1976, pp 313–326.
2. N. Inou, N. Shimotai and T. Uesugi, "A Cellular Automaton Generating Topological Structures", in "Proceedings of The Second European Conference on Smart Structures and Materials", 1994, pp 47–50.
3. A. G. M. Michell, "The Limits of Economy of Material in Frame-structures", *Philosophical Magazine*, 8, 47, November 1904, pp 589–597.
4. G. R. Tomlinson, "Using Viscoelastic Materials for Practical Damping Applications", Notes for One-Day Course, Department of Mechanical and Process Engineering, University of Sheffield, UK, Dec 1995.
5. K. Worden and G. R. Tomlinson "On Structures From Cellular Automata", in "Proceedings of International Symposium On Microsystems, Intelligent Materials and Robots", Sendai, Japan, 1995, pp 390–394.

6. Y. M. Xie and G. P. Steven, "A Simple Evolutionary Procedure for Structural Optimization", *Computers and Structures*, 49, 5, 1993, pp 885-896.

Smart Structures, MEMS and Smart Electronics for Aircraft

Vijay K. VARADAN and Vasundara V. VARADAN
 Alumni Distinguished Professors of
 Engineering Science and Mechanics and Electrical Engineering
 &
 Co-Directors
 Research Center for the Engineering of Electronic and Acoustic Materials
 Pennsylvania State University, University Park, PA 16802

1. SUMMARY

In this paper, the integration of multifunctional smart materials, MicroElectroMechanical Systems (MEMS) and smart electronics is presented with examples covering smart structures and devices applicable to aircraft. Some applications include systems for a) noise suppression in aircraft cabin using 'smart wall paper', b) drag sensing and reduction in aircraft, c) sensing and control of ice formation and deicing on aircraft, d) remote measurement of tip deflection of helicopters using MEMS sensor and electronically tunable antenna, e) smart skin antenna for communication between sensors and actuators (telemetry device), and f) health monitoring of rotorcrafts using MEMS sensors along with fiber optics sensor and remote antenna system.

2 INTRODUCTION

The term multifunctional polymeric composite refers to a material that can sense changes in its environment and makes a useful or optimal response by either changing its material properties, geometry, mechanical or electromagnetic response. Both the sensor and actuator functions with the appropriate feedback must be integrated and comprises the 'brain' of the material. The materials belong to this category may include a range of artificial materials from optically active or chiral polymers to multifunctional polymers, ferroelectric or other active ceramics. Advanced smart polymeric composites are a new generation of multifunctional polymers, piezopolymers and conducting polymers that must be distinguished from piezoelectric polymers such as PVDF that are in current use. Piezopolymers involve the integration of polymers and nanoceramic particles by chemical bonding as side groups on a polymer backbone. The nanoparticles have active surfaces or functional groups that can bond with the polymer chain. The ceramic side groups provide the piezoelectric function in the polymer while the backbone provides mechanical strength and structural integrity, electrical conductivity, etc.

Microelectromechanical systems (MEMS) refer to a collection of microsensors and actuators which can both sense its environment and have the ability to react to changes in that environment with the use of a microcircuit control. They include, in addition to the

conventional microelectronics packaging, integrating antenna structures for command signals into micro electro-mechanical structures for desired sensing and actuating functions. The system also may need micro-power supply, micro-relay and micro-signal processing units. Silicon micromachining has become the fundamental technology for the fabrication of micro electromechanical devices and, in particular, miniature sensors and actuators. Silicon micromachining is the most mature of the micromachining technologies and it allows for the fabrication of MEMS that have dimensions in the sub millimeter range. These microdevices can also be micromachined using semiconductor processing technologies on the polymeric multifunctional sheets mentioned above. In case of difficulty on the polymeric materials, some of these devices can be micromachined in silicon and the system architecture can be obtained by photoforming processing. Batch processing of such devices thus seem feasible.

The combined architecture may also result in sheets of smart skin with integrated sensors and actuators at the μm to mm scale. The control loop between the sensors and actuators employs the multifunctional materials which provide electrical functionality at selected locations using conductive polymers and electrodes that are connected to on-site antennas communicating with a central antenna. A related and difficult problem, and one which has been largely unaddressed is the method for telemetry of the data. In some applications, stresses and strains to which the structure is subjected to may pose a problem for conventional cabling. In others, environmental effects may affect system performance. Advances in ultra flat antenna technology coupled with MEMS sensors/actuators seems to be an efficient solution.

The smart electronics referred to in this paper is a microelectronics circuitry such as CMOS, flip-chip electronics, microprocessors and wireless remote and continuous telemetry system which integrate various electronic components and microsensors and actuators. The wireless communication obviates the need for complicated wiring to accomplish the telemetry. For such integration the antenna should be compatible with the standard IC technology and micromachined along with other microsensors, microactuators and control devices. The integrated MEMS actuators with suitable smart electronics etched onto the structure are controlled by the built-in

antennas through feedback and feedforward control architecture.

3. MULTIFUNCTIONAL POLYMERIC COMPOSITES

Multifunctional polymeric composite materials involve the integration of polymers and nanoceramic particles by chemical bonding as side groups on a polymer backbone. The polymers in general may be chiral with conductive side groups. They consist of a backbone structure with functional groups that serve as anchor points for the metal oxides as well. The chiral groups serve as passive damper for noise and acoustic fields converting them into two longitudinal waves (a fast wave and a slow wave) and four components of shear waves (usual shear waves in an elastic continua and left, LCP and right, RCP circularly polarized waves traveling with two different wave speeds). The nanoparticles such as PZT, PLZT, etc. have active surfaces or functional groups that can bond with the polymer chain. The nanoparticles provide the piezoelectric function (and other ferroelectric functions necessary with a family of ferroelectric materials) in the polymer and the backbone provides mechanical strength and structural integrity, electrical conductivity, etc. Further active sensing and control of noise can be achieved by microsensors and microactuators etched on or micromachined on these functional polymers through microprocessors. The conductivity nature of the polymer serves as semiconductor silicon wherein MEMS devices can be etched on.

A new class of functional polymers are being synthesized at Penn State which can serve as the host for piezoelectric nanoceramics and even Ni/Ti shape memory films, as well as a protective coating layer on structural parts. For these polymers to be used as smart skins or smart devices in structures, they have to meet the following requirements: (1) interactions (chemical or physical) between functional polymer and nanoceramics; (2) strong interfacial adhesion between functional polymer and conducting polymer layers; (3) suitable elastic moduli to support the deformation initiated by MEMS actuator devices; (4) excellent overall dimension stability (allowing local mobility); (5) processes conducive to the attachment of nanoceramics and /or conductive phases and formation of a uniform coating layer ; (6) long term environmental stability.

The functional groups provide strong interactions (chemical, physical or both) between polymer and piezoelectric nanoceramic or Ni/Ti particles. Some of the functional groups also serve as the anchor sites at the interface of smart composite and conducting polymer layers as well as the active species for crosslinking reaction between polymer chains if

needed. The polyolefin polymers, for example, offer good mechanical strength, excellent processability, low moisture permeability and excellent environmental stability. The elastic property of polyolefin is strongly dependent on the percentage of crystallinity which can be controlled during the polymerization. With the attachment of nanoceramic smart materials, the functional polymer composites form two-phase morphological structure, a continuous polyolefin elastic phase and a discrete hard phase which mainly consists of functional groups to piezoelectric nanoceramic particles. The strength of interfacial interactions is governed by the nature and the concentration of functional groups.

Many polymers cannot withstand the high electric fields needed to pole ceramics. So it may be preferable to pole the calcined nanoparticles before chemical attachment to the backbone polymer chain. In this way thin films of the nanoparticles held together with a binder can be poled without the need for extremely high voltage poling equipment, which would be the case if thick samples are to be poled. After the thin film samples are poled, the binder can be removed and one now has poled, piezoelectric nanoceramic particles. The surface of the particles must be activated to allow for chemical attachment to the polymer as well as alignment of groups of particles in required directions during attachment.

4. MICROELECTROMECHANICAL SYSTEMS (MEMS)

The basic MEMS utilize a diaphragm-based, a microbridge-based or a cantilever-based structure. For a given application, it may be necessary to have integrated MEMS employing one or more of the basic structure. These three structures provide some feasible designs for microactuators that eventually perform the desired task in most of smart structures. However, the main issues with respect to implementing these structures are the choice of materials that are to be used in fabricating these devices and the micromachining technology that may be utilized. To address the first issue, we note that in all of the three structures proposed the actuation occurs as a result of exciting a piezoelectric layer by the application of an electric field. This excitation brings about actuation in the form of expansion in the diaphragm, or in the free-standing beam in the microbridge structure, or in the cantilever beam. In the former two cases the expansion translates into upward curvature in the diaphragm or in the free-standing beam, hence, resulting in a net vertical displacement from the unexcited equilibrium configuration. In the cantilever case, however, and upon the application of electric field the actuation occurs by a vertical upward movement of the

cantilever tip. Evidently in all three designs the material system structure of the active part (diaphragm, free-standing beam, or cantilever beam) in the microactuator must comprise at least one piezoelectric layer as well as conducting electrodes for the application of electric field across this layer. Piezoelectric force is used for actuation for many of the applications mentioned above.

Microsensors and actuators are fabricated using the well known micromachining techniques in microelectronics industry (for recent developments, please refer to Refs. 1-4) Three dimensional microactuators in polymer structures can be achieved using stereo lithography on UV curable backbone type polymers (Refs. 5 and 6). In the integrated MEMS device, we may use photoforming processing in achieving the combined sensor and actuator architecture as outlined by Takagi and Nakajima (Ref. 7). For large actuation, one could use a flex tensional transducer consisting of a piezoelectric diaphragm bridged into a cavity (Ref. 8)

Micro-Interdigital Transducers (IDT) and Micro-Surface acoustic wave (SAW) devices are ideal sensors for many applications mentioned in the abstract. They were first used in radar and communication equipment as filters and delay lines and, then, were found to be attractive sensors for various physical variables such as temperature, pressure, force, electric field, magnetic field, and chemical compounds. A SAW device usually is a piezoelectric wafer with inter-digital transducers (IDT) and reflectors on its surface. The principle of SAW sensors is based on the fact that SAW traveling time between the components, e.g. IDTs and reflectors, changes with the variation of physical variables. To obtain a high sensitivity, SAW sensors are usually constructed as electric oscillators using the SAW device as frequency control components. By accurately measuring the oscillation frequency, a small change of the physical variables can be detected by the sensors. A typical SAW oscillator sensor schematic is shown in Fig. 1. An amplifier connects two IDTs on a piezoelectric wafer so that oscillations result because of the feedback of the SAW propagating from one IDT to the other. The oscillation frequency satisfies the condition that the total phase shift of the loop equals 2π and varies with the SAW velocity or the distance between the IDTs. The oscillator includes an amplifier and require electrical power supply and cannot be wireless. The operating frequency range of the SAW devices is from ten megahertz to a few gigahertz which directly matches the frequency range of radios and radar. When an IDT is directly connected to an antenna, SAW can be excited remotely by electromagnetic waves. The fact suggests that it is possible to realize passive, wireless or remotely operable SAW devices. The application to remote sensors was first reported in (Ref.9). The temperature of a passive SAW device with a small antenna was remotely read out by a

microwave system (Ref. 10). In this paper, a passive, wireless SAW deflection and strain sensor system is described and experimentally tested. The sensing of ice on structures and deicing are also discussed. The analysis using a simple model is confirmed by experimental results. Additional applications of sensing drag on structures are presented. At Penn State, they have been used for health monitoring of cracks and flaws at or in the vicinity of rivet holes on aircraft surfaces.

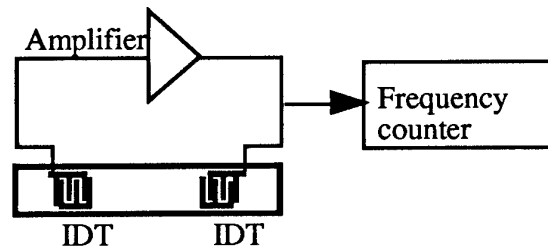


Figure 1. Schematic diagram of an oscillator SAW sensor with a SAW resonator

The schematic diagram of IDT and reflectors in Fig. 2 shows the basic operating principle of the system. An IDT and two reflectors are made on the surface of a piezoelectric crystal wafer. The IDT connects directly to a small antenna called the device antenna. This antenna-IDT configuration is able to convert the microwave signal from air to SAW signal on the wafer surface and vice versa. The reading system has a linear Frequency Modulated (FM) signal generator. The FM signals are transmitted by a system antenna. The signals are received by the device antenna and converted by the antenna-IDT to SAWs propagating along the surface of the wafer. The echoes from the two reflectors are picked up by the antenna-IDT and sent back to system antenna. The echo signals are delayed copies of the transmitted FM signal. The delay times mainly depend on the velocity of the SAWs and distance between the IDT and the reflectors. A mixer which takes the transmitted FM as reference signal, outputs the signals of frequency difference between the echoes and the transmitted signals. Because the transmitted signal is linear frequency modulated, the frequency difference is proportional to the delay time. By using spectrum analysis technique like FFT, the two echo signals can be separated in the frequency domain since the delay times are different. Although the frequencies of the echoes included the information of delay times and the latter are sensitive to the strain on the wafer surface, the sensitivity of frequency to strain still too low. The phases of the two echoes are also dependent on the delay times and much more sensitive than the frequency as shown in the following analysis. The system detects the phase difference of the two echoes to figure out the strain, so that the interferences to the common path of the two echoes cancel each other and will not affect the strain measurement.

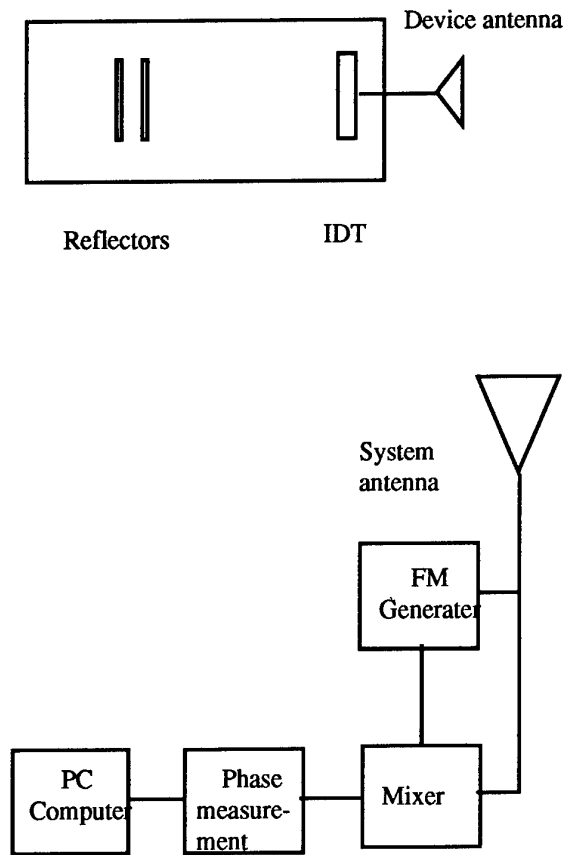


Figure 2. Schematic diagram of remote reading sensor system with passive SAW sensor

Comb-type MEMS sensor: At Penn State, the comb-type MEMS sensor is being used for studying acceleration and for sensing and suppression of cabin noise in aircraft (Ref. 11 and 12). The sensor design is shown in Figure 3.

It consists of interdigital finger structures forming a differential capacitor with movable fingers mounted on a movable mass while the fixed electrodes are anchored onto the silicon substrate. A force-feedback operation mode increases the sensor performance.

In the fabrication process a BiCMOS two chip approach is adopted. An n+ implantation is performed on a (100) silicon substrate. The purpose of this implantation is to provide an electrical contact to the polysilicon layer which will be deposited on the top of a low temperature oxide layer that acts like a sacrificial layer. A detailed process description is described in Guckel et.al. A close-loop sensitivity of 8mV/g and bandwidth of 10 kHz can be achieved.

Silicon micromachining has been a key factor for the vast progress of MEMS in the last decade. This refers to the fashioning of microscopic mechanical parts out of a silicon substrates and more recently other materials. It is used to fabricate such features as clamped beams, membranes, cantilevers, grooves, orifices, springs, gears, suspensions, etc. These can

be assembled to create a variety of sensors. Recently, the Japanese exhibited a complete functioning micromachined automobile that operated for several minutes. Bulk micromachining is the commonly used method but it is being replaced by surface micromachining which offers the attractive possibility of integrating the machined device with microelectronics which can be patterned and assembled on the same wafer. Thus power supply circuitry, signal processing using ASICs (Application Specific Integrated Circuits). It is the efficiency of creating several such complete packages using existing technology that makes this such an attractive approach. At present universities have access to several centers that can manufacture to customer design. The Microelectronics Center of North Carolina (MCNC) funded by ARPA, the NSF funded Nano Fabrication Centers at Cornell University and the Pennsylvania State University are a few.

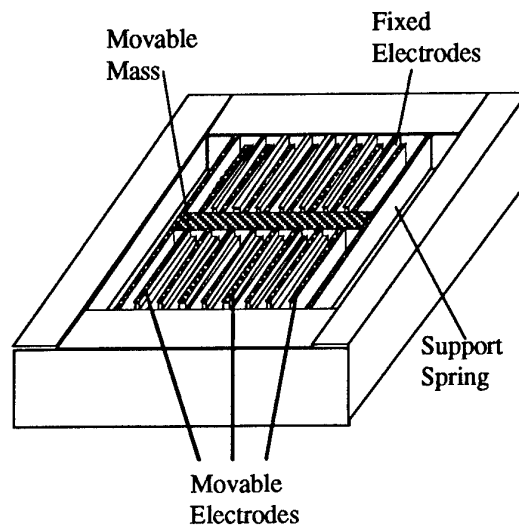


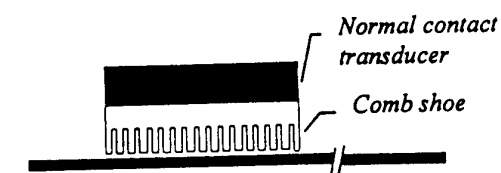
Figure 3. MEMS Vibration Sensor designed and implemented at Penn State

The active component of many MEMS devices may involve a moving part that changes the capacitance by changing the spacing between two closely spaced electrodes. The accompanying examples illustrate, a MEMS accelerometer that can also be used as a vibration sensor based on changes in electrical capacitance between moving fingers, a MEMS microflow sensor where the deformation of a piezoresistive coating on a micro-cantilever actuated by a flow field leads to changes in resistance and hence the current and voltage. The design possibilities are almost limitless. The design of a MEMS accelerometer was modified for use as a vibration sensor and was successfully demonstrated as being superior to conventional piezoelectric wafer sensors in sensitivity occupying far less space and at a fraction of the weight (Ref.11).

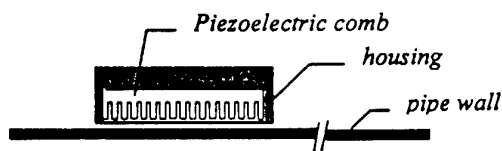
A less expensive and quicker method that is just emerging is the use of photoforming by exposure to UV radiation. The attractive feature of this technique

is that electroactive polymer layers can be deposited layerwise in a desired fashion to create various mechanical components at the micron level. As this technology develops, the application of polymer based MEMS to structural health monitoring and process control will be revolutionized.

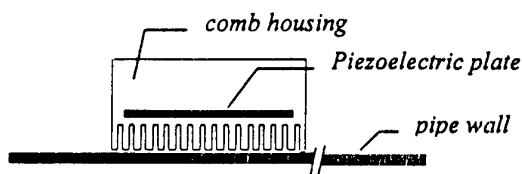
Another type of comb transducer is currently being used for non-destructive evaluation and health monitoring of aging aircraft (Ref. 13) The comb transducer can be made in different ways. As shown in Figure 4 (a), the comb transducer can be a comb shoe attached to the front face of a normal beam transducer. The normal beam transducer drives all of the elements to vibrate in phase so as to excite guided waves. As in Figure 4(b), a piezoelectric plate is directly placed in a housing with the comb at the bottom. Similar to Figure 4(a), the piezoelectric plate drives the comb to vibrate in phase. The comb transducer in Figure 4(c) consists of a group of independent elements that are equally spaced arranged in parallel order. An ultrasonic pulsar/receiver sends electrical pulses in phase to all elements to excite guided waves as transducers in (a) and (b). The generated guided wave on a plate may be received using three methods as illustrated in Figure 5. Figure 5(a) is the pulse echo method: the comb transducer serves as both sender and receiver; and the echo is received by the comb. Figure 5(b) is the through transmission method using a comb transducer to receive the signal. Both Figure 5(a) and (b) receive a particular selected wave mode because the comb transducers are designed for it. (c) is the through transmission method using an angle beam transducer to receive the signal. This method is also very effective in receiving the particular excited mode because Snell's Law allows a particular mode conversion to a longitudinal wave that is received by the angle beam transducer.



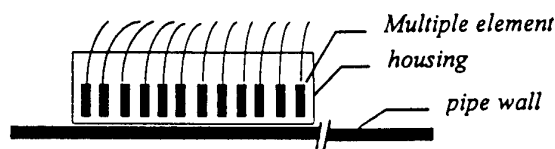
(a) Transducer on top of comb shoe



(b) A piezoelectric comb in a comb housing

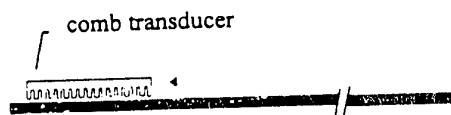


(c) A piezoelectric plate in a comb housing

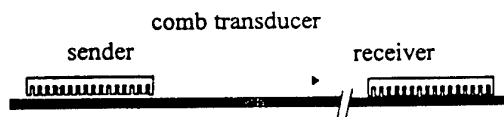


(d) A multiple element comb transducer

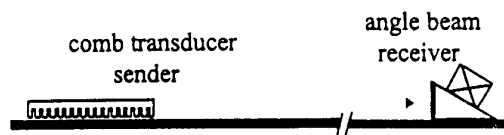
Figure 4. Configuration possibilities of comb transducers.



(a) pulse echo



(b) comb/comb through transmission



(c) comb/angle beam through transmission

Figure 5. Experimental setups using the comb transducer technique.

5. SMART ELECTRONICS AND CONFORMAL ANTENNAS

The development of integrated smart electronics involve microelectronics circuitry, low-power signal processing electronics, microcontroller and wireless communication between microsensors and microactuators. Three different approaches are being pursued: 1) CMOS microelectronics-first followed by MEMS device integration using polysilicon surface micromachining(Ref. 14), 2) micromechanics-first followed by CMOS integration (Ref.14) and 3) flip-chip integration of MEMS chips with that of microelectronics circuitry chips (Ref. 15).

Wireless remote and continuous telemetry systems for application to smart structures can be achieved using Penn State's novel antenna architecture using

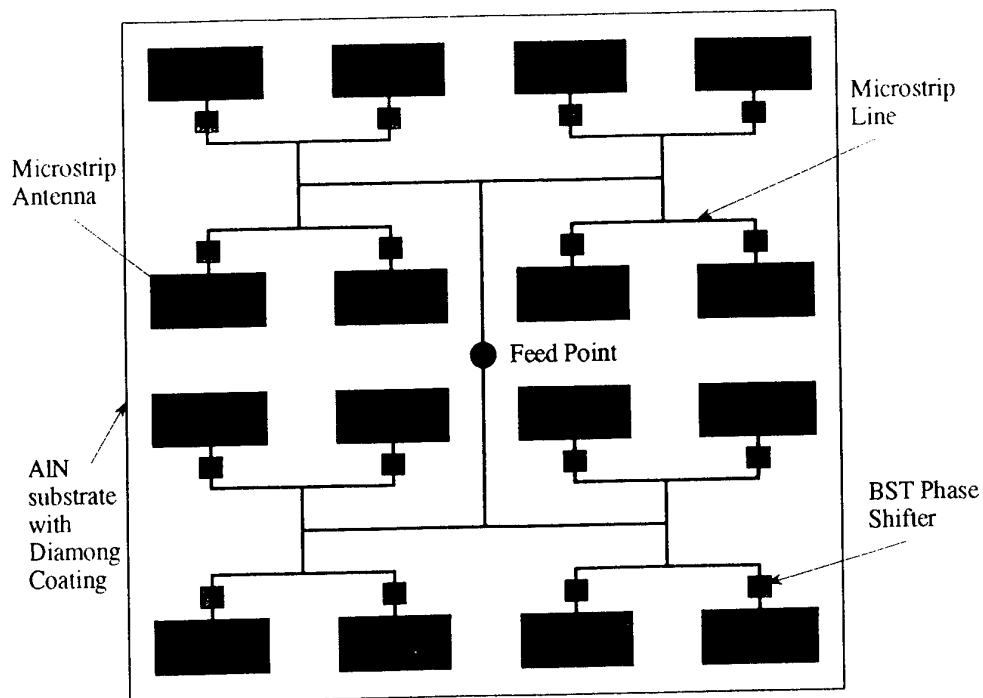


Figure 6. Electronically Steerable Microstrip Antenna with Ferroelectric Phase Shifters

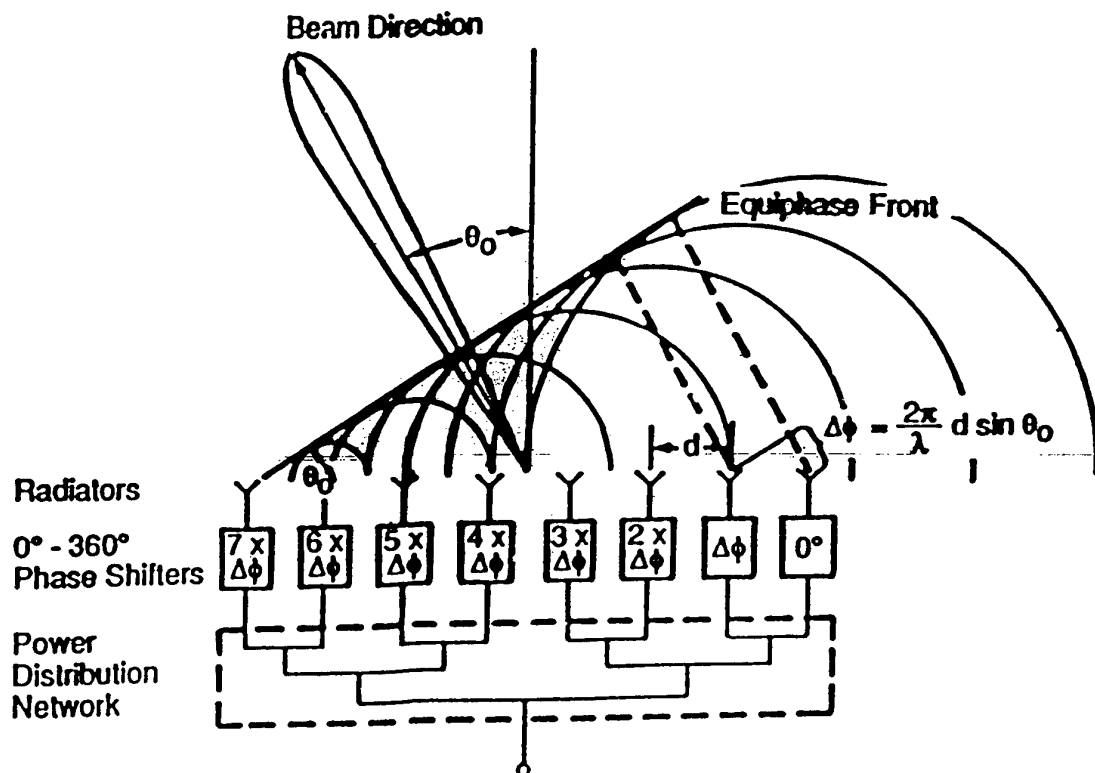


Figure 7. Beam Steering with Ferroelectric Phase Shifters

ferroelectric on-line or filter phase shifters to interact with MEMS, piezoelectric polymer skins and SAW sensors wherein the communication from sensors to control systems and back to the actuators is accomplished by wireless telemetry using antennas specially designed for such purpose and integrated into the structure. The ferroelectric ceramics are used to develop new, lightweight, flat, large bandwidth antennas whose output beams can be steered electronically by tuning the dielectric properties of the ceramic, Fig. 6 Beam steering, see Fig. 7 can be used to advantage for monitoring and communicating with several sensors and actuators distributed over a large structure using a single central antenna.

A sensor bus can be used when sensing many parameters at the same time. The sensors can be electronically scanned, and the information is 'passed' on to the microcontroller. Separate software code has to be assigned in the microcontroller to each sensor. The wireless communication link consists of a transmitter and receiver with a message format consisting of eight data bits preceded by a starter bit and followed by parity bit and stop bit. The antenna for this application is a conformal one employing high dielectric and low loss ferroelectric material with tunable capability. Planar phase shifters controlled only by bias voltage are used for electronic steerability (Refs. 16-21)

6. APPLICATION TO AIRCRAFT

6.1 Deflection and strain of flex type beam structures

In this section a remote SAW strain sensor system is employed to study the deflection and strain of "flex-beam" type structure of a helicopter. The system consists of remotely-readable passive SAW sensors and a microwave reading system. The experimental results confirm the theoretical analysis using a simple model and show the feasibility of using passive SAW sensors to measure structural strains.

The microwave reading system used in this system is actually a FM radar. The FM signal send by the system antenna is expressed as

$$S(t) = A \cos(\omega_0 + \mu t / 2)t \quad (1)$$

where ω_0 is the start frequency of the FM signal, μ is the rate of the modulation, and t is time.

The echoes from the reflectors, $S_1(t)$ and $S_2(t)$, are the same as the transmitted signal $S(t)$ but with

time delays t_1 and t_2 respectively. They are written as

$$S_1(t) = S_1 \cos(\omega_0 + \mu t / 2)(t - t_1) \quad (2)$$

and

$$S_2(t) = S_2 \cos(\omega_0 + \mu t / 2)(t - t_2) \quad (3)$$

where

$$t_1 = 2d_1 / v + \tau_e \quad (4)$$

$$t_2 = 2d_2 / v + \tau_e \quad (5)$$

where v is the SAW velocity, d_1 and d_2 are the distances from the IDT transducer to the reflectors respectively, and τ_e is the total of other delays such as electromagnetic wave traveling time, delay in electronic circuit and devices, which is the same for both echoes.

Through the mixer, which uses the transmitted signal as reference, and low-pass filter, frequency differential signals are obtained as

$$E_1(t) = E_1 \cos[\mu t_1 t + (\omega_0 t_1 - \mu t_1^2)]$$

$$= E_1 \cos[\omega_1 t + \phi_1] \quad (6)$$

and

$$E_2(t) = E_2 \cos[\mu t_2 t + (\omega_0 t_2 - \mu t_2^2)]$$

$$= E_2 \cos[\omega_2 t + \phi_2] \quad (7)$$

respectively. The frequencies and phases of these two signals both depend on the delay times. The two signals can be separated in the frequency domain. Since the ω_0 is usually much greater than m , the phase shift is more sensitive to the variation of delay time than the frequency.

The difference of the two phase can be written as

$$\phi = \phi_1 - \phi_2 = [\omega_0 - \mu(t_1 + t_2) / 2](t_2 - t_1) \quad (8)$$

where the extra delay time of the second echo referring to the first is equal to the round trip time of the acoustic wave traveling from the first reflector to the second and is presented as

$$\tau = t_2 - t_1 = \frac{2d}{v}$$

where d is the distance between the two reflectors.

The phase difference is sensitive to the change of the delay times. The variation of the phase difference due to the change of the delay times is expressed as

$$\Delta\phi = [\omega_0 - \mu(t_1 + t_2) / 2] \Delta\tau \quad (9)$$

Since ω_0 is usually much larger than the item of $\mu(t_1 + t_2) / 2$, then we have

$$\Delta\phi = \omega_0 \Delta\tau$$

The wave traveling time t is proportional to the distance between the two reflectors and inversely proportional to the velocity. If neglecting the possible velocity variation of the SAW under strain and taking in count only the direct effect of the distance change, we have

$$\Delta\phi = \omega_0 \frac{2\epsilon d}{v} = \omega_0 \epsilon \tau_0 \quad (10)$$

where ϵ is strain and τ_0 is the traveling time when the strain is zero. The sensitivity of this remote sensor system depends on operating frequency and the round traveling time of the SAW between the two reflectors.

Experimental setup and results

The test setup is shown in Fig. 8. The SAW wafer package is glued to a fiberglass cantilever beam of the dimensions of 172 mm in length, 25 mm in width and 1.5 mm in thickness.

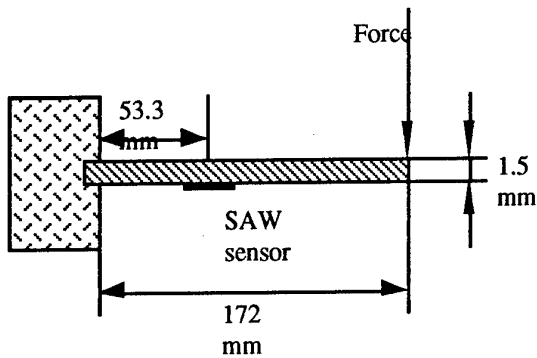


Figure 8. Passive SAW sensor on test cantilever beam

The center of the SAW wafer is 53.3 mm from the root of the beam and the SAW propagating direction is along the beam length. If we neglect the effect of the bonded SAW wafer, the strain on the surface of the beam can be calculated by simple beam theory

$$\epsilon_x = -d_s \frac{3t_b(l-x)}{2l^3} \quad (11)$$

where l is the length of the beam, x is the distance of the location from the root, t_b the thickness, and the d_s is the displacement at the tip of the beam. In the experiment, the beam is bent by a force at the tip and the tip displacement is measured by a dial indicator.

The remote SAW sensor system successfully detected the shift of the phase difference of the two echoes with the variation of the tip displacement. The results are presented in Fig.9 in the form of the shifts versus strains. The strains are calculated according to the tip displacements by Eq. (11).

The data show that the phase shift varies with the strain linearly when the strain is less than .0012. For larger strains, nonlinearity and larger fluctuation appear. The nonlinearity may due to the glue used to bond the SAW package, the large deformation of the beam and other causes. The maximum tip displacement in the test is 34 mm. It is compatible with the length of the beam and beyond the range where simple beam theory is valid.

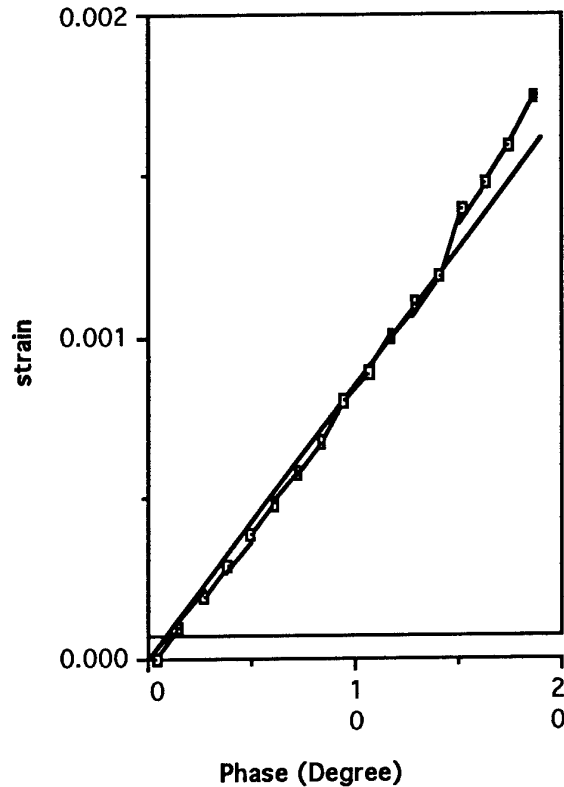


Figure 9. Experimental results of strain versus phase change

The sensitivity and resolution converted from the measurement data is about $1.09 \cdot 10^4$ degrees and

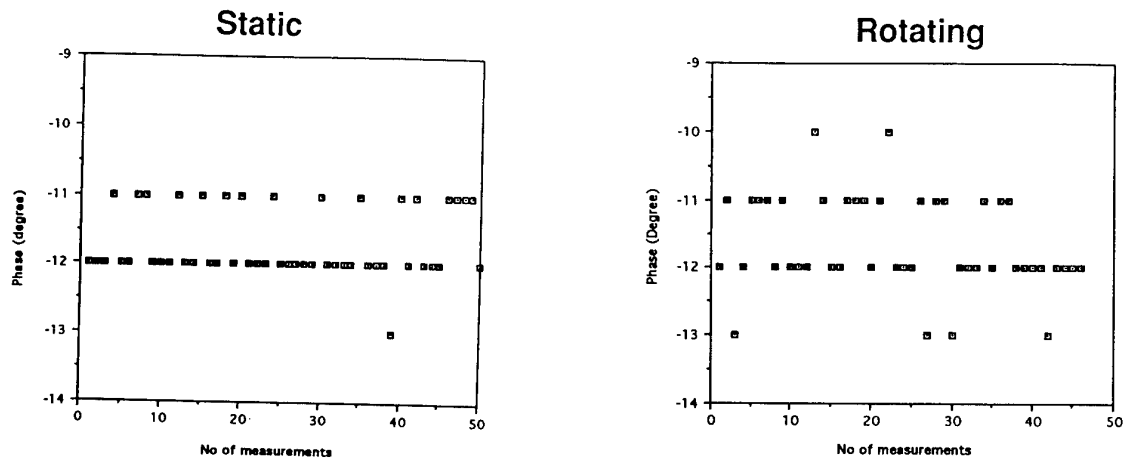


Figure 10. Phase shift and hence the strain measurement of stationary and rotating blades

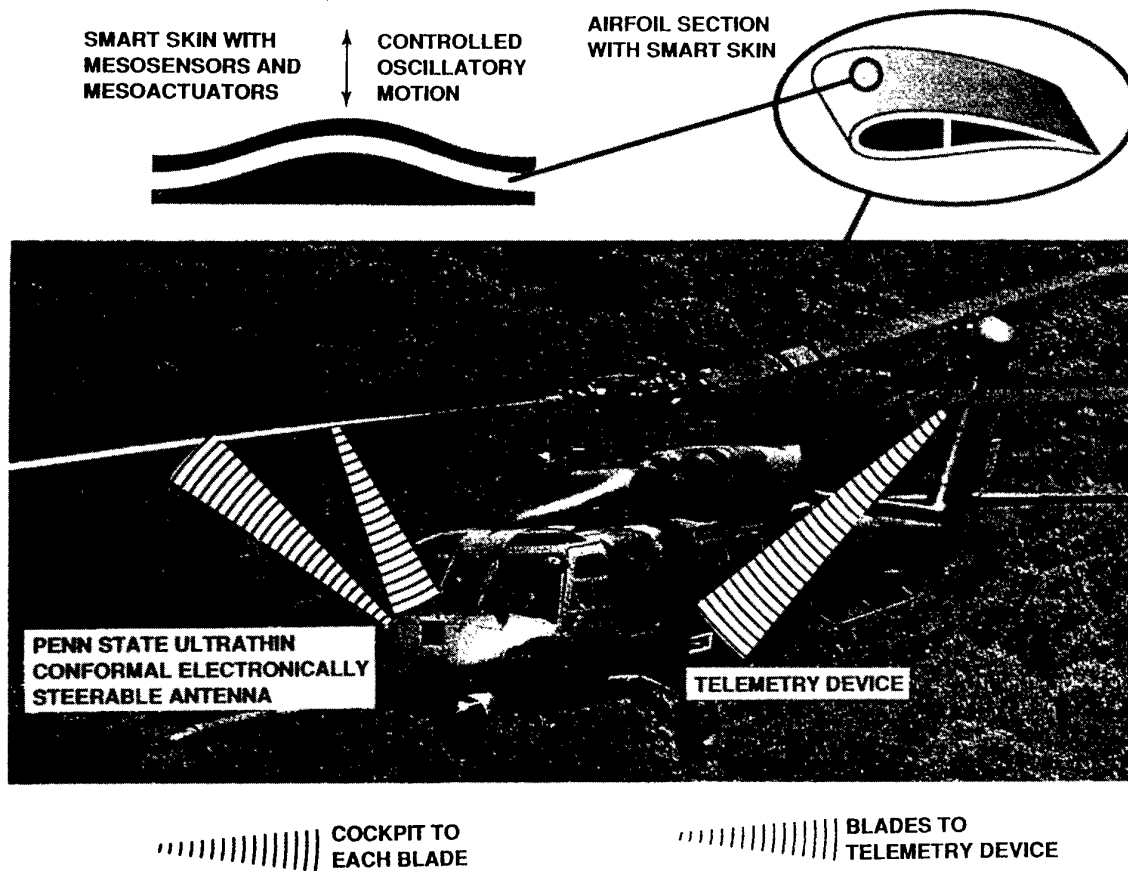


Figure 11. Helicopter with built-in sensors and electronically steerable antenna

$0.92 \cdot 10^{-4}$, respectively. They are lower than the theoretical estimation of $3.3 \cdot 10^{-4}$ degrees and $3 \cdot 10^{-5}$. Since that the thickness of the SAW wafer and the plastic case is not negligible, comparing with the thickness of the cantilever beam in the test, it is expected that the strain on the wafer surface is less than the strain on the surface of the cantilever beam when the SAW sensor is absent. The latter is used to calculate the sensitivity and resolution.

Considering this factor and the softness of the plastic case also may decrease the sensitivity of the inside SAW sensor, the test results reasonably confirm the theoretical estimation.

The concept presented above has been implemented on rotating blades. First the strain and the deflection were measured remotely by the antenna communicating with the sensors (via the built-in antenna) while the blades were stationary and then when the blades were rotating. The rotational speed is close to that of an actual helicopter. The results presented in Figure 10 are encouraging for further research.

CEEAM

PENN STATE

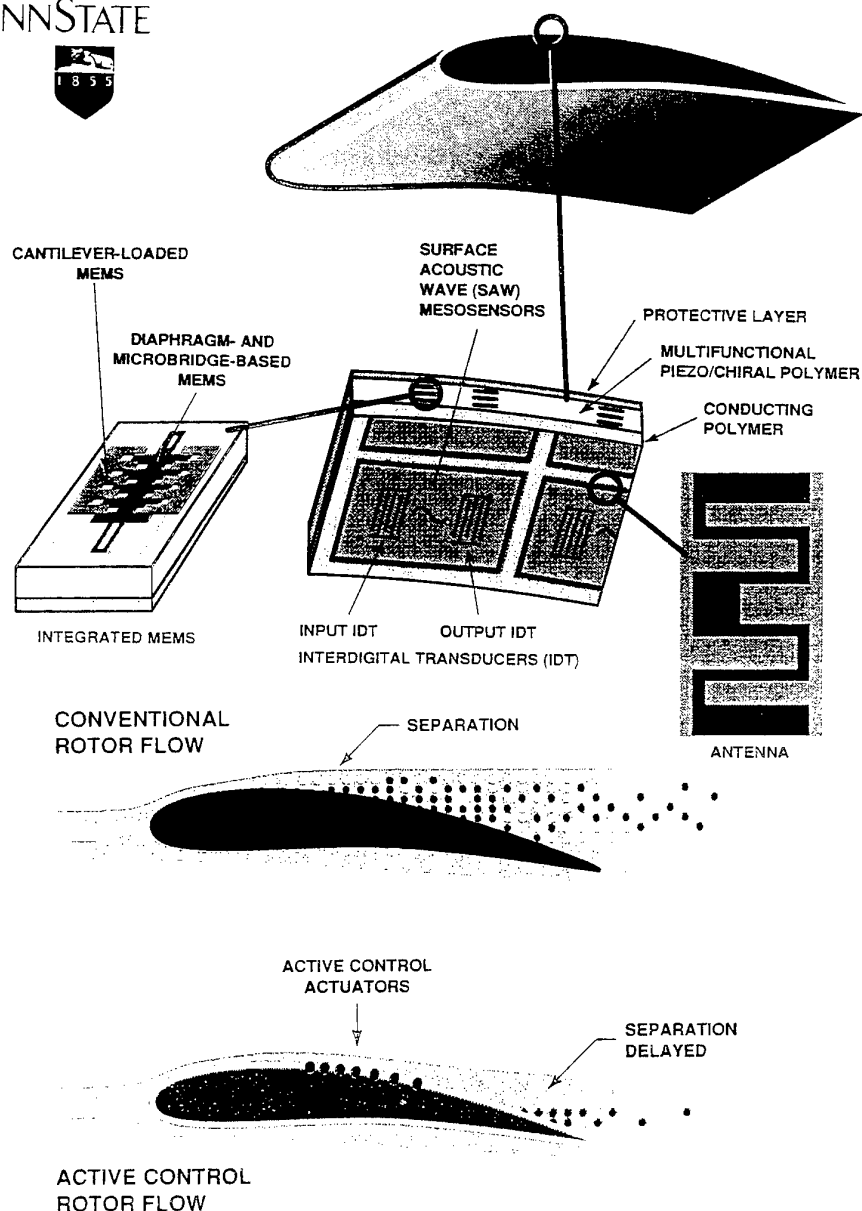


Figure 12. Airfoil section with MEMS and actuators

6.2 Local and global sensing and control of vibration and drag in aircraft

In this case the sensors described above are used to measure both pressure and shear of the fluid flow on aerospace structures. The wave form measurements may be monitored at a remote location either at the cockpit or elsewhere via the antennas in the sensors and an outside antenna. The integrated MEMS actuators with suitable smart electronics etched onto the structure are controlled by the built-in antennas through feedback and feedforward control architecture.

The integration of such materials and smart electronics into the skin of airfoil is ideal for sensing and controlling vibration and drag. The basic idea of this concept involves detection of the point of transition from laminar to turbulent flow and transmitting acoustical energy into the boundary layer so that the low energy fluid particles accelerate in the transverse direction and mix with the high energy flow outside of the boundary layer.

A schematic arrangement which connects SAW and MEMS devices to antenna onto the airfoil of aircraft is shown in Figures 11 and 12.

The smart skins derived from this integration are ideally suited for drag sensing and control of aircraft and spacecraft. One can also induce microriblets on the smart skin for drag reduction using micromachining techniques. These microriblets can be actively produced by the MEMS techniques at the desired location. The detection and control of noise and vibration as caused by both external and internal forces may be countered through the use of polymeric piezosensors and actuators.

For sensing drag pressure and shear, SAW MEMS devices are used as described below. In principle, two SAW sensors are normally employed as shown in Figure 13, in one of the SAW device the waves propagating in the same direction of the air flow while in the other the waves propagating in the opposite direction. Using the velocity V_0 as the reference when there is flow, we could relate the pressure and the shear from these two SAW sensors as shown in Figure 13.

The sensors arranged in the form rosette can provide the direction of the flow, see Figure 14. A cantilever-beam SAW force sensor attached to a floating thin and flat membrane will enhance the stress many orders of magnitude, see Figure 15.

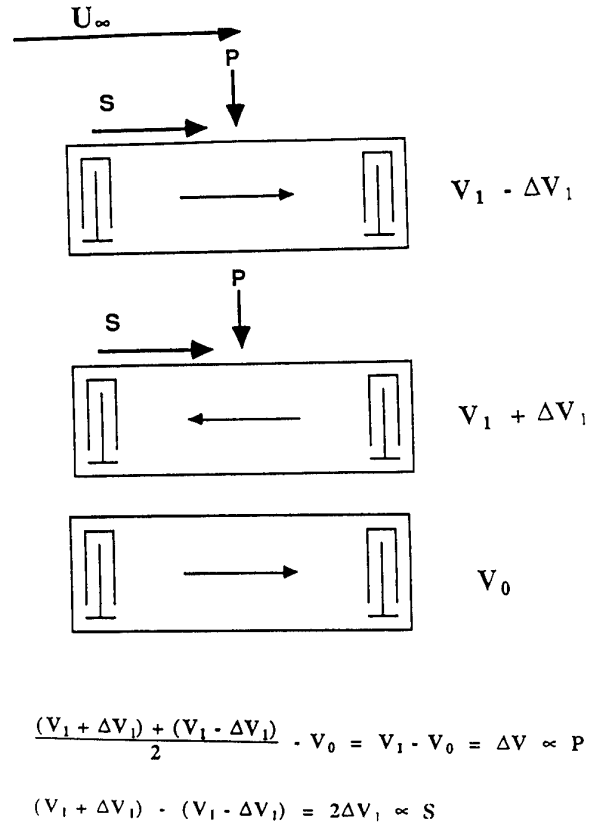


Figure 13. SAW pressure and shear sensor

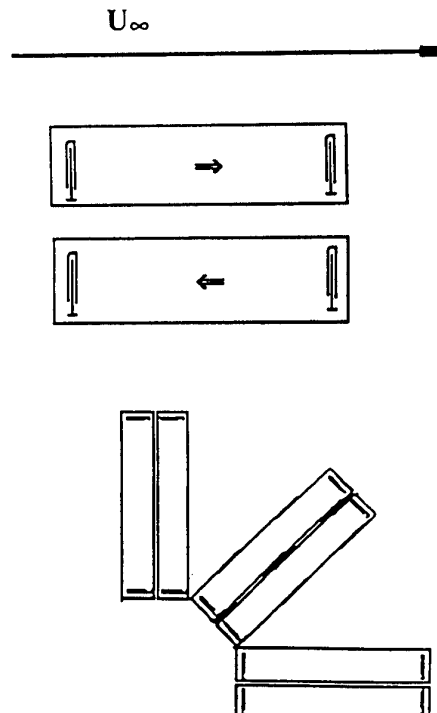


Figure 14. Rosette arrangement of SAW sensors

The device can be flush mounted in an aircraft. The composite cantilever beam has two SAW devices fabricated by using Lithography. The active areas of the two devices, where surface acoustic waves propagate, face opposite sides. The moment applied by the attached membrane exposed to shear, one active surface is in tension and the other is in compression. Dual sensor approach provided also compensates for changes if any in other physical variables such as temperature, pressure, etc. Preliminary experiment was performed at Penn State Wind Tunnel. The tunnel is 16 inch low speed unsteady boundary layer wind tunnel. The sensor system was mounted on a horizontal internal plate which divides the tunnel of rectangular cross section into two equal parts. The sensing membrane of the sensor was in the up position. The velocity of the wind in the tunnel was monitored by a pressure sensor close to the air inlet. The output of the pressure sensor is voltage, which is proportional to $P=m(V-V_0)$ with $m = 66.89 \text{ Pa/V}$, where V_0 is the

A calibrated curve of the wall shear stress t and pressure P is also available for the tunnel. The shear stress is proportional to the pressure P , $t = kP$ where k is approximately equal to 0.003129 for the wind tunnel under consideration. First the sensor is calibrated and the relation between the pressure and shear vs the phase shift is determined. In the experiment, the wind speed was increased step by step to a maximum first and then decreased gradually. The output frequency of the SAW sensor and time was recorded. The results are shown in Figures 16 and 17. The sensor system will be implemented in model airfoil and the performance will be assessed later.

The concept of micro riblets for drag reduction has been presented by Haund and Ho (Ref. 22) and Varadans (Ref. 23 and 24). Using 3D MEMS structure as presented by Varadan (Ref. 6), one could produce active microriblets to control the drag. Even a 5% drag reduction will result in an enormous fuel savings, see (Ref. 25)

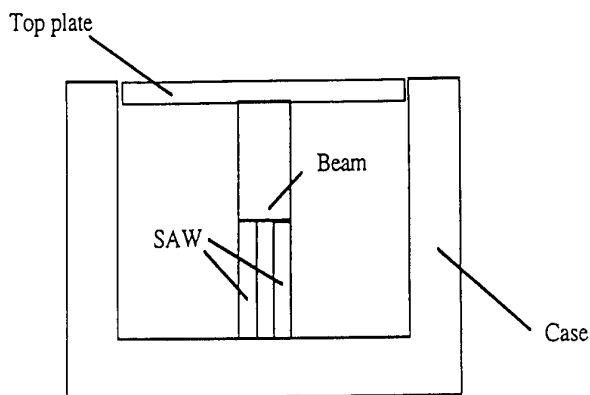
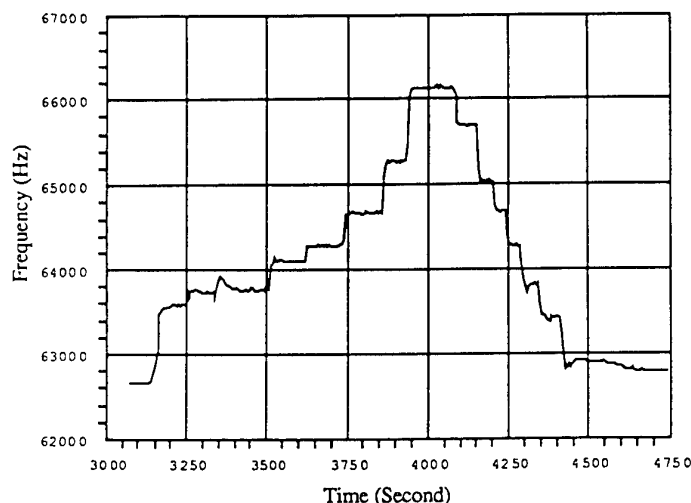


Figure 15. Cantilever beam SAW sensor



Frequency shift vs time in wind tunnel as flow is gradually turned on and then off, SAW sensors on continuously (SAW # 1 frequency increases, SAW # 2 frequency decreases)

Figure 16. SAW results in wind tunnel

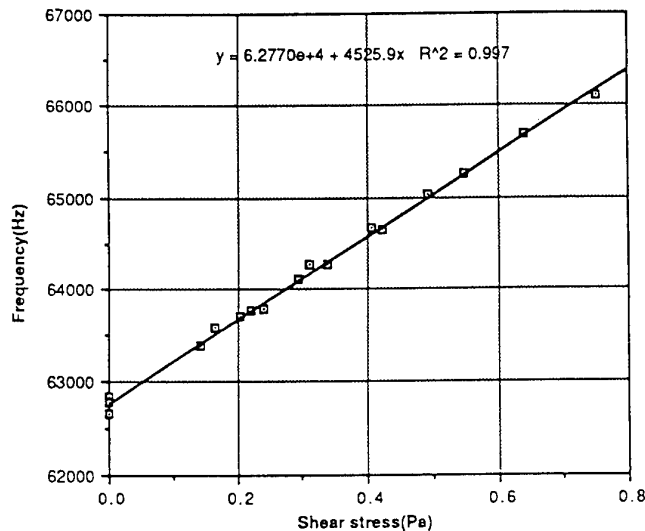


Figure 17. Frequency shift vs. wall shear stress using calibration

6.3 "Smart Plate" for Noise Reduction using MEMS Technology

Active structural acoustic control has attracted growing attention in recent years. Piezoelectric sensors and actuators are widely used because they can be embedded in structures or bonded to surfaces with minimum interference to the structure design. Numerous researches has been devoted to sound transmission through plates or shell (Refs. 26-28). A theoretical analysis by Fuller showed the feasibility to actively control the sound transmission/radiation with a few actuators applying forces to the plate (Ref.26). The concept was proved by later experiments (Ref.28). The analysis work aimed at applying the technique to cylindrical shell, like aircraft fuselage, also shows encouraging results (Ref.29). The possibility to use on-plate error sensors to achieve significant global reduction has been addressed (Ref. 27). Most of these investigations deal with the cases of transmission between two free acoustic fields or into cylindrical enclosures and the boundary conditions involved are ideal, such as simple support.

The present experimental investigation addresses to the active control of the sound transmitted from an enclosure through plates by using on-plate MEMS sensors and actuators (Ref. 30 and 31). This experiment will provide the foundation for the cabin noise reduction in aircraft. In cabin noise reduction, the problem becomes simpler since we want to control the noise coming from out side to the interior of the cabin. The plate is mounted at an opening of a cubic sound enclosure. The boundary condition of the plate is not ideal rather close to the mounting in most practical applications. The sound transmitted through the plate is measured by a

microphone array that scans a hemispherical surface. Measurements show that the spectrum of the transmitted sound has peaks that coincide with the resonance of the plate. The target of the active control is first to reduce these transmission peaks that result in a poor isolation performance. This strategy requires a relatively simple, low-cost control system and may be applied to a wide variety of structures such as machine cases, windows, etc. The capability of a one-sensor one-actuator control system is evaluated. Significant reductions of 15 - 22 dB are obtained by use of this simplest control system at the resonance frequencies of the first three symmetric modes.

In this study, an aluminum square plate is used as a test sample. The dimensions of the plate are 14"x14" in area and 0.015" in thickness. The MEMS sensor fabricated is 400mm x 400 mm. Its performance is compared with regular PZT sensor and actuator as shown in Figure 18. Three PZT (Lead Zirconate Titanate) pieces are bonded on the plate by epoxy as shown in Fig. 18. One is used as an actuator, which is indicated as A1 in the figure. Those marked as S1 and S2 in the figure are sensors. The geometry of A1 and S2 are the same. They are disks with a diameter of 1.5" and a thickness of .02". The size of S1 is 1" in diameter. The actuator A1 is located at the center of the plate, the sensor S1 at the middle from the center to an edge, and the sensor S2 at the middle from the center to a corner. To compare the performance of the MEMS sensor, it is located on the actuator at the center of the plate.

Since that the actuator is located at the center of the plate, we expect the actuator has good couplings to most symmetric vibration modes such as (1, 1), (3, 1) and (1, 3). The symmetric modes are usually more efficient in sound radiation as compared with the anti-symmetric ones especially in low frequency range.

The plate is mounted on a five-side wood box in a semi-anechoic chamber as shown in Fig. 19. The sizes of the box are 12"x12"x12" inside. The walls of the box are made from thick (1") oak plates and fiber-rubber-fiber acoustic isolation mats are put in front of the walls to prevent the sound in the box from being transmitted through the walls. The plate is clamped on the edges of the opening of the box by a steel frame. The movable area of the plate is 12"x12". A soft rubber gasket is placed between the plate and the wood. The boundary condition is somewhere between the clamped and the simple support. A loudspeaker generates the sound field in the enclosure. The sound level outside is measured by a microphone array. The eleven elements of the array are uniformly distributed in a half circle in a distance of 15" from the center of the plate. The array is able to rotate in 180° to cover a hemispherical surface above the plate and the baffle. The baffle is a 0.75"-thick plywood board.

The global power reduction obtained by active control may be defined as

$$R = 10\log(W_o/W_c) \quad (12)$$

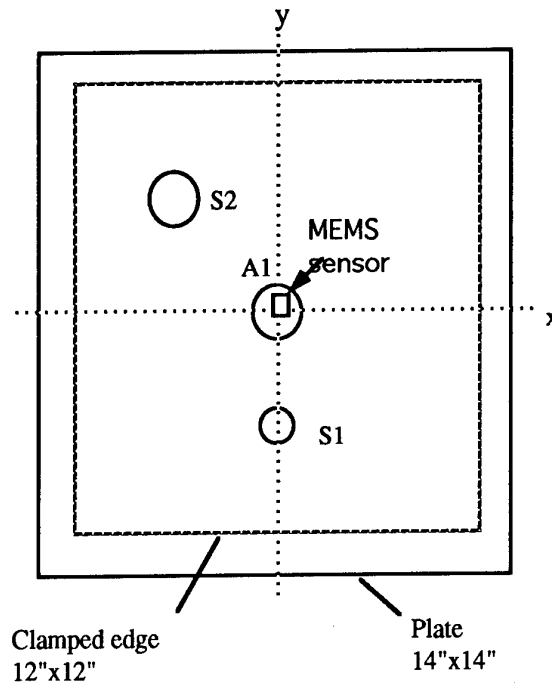


Fig. 18 The aluminum plate with piezoelectric actuator and sensors and MEMS sensor

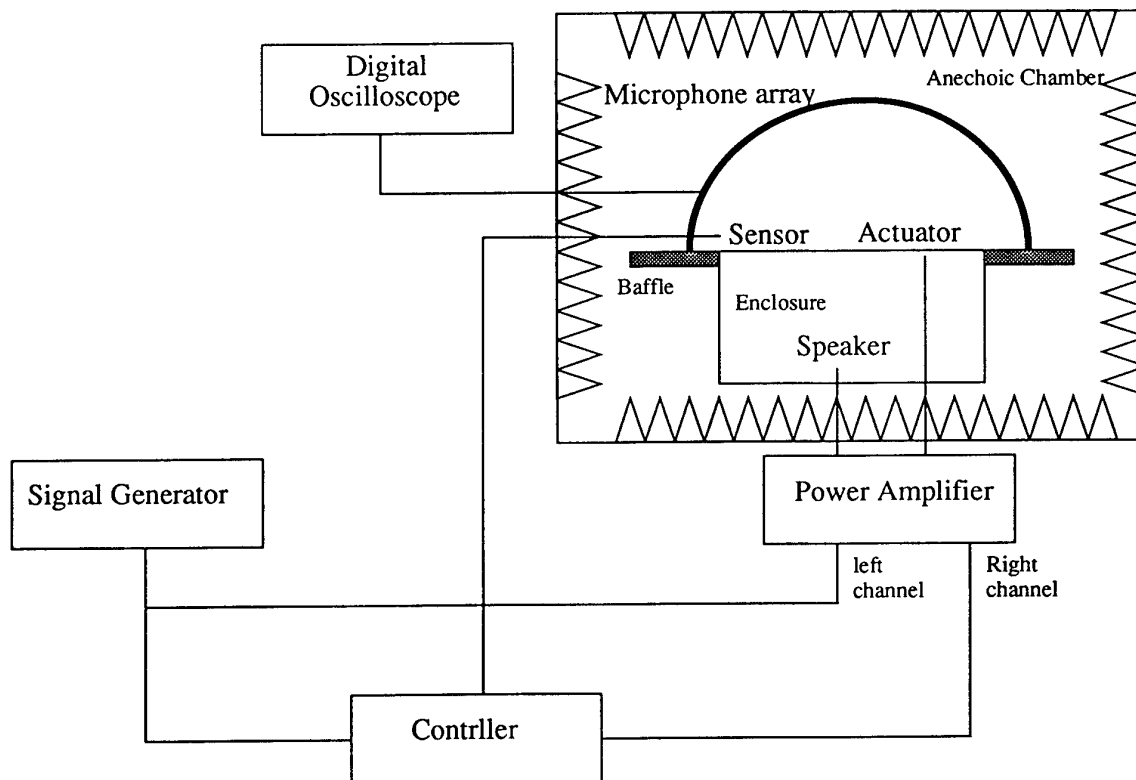


Figure 19. Measurement Set Up

where the W_O and W_C are the sound power radiated from the original and controlled plate respectively. Although the measuring surface in this experiment is not far enough to satisfy far field condition, we estimate the global reduction for convenience. Approximately, we have

$$R = 10 \log \left(\frac{\int_{S_h} (|p_O|^2) ds}{\int_{S_h} (|p_C|^2) ds} \right) \quad (13)$$

where S_h is the hemispherical surface and p_O and p_C are the original and control pressures, respectively.

Actually, the sound pressure is measured at discrete points. The integrals are replaced by the sum of the multiplication of the square of sound pressure and the surround area.

First, the original plate without active control was investigated. In the measurement, a white noise with a bandwidth from 20 Hz to 2 kHz was applied to the loudspeaker. The sound pressure at the position 15" up to the center of the plate and the outputs of sensor S1 and S2 and that of the MEMS sensor were recorded.

The performance of the one-sensor/one-actuator system was tested in this experiment. The signal from sensor S1 or S2 was taken as an error signal by the controller. The controller adjusted the amplitude and phase of the voltage applied to the actuator in such a way as to make the error signal minimal, while the voltage applied to speaker remained constant. In this experiment, it was usually more than 40 dB less than the original. We chose S1 as the basic sensor because the output appears to be more sensitive to the modes with stronger sound radiation and less sensitive to the inefficient radiating modes. In the case that the sensor S1 did not result in a reasonable sound control, the sensor S2 was tested.

The best result was obtained at the first resonance frequency of 79 Hz. The sensor S1 was used as the error sensor. The reduction by the active control is shown in Fig. 19. The original sound field on the hemispherical surface was quite uniform. The variation was about ± 1.5 dB. The active control reduced the sound level at all the measuring positions on the hemispherical surface by 20 to 26 dB. The global reduction was 22 dB. The same kind of result was also obtained using MEMS sensor at this frequency.

Comparisons were then made for other frequencies using PZT and MEMS sensor as shown in Figures 20-21. It is to be noted that the MEMS sensor performance is comparable and sometimes better than the conventional large size PZT sensor.

The use of MEMS technology for the cabin noised reduction using the multifunctional polymer mentioned as 'smart wall paper' will be reported later.

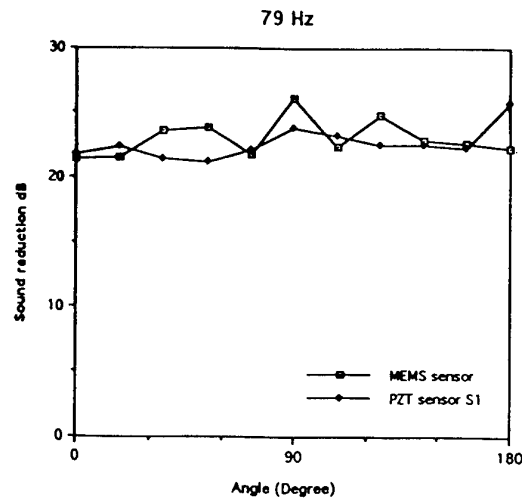


Figure 20. Comparison of MEMS and PZT sensors at 79 Hz

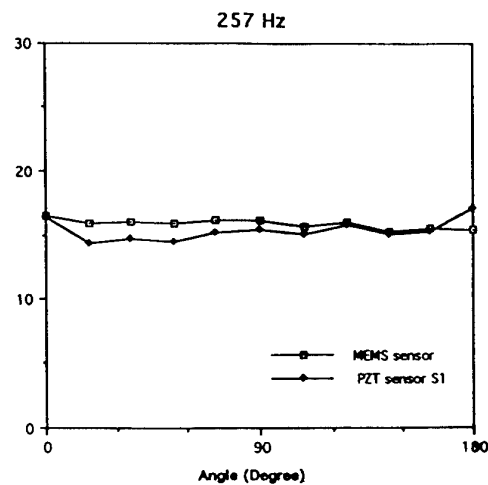


Figure 21. Comparison of MEMS and PZT sensors at 257 Hz

6.4 Health Monitoring of Aircraft Structures

The theoretical and numerical challenges in simulating a structure with embedded sensors using comb transducers, MEMS, SAW devices, etc., are many. The material may be inhomogeneous, the piezoelectric phases are anisotropic and involve coupled elastodynamic and electric fields, the structure may have protective coatings, the structure may be exposed to a semi-infinite environment (liquid). A numerical simulation method that can be applied to arbitrary geometry, material constituents, coupled field problems and transient effects calls for techniques such as hybrid finite element methods.

Several versatile codes have been developed by the authors which can look at optimization of sensor design, sensor placement, and antenna interfaces. Useful sensor parameters such as electrical conductance and susceptibility, crosstalk between sensor elements, sensor fidelity and efficiency, sensor/structure interface problems, effect of material damping etc. can all be calculated and studied numerically. Simpler calculations for the design and performance simulation of various designs for MEMS and SAW devices as well as transducer arrays and comb transducers can also be done in a much shorter time at much less cost. There is a well established precedent for the finite element and boundary element modeling (FEM and BEM) of structures with embedded sensors [Ref. 32-37]. This is now interfaced with new models that have been developed

for various types of transducers. Transient problems can also be handled using the unconditionally stable α -method for time stepping the dynamical equations of the system.

It is generally well known in the NDE community that inspection redundancy can often improve the overall probability of detection of defects. In addition to bulk wave, surface wave and guided wave ultrasonic NDE techniques, we are currently pursuing research on a multi-technology program including MEMS devices and microwave NDE. The overall NDE methodology and decision algorithm development program is illustrated in Figure 22. The application to aircraft structures is given in Figures 23 and 24. In Figure 24 a combination of fiber optics and antenna technology is given for future health monitoring of structures.

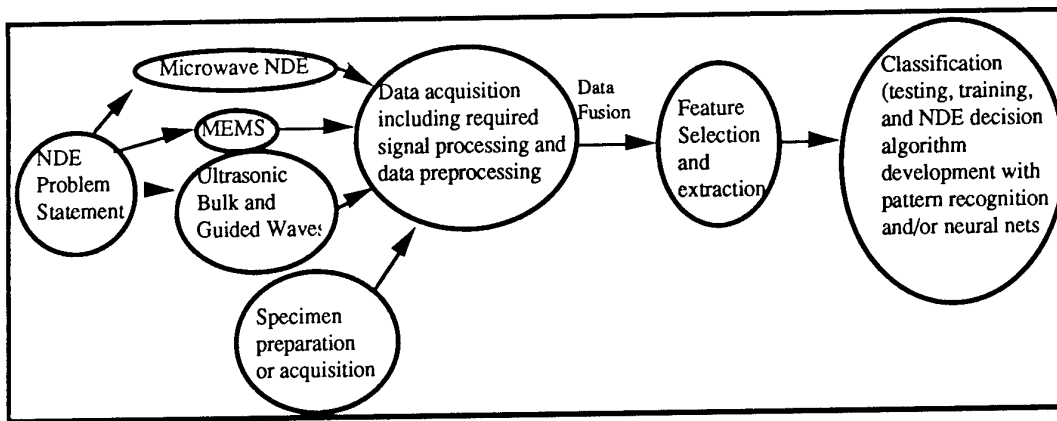


Figure 22 Decision algorithm program

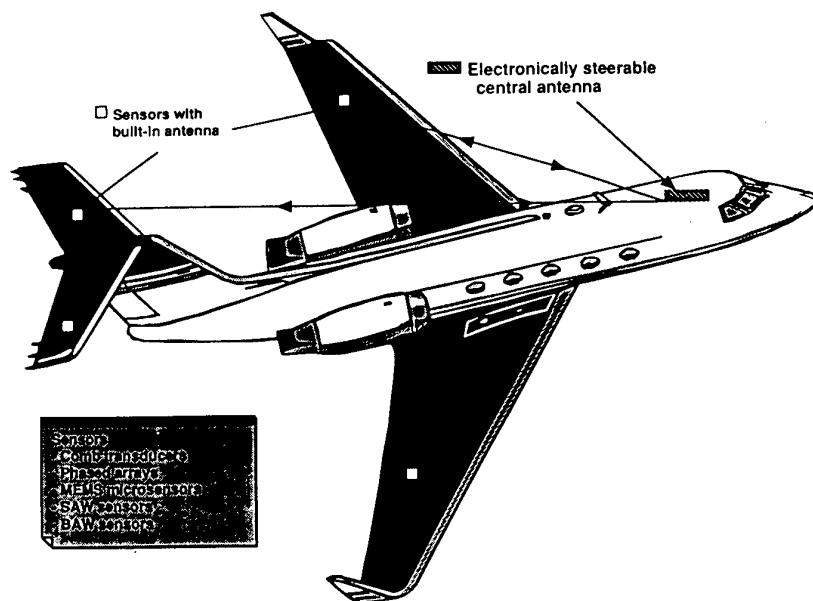


Figure 23 Wireless Telemetry for Health Monitoring of Aircraft

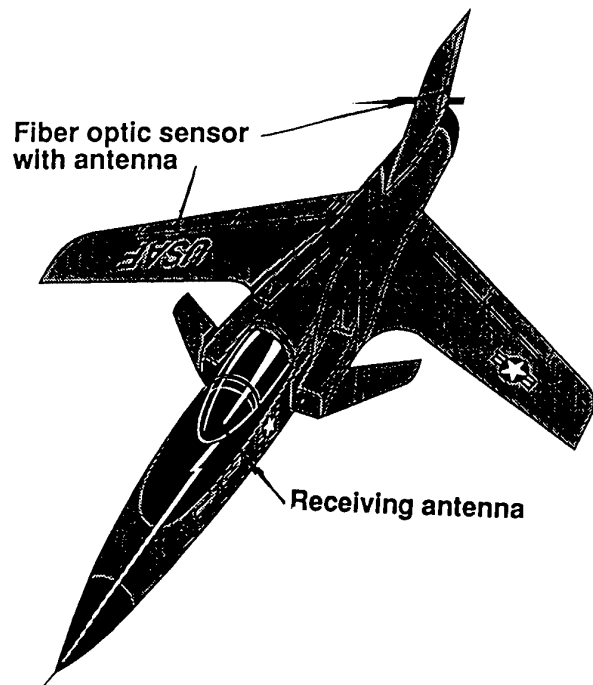


Figure 24. Health monitoring of structures using fiber optics and antenna technology

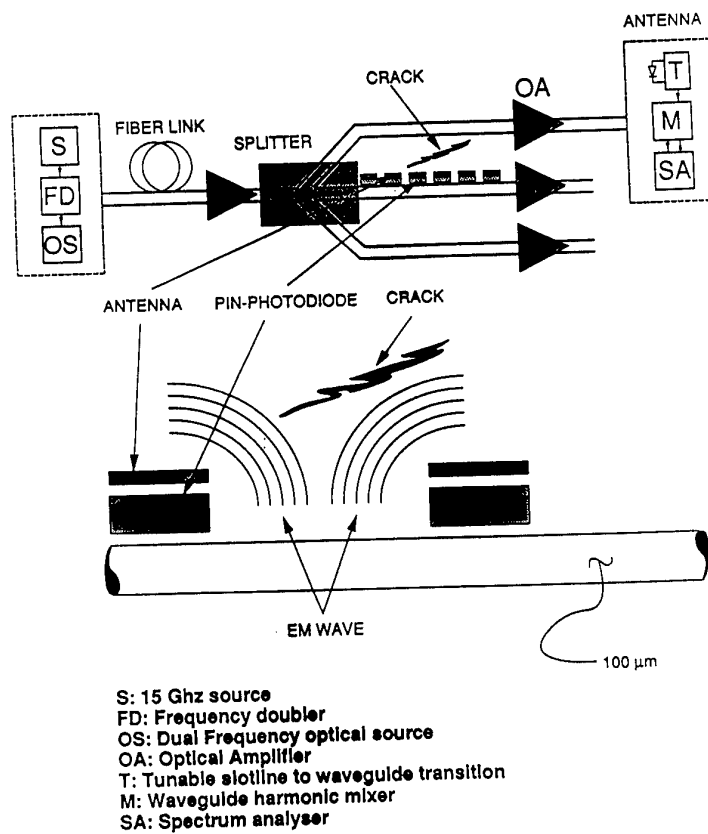


Figure 25. Fiber Optic Sensor with Antenna for 3D Imaging of Flaws in Structures

In Figure 27, an optical carrier wave with microwave signal is fed through an optical fiber. Using a pin-photodiode, the microwave signal is transmitted into the structure containing cracks via an antenna. The signal is scattered by the crack and the scattered signal is received by the antenna. A three dimensional image of the flaws can then be constructed using the ramp response signature as shown in Ref. 32.

Feature selection takes place from the physically based domains of guided waves, MEMS, microwave, etc. The classification will use state of the art artificial neural networks. This multi-technology approach to NDE vastly improves our ability to monitor the health of aircraft, civil structures and manufacturing processes. The goal, of course, is to finally develop a physically based feature vector for a complex system from which data fusion can be used in the development of a decision algorithm for criticality of system performance based on detection, classification, and sizing. The feature vector established with this multimode and multi-technology approach is rich and robust. Rather than filling in the elements of a feature vector with a long list of statistically or probabilistic based features on a single modality NDE approach in an attempt to solve the problem, the approach here with a multimode and multi-technology approach is to initially have tremendous sensitivity potential hence improving the overall probability of detection and decision algorithm performance potential. Once the feature vector is completely formulated, procedures for algorithm development follows traditional guidelines of pattern recognition whereby probability density function curves could be plotted to select the most useful features for final input into a pattern recognition or neural net algorithm, hence establishing a decision function with appropriate weights for the physically based features selected.

Thus, the multi-technology approach to health monitoring of systems and processes, is not simply a set of disparate and complementary technologies, but rather a multi-scale inspection ability that can be combined together for a powerful new approach to NDE.

7. CONCLUSION

An integration of smart materials, MEMS and control devices have been presented for aerospace structures. The smart skins derived from this integration are ideally suited for drag sensing and control of aircraft and spacecraft. One can also induce microriblets on the smart skin for drag reduction using micromachining techniques. These microriblets can be actively produced by the MEMS techniques at the desired location. The detection and control of noise and vibration as caused by both external and internal forces may be countered

through the use of MEMS sensors and piezoelectric actuators. An array of shear wave sensors introduces a method for localization of the internal stress field throughout the structure. The wireless remote and continuous telemetry systems do not weaken the structure. The wireless telemetry system can be incorporated along with fiber optic sensor for health monitoring of aerospace structures. The advanced polymeric smart materials may also serve as a "smart wall paper" for cabin noise sensing and control of aircraft.

8. ACKNOWLEDGMENTS

The work is in part supported by the US Army CECOM, the Office of Naval Research and the industrial members of the Center for the Engineering of Electronic and Acoustic Materials of the Pennsylvania State University. The authors would like to thank many of their graduate students in particular, Y. R. Roh, F. Selmi, J. Kim and Z. Wu and their colleague Dr. Bao

9. REFERENCES

1. Ikuta, K. and Higuchi, T., ed., *Proceedings of the IEEE Micro Electro Mechanical Systems* (Piscataway, NJ, 1994)
2. Varadan, V. K., ed., *Smart Electronics*, SPIE Proceedings (Bellingham, WA, 1995) vol. 2448
3. Tani, J. and Esashi, M., ed., *Proceedings of the International Symposium on Microsystems, Intelligent Materials and Robots* (Tohoku University, Japan, 1995)
4. Varadan, V. K., ed., *Smart Electronics and MEMS*, SPIE Proceedings (Bellingham, WA, 1996) vol. 2722
5. Ikuta, K. and Hirowatari, K., "Real Three Dimensional Micro Fabrication using Stereo Lithography and Metal Molding" (*Proceedings of the IEEE Micro Electro Mechanical Systems*, 1993), 42.
6. Varadan, V. K. and Varadan, V. V., "3D MEMS Structures and their Applications" (Invited Paper presented at the International Symposium on Microsystems, Intelligent Materials and Robots, Tohoku University, Japan, 1995)
7. Takagi, T. and Nakajima, N., "Photoforming Applied to Fine Machining" (*Proceedings of the IEEE Micro Electro Mechanical Systems*, 1993), 173.
8. Chin, L.C., Varadan, V.V., Varadan, V.K. "Hybrid Finite Element Formulation for Periodic Piezoelectric Arrays Subjected to Fluid Loading", *International Journal for Numerical Methods in Engineering*, Vol. 37, pp. 2987-3003, 1994.
9. Bao, X. Q., Varadan, V. V. and Varadan, V. K., SAW temperature sensor and remote reading system 1987 *Proc. IEEE Ultrasonic Symposium* 1 583-585

10. Varadan, V. K., Varadan, V. V. and Bao, X. Q., "Wireless Telemetry Systems and their Applications", *Journal of Smart Materials and Structures*, accepted for publications
11. Varadan, V. K., Varadan, V. V. and Bao, X. Q., "Integration of Interdigital Transducers, MEMS and Antennas for Smart Structures", in *Smart Electronics and MEMS*, edited by V. K. Varadan and P. J. McWhorter, SPIE Proceedings, Vol. 2722, pp. 95-106, 1996
12. Varadan, V. V., Varadan, V. K. and Bao, X. Q., "Smart Plates for Noise Reduction using MEMS Technology", in *Smart Electronics and MEMS*, edited by V. K. Varadan and P. J. McWhorter, SPIE Proceedings, Vol. 2722, pp. 230-240, 1996
13. Rose, J. L., Rajana, K. M. and Pilarski, A., "Guided waves for composite patch repair of aging aircraft", *Symposium on Composite Aircraft Repair of Aging Aircraft*, Vancouver, B.C., 1995
14. Smith, J. H., Montage, S. and Sniegowski, J. J., "Material and processing issues for the monolithic integration of microelectronics with surface-micromachined polysilicon sensors and actuators, *Micromachining and Microfabrication Process Technology*, edited by Karen W. Markus, SPIE, vol. 2639, 1995
15. Markus, K. W., Koester, D. A., Cowen, A., Mahadevan, R., Dhuler, V. R., Roberson, D. and Smith, L., "MEMS infrastructure: The Multi-User MEMS Processes (MUMPS)", *Micromachining and Microfabrication Process Technology*, edited by Karen W. Markus, SPIE, vol. 2639, 1995
16. Varadan, V. K., Ghodgaonkar, D. K., Varadan, V. V., Kelly, J. and Glikerdas, P., "Ceramic Phase Shifters for Electronically Steerable Antenna Systems", *Microwave Journal*, 35, pp. 116, 1992.
17. Varadan, V. K., Jose, K. A., Varadan, V. V., Hughes, R. F. and Kelly, J. F., "A novel microwave planar phase shifter," *Microwave Journal*, vol. 38, No. 4, pp. 244-254, 1994
18. Jose, K. A., Hollinger, R., Varadan, V. K., Varadan, V. V. and Kelly, J. F., "Experimental Investigations of Electronic Beam Steering Array Antennas", *Journal of Wave-Materials Interaction*, vol. 8, p. 311, 1993
19. Varadan, V. K., Varadan, V. V., Jose, K. A. and Kelly, J. F., "Electronically Steerable Leaky-wave Antenna using Tunable Ferroelectric Materials", *Journal of Smart Materials and Structures*, vol. 3, pp 470-475, 1994
20. Varadan, V. K. and Varadan, V. V., "Electronically Steerable Automobile Collision Warning Antennas Using Tunable Ferroelectric Materials", *Wireless Symposium*, Santa Clara, CA, February, 1994
21. Varadan, V. K., Selmi, F. and Varadan, V. V., Voltage Tunable Dielectric Ceramics which Exhibit Low Dielectric Constants and Applications thereof to Electrical Structures, US Patent (Serial No. 08/260,053) awarded 1996
22. Huang, J-B. and Ho, C-M., "Micro Riblets for Drag Reduction", SPIE Proceedings, edited by V. K. Varadan, vol. 2448, pp. 245-250, 1995
23. Varadan, V. K. and Varadan, V. V., "Drag Reduction in Aircraft Structures", SPIE Conference, San Diego, 1995
24. Varadan, V. V. and Varadan, V. K., "Microriblets for Drag Reduction using MEMS Technology" SPIE Conference, San Diego, 1995
25. Walsh, M. J., *AIAA journal*, vol. 21, p. 485, 1983
26. Fuller, C.R., *J. Sound and Vibration*, Vol. 139, p. 1-15, 1990.
27. Clark, R.L. and Fuller, C. R., *J. Acoust. Soc. Am.*, Vol. 92, p. 1521-1533, 1992.
28. Guckel, H., Burns, D.W., Rutigliano, C.R., Showers, D.K. and Uglow, J., *Technical Digest 4th Int. Conf. Solid-State Sensors and Actuators*, Tokyo, Japan, pp. 277-282, June 1987.
29. Metcalf, V.L., Fuller, C.R., Silcox, R.J. and Brow, D.E., *J. Sound and Vibration*, Vol. 153, pp. 387-402, 1992.
30. Thomas, D.R., Nelson, P.A. and Elliott, S.J., *J. Sound and Vibration*, Vol. 167, pp. 113-128, 1993.
31. Varadan, V.V., Varadan, V.K., Bao, X.Q., Jeng, J.H. and Sung, C.C., *J. Sound and Vibration*, Vol. 167, pp. 263-275, 1993.
32. Varadan, S. J. Tsao, V. K. Varadan and B. R. Tittman, "Image Reconstruction of Flaws using Ramp Response Signature", *Journal of Wave-Material Interaction*, vol. 10, no. 1, pp. 67-78, 1995

STRUCTURAL HEALTH MONITORING OF AIRCRAFT COMPONENTS

Jayanth N. Kudva, Allen J. Lockyer, and Craig B. Van Way
 Northrop Grumman Corporation
 Military Aircraft Systems Division
 Dept. 9B71/63, One Hornet Way
 El Segundo, CA - 90245, USA

SUMMARY

Since the late fifties when fatigue problems in aircraft structures were first encountered, aircraft maintenance has evolved through research, and subsequent implementation in well-orchestrated programs in several NATO countries. In the United States Air Force, the Aircraft Structural Integrity Program (ASIP) [1], and similar programs in other US service organizations, deserve much of the credit for establishing a first class record for US fleet readiness. ASIP's success, similar to other NATO programs, rely heavily (still) on frequent aircraft inspections to ensure fatigue cracking, or other flaws, get the necessary attention, and appropriate corrective action, before vehicle safety is compromised. Recent initiatives at Northrop Grumman, together with research elsewhere [2-5] in structural health monitoring systems (SHMS), now point one step further toward improved safety and maintenance costs reductions. Though not yet mature, recent technological advances in sensors, data acquisition, electronic miniaturization, and sensor system integration, now make it conceivable, at least, to replace current scheduled driven inspection practices - prevalent in aerospace systems maintenance throughout NATO - with "maintenance-on-demand." Put simply, aircraft structural inspections and maintenance will be performed only when really necessary and there is a high probability of finding damage, rather than scheduled, when often there is no damage detected.

An overview of ASIP is first introduced as background to the subject of structural health monitoring in the US reviewing inspection requirements, critical flaw sizes, and operational load environments. SHMS technologies are subsequently reviewed featuring requirements, architectures and components, sensors, processors, analysis algorithms and software, and SHMS component technology status. Finally, conclusions and recommendations for technology transition and future work are reported.

1.0 INTRODUCTION AND BACKGROUND

Aircraft and other aerospace structures experience various types of flight and operationally induced damage, such as fatigue and corrosion in metallic structures, and delaminations and disbonds in composite structures. Combat aircraft may additionally incur large-scale battle damage. To maintain military fleet safety and reliability,

life cycle tracking of aircraft is performed. In the USAF, aircraft tracking is dictated by the aircraft structural integrity program (ASIP) [1].

ASIP has fashioned over 20 years of experience of structural integrity monitoring into a comprehensive plan acquiring US fleet operational usage data to establish individual aircraft structural integrity. In general terms, ASIP's goal is to minimize the possibility of catastrophic structural failure resulting from unanticipated or undetected structural or material degradation. Logistics, structural inspections and maintenance, together with fleet rotation, all play an integral part in determining whether an aircraft is unsafe, or should be retired. Figure 1 illustrates the depth of the program. If we had to choose a single ASIP task that would derive most benefit from an on-board structurally integrated SHMS it would probably be Task 5, force management (FM), though all tasks are functionally interrelated.

Task 1	Task 2	Task 3	Task 4	Task 5
Design Information	Design Analysis & Development Tests	Full Scale Testing	Force Management Data Package	Force Management
ASIP Master Plan	Material & Joint Allowables	Static	Final Analysis	Loads / Environment Survey Support
Structural Design Criteria	Analysis • Loads • Temperature • Stress • Damage Tolerance	Fatigue	Force Structural Maintenance Plan	IAT Data Collection
Fracture and Fatigue Control Plan	• Fatigue • Sonic Fatigue • Vibration • Flutter	Sonic Fatigue	Loads / Environment Spectra Survey	Service Inspections, Maintenance & Repair
Selection of Materials, Processes & Joining Methods	• Nuclear Effects • Weapons Effects	Flight & Ground Loads Survey	Individual Aircraft Tracking Program	Structural Performance Records
Planned Operational Usage	Design Verification Tests	Loads Environment Spectra Survey		

96-158

Figure 1. ASIP Functional Tasks

FM is further subdivided into: 1) an individual aircraft tracking program (IAT), 2) an aircraft loads and environment spectra survey (L/ESS), and a 3) a force structural maintenance plan (FSMP). These elements are collectively used to determine maintenance and inspection

actions among US fleet aircraft, as well as ensure that over time, all aircraft maintain similar levels of usage to balance the effects of structural degradation. (Figure 2).

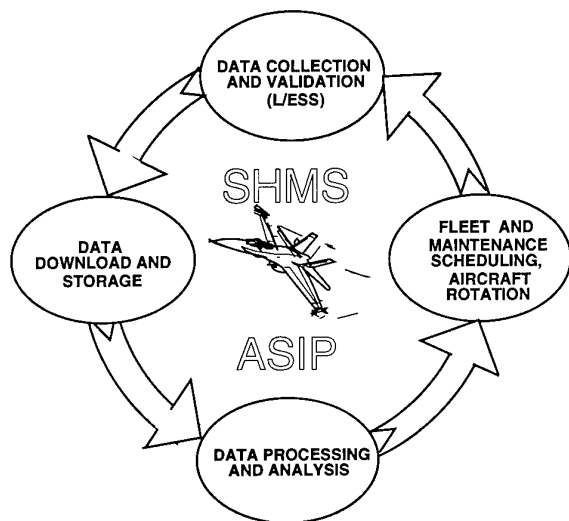


Figure 2. ASIP Structural Integrity Monitoring Functions.

Over the last few decades, ASIP and similar programs have contributed substantially to improving the safety and reliability of NATO military aircraft. Ideas published in the literature [2-5] to further enhance the effectiveness of NATO aircraft force management and tracking programs generally recommend:

- Reduce aircraft inspection intervals
- Improve maintenance procedures
- Improve data collection

All the above, individually or collectively, have a multiplicative effect for overhead reduction in terms of man power, time and equipment.

Other recommendations to improve NATO FM and tracking programs relate more specifically to details in the processing, monitoring methods, inspection, analysis and automation:

- (a) Increase stress monitoring - more sensors/locations
- (b) Reduce dependence on interpolation for stress measurements
- (c) Increase number of fleet aircraft instrumented for L/ESS - place less reliance on data extrapolations from few instrumented aircraft to entire fleet
- (d) Monitor damage directly (if feasible)
- (e) Automate aircraft usage data collection
- (f) Increase inspection interval

Items (a) through (c) are to a degree self explanatory, although for (c) it should be emphasized, that the difficulty of extrapolating the results from a few instrumented aircraft to the entire fleet is endemic to all NATO FM and tracking programs. An important point relating to (e) apart from the obvious cost reductions discussed previously, is that currently analytical methods and data collection play a central role in predicting the duration between inspections. Intervals are based on flaw (crack) growth rate, which is predicted analytically from such entities as aircraft loads, materials allowables, structural design and environmental factors, and others depending on the analytical mode used. All of the foregoing entities come from the data collection of the FM program and are subject to a degree of uncertainty. Inspection interval determination is not therefore an exact science. Item (e) is an integral part of (f) and could also be improved in terms of collection time, centralization, inaccuracies or missing data, and lengthy processing delays from collection and transmittal back to the fleet. It is perhaps item (f) that would benefit most from a structurally integrated health monitoring system that could replace the uncertainties of analytical methods by actual measurement, provided of course that the probability of flaw detection with an installed SHMS is better than the analytical uncertainties of current methods.

A related item not directly part of SHMS but important for inspection intervals is the accuracy of current non destructive inspection (NDI) techniques. If smaller flaws can be detected during ground maintenance, naturally inspection intervals can be increased.

In recent years, a significant amount of research [2-17] has addressed utilizing advanced sensors, software, and data processing technologies to overcome some of the above limitations by developing a structural health monitoring system. (a structure with an integrated SHMS is often referred to conceptually as a smart structure, implying a structure that senses its environment and assesses the impact of any resulting damage.) An SHMS could conceivably provide an accurate and detailed stress history, locate incipient damage, and ultimately lead to maintenance-on-demand.

2.0 STRUCTURAL HEALTH MONITORING REQUIREMENTS

An ideal SHMS implemented in an operational aircraft will need to address both large area damage (i.e. battle damage) and localized damage caused by everyday usage. Large area damage, while obviously more critical to the immediate safety of the aircraft, is easier to detect, and the real challenge in developing an SHMS is detecting minute flaws which may, over time, lead to structural failures [13]. ASIP requires that an airframe be capable of withstanding the growth of an assumed initial flaw under normal operational usage over a prescribed time interval. Typically, the assumed structural damage is set at the minimum detectable by standard non-destructive inspection (NDI). The inspection interval is set based on one half of the time it takes for the assumed flaw to cause a structural failure. A

summary of some typical damage modes are shown in Figure 3 (these are discussed in detail in References 11-13).

Metallic Structures	Composite Structures
<ul style="list-style-type: none"> Cracks ($\geq 0.05"$) Corrosion Stress Corrosion Cracking 	<ul style="list-style-type: none"> Impact Damage (up to 100 ft-lbs) Delaminations (2" Dia.) Stiffener Debond Joint Failures

Strains up to 10,000 Microstrains; Temperatures from -65° to 375°F

Figure 3. Structural Health Monitoring Requirements.

In metallic structures, the predominant damage modes are fatigue cracking, corrosion, and stress corrosion cracking. Cracks typically occur around fastener holes, cut-outs and sharp bends, and critical crack length could be as small as 0.1 inches. Hence, a monitoring system will have to be capable of detecting minute cracks in geometrically complex areas where the precise location is not known a priori. While corrosion is a serious problem, especially for naval aircraft, there are no quantitative ASIP requirements for corrosion monitoring, as yet. Difficulties arise in trying to correlate corrosion and performance degradation because the relationship is not quantitatively well understood, or easily predicted by analytical or statistical methods. The rapid growth of corrosion and the extent of corrosion propagation is similarly difficult to assess or quantify, and structural components with noticeable corrosion damage are typically replaced. Monitoring stress corrosion cracking will require detection of both cracks and corrosive environments.

For composite structures, four important failure/damage modes need to be addressed. These are low-velocity impact damage, delaminations, stiffener-skin separation, and failure of bolted and bonded joints. Of these, impact damage caused by dropped tools, runway debris, etc., is the most prevalent and its detection would perhaps have the most significant benefits of an SHMS.

In addition to damage detection, an SHMS must be capable of performing the ASIP functions of L/ESS and IAT monitoring. The L/ESS program is used to obtain time history records of the parameters necessary for defining the stress state of the airframe, and the IAT program predicts flaw growth in critical areas of the structure. By enhancing current tracking programs, a SHMS would provide increased data validity and return rates, while at the same time improving overall program efficiency.

3.0 SHMS ARCHITECTURE AND COMPONENTS

Figure 4 illustrates the main components of an SHMS. They include sensors, local preprocessors, a central processor, and software capable of making aircraft maintenance and logistics decisions. Individual sensors track strain, acceleration, temperature, corrosive environment, and structural damage. Local and central processors perform the functions of data collection,

processing, and analysis. Figure 5 (adapted from Reference 16) presents a more detailed architecture of an SHMS currently under development at Northrop Grumman.

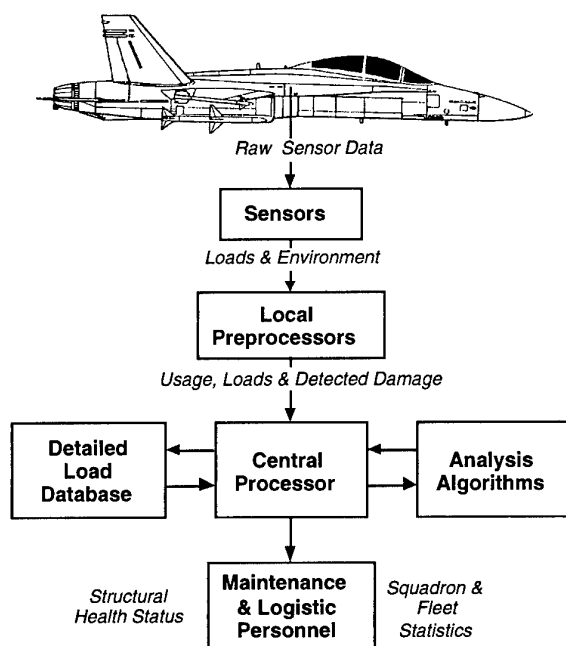


Figure 4. Overview of SHMS Components

The system architecture is designed to be modular and adaptable to different structural and system geometries. Raw sensor data is collected from each of the monitored zones and passed to the local processors. The central processor interrogates each of the local processors in turn to extract the sensor data. The system communicates with the central flight computer as necessary and stores flight parameters and summary information in the Standard Flight Data Recorder (SFDR).

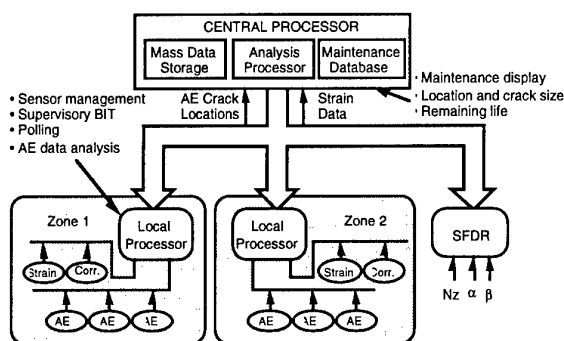


Figure 5. SHMS Architecture

The SHMS architecture is organized as a physically distributed and logically centralized configuration. Each major structural zone within the aircraft will contain a distributed sensor network and dedicated sensors. The significant advantages of this architecture are as follows:

excellent flexibility that accommodates system growth and ease of replacement without impacting the baseline design, a modular design to minimize system maintenance and repair costs, and tolerance to faults occurring at the embedded sensor (i.e., if a failure exists in one sensor element, the other sensors and processors will continue to operate).

3.1 Sensors

For structural health monitoring, load, temperature, moisture, fatigue, corrosion, delaminations, impact damage, and battle damage need to be monitored. To determine aircraft usage, flight parameters such as airspeed, altitude, pressure, angle-of-attack, etc., need to be recorded.

The sensors monitor all required environmental and damage parameters. In particular, acoustic emission and fiber-optic sensors are promising for health monitoring applications. Acoustic emission based sensors provide the only established technique capable of remote sensing, i.e., they do not have to be located in the immediate vicinity of the damage [8, 9]. Fiber-optic sensors exhibit high strain sensitivity, excellent strain resolution, and multiplexing capability. Additionally, fiber-optic sensors demonstrate an immunity to electromagnetic interference (EMI), a common source of sensor impedance in an aircraft environment [10].

Candidate sensors and their applications are discussed in Reference 15. Status of current sensing technology is discussed in Reference 13 and summarized in Section 4.

3.2 Processors

The zone sensors (AE, strain, and corrosion in Figure 5) are controlled by a local processing unit which contains a data acquisition board, a bus controller, and an analog to digital (A/D) converter. The local processors perform the tasks of data acquisition, basic signal conditioning, transducer error compensation, local data storage, and built-in-test (BIT). The raw sensor data are collected by the local processors, digitized, and stored for subsequent retrieval by the central processor.

The central processing unit consists of a system control processor, a health assessment processor, and a mass storage unit. It performs the functions of system control, data storage, flaw location, usage tracking, and health assessment. The central processor interrogates each of the local processors to obtain the processed sensor information, receives the data, stores it, performs a health assessment, and reports any critical information. The system controller is additionally responsible for interrogating the central flight computer to collect pertinent aircraft usage data. Details of a current SHMS design are presented in Reference 17.

Data transmission in the SHMS is driven by the requirements of the acoustic emission sensors. Significant data processing is required to accommodate the broadband acoustic emission monitoring technique [9,17]. Specifically, the sensing system samples acoustic events

at rates up to 10 MHz at an anticipated event rate of 10 Hz (10 valid AE events per second).

3.3 Analysis Algorithms and Software

Software for the SHMS must include data collection, storage, retrieval, and analysis algorithms. The software must be capable of collecting the sensor input, analyzing it, and making maintenance and inspection decisions based on the results. A detailed discussion of the system software appears in References 16 and 17.

4.0 STATUS OF CURRENT TECHNOLOGIES

An overview of technology assessment is shown in Figure 6. In the figure 0% implies the technology does not exist and 100% implies that the technology is ready for implementation onto an operational aircraft without any developments. The computer and analysis algorithm requirements of the health monitoring system are well developed, and can be sufficiently satisfied with current technology. System integration and technology demonstration is being addressed by the work at Northrop Grumman, however, further effort remains to be done in the area of sensor development. While standard sensors such as strain gages, accelerometers, and crack gages are well developed and widely accepted, the acoustic emission and fiber optic sensors will both require some further development and testing. In the case of the AE sensors, greater sensitivity and fidelity will be required to increase the accuracy and reliability of the AE damage detection technique. The fiber optic sensors are well developed, but lack a general acceptance in the military aircraft operational environment.

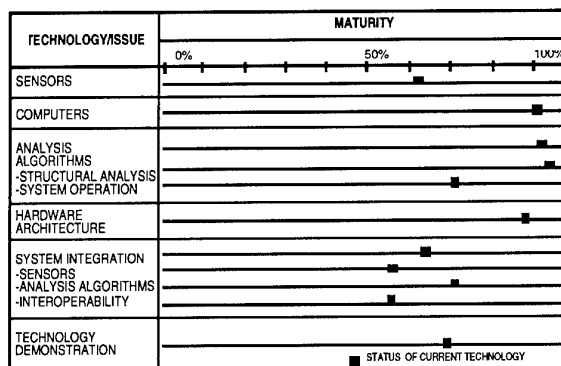


Figure 6. Current Technology Assessment.

The work at Northrop Grumman [11-17] has focused on the development of a prototype health monitoring system with the intent of performing a final demonstration test on a full scale F/A-18 wing attach bulkhead. The system has been demonstrated on complex subelements such as a simulated wing spar (Figure 7) and a multi-bay specimen simulating a wing carry through bulkhead (Figure 8). These demonstration tests have verified the ability of the acoustic emission system to identify flaws in complex structures. However, the test results have shown that the acoustic sensors can detect cracks as far away as 18 inches in simple

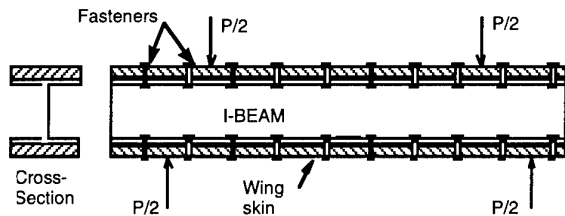


Figure 7. Simulated Wing Spar Subelement.

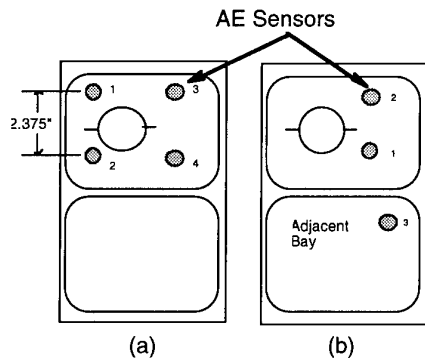


Figure 8. 2-Bay Subelement Sensor Placements (Two Configurations).

geometries like the wing spar web, but in more complex geometric configurations such as the stiffeners between the bays in the bulkhead specimen, or in the rows of fasteners in the beam, the crack signals are much more difficult to detect. The AE sensors had to be located within a few inches of the flaw to obtain positive identification and tracking. Further sensor development will alleviate these sensor spacing issues. The fiber optic sensors demonstrated excellent fidelity during these tests, to the point of detecting a small torsion in the wing spar specimen which was not detectable with standard strain gages. The successes in these tests have validated the design of the health monitoring system, and have yielded valuable information about crack detection which will be applied to the final test. These tests are discussed in detail in References 16 and 17.

The final step in this program will be to conduct a full scale fatigue test on the F/A-18 F.S. 488 bulkhead (Figure 9) and demonstrate the ability of the monitoring system to track the loads and environment, and detect structural damage in the structure. This test is presently scheduled for November 1996 and will be conducted at USAF Wright Laboratory, Wright Patterson Air Force Base, OH.

Thus, the technologies for the development of a health monitoring system for monitoring local areas (i.e. hot spots) are fairly mature, and with minor effort could perhaps be implemented in the near future. The next step in the development of this system will be to provide flight qualification through a flight test demonstration.

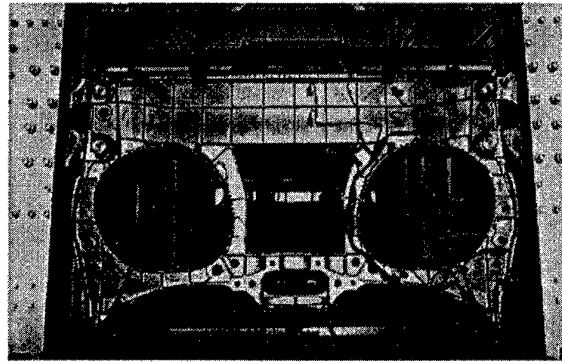


Figure 9. F/A-18 Wing Attach Bulkhead Mounted in Fatigue Test Frame.

5.0 SYSTEM BENEFITS AND PAYOFFS

The long-term goal of health monitoring is to create an aircraft with a 'maintenance-on-demand' system. In other words, replace analytical flaw tracking with automated structural damage detection and evaluation. While ideal performance capabilities have yet to be attained, health monitoring applications could enhance current methods of analytic flaw tracking. Payoffs include fewer special inspection requirements at repaired or known critical locations as well as improved mission readiness. In addition, initial steps to automate the data collection and transmission procedures can improve data validity and reduce turnaround times.

Preliminary studies indicate savings can be achieved by eliminating the manpower effort associated with aircraft inspections. For the F-18, savings in excess of \$35 million per year were estimated (assuming 33 hours of flight per aircraft per month, 1000 aircraft fleet) [13]. Estimates for the T-38 show a savings of more than \$9 million per year (based on 420 flight hours per aircraft per year, 720 fleet aircraft) [7].

The most significant potential savings for the SHMS, however, could result from the elimination of logistics personnel. By eliminating the need for various maintenance and tracking operations, the SHMS would replace one or more of the personnel assigned to the aircraft. The automation of just one logistics function could result in an approximate savings of \$100,000 per year in manpower and equipment [5]. When the total savings (inspections and logistics effort) are examined, the potential savings can become quite significant. Further, there is the consideration of the rare but plausible savings due to prevention of a catastrophic structural failure (failure resulting in loss of aircraft).

6.0 CONCLUDING REMARKS AND RECOMMENDATIONS FOR FUTURE WORK

The transition from current processes to a fully automated health monitoring system will not be immediate. Further R&D efforts are required in the areas of damage detection, aircraft system integration, and ASIP automation. Significant developments are needed particularly in the area

of damage detection sensors. Work currently underway at Northrop Grumman addresses some of these issues. In particular, a prototype health monitoring system is currently under development. Hardware components, data busses, software requirements, and anticipated data collection rates have been identified. Recent work has focused on assembling and testing a prototype system based on the developed candidate architecture. This work will lead to a full scale structural fatigue test towards the end of this year, and eventually to a qualification flight test of an aircraft health monitoring system.

Ongoing efforts collectively will pave the way towards the development of a completely automated SHMS providing total aircraft coverage and resulting in unprecedented levels of fleet readiness, flight safety, and life-cycle cost reduction.

7.0 ACKNOWLEDGMENTS

The work documented in this paper was performed under a government contract to a team lead by Northrop Grumman Corporation entitled "Smart Metallic Structures (SMS)," F33615-92-C-3203. The contract monitors are Mr. Michael Ziegler of the Air Force Wright Laboratories and Dr. James Alper of the Naval Air Warfare Center; their support and technical guidance is greatly appreciated.

The team members of the multidisciplinary team include Honeywell Corporation (system hardware development), Digital Wave Corporation (acoustic emission monitoring), Mission Research Corporation (system software), and Fiber & Sensors Technologies (fiber optic sensing system).

The authors would also like to thank Mr. Mark Roberts and Ms. Carlene Lau for the diligent and dedicated help they provided in preparing this paper.

8.0 REFERENCES

1. MIL-STD-1530A, Military Standard, Aircraft Structural Integrity Program, Airplane Requirements, December 1975.
2. Schmidt, W., and Boller, C., "Smart Structures - A Technology for the Next Generation Aircraft", Paper No. 1 AGARD-CP-531, Presented at the 75th Meeting of the AGARD Structures and Materials Panel, Lindau, Germany, Oct. 1992.
3. Boller, C., Dilger, R., "In-flight Aircraft Structures Health Monitoring Based on Smart Structures Technology", Paper No. 17, AGARD-CP-531, Presented at the 75th Meeting of the AGARD Structures and Materials Panel, Lindau, Germany, Oct. 1992.
4. Hickman, G. A., Gerardi, A., "Application of Smart Structures to Aircraft Health Monitoring", *Journal of Intelligent Material Systems and Structures*, Vol. 1, pp. 411 - 430, July 1991.
5. Gentry, J.D., et al., "The Impact of Smart Structures on Aircraft Structural Integrity Programs", 1992 USAF ASIP Conference, San Antonio, TX, December 1992.
6. Appels, A.J., Capt., "The cost effectiveness of aircraft structural integrity programs", 1993 USAF ASIP Conference, San Antonio, TX, December 1993.
7. Van Way, C.B., et al., "Integration of smart structures concepts for improved structural integrity monitoring of the T-38 aircraft," 1993 USAF ASIP Conference, San Antonio, TX, December 1993.
8. McBride, S. L., et al., "Acoustic Emission Determination of Crack Presence and Crack Advance During Flight", *Journal of Acoustic Emission*, Nov. 8, pp. 4 - 7, 1989.
9. Gorman, M.R., "Acoustic emission for the 1990s," *Proceedings of the IEEE: Ultrasonics, Ferroelectrics and Frequency Control*, 1992.
10. Murphy, K.A., et al., "Elliptical-core, two-mode optical fiber sensor implementation methods," *Journal of Lightwave Technologies*, November 1992.
11. Kudva, J.N., et al., Smart Structures Concepts Requirements Definition (SSCORE) Phase I Interim Report, WL-TR-93-3041, March 1993.
12. Van Way, C.B., et al., Smart Metallic Structures (SMS) Task 1 Report, Northrop Corp., Contract No. F33615-92-C-3203, Feb., 1993.
13. Kudva, J.N., et al., "Smart structures concepts for aircraft structural health monitoring", 1993 SPIE Smart Structures Conference, Albuquerque, NM, February 1993.
14. Marantidis, C., et al., "Acoustic emission in an on-board structural health monitoring system for military aircraft," 1994 SPIE Smart Structures Conference, Orlando, FL, February 1994.
15. Marantidis, C., et al., "Sensor and sensing technologies for structural health monitoring of aircraft," 1993 SPIE Smart Structures Conference, Albuquerque, NM, February 1993.
16. Van Way, C.B., et al., "Aircraft structural health monitoring system development - overview of the Air Force/Navy Smart Metallic Structures program," 1995 SPIE Smart Structures and Materials Conference, San Diego, CA, February, 1995, Paper No. 2443-30.
17. Van Way, C.B., et. al., "Development of an Automated Aircraft Structural Integrity Monitoring System-Overview of the Air Force/Navy Smart Metallic Structures Program," AIAA-96-1615-CP, paper presented at the 37th AIAA SDM Conference, Salt Lake City, UT, April 1996.

ADAPTIVE AIRCRAFT WING

Jayanth N. Kudva, Allen J. Lockyer and Kari Appa
Northrop Grumman Corporation
Military Aircraft Systems Division
Dept. 9B71/63, One Hornet Way,
El Segundo, CA, USA - 90245

SUMMARY

The concept of an adaptive aircraft wing, i.e., whose shape parameters such as camber, span-wise twist, and thickness can be varied to optimize the wing shape for various flight conditions, has been extensively studied by numerous researchers [1-8]. While the aerodynamic benefits (in terms of increased lift/drag ratios, improved maneuverability, and delayed flow separation) have been analytically and experimentally established, the complexity and weight penalty of the designs and actuation mechanisms have limited their practical implementation. Recent developments in sensors and actuators using smart materials could potentially alleviate the shortcomings of prior designs, leading the way to a more practical "smart" adaptive wing which responds to changes in flight and environmental conditions by optimally modifying its shape.

A summary of recent work in the area of adaptive wing concepts incorporating smart structures technologies is presented. Emphasis is placed on continuing research at Northrop Grumman under a United States Defense Advanced Research Projects Agency (DARPA) contract entitled "Smart Structures and Materials Development - Smart Wing," [8]. Limitations and potential benefits of adaptive wing designs, applications and advantages of smart material actuators and sensors, and results of recent tests are discussed. Recommendations for future work required to develop an operational smart adaptive wing are also outlined.

1.0 INTRODUCTION AND BACKGROUND

Since the dawn of manned flight, aircraft engineers have dreamed of adaptive wings to provide optimal flight performance at all points in a flight envelope. The terms active and adaptive are used to broadly convey a family of concepts wherein the structure senses the environment and responds actively to optimize performance. For aircraft, concepts include: (1) active feedback control systems for flutter suppression, load alleviation, and improvements in ride quality; and (2) changing the shape of the wing (to vary camber, span-wise twist or airfoil cross-section) for optimal performance at different flight conditions (take-off, landing, maneuver, and multiple cruise conditions).

Whereas active load alleviation systems are quite well developed and installed on several commercial and military

aircraft, active flutter suppression systems have yet to be incorporated in operational aircraft. Current experimental efforts are based on actively deploying conventional control surfaces (for flutter suppression the actuation rate is on the order of several hundred Hz).

The theoretical benefits of active control of wing shape are well known. For instance, hingeless contoured control surfaces provide improved aerodynamic performance. Deployment of conventional control surfaces in effect changes the overall wing camber but the rigid control surfaces give rise to discontinuous boundaries resulting in early air flow separation, leading to reduced lift and increased drag. On the other hand, the use of smooth continuous control surfaces delays the onset of flow separation and also improves the lift and stall angle characteristics as depicted in Figure 1.

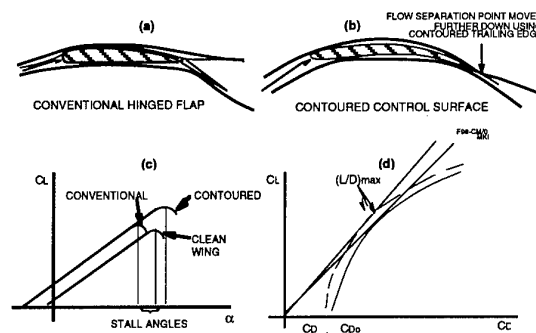


Figure 1. Comparison of Conventional and Contoured Control Surfaces

Two extensive studies in this area are the mission adaptive wing (MAW) and the active flexible wing (AFW) programs [1-5]. The MAW design used a mechanical actuation system to smoothly deploy leading and trailing edge control surfaces which were fully enclosed by flexible wing skins to provide increased efficiency by elimination of discontinuities in the airfoil cross-section. Performance benefits over a conventional fixed camber wing in the subsonic regime were demonstrated in flight tests on a modified F-111. However, the complexities of the mechanical actuation system and increase in overall weight rendered the design impractical for fleet operations.

The AFW concept on the other hand involves reducing the wing flexibility (and hence weight). To improve maneuver performance, the wing was twisted using aerodynamic torque provided by control surface deflections. Aeroelastic performance degradation was offset using active controls. While the anticipated aerodynamic performance benefits were somewhat compromised by the drag due to the use of control surfaces to both twist the wing and for normal flight control operations, the concept has sufficient weight benefits and a detailed flight test is currently being planned [5].

The smart wing concept is based on both the AFW and MAW designs and potentially improves the benefits by making judicious use of smart materials and structures technologies. Under an DARPA/WL contract to Northrop Grumman, the smart wing concept is being investigated incorporating new ideas in integrated sensing and actuation systems. Details of the program are discussed below.

2.0 SMART WING REQUIREMENTS, DESIGN, AND TESTING

Under the smart wing program, three key features are being studied: 1) hingeless, smoothly contoured trailing edge (TE) control surfaces, 2) variable wing twist, and 3) real-time pressure distribution data for feedback control. To evaluate the concepts and quantify performance improvements, two 16% scaled models (of a present generation fighter aircraft), one conventional and the other incorporating the above features (Figures 2 and 3), have been fabricated and tested in a wind tunnel to quantify performance benefits of the smart wing concept. Prior to undertaking the design, actuation requirements for the smart wing were established.

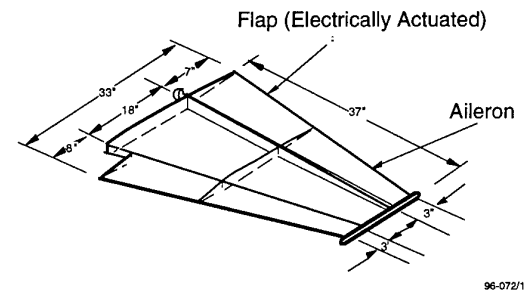


Figure 2. Conventional Wing Model

2.1 Requirements

Details of the requirements analysis performed in the program are provided in References 8 and 9. Figure 4 shows the actuation rates needed for various flight operations. Figure 5 shows calculated values of torque at wing mid-span and tip to achieve 2 and 5 degrees of twist for a full-scale aircraft and scaled models. (The torque requirements increase essentially as the fourth power of the geometric scaling factor - the values shown in the figure are slightly different because of differences in the materials used.) While it is feasible to achieve the torque requirements for the models, it is obvious that meeting

scaling requirements will be a significant challenge to transition this technology to a full-scale aircraft. This is discussed further in Section 3.

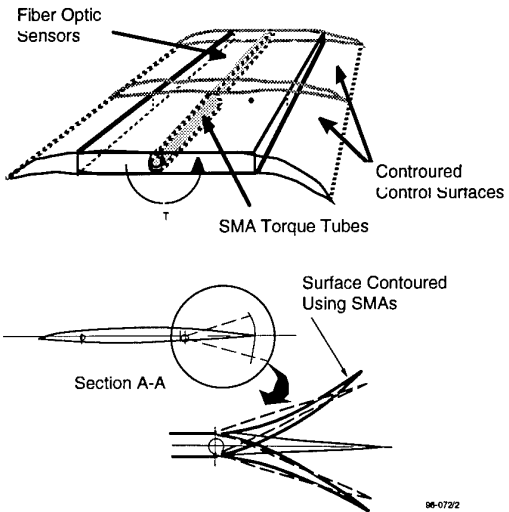


Figure 3. Smart Wing Model

Flight Condition	Actuation Rate
Cruise	0.3 to 1 Hz
Take-off/Landing	0.3 to 1 Hz
Maneuver	1 to 10 Hz
Flutter Suppression	50 to 100 Hz

Figure 4. Actuation Rate Requirements

Wing Twist	Full-scale	16% Model	10% Model	Twist (deg)
@ 50% span	2.0x10 ⁶	1.5x10 ³	220	2°
@ wing tip	0.16x10 ⁶	3.0x10 ²	165	5°

Figure 5. Torque Requirements for Wing Twisting (in.lbs.)

2.2 Design

Wing Twist: Several design concepts (Figure 6) were considered for twisting the wing for the wind tunnel models. Initial trade studies indicated that the integrated torque box concept was structurally most efficient. However, on further examination, the design presented severe manufacturing difficulties and appears to be somewhat impractical. Hence the shape memory alloy (SMA) torque tube actuation was chosen and a design with two concentric tubes as shown in Figure 6A was implemented. This technique functioned well in the tunnel, but because the final wind tunnel model was significantly stiffer than the scaled model (primarily due to escalation of wing skin and spar web thicknesses from the original scaled values to prevent local panel buckling), maximum wing tip twist of only about 1.25 degrees was realized. If

the stiffnesses were scaled exactly, 3 to 5 degrees of twist at the wing tip could easily have been achieved. Further details of the torque tube design are presented in Reference 10.

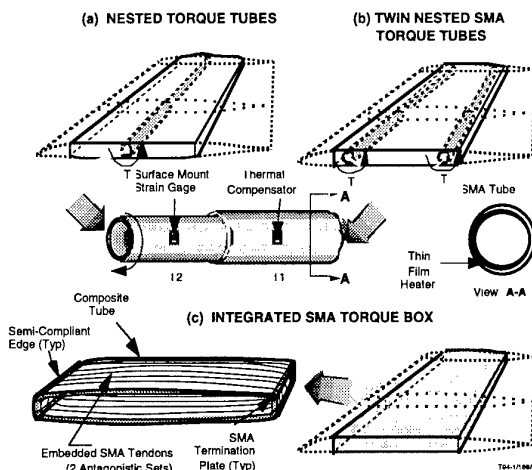


Figure 6. Wing Twist Activation Concepts

Adaptive Control Surfaces: The aerodynamic benefits of contoured hingeless surfaces are well known [1-3]. To implement these types of control surfaces, SMA based actuation systems are ideal because of their high force and high strain capabilities [11,12]. Figure 7 shows a schematic of the adaptive control surfaces with embedded SMA wires in top and bottom face sheets which provide two-way "antagonistic" actuation. Figure 8 shows the final system used for the wind tunnel model. Approximately forty 20 mil diameter wires were used to obtain the equivalent of ten degrees of rotation. Because of the complex thermo-mechanical behavior of the SMA wires, it was essential to incorporate sensors to determine the true position of the control surfaces. The most suitable sensors were fiber-optic sensors, and a suite of extrinsic Fabry-Perot interferometric (EFPI) strain sensors were embedded in the control surfaces and calibrated to provide an accurate measure of control surface actuation. This information was used for feedback to command, achieve and maintain a desired deflection.

A modified version of the EFPI strain sensor was also developed for pressure sensing and was shown to be highly accurate (resolution of 0.001 psi was achieved.)

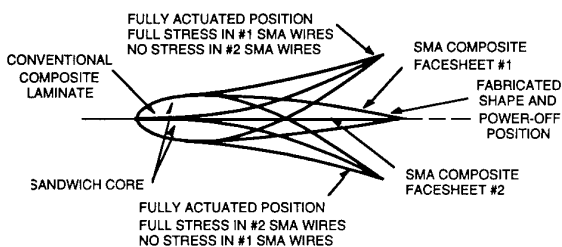


Figure 7. Antagonistic Actuation Concept

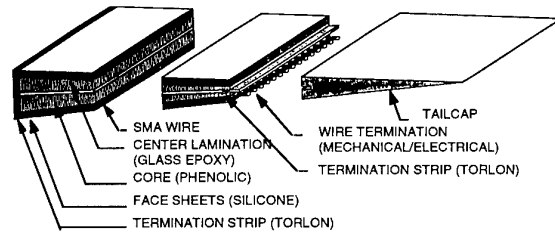


Figure 8. Details of Smart Trailing Edge Design

2.3 Testing

Figure 9 shows the range of test parameters used at the NASA Langley tests conducted during May 1996. A photograph of the smart wing model is shown in Figure 10. In addition to pressure data at approximately 130 points, six component balance data were recorded. Data reduction is currently under progress but preliminary results are encouraging. Approximately 8% increase in lift was obtained due to a wing twist of only 1.25 degrees (Figure 11). The hingeless control surface typically provided between 8 and 20% increase in rolling moment compared to a conventional design (Figure 12). (Complete results will be presented at the SPIE smart structures conference to be held in San Diego in Feb. 1997.)

Pressure (psf)	Aileron (deg)	Flap (deg)	Wing Tip Twist (deg)	Q (psf)
2200, 1100	0, 5, 10	$\pm(0, 5, 10)$	0, 1.25	40-120

Figure 9. Wind Tunnel Test Parameters

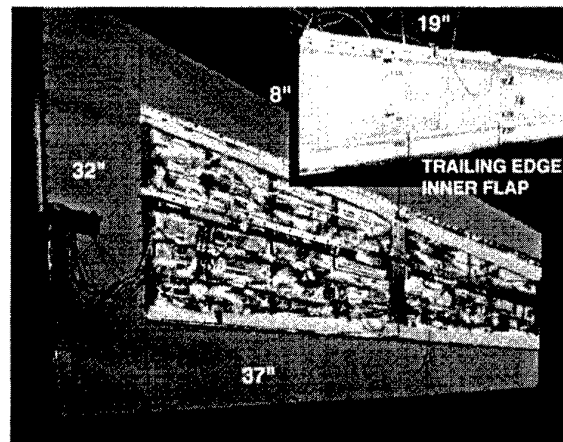


Figure 10. Smart Wing Wind Tunnel Model with SMA Flap (inset)

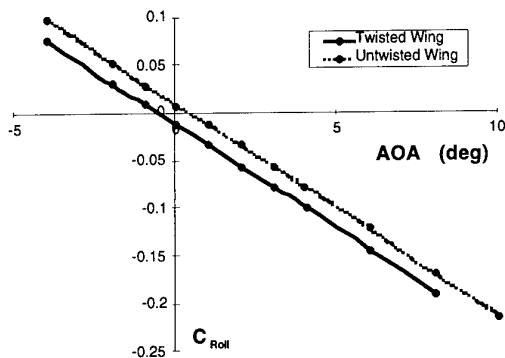


Figure 11. Rolling Moment Comparison of Twisted and Untwisted Wing

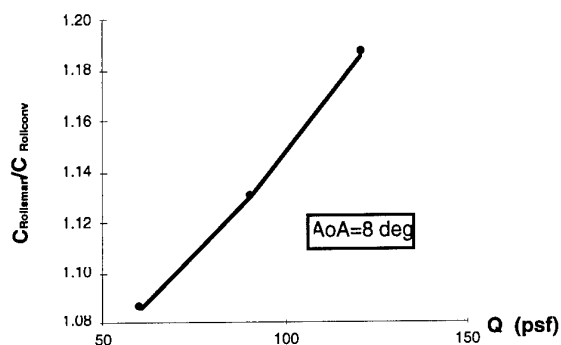


Figure 12. Rolling Moment Comparison of Smart and Conventional Wing Designs

3.0 FUTURE PLANS AND TECHNOLOGY TRANSITION

After data reduction and assessment of the results from the first wind tunnel test, efforts will be directed towards a) addressing manufacturing and system reliability issues, b) unsteady maneuver conditions and flutter suppression. In this regard, extendible leading edge control surfaces which can be activated at 30 to 50 Hz appear to have significant potential. The final goal of the smart wing development effort is to facilitate incorporation of smart material and structures technologies to improve the performance of military aircraft. This includes take-off and landing, cruise, maneuver, and aeroelastic stability boundary conditions.

As mentioned earlier, the raw requirements for wing twisting, control surface contouring etc., scale-up as the fourth power of the linear dimension and a direct implementation of the concepts discussed here may not be feasible and in fact, may not be the most efficient way to proceed. Smart wing technologies will need to be considered as one part of the total solution to obtain adaptive wing designs along with other related concepts such as aeroelastic tailoring, active flutter suppression, flow control etc. A system level optimization approach, wherein the load distribution is varied to optimize performance at different flight conditions using aeroelastic

tailoring and a judicious combination of conventional and smart control systems, is recommended. A phase two smart wing effort along these lines is currently being planned.

4.0 CONCLUDING REMARKS

Sensors, actuators and innovative designs incorporating smart materials and structures technologies could lead to the design of a truly adaptive "smart" aircraft wing which would provide optimal performance at all points in the flight regime by changing its shape parameters and actively responding to external loads and operating conditions. On-going work sponsored by DARPA and the United Air Force are laying the foundation for the eventual realization of this goal. While preliminary results are encouraging, much work remains to be done, particularly in the areas of design, optimization, system level integration, and cost-benefits analysis.

5.0 ACKNOWLEDGMENTS

Much of the work reported here was performed under a United States Defense Advanced Research Projects Agency (DARPA) contract to a team led by Northrop Grumman, entitled "Smart Materials and Structures Development - Smart Wing". The DARPA program manager is Dr. Robert Crowe. The contract is monitored by Dr. George Sendekyj of the Air Force Wright Laboratory, Wright Patterson Air Force Base, OH. The support and technical guidance provided by Dr. Crowe, Dr. Sendekyj and Mr. Terry Harris (USAF/WL) is greatly appreciated. The wind tunnel testing was conducted at the NASA Langley Transonic Dynamic Tunnel (TDT) in Hampton, VA; Dr. Tom Noll, Ms. Anna McGowan, Mr. Bob Moses, Ms. Sherry Hoadley, Ms. Renee Lake and Dr. Tony Rivera provided excellent support above and beyond the call of duty during six strenuous weeks of wind tunnel testing.

Besides the authors, key members of the smart wing development team at Northrop Grumman include Dr. Peter Jardine (SMA torque tube design and development), Mr. Chris Martin (model design and testing), Mr. Larry Jasmin (hardware design), Mr. Lewis Scherer (wind tunnel testing), Mr. John Flanagan (model fabrication) and Mr. Rich Votava (instrumentation).

Other members of the team include Dr. Bernie Carpenter of Lockheed Martin (SMA control surface development), Mr. Mark West, Mission Research Corporation (system software), and Mr. Paul Duncan, Fiber and Sensor Technologies (fiber optic sensors).

The authors would also like to thank Mr. Mark Roberts and Ms. Carlene Lau for the diligent and dedicated help they provided in preparing this paper.

9.0 REFERENCES

1. Hall, J.M., "Executive Summary AFTI/F-111 Mission Adaptive Wing," WRDC-TR-89-3083, September 1989.
2. Wong, K.J., "AFTI/F111 Mission Adaptive Wing Lift and Drag Flight Test Results," AFFTC-TR-86-42, Final Report, March 1987.

3. Cogburn, L.T., "AFTI/F111 Mission Adaptive Wing Flutter and Aeroservoelastic Test Program," AFFTC-TR-86-42, Final Report, April 1987.
4. Miller, G.D., "Active Flexible Wing (AFW) Technology," AFWAL-TR-87-3096, February 1988.
5. Pendelton, E., et. al., "A Flight Research Program for Active Aeroelastic Wing Technology," AIAA Paper No. 96-1574, presented at the 37th AIAA SDM Conference, Salt Lake City, UT, April 15-17, 1996.
6. Fielding, J.P., and Vaziry-Zanjany, M.A.F., "Reliability, Maintainability, and Development Cost Implications of Variable Camber Wings," Aeronautical Journal, pp. 183-195, May 1996.
7. Redeker, G., Wichmann, G., and Oelker, H-C., "Aerodynamic Investigations Toward an Adaptive Airfoil for a Transonic Transport Aircraft," Journal of Aircraft, Vol. 23, No. 5, pp. 398-405, May 1986.
8. Kudva, J.N., et. al., "Overview of the ARPA/WL 'Smart Structures and Material Development-Smart Wing' Contract," Paper No. 2721-02, SPIE North American Conference on "Smart Structures and Materials," San Diego, CA, February 26-29, 1996.
9. Kudva, J. N., et al., "Adaptive smart wing design for military aircraft: requirements, concepts and payoffs," Paper No. 2447-04, SPIE North American Conference on "Smart Structures and Materials," San Diego, California, February 26 - March 3, 1995.
10. Jardine, A. P., et al., "Shape Memory Alloy TiNi Actuators for Twist Control of Smart Wing Designs," Paper No. 2716-10, SPIE North American Conference on "Smart Structures and Materials," San Diego, California, February 26 - February 29, 1996.
11. Maclean, B.J., Carpenter, B.F., Draper, J. S., and Misra, M.S., "A Shape Memory Actuated Compliant Control Surface," SPIE, Vol. 1917, "Smart Structures and Intelligent Systems," 1993, pp. 809-818.
12. Misra, M.S., et. al., "Adaptive Structure Design Employing Shape Memory Actuators," Paper No. 15, AGARD-CP-531, presented at the 75th meeting of the AGARD Structures and Materials Panel, Lindau, Germany, 5-7 October 1992.

ELECTROMAGNETIC ANTENNA AND SMART STRUCTURES

A. PRIOU, Professor at the University of Paris X

Radar Technologies Division Head

DGA/DRET/STRDT-G.22

00460 ARMEES France

SUMMARY

One of the future applications of smart structures and materials for aircraft of new generation could be the electromagnetic smart skin antennas integrated on the aircraft. Military aircraft contains a proliferation of antennas to support advanced weapon system avionics. A tendency is to reduce the number of antennas sites on an aircraft to a minimum set of multifunction smart skin apertures that will provide equivalent or superior coverage and that will satisfy all the requirements of advanced weapon system avionics. Up to 50 % of the air vehicle could be used for embedment of antennas. Controlable and reconfigurable antennas or conformal antennas are needed for mission flexibility and for reducing component failure or battle damage. Pay-offs are mainly cost saving and weight saving per aircraft with additional properties such as improved low observable performances, supportability and drag reduction, etc...

In the first part of the presentation, we will review the present international activity in this area. We will develop some arguments to answering the question : why to do it ?

In the second part, we will introduce the concept of multifunctional smart skin antenna passing through the elementary radiating element, the adaptive antenna, and the antenna array. The electronic scanning and steering antenna array as well as the conformal antenna array is approached.

We end the presentation by a concept of electromagnetic smart skin antenna array that can be developed in the future and integrated to military or civilian aircrafts.

During this presentation, a lot of examples will be given for each case. We will address the critical enabling technologies required to implement an electromagnetic smart antenna. We will show the main advantages of such new technologies and concept for military aircraft of new generation (benefit and pay-offs).

I - INTRODUCTION

A smart structure is considered to be a structure that contains embedded microsensors, sensors and actuators with associated modern control system capabilities that spontaneously respond to external stimuli in proportion to their intensity to compensate undesired effects or to enhance desired effects.

Smart structures must be able to reproduce the reactive and sensitive capabilities of a skin by using artificial, technical

and industrial processes and to instantaneously transmit all variations to a local or non local central command center.

It is an interdisciplinary topic. Smart Structures and Materials will influence many basic research programmes :

- materials sciences (both chemical and physical),
- mechanical science,
- fabrication (involving chemistry, fluid mechanics and processing),
- engineering research (integration of micro-sensors, actuators, optical sensors, micro-electro-mechanical systems, devices)
- data processing (signal analysis and interpretations).

The possible applications for Smart Structures will include mainly : health and usage monitoring, damage detection and control, sound attenuation, noise reduction, active control of vibrations, shape control, monitored repairs, manufacturing control and smart skins antennas.

A lot of international programmes start few years ago (US, Japanese and European) to make progress in the material science, in fabrication and assembling techniques, in sensors and microsensors technologies and signal and data processing related to smart structures.

SPICES program (Synthesis and Processing of Intelligent Cost Effective Systems) sponsored by Advanced Research Project Agency (ARPA) for two years is one of those programmes trying to develop and fabricate micro sensors, microsystems at controlled fabrication cost.

In the domain of aircraft, several recent attempts are made. Among others, we will mention the following activities :

- Northrop Grumman (1) will study smart adaptive wing concepts under a two-year contract from ARPA. They study several materials that can change the shape of the wing. The main objective is to explore, define and demonstrate the applicability of Smart Materials and Structures in military or civilian aircraft in order to improve their performances,
- Smart electronics with interdigital electrodes antennas and MEMS for aerospace structure developed by V.V and V.K Varadan (2). The sensors are designed to measure both pressure and shear of the fluid flow an aerospace structures.

Returning to smart skins antennas, it is well recognized that military aircraft contain a proliferation of antennas to support advanced weapon system avionics. There is much redundancy and inefficiency with many single function antennas operating at similar power levels, operating bands and signal bandwidths. The situation becomes more complex as technology advances.

As example, 66 - antenna apertures located at 37 sites are implemented on the F-18, covering various frequency bands (from 200 Mz to 18 GHz) and various communications or radar functions (UHF communication medium and long range, navigation and location, identification, smart weapons communication, altimeter and warning radars).

The solution to the proliferation problem is to reduce the number of apertures to a minimum set of multifunction smart skins apertures that will provide equivalent or superior coverage.

In a recent paper (3) the authors from Northrop Grumman TRW and WP propose to have only 9 apertures in 9 sites to divide the weight by a factor near 2, to reduce the cost of 30 %. They propose several candidate locations for smart skin panels for a realistic aircraft installation (dorsal deck centerline, weapon bay door, front landing gear bay door, outer wing, radome, forward wing root lower surface, trailing edge flaps and vertical tail). The performance, easy installation, repair, load conditions are compared and ranked for ease of installation.

It is an Air Force Wright Lab initiative in the area of "Smart Skins Structure Demonstration Program S³D" (5). The objective is to design, develop and test a conformal structural load-bearing communication navigation and identification (CNI) antenna in the 0,15 to 2 GHz frequency bands suitable for a military aircraft.

The same authors propose the development of a conformal antenna installation in vertical tail of a military aircraft (4). Excitation of the large vertical tail surface improves radiation efficiency in the VHF-FM, VHF-AM and VHF frequency bands. The main idea is the volume reduction in antenna avionics packaging afforded by semi conductor miniaturization and low cost multifunction conformal antenna installed in the vertical tail. An increased antenna gain without degrading structural integrity could be obtained for such smart skins embedded antenna in the vertical tail.

Other attempts and idea are under development :

- a thermoadaptative antennas by Mc Donnell Douglas Aerospace (6),
- an electrochromic adaptive antennas by Mc. Donnell Douglas Aerospace (7),
- conformal Load Bearing Antenna Structure : CLAS concept by Mc. Donnell Douglas,
- a conformal spiral antenna (8) by Pennstate University,

- a NATO RSG Group on Smart Structures under Panel 3 for physics and electronics.

In exploring those programmes published in open literature. We can deduce the main reasons for why to do it :

- about 50 % of an aircraft can be used for embedding antennas,
- there is a need to decrease the number of apertures and aperture sites on an aircraft,
- there is a need to have controllable and reconfigurable (conformal and adaptive) antennas on an aircraft to get more flexibility and create new mission flexibility,
- there is a need to develop multifunctional, multimode and multiband systems.

With such concepts, it is expected to get the following main advantages :

- reduction in weight per aircraft,
- reduction in fabrication cost per aircraft associated with other increased properties such as the low observable radar performances, the supportability and the drag reduction.

II - CONCEPT OF MULTIFUNCTIONAL SMART SKIN ANTENNA

Microstrip antennas, slotted antennas, helical and spiral antennas are some candidates for large bandwidth elementary radiating elements [10]. They can be mounted such as to form a large antenna array in order to obtain large antenna gain and more directing radiation pattern.

The main requirements for elementary radiating elements or antenna array are :

- multifrequency and broad-band,
- low weight,
- fabricated with flexible materials (composite material having structural properties),
- as possible built-in technology to get a low cost fabrication.

With the advancement of recent semi conductor, high speed data processing, material and machining technologies, a variety of systems using phased array technologies are being put into practical uses. The phased array antennas that uses electronic beam scanning by controlling the phase shifters (ferrite or diode phasers) has been widely employed because it can scan beams speedily and freely.

Passive phased array antennas were first developed for ground-based radar such as landing system [11] or others. Active, semiactive or passive electronic beam steering in reception allows by an appropriate treatment on the signals coming from each radiating elements of the array to form one or more antenna lobe having special properties.

Primitive active phased array antennas, however, had many restrictions for practical use, because of high price, low power, and the difficulty of attaining compact size and light weight.

Remarkable advancement of semiconductor technology solved these problems in the 1980. Power amplifiers, low noise amplifiers, phase shifter and diplexers are now being made smaller and cheaper. Microwave monolithic integrated circuit (MMIC) technology is successfully realized low cost, high power, compact size, light weight of these parts [12].

The advantage of the active phased array antenna is highly flexible design of radiation pattern characteristics and beam scanning methods. The second advantage is that it is able to have multiple beams by using multiple exciting apertures designed by using switching circuits. The adaptive beam scanning which is effective for radar becomes possible.

The adaptive array can automatically form nulls in the radiation pattern in the unknown direction of undesired signals and architectures applying digital beamforming techniques have been proposed [13].

Principally all these techniques are applied to ground-based radars not yet to aircraft radar. But the characteristics obtained by such adaptive array are very attractive and can be used in military aircraft when the fabrication cost of all systems, subsystems associated with this kind of array will decrease drastically.

The next step is to try to realize a multilayered concept for multifunctional skins. The different functions are distributed to separate layers which are stacked together. This multilayered structure must include environmental protection sheet, sensors with variable radar absorbers, radar absorbing structure, EMI/EMP shielding, structure health monitoring, communication and power supply, electronics such as TR modules and electronic command, internal environmental protection, cooling systems and signal processing systems.

Several architectures are under investigation either in the range of 100 Mz to 2 GHz [1-3] or at higher frequency range from 2 to 18 GHz. Also flexible materials are used for this multifunctional skins in order to obtain conformal array antenna. Fig. 1 is the crosssection artistic view of a multilayer radiating elements and distribution structure for a smart skins. Fig. 2 is the view of a possible smart skin antenna array including all the various layers with the cooling system.

For aircraft, depending where such kind of smart skin antenna array is located, we need to have, furthermore, sensors or actuators to control mechanical deformation or vibration. These sensors microensors or actuators have to be embedded directly in the antenna array in a place where they don't create interferences with the impinging electromagnetic wave.

Many questions arise : what sensors we needed and for what action ? How is it possible to use the signal delivered by these sensors to reconfigure the antenna array radiating pattern ?... What are the new algorithms to be developed ?

All these questions are related to the mean topic "how to do it" ?

III - ADVANTAGES, PAY-OFFS AND CONCLUSIONS

The expected advantages and benefits are the following :

- réduction in weight, volume, life cycle,
- reduction in energy consumption,
- improvement of system performances, more flexibility and new mission
- wide instantaneous bandwidth with high gain and coverage
- avionic multifunctionality : multifunctional radar and electronic warfare shared apertures,
- reduction in cost due to a reduction in replication and better repairing and system maintenance
- lightning susceptibility and electromagnetic compatibility.

The main pay-offs for military systems will be ranked as follow :

- safety, availability and effectiveness increased,
- downtime and cost of maintenance reduced.

It is now a real challenge to build a first prototype of a smart skin antenna array for aircraft. The associated technologies is merging maturing Smart Skins concepts. Performing the multidisciplinary trades becomes necessary for air vehicle integration. The advantages and disadvantages of such new techniques must be clearly verified bringing in mind the demonstration of reduction of weight, volume and the reduction in cost per aircraft.

References

- 1) J.N. Kudva et al, Nortrop Grumman Corporation
Smart Structure and Materials Development
Smart Wing
SPIE meeting on Smart Structures and Materials - San Diego - February 1996.
- 2) V.V. and V.K. Varadan, Pennstate University,
Smart electronics with interdigital electrodes antennas and MEMS
SPIE Meeting on Smart Structures and Materials - Orlando - February 1995 and SPIE - Vol 2448.
- 3) A.J. Lockyer et Al, Northrop Grumman Corp,
A.C. Goetz, TRW and J. Tuss, Wright Patterson, AF
Development of a conformal load carrying
Smart skin antenna for military aircraft
SPIE Meeting on Smart Structures and Materials - Orlando - February 1995 and SPIE - Vol 2448/53

- 4) A.J. Lockyer et al, Northrop Grumman Corp, A.C. Goetz
TRW
Smart skin technologies to the development of a
Conformal Antenna installation in vertical tail of a
military aircraft
SPIE Meeting on Smart Structures and Materials -
Orlando - February 1995 and SPIE - Vol 2448/42
- 5) K. H. Altandal Northop - Grumman Corp
Smart skin structure technology demonstration.
SPIE Meeting on Smart Structures and Materials - San
Diego - February 1996
- 6) B.M. Howard et al, Mc Donnell Douglas
Thermoadaptive antennas.
SPIE Meeting on Smart Structures and Materials
San Diego - February 1996
- 7) B.M. Howard et al Mc Donnell Douglas
Electrochromic adaptive antennas
SPIE Meeting on Smart Structures and Materials - San
Diego - February 1996
- 8) V.K. Varadam, Pennstate
Design and development of a conformal spiral antenna
SPIE Meeting on Smart Structures and Materials - San
Diego - February 1996
- 9) V.V. Varadan
Electronically steerable millimeter antenna.
SPIE Meeting on Smart Structures and Materials
Orlando - February 1995 - SPIE Vol 2448
- 10) G. Dubost - S. Zisler
Antennes a large bande : theorie and applications
Masson 1976
- 11) Y. Kuwahara, M. Sato, NEC
Some latest phased array systems
1994 - Asia Pacific Microwave Conference
- 12) M. Sato, M. Sugano et Al, NEC
Cylindrical Active Phased Array Antenna
IEICE trans Comm - Vol I 76 - B N010
October 1893
- 13) S. Takeya, M. Sinonago, Y. Susaki, . H. Myanchi, Toxiba
Corporation
Applications of DBF techniques to radar systems
IEICE trans Com. - Vol E 77 - B n° 2 - February 1994

Smart Skins : Mechanical and Microwave Active Structures

Smart Skin Realization : Multilayer radiating elements / distribution structure

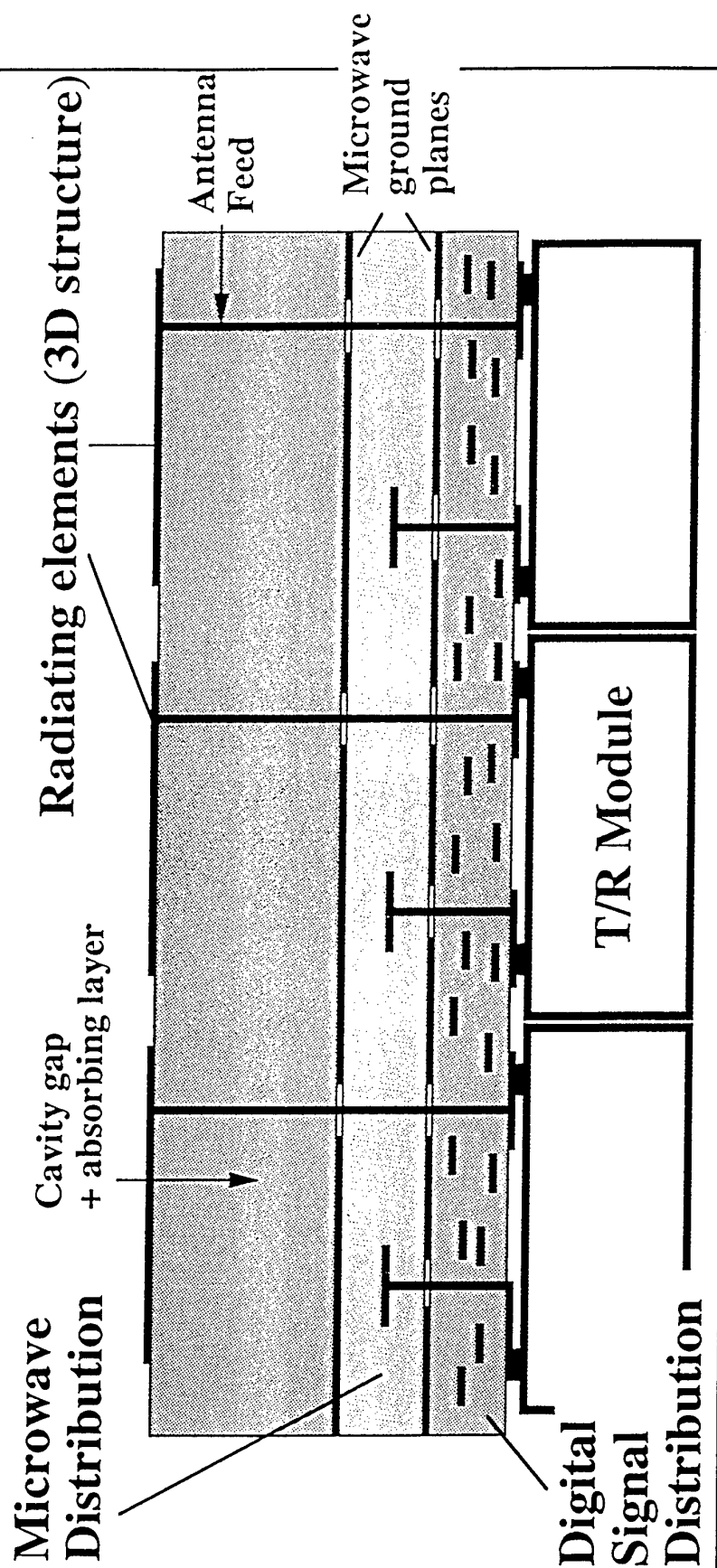


Figure 1 : artistic view of a smart skin

**EXPLORATORY TEAM ON SMART STRUCTURES
AND MEMS OF NATO, PANEL 3, AC 243 RSG**

**A. PRIOU, Professor at the University of Paris X
Radar Technologies Division Head
DGA/DRET/STRDT-G.22
00460 ARMEES France**

SUMMARY

In 1995 the NATO Panel 3, related to Physics and Electronics, decided to create an Exploratory Team on Smart Structures and MEMS. France is Pilot Nation of the Exploratory Team. During 1995 and 1996 several meetings have been held in European Countries and in USA in order to prepare the term of Reference, (TOR) describing the background and objectives, the Programme of the work (POW) for the method and programme which addresses the enabling technologies required to implement a smart structure or system.

In the first part the Term of Reference (version september 13 1995) is presented. The second part includes the proposal for a Programme of work (version November 1995). In the last part, the decision taken at 1996 Paris and San Diego meetings to organize several workshops in 1996 and 1997 has been mentioned.

**I - TERM OF REFERENCE (TOR) : RESEARCH
STUDY GROUP ON SMART STRUCTURES**

1-1 Origin

a) Background

An exploratory team on the use of Micro Electro Mechanical Systems (MEMS) in Smart Structures has been created for a one year term. The first meeting took place in Brussels on January 16-17, 1995. As a pilot nation, France chaired this meeting.

This exploratory team evaluates the desirability and/or need for NATO wide cooperation between countries on MEMS in Smart Structures in order to develop and find specific application of these structures to solve military mission.

The exploratory team recommends the creation of RSG group on Smart Structures integrating microsensors, actuators and MEMS in composite materials.

A smart structure is considered to be a structure that contains embedded sensors and/or actuators with associated modern control system that spontaneously respond to external stimuli in proportion to their intensity to compensate undesirable effects or to enhance desirable effects.

Smart Structures are a truly interdisciplinary topic and will influence many basic research programmes simultaneously :

- materials science (both chemical and physical),
- mechanical science,
- fabrication (involving chemistry, fluid mechanics, and processing),
- engineering research (involving integrated systems of sensors, actuators, MEMS and optical sensors or other devices),
- data processing (signal analysis and interpretations).

The current programmes hardly scratch the surface of the basic science and engineering research issues which must be addressed to fully realize the benefits of integrated sensors and actuators.

Smart Structures offer a new challenge especially in the area of microwave antennas or microwave array structures that can be embedded directly on vehicle or aboard an aircraft. It is a redefinition of the efficiency and the behaviour of the target skins. It offers, in principle, many advantages. It covers a large range of research topics such as the passive and active materials, instrumentations, data treatment and control of Smart Structures. Progress has to be made in the future to define and design Smart Structure devices or equipments. Both basic and applied researches are needed in many disciplines.

Research in Smart Structures includes encompasses materials research on surface morphology and the application of MEMS to microprocess control in materials processing. It addresses research on alternate materials (e.g. polymers) for MEMS applications.

Micromachining (e.g. etching) research for a wide array of materials other than silicon, and research on the adaptation of the thin film techniques for MEMS is also envisioned. Characterization of mechanical and other properties of these materials on small scales is essential (order of magnitude differences in material properties have been observed in small scale material samples). Revolutionary embedded instrumentation for researching such material properties can be provided within the MEMS framework itself.

The application of Smart Structures concept to **structural aspects** could be explored including :

- * **Health and Usage monitoring**
 - + Starting from cure monitoring to damage detection (against impact, ageing) on composite structures.
- * **Active control of structural vibrations**
 - + Higher harmonic control of helicopter blade.

- + Microvibrations of spacecraft (or optical high precision device, antennas).
- + Thin buffet alleviation of fighter aircrafts.

- * Active shape control
- + Antenna structures.

The application of the smart structure concept could be extended to coupled system aspects. Taking into account the coupling between the structural and internal/external environment could also be explored with special interest to :

- * Internal environment : Reduction of noise inside helicopter cabin - inside ground vehicles.
- * External environment :
 - (1) Reduction of external radiated noise.
 - (2) External electromagnetic field for the influence of structural deformation on radiation pattern efficiency on conformal antennas.

New scientific instrumentation for research in many disciplines both basic and applied will be an important result of this initiative.

b) *Military benefit*

Smart Structures have important military benefits in all the services, air, land and sea, including : fixed and rotary wing aircrafts, fighting vehicles, bridges, above and below water vessels. These benefits include :

- increased overall system performances and functionality,
- increased system reliability and survivability,
- increased system and personal safety,
- increased service lifetime,
- reduce maintenance,
- increased payload of missiles and airplanes.

The applications to the future are :

- active control of structures (vibration/flutter suppression),
- multisensor integration approach,
- health monitoring/damage detection,
- sound attenuation,
- electromagnetic smart skins : conformal and active antenna array,
- new measuring techniques.

The applications of MEMS and other microsystem components in Smart Structures have the following specific benefits :

- light weight, high quality aspects,
- rugged, reliable, robust,
- self test and diagnostics,
- high functionality for single components.

1-2 Objectives

The aim of the RSG is to conduct mutual research projects in the various areas of the microsensor, actuator, MEM integration in Smart Structures and to initiate collaboration in research activities in the participating nations.

Activities of the RSG are based on selected efforts from the following areas :

- a) study of critical environmental parameters.
- b) modelling of component performances and technology of microsensors, actuators, MEMS, optical packages and control systems,
- c) integration of sensors and actuators in material, structures and processing.
- d) impact of Smart Structures on system performances.

The aim of the work by the participating nations should be the demonstration of proofs of principles or technological concepts.

The RSG conducts specific cooperative research projects. Each project is proposed to and approved by Panel 3. More than one project can run in parallel. After completion of each project a report is submitted to NATO for publication.

The guidelines for performing the work are :

- a) Developing common technical projects using the existing specialties of each agency of the participating countries. Participating countries are not expected to commit new funding towards this RSG, however some redirection of resources may be necessary in few cases to achieve the final goals of the RSG.
- b) Exchanging technical information between participating agencies on microsensors, actuators, MEMS, Smart Structures and standard materials embedded in Smart Structures. Providing a large forum for discussions to all the participating nations for examining cooperation between agencies.
- c) Organizing international workshops.

1-3 Resources

Members should be scientists involved in multidisciplinary research programs in the domain of the integration of microsensors, actuators, MEMS in Smart Structures.

1-4 Participating industry

Industrial participation is by invitation of the RSG Group members.

1-5 Security level

Up to and including NATO SECRET.

1-6 liaison

Liaison is obtained in connection with other RSG groups such as RSG16, RSG20, AC Panel 3.

1-7 Policy and procedures

The RSG is only open to participating nation.

1.8 Expected duration of TOR

Four years

II - PROGRAMME OF WORK (POW) : SMART SYSTEMS - ENABLING TECHNOLOGIES

2.1. Introduction

A smart structure is considered to be a structure which contains embedded sensors and actuators with an associated modern control system which is capable of a spontaneous response to external stimuli in proportion to the intensity in order to compensate undesirable effects or to enhance desirable effects.

Smart structures or systems comprise an extensive range of enabling technologies all of which have significant interdependencies. Such technologies include: structural analysis; sensor technology; actuator technology; control systems; signal processing; system modelling; novel materials; integration of technology into structures; evaluation of 'smart' structural integrity.

A large number of European and US research groups (representing government & military, commercial and academia) are actively involved in the field of smart structures, researching the enabling technologies required for particular applications. It is the intention of this NATO Research Study Group (RSG) to promote participation and collaboration in a number of enabling technologies or tasks thereby furthering progress in this field which will benefit a broad range of systems applications. The programme is a multidisciplinary study undertaken for four years with the emphasis in the first two years on enabling technologies, establishing where mutual expertise and applications exist, thus allowing a focus on demonstrating the technology for particular applications in the final two years.

This document describes the method and programme which addresses the enabling technologies required to implement a smart structure or system. The programme of work is particularly focused on a range of systems applications including structural health monitoring, smart antennas and aerodynamic/structural control.

The generic applications currently foreseen by participating groups in the NATO Exploratory Team are outlined in the next sections.

2.1.1. Smart Antenna

In a smart phased antenna array, the antenna is directly glued on the radome which protect it, instead of being a rigid and flat structure behind the radome and not firmly attached. Because the radome must fit the skin of the aircraft or vehicle or ship, the smart antenna must be conformal. One of the main interest is to increase the bandwidth of that antenna thanks to the suppression of any air gap (i.e parasitic microwave cavity) between the antenna and the radome. An other aspect is to increase the integration of the antenna and

to facilitate the maintenance of the antenna array. Such an antenna will be subject to mechanical constraints, mainly vibrations, which will cause deformations of the total antenna. To get an antenna correctly working it will be necessary to control precisely the phase and amplitude of the emitted wave. This could be obtained only with a strict knowledge of the amplitude and frequency of the deformations, and to correct their effects.

Smart antennas will be composed of a multilayered conformal printed circuit board integrated within a radome which itself made up with stacking of foams, honeycombs, absorbing layers and thermoset films (PEEK for example). The total thickness of the structure should be close to 1 inch, and the global dimensions of the antenna will approach 2 to 3 feet wide. The curvature radius could be between 1/2 and 4 feet.

Smart antenna placed in the skin of an aircraft will be subject to static deformations, vibration modes and susceptibility to impact damages. Typically the vibration spectrum will be as wide as 10 to 2000 Hz, with a spectral density of 1 to 0,01 g^2/hz . The vibration amplitudes could be as large as several millimeters. For example, to have an antenna working correctly at 10 Ghz, the deformations must be lower than 1mm. All these effects have to be known and characterized.

The basic need is to get a reliable measurement of the shape of the antenna during the flight : $f(x,y,z,t)$. The use of electromechanical and optical sensors embedded in the antenna array seems to be one of the best ways to solve the problem. These sensors must be embedded into the multilayered structure without generating delaminations. One has to take care, also, that the electromechanical sensors and their electrical connections must not disturb the microwave working of the antenna, so they must be placed behind a metallic ground plane at 1/4 to 1/2 inch from the radiating elementary patch antenna. Optical sensors give an other solution to this last problem.

The second step is to correct the effects of the vibrations, if their amplitudes are unacceptable. Two ways must be investigated: the first is to make the corrections directly by using the phase-shifters in the T/R module (transmitter and receiver). These corrections have direct effect on the emitted wave and don't need any mechanical compensation. The second way is to embed combination of actuators and sensors which correct in real-time the mechanical deformations of the antenna. The second way has the double advantage to simplify the driving circuits of the phase-shifters and to increase the thermomechanical reliability of the structure. The localization of the sensors and or actuators must be a compromise between a good mechanical working and a lack of interference with the electromagnetic wave in order to avoid disturbance in the radiation pattern of the antenna.

2.1.2. Structural Health Monitoring

A number of assumptions have to be made during the design of any structure. The most important assumptions are the applied loading, material properties and presence

and size of defects. By making conservative assumptions a design life can be estimated. The presence of a health monitoring system can bring substantial advantages, including :

- verification of design assumptions. Loading conditions in particular have a profound influence on life, and these can be effectively monitored,
- the presence of significant defects can be detected and their growth estimated. This provides an increase in safety since the health of the structure is judged on actual performance rather than assumed properties,
- the structure can be made more efficient by reducing the conservatism in design assumptions without compromising safety,
- other influences which affect life, but cannot be readily estimated during design, can be detected before safety is reduced. Corrosion is an example of such an influence.

2.1.3. Aerodynamic/Structural Control

Structural acoustic control and machinery vibration control are of major importance to submarine operations and to an extent for surface ships stealth. Smart materials are perceived to play a major role as sensors and actuators in the control of machinery vibration and structural acoustics. Preliminary estimates indicate that the requirements in naval structures are such that existing, commercially available, smart materials are inadequate for these applications. The basic technology issues addressed are the need for actuator materials with large strains and high frequency and the need for high force actuators. In effect the performance envelop of all types of smart materials needs to be pushed further out.

The following basic developments are addressed :

- high-strain ferroelectric ceramic materials for actuators,
- constructive models and fatigue and fracture methodology for the design of high strain ferroelectric actuators,
- new fast shape memory materials for high-force / high-frequency actuators,
- hybrid active materials with superior properties,
- methodology for design and fabrication of embedded sensors and actuators in structural materials,
- novel actuators for high-strain / high-force and high frequency,
- methodology for nonlinear control

2-2 Programme of work

Through the discussions within the Exploratory Team the range of disciplines and enabling technologies which comprise smart structures research can be categorised as follows.

European and US research groups can contribute to any number of the identified parallel tasks through information interchange at dedicated organised fora (meetings, workshops and conferences). Establishing collaborations between groups is encouraged during these tasks, this leading into the second phase of the programme which is

focused on the demonstration of the technology in specific application areas of mutual interest.

Phase 1 : Enabling Technologies : 1996 - 1997

- Task 1** Data collection on environment where smart systems are to be applied (mechanical, stresses, temperature range, pressure, electromagnetic conditions).
- Task 2** Data collection on available technologies for sensing and actuation : piezoelectric polymers & ceramic; magnetostrictive & electrostrictive; shape memory alloy; optical fibres; acoustic/ultrasonic; electro-rheological; semiconductor devices (including silicon microelectromechanical structures and microtechnology); novel materials (micro, macro, meso-scale etc.).
- Task 3** Modelling and simulation of sensors and actuators integrated in smart structures, including structural finite element, electromagnetic simulation.
- Task 4** Integration of sensors, actuators and control methodology in smart structures, including compatibility, requirements, performance metrics, placement, networking, communication, powering.
- Task 5** Identification of control methodology and architecture, including neural networks, algorithms, open/closed loop systems.
- Task 6** Signal processing, including data acquisition, treatment and manipulation.
- Task 7** Reliability of sensors, actuators and control systems and structures, including performance of integrated smart system, effect of smart system on overall structural performance.
- Task 8** Future smart systems design concepts ie. designing systems with possible novel 'smart' structural materials.
- Task 9** Organised fora to disseminate results from research in tasks 1 to 8 to RSG members and wider international community working in the field. Establish collaborations and overlaps of expertise within participating members.

Phase 2 : Applications : 1998 - 1999

Applying and demonstrating the research into the enabling technologies from Phase 1 and the establishing of collaborations geared to particular applications will be performed in Phase 2. The type of approach and general sequence of tasks in this phase is envisaged as follows.

- Task 10** Selection of sensors and actuators compatible with each application.

- Task 11** Design of the bread-board : technological structure, positioning of embedded sensors and actuators, others.
- Task 12** Manufacturing the bread board system.
- Task 13** Mechanical, thermal, electromagnetic and optical trials on each components.
- Task 14** Studies of the electronic control of the structure under mechanical vibrations and or stresses,
- Task 15** Data acquisition from sensors, data treatment and control methods,
- Task 16** Organize workshops based on the results of tasks 10 to 15 with the participation of the wider international community who have worked in tasks 10 to task 15,
- Task 17** Identify the relevance of the results with respect to military applications.

The first workshop is scheduled in Paris on November 25-26, 1996 and will be related to future EM Smart structures Antennas.

III - LAST EVENTS AND CONCLUSIONS

During the November 1995 meeting of the Panel 3, the term of Reference and the Programme of work have been presented. It was decided to organize under Panel 3 umbrella several workshops ; in two years period, in order to clarify items included in task 1 to 9 of phase 1 of the POW.

During January 29, 1996 meeting in Paris and February, 27 meeting in San Diego, it was decided to organize three workshops :

- Future Electromagnetic Smart Structures Antennas to be held in Paris, November 25-26, 1996, Point of Contact Prof. A. Priou,
- Health monitoring to be held in 1997 in UK. Point of Contact : P. Lloyd from DRA Farnborough, UK,
- Aerodynamic/Structural Control in 1997 or 1998. Point of Contact : Dr. G. Anderson US ARO + someone from Germany.

For each workshop three parts will be organized :

- **Part I :** Why to do it ? with overviews from industries or national agencies,
- **Part II :** How to do it ? Open to presentation from various countries and including several sub-topics,
- **Part III :** Future Direction : round table with attendees for preparing the future direction and phase II of POW.

The objectives and goal of the workshops are to produce a clear view for Panel 3 on the :

- state-of-the art in the area,
- current and future opportunities for military applications,
- definition of gaps and need for future activities,
- areas for future cooperation for future activities.

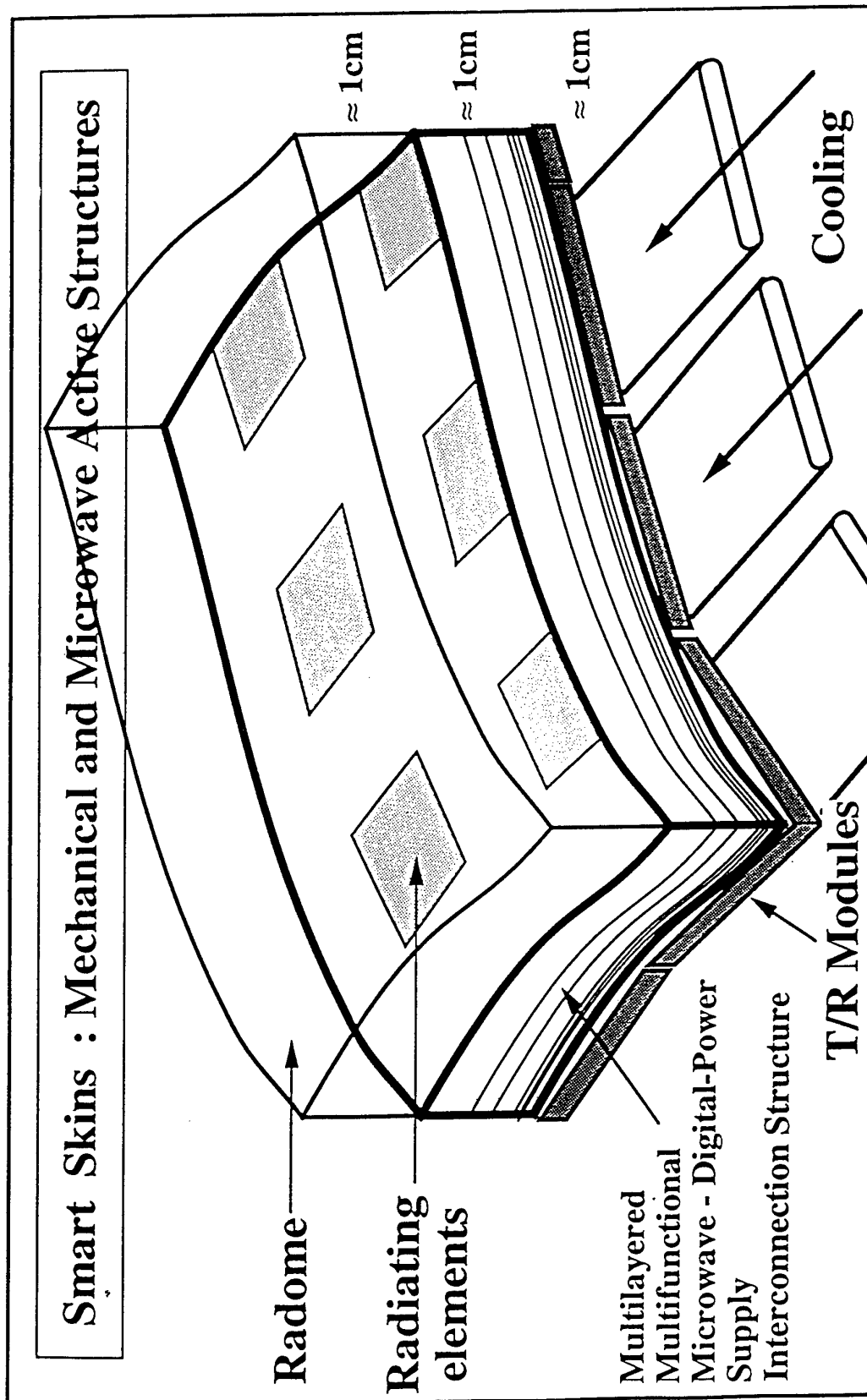


Figure 2 : possible smart thin antenna array panel

REPORT DOCUMENTATION PAGE

1. Recipient's Reference	2. Originator's Reference AGARD-LS-205	3. Further Reference ISBN 92-836-1042-3	4. Security Classification of Document UNCLASSIFIED/ UNLIMITED																
5. Originator Advisory Group for Aerospace Research and Development North Atlantic Treaty Organization 7 rue Ancelle, 92200 Neuilly-sur-Seine, France																			
6. Title Smart Structures and Materials: Implications for Military Aircraft of New Generation																			
7. Presented at/sponsored by The AGARD SMP Lecture Series held on 30-31 October 1996 in Philadelphia, USA, 18-19 November 1996 in Amsterdam, the Netherlands, 21-22 November 1996 in Paris, France.																			
8. Author(s)/Editor(s) Multiple			9. Date October 1996																
10. Author's/Editor's Address Multiple			11. Pages 152																
12. Distribution Statement There are no restrictions on the distribution of this document. Information about the availability of this and other AGARD unclassified publications is given on the back cover.																			
13. Keywords/Descriptors <table><tr><td>Fighter aircraft</td><td>Actuators</td></tr><tr><td>Airframes</td><td>Microprocessors</td></tr><tr><td>Smart materials</td><td>Neural nets</td></tr><tr><td>Smart structures</td><td>Fuzzy sets</td></tr><tr><td>Fiber optics</td><td>Signal processing</td></tr><tr><td>Piezoelectric materials</td><td>Sensor characteristics</td></tr><tr><td>Electrostriction</td><td>Shape memory materials</td></tr><tr><td>Rheological properties</td><td></td></tr></table>				Fighter aircraft	Actuators	Airframes	Microprocessors	Smart materials	Neural nets	Smart structures	Fuzzy sets	Fiber optics	Signal processing	Piezoelectric materials	Sensor characteristics	Electrostriction	Shape memory materials	Rheological properties	
Fighter aircraft	Actuators																		
Airframes	Microprocessors																		
Smart materials	Neural nets																		
Smart structures	Fuzzy sets																		
Fiber optics	Signal processing																		
Piezoelectric materials	Sensor characteristics																		
Electrostriction	Shape memory materials																		
Rheological properties																			
14. Abstract <p>Smart materials and structures technology is the integration of sensing and actuation elements into a structure or even more ambitiously into a material, with sensor and actuator being linked by a controller. Materials actually favoured for integration include optical fibres and piezoelectric materials with respect to sensors, piezoelectric and electrostrictive materials, shape memory alloys or electro-rheological fluids with respect to actuators and microprocessors, neural networks, fuzzy logic and various types of signal processing with respect to control. The first part of the lecture series is mainly focussed on understanding the fundamentals of smart materials and structures technology and achieving the capability to judge the use of that technology with respect to individual applications. Presentations related to sensor and actuator materials, mechanics of smart structures, control and data processing, as well as structural integration of sensors, actuators, and generally electronics are therefore be the focus of this part. In a second part, applications of smart structures technology are considered with respect to aircraft. Topics to be covered include monitoring the health/damage of aircraft structures or components, conceptual design of an adaptive wing, and electromagnetic antennae and their structural integration.</p>																			

Aucun stock de publications n'a existé à AGARD. A partir de 1993, AGARD détiendra un stock limité des publications associées aux cycles de conférences et cours spéciaux ainsi que les AGARDographies et les rapports des groupes de travail, organisés et publiés à partir de 1993 inclus. Les demandes de renseignements doivent être adressées à AGARD par lettre ou par fax à l'adresse indiquée ci-dessus. *Veuillez ne pas téléphoner.* La diffusion initiale de toutes les publications de l'AGARD est effectuée auprès des pays membres de l'OTAN par l'intermédiaire des centres de distribution nationaux indiqués ci-dessous. Des exemplaires supplémentaires peuvent parfois être obtenus auprès de ces centres (à l'exception des Etats-Unis). Si vous souhaitez recevoir toutes les publications de l'AGARD, ou simplement celles qui concernent certains Panels, vous pouvez demander à être inclu sur la liste d'envoi de l'un de ces centres. Les publications de l'AGARD sont en vente auprès des agences indiquées ci-dessous, sous forme de photocopie ou de microfiche.

CENTRES DE DIFFUSION NATIONAUX

ALLEMAGNE

Fachinformationszentrum Karlsruhe
D-76344 Eggenstein-Leopoldshafen 2

BELGIQUE

Coordonnateur AGARD-VSL
Etat-major de la Force aérienne
Quartier Reine Elisabeth
Rue d'Evere, 1140 Bruxelles

CANADA

Directeur, Services d'information scientifique
Ministère de la Défense nationale
Ottawa, Ontario K1A 0K2

DANEMARK

Danish Defence Research Establishment
Ryvangs Allé 1
P.O. Box 2715
DK-2100 Copenhagen Ø

ESPAGNE

INTA (AGARD Publications)
Carretera de Torrejón a Ajalvir, Pk.4
28850 Torrejón de Ardoz - Madrid

ETATS-UNIS

NASA Goddard Space Flight Center
Code 230
Greenbelt, Maryland 20771

FRANCE

O.N.E.R.A. (Direction)
29, Avenue de la Division Leclerc
92322 Châtillon Cedex

GRECE

Hellenic Air Force
Air War College
Scientific and Technical Library
Dekelia Air Force Base
Dekelia, Athens TGA 1010

ISLANDE

Director of Aviation
c/o Flugrad
Reykjavik

ITALIE

Aeronautica Militare
Ufficio del Delegato Nazionale all'AGARD
Aeroporto Pratica di Mare
00040 Pomezia (Roma)

LUXEMBOURG

Voir Belgique

NORVEGE

Norwegian Defence Research Establishment
Attn: Biblioteket
P.O. Box 25
N-2007 Kjeller

PAYS-BAS

Netherlands Delegation to AGARD
National Aerospace Laboratory NLR
P.O. Box 90502
1006 BM Amsterdam

PORTUGAL

Estado Maior da Força Aérea
SDFA - Centro de Documentação
Alfragide
2700 Amadora

ROYAUME-UNI

Defence Research Information Centre
Kentigern House
65 Brown Street
Glasgow G2 8EX

TURQUIE

Millî Savunma Başkanlığı (MSB)
ARGE Dairesi Başkanlığı (MSB)
06650 Bakanlıklar-Ankara

Le centre de distribution national des Etats-Unis ne détient PAS de stocks des publications de l'AGARD.

D'éventuelles demandes de photocopies doivent être formulées directement auprès du NASA Center for AeroSpace Information (CASI) à l'adresse ci-dessous. Toute notification de changement d'adresse doit être fait également auprès de CASI.

AGENCES DE VENTE

NASA Center for
AeroSpace Information (CASI)
800 Elkridge Landing Road
Linthicum Heights, MD 21090-2934
Etats-Unis

ESA/Information Retrieval Service
European Space Agency
10, rue Mario Nikis
75015 Paris
France

The British Library
Document Supply Division
Boston Spa, Wetherby
West Yorkshire LS23 7BQ
Royaume-Uni

Les demandes de microfiches ou de photocopies de documents AGARD (y compris les demandes faites auprès du CASI) doivent comporter la dénomination AGARD, ainsi que le numéro de série d'AGARD (par exemple AGARD-AG-315). Des informations analogues, telles que le titre et la date de publication sont souhaitables. Veuillez noter qu'il y a lieu de spécifier AGARD-R-nnn et AGARD-AR-nnn lors de la commande des rapports AGARD et des rapports consultatifs AGARD respectivement. Des références bibliographiques complètes ainsi que des résumés des publications AGARD figurent dans les journaux suivants:

Scientific and Technical Aerospace Reports (STAR)
publié par la NASA Scientific and Technical
Information Division
NASA Langley Research Center
Hampton, Virginia 23681-0001
Etats-Unis

Government Reports Announcements and Index (GRA&I)
publié par le National Technical Information Service
Springfield
Virginia 22161
Etats-Unis
(accessible également en mode interactif dans la base de
données bibliographiques en ligne du NTIS, et sur CD-ROM)



AGARD holds limited quantities of the publications that accompanied Lecture Series and Special Courses held in 1993 or later, and of AGARDographs and Working Group reports published from 1993 onward. For details, write or send a telefax to the address given above. *Please do not telephone.*

AGARD does not hold stocks of publications that accompanied earlier Lecture Series or Courses or of any other publications. Initial distribution of all AGARD publications is made to NATO nations through the National Distribution Centres listed below. Further copies are sometimes available from these centres (except in the United States). If you have a need to receive all AGARD publications, or just those relating to one or more specific AGARD Panels, they may be willing to include you (or your organisation) on their distribution list. AGARD publications may be purchased from the Sales Agencies listed below, in photocopy or microfiche form.

NATIONAL DISTRIBUTION CENTRES**BELGIUM**

Coordonnateur AGARD — VSL
Etat-major de la Force aérienne
Quartier Reine Elisabeth
Rue d'Evere, 1140 Bruxelles

CANADA

Director Scientific Information Services
Dept of National Defence
Ottawa, Ontario K1A 0K2

DENMARK

Danish Defence Research Establishment
Ryvangs Allé 1
P.O. Box 2715
DK-2100 Copenhagen Ø

FRANCE

O.N.E.R.A. (Direction)
29 Avenue de la Division Leclerc
92322 Châtillon Cedex

GERMANY

Fachinformationszentrum Karlsruhe
D-76344 Eggenstein-Leopoldshafen 2

GREECE

Hellenic Air Force
Air War College
Scientific and Technical Library
Dekelia Air Force Base
Dekelia, Athens TGA 1010

ICELAND

Director of Aviation
c/o Flugrad
Reykjavik

ITALY

Aeronautica Militare
Ufficio del Delegato Nazionale all'AGARD
Aeroporto Pratica di Mare
00040 Pomezia (Roma)

LUXEMBOURG

See Belgium

NETHERLANDS

Netherlands Delegation to AGARD
National Aerospace Laboratory, NLR
P.O. Box 90502
1006 BM Amsterdam

NORWAY

Norwegian Defence Research Establishment
Attn: Biblioteket
P.O. Box 25
N-2007 Kjeller

PORTUGAL

Estado Maior da Força Aérea
SDFA - Centro de Documentação
Alfragide
2700 Amadora

SPAIN

INTA (AGARD Publications)
Carretera de Torrejón a Ajalvir, Pk.4
28850 Torrejón de Ardoz - Madrid

TURKEY

Millî Savunma Başkanlığı (MSB)
ARGE Dairesi Başkanlığı (MSB)
06650 Bakanlıklar-Ankara

UNITED KINGDOM

Defence Research Information Centre
Kentigern House
65 Brown Street
Glasgow G2 8EX

UNITED STATES

NASA Goddard Space Flight Center
Code 230
Greenbelt, Maryland 20771

The United States National Distribution Centre does NOT hold stocks of AGARD publications.

Applications for copies should be made direct to the NASA Center for AeroSpace Information (CASI) at the address below. Change of address requests should also go to CASI.

SALES AGENCIES

NASA Center for
AeroSpace Information (CASI)
800 Elkridge Landing Road
Linthicum Heights, MD 21090-2934
United States

ESA/Information Retrieval Service
European Space Agency
10, rue Mario Nikis
75015 Paris
France

The British Library
Document Supply Centre
Boston Spa, Wetherby
West Yorkshire LS23 7BQ
United Kingdom

Requests for microfiches or photocopies of AGARD documents (including requests to CASI) should include the word 'AGARD' and the AGARD serial number (for example AGARD-AG-315). Collateral information such as title and publication date is desirable. Note that AGARD Reports and Advisory Reports should be specified as AGARD-R-nnn and AGARD-AR-nnn, respectively. Full bibliographical references and abstracts of AGARD publications are given in the following journals:

Scientific and Technical Aerospace Reports (STAR)
published by NASA Scientific and Technical
Information Division
NASA Langley Research Center
Hampton, Virginia 23681-0001
United States

Government Reports Announcements and Index (GRA&I)
published by the National Technical Information Service
Springfield
Virginia 22161
United States
(also available online in the NTIS Bibliographic
Database or on CD-ROM)



Printed by Canada Communication Group
45 Sacré-Cœur Blvd., Hull (Québec), Canada K1A 0S7